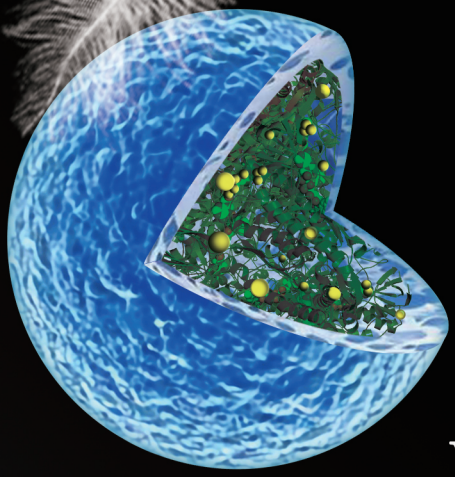

VALORIZATION OF CHICKEN FEATHERS : BIOBASED NANOCARRIERS FOR BIOMOLECULE DELIVERY

XIAOJIE QIN

Propositions

1. Feather keratin is a severely undervalued biomass for its application in biomaterials.
   (this thesis)

2. Keratin-based formulations enhance the implementation rate of biomolecules in food and pharma applications.
   (this thesis)

3. Integrating multiple research areas will yield novel insights greater than the sum of individual parts.

4. The visualization of scientific data will make the public understand scientific research easily.

5. Having a Plan B is always beneficial for work and life.

6. Communicating with others is an effective way of getting out of a dilemma.

Propositions belonging to the thesis, entitled

Valorization of chicken feathers: biobased nanocarriers for biomolecule delivery

Xiaojie Qin

Wageningen, 19 June 2024

VALORIZATION OF CHICKEN FEATHERS: BIOBASED NANOCARRIERS FOR BIOMOLECULE DELIVERY

Xiaojie Qin

Thesis committee

Promotor

Prof. Dr Johannes H. Bitter
Professor of Biobased Chemistry and Technology
Wageningen University & Research

Co-promotors

Dr Elinor L. Scott
Assistant professor, Biobased Chemistry and Technology
Wageningen University & Research

Prof. Dr Chunhui Zhang
Professor of Food Science and Technology
Chinese Academy of Agricultural Sciences, Bejing, China

Other members

Prof. Dr Aldrik Velders, Wageningen University & Research
Prof. Dr Michel Eppink, Delft University of Technology
Dr Yuemei Lin, Delft University of Technology
Dr Carlos Cabrera, Greencovery, Wageningen

This research was conducted under the auspices of the VLAG Graduate School (Biobased, Biomolecular, Chemical, Food and Nutrition Sciences)

VALORIZATION OF CHICKEN FEATHERS: BIOBASED NANOCARRIERS FOR BIOMOLECULE DELIVERY

Xiaojie Qin

Thesis

submitted in fulfilment of the requirements for the degree of doctor
at Wageningen University
by the authority of the Rector Magnificus,
Prof. Dr C. Kroeze,
in the presence of the
Thesis Committee appointed by the Academic Board
to be defended in public
on Wednesday 19 June 2024
at 1:30 p.m. in the Omnia Auditorium.

Xiaojie Qin

Valorization of chicken feathers: biobased nanocarriers for biomolecule delivery, 206 pages.

PhD thesis, Wageningen University, Wageningen, the Netherlands (2024)
With references, with summary in English

DOI https://doi.org/10.18174/656823

Table of contents

1

CHAPTER 1

General Introduction

1.1 Feather keratin

1.1.1 Keratin resources

Keratin dominates the largest family of intermediate filament proteins, widely existing in feathers, wool, hair, horns, nails, etc. [1, 2]. As the main byproducts from poultry farms, slaughterhouses and leather industries worldwide, keratin is the third most abundant natural polymer after cellulose and chitin [3, 4]. Especially, with a great demand for chicken meat and eggs, about 50 billion chickens are raised globally every year, producing millions of tons of feather waste [3, 5]. Chicken feathers contain more than 90% keratin, serving as a huge alternative protein reservoir. As an abundant, cost-effective and readily available natural biopolymer, feather keratin shows promise for diverse applications [6].

1.1.2 Properties and applications of feather keratin

Feather keratin is a natural biopolymer with an average molecular weight of about 10 kDa, rich in certain amino acids (e.g. glycine, serine, valine, alanine and cysteine) [7, 8]. The polypeptide chains form α-helix and β-sheet structures, providing keratin with mechanical property [9]. Feather keratin contains about 7 mol% cysteine forming abundant disulfide bonds [10]. The abundant presence of inter- and intra-chain crosslinks, along with hydrogen bonds, ionic bonds and hydrophobic interactions confer an intrinsically stable chemical structure (**Figure 1.1**), resulting in high stability, low solubility and resistance to enzymatic and thermal treatments [9]. As well as this, abundant carboxyls, amines and active thiols allow keratin to undergo chemical modification, functionalization and conjugation [11, 12], demonstrating the adjustability of functional properties.

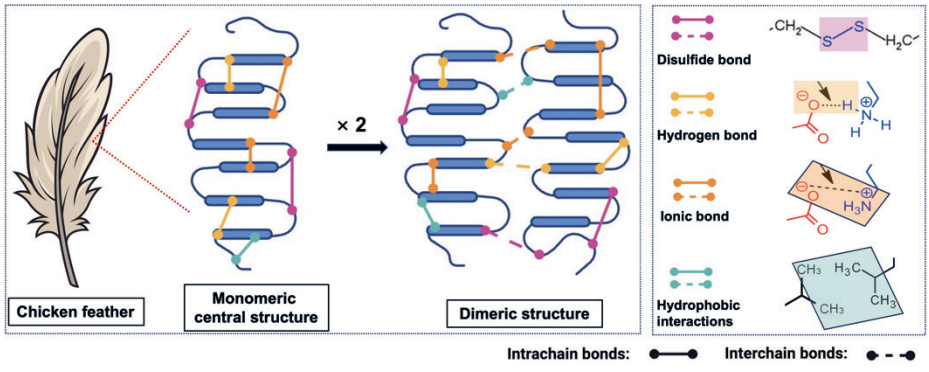

Figure 1.1. The central monomeric structure, dimeric structure and main bonds of chicken feather keratin.

As a natural biopolymer, keratin exhibits good biocompatibility, biodegradability and low toxicity [13-15], without burden on the environment and human health. Despite its resistance to common proteases, researchers found that keratin can be degraded by keratinolytic b1acteria and some specific enzymes, such as keratinase and proteinase K [16, 17]. Earlier studies have also reported the ability of keratin degradation *in vivo* without immune rejection [18, 19]. Additionally, the specific composition of functional groups (e.g. -COOH, -SH, -NH_2 and -OH), amino acids and tripeptide structures (e.g. Arg-Gly-Asp and Leu-Asp-Val) contribute to its potential biological functions [8, 16, 20]. As outlined in previous reviews [9, 12], keratin presents biological capabilities involving hemostasis, wound healing, anti-inflammatory, cell adhesion, cell proliferation, antibacterial and oxidation-reduction properties.

Feather keratin has been taken as an alternative protein resource for new upcycling processes for targeting applications such as fertilizers, feed, cosmetics and biomedical materials [21, 22]. Specifically, the biomedical applications mainly include hemostasis, wound healing, drug delivery, tissue engineering, involving products of hydrogels, nanoparticles, micelles, scaffolds, sponges and biofilms [12]. As an abundant natural biopolymer, keratin holds significant economic benefits and environmental importance.

1.1.3 Limitations of feather keratin utilization

Despite the appealing properties, it is still challenging to fully utilize feather keratin. The combination of disulfide bonds, hydrogen bonds, ionic bonds and hydrophobic interactions resulted in a chemical robust nature, indicating resistance to various chemicals/conditions and conventional proteases (e.g. pepsin and trypsin) [4, 23]. It is often costly and difficult to efficiently dispose feather waste in a large scale. The majority of them end up in landfills, leading to both resource waste and environmental problems, such as land, water and air pollution [3]. Only a minor fraction undergoes processing into animal feeds, fertilizer and biomaterials abovementioned [22]. Nevertheless, various issues arise during the utilization of feather keratin. Most keratin extraction processes exhibit drawbacks, including time consumption, high cost, small scale, residual chemicals, etc. [24]. The resulting products are often with low economic value and unevenly qualified. For example, alkali reagents can damage the polypeptide chain structure [25], and keratin tends to aggregate when removing chemicals during extraction, which further results in poor

solubility and dispersibility [1, 26, 27].

1.1.4 Available techniques for keratin extraction

Approaches to extract keratin are in general based on solubilization followed by extraction. To solubilize often oxidation, reduction, alkaline hydrolysis, microwave irradiation, steam explosion, ionic liquids, sulfitolysis and enzymatic hydrolysis are used [28]. Although chemical hydrolysis possesses high efficiency in solubilizing keratin, most of the current methods result in residual chemicals (e.g. mercaptoethanol (MEC) and sodium dodecyl sulfate (SDS)), which limits the application in food and pharmaceutical areas [22]. Additionally, the methods of oxidation, reduction, alkaline and sufitolysis have been reported to carry the risk of damaging the protein backbone and amino acid residue (e.g. tryptophan and methionine) [29-31], while thermal hydrolysis may result in severe degradation and chemical modification though with less requirement of reagents [32]. The methods with microwave and ionic liquids are more eco-friendly compared to other methods, however, exhibiting drawbacks as well, such as cysteine loss and low yield [22, 33]. For instance, a maximum yield of 21.5% of feather keratin was recycled through the ionic liquid after four hours [34].

Enzymatic hydrolysis stands out owing to its relatively mild treatment conditions and the preservation of functional properties [35]. It offers numerous advantages over chemical and hydrothermal treatments, e.g. environmental safety and lower energy, making them extensively employed in various industrial and biotechnological processes [28, 36]. Enzymatic hydrolysis is an applicable technique for safeguarding functional groups and yielding bioactive peptides [16, 37]. Beyond that, it also shows prospects in other aspects. The emergence of amphiphilic structures after enzymatic hydrolysis can spontaneously self-assemble into various well-defined nanostructures, such as nanoparticles, nanotubes, nanofibrils, nanorods and micelles [38, 39]. Previously, partial enzymatic hydrolysis was found to be an efficacious approach for preparing soy protein nanoparticles, exhibiting spherical shapes, enhanced solubility, stability and improved biomolecule encapsulation efficiency [40]. Thus, enzymatic hydrolysis is promising in producing high-valued bioactive keratin peptides and keratin-based nanoparticles. In this thesis, enzymatic hydrolysis will be considered as a key technique to formulate a more efficient and eco-friendly process for reusing feather keratin.

Overall, keratin is a promising natural biomaterial deserving anticipated exploration to bring further benefits to humanity. However, how to convert feather waste into value-added products from both economic and environmental viewpoints needs to be addressed. This thesis aims: 1) to develop a more sustainable strategy for efficiently extracting/utilizing keratin; 2) to investigate the potential biological activities (antimicrobial and cell-penetrating ability) of hydrolyzed keratin; 3) to develop keratin-based material into high-valued nanocarrier products.

1.2 Bioactive molecules

1.2.1 Bioactivities and applications

In recent years, bioactive molecules (biomolecules) have gained attention among researchers, producers and consumers, owing to their recognized potential for promoting health benefits and well-being [41]. The most-reported biomolecules encompass fatty acids, polyphenols, flavonoids and bioactive peptides [42, 43], such as insulin, curcumin and resveratrol [44-46]. Many preclinical, clinical and epidemiological investigations have been conducted *in vitro* to elucidate their chemical properties and explore their applications [47]. The functional properties, including anti-oxidant, anti-cancer, anti-diabetes, anti-aging and anti-inflammatory bioactivities, etc. are beneficial for human health and preventing and managing diseases [41, 48]. They have been applied to kinds of products, including functional foods, nutraceuticals, pharmaceuticals and cosmeceuticals [49].

1.2.2 Physicochemical properties and limitations

However, despite the favorable bioactivities, their bioavailability and applications are often restricted by poor physicochemical properties. Biomolecules exhibit diverse chemical structures, encompassing both hydrophilic and lipophilic properties, the chemical structures of which are highly heterogeneous [47]. The intrinsic nature, such as large molecular weight, hydrophilicity and lipophilicity, will hinder their passive diffusion, biomembrane permeation and solubility in the intestine [50-52]. The degradation by low pH and enzymes, bioconversion by gut microbiota and elimination by efflux mechanism in the gastrointestinal (GI) tract will also lead to low absorption and bioavailability [53-55]. The properties of solubility, stability, permeability and metabolic interconversions play a key role in the bioaccessibility of biomolecules [56]. Additionally, the environmental conditions during processing, storage and transportation (e.g. heating, oxygen levels, humidity,

pH, ionic strength and light exposure) can also result in biomolecule degradation [47, 57, 58]. To achieve effective health responses, the stability enhancement of biomolecules is crucial for ensuring their successful delivery to the intended site of action at an optimal dosage [59, 60].

1.2.3 Insulin—A typical representative

Insulin is a typical polypeptide biomolecule with the main administration of daily injection, but 45-60% of diabetic patients intentionally skip insulin doses due to the fear of injections [61]. Oral administration is a more suitable and ideal route to enhance compliance and therapeutic outcomes for diabetic patients. However, the special characteristics make insulin easily denatured and degraded. The physicochemical properties, such as poor stability and sensitivity to harsh pH and enzymes, pose significant limitations on its bioavailability when administered orally.

As outlined in the previous review, the key features of insulin can be summarized as follows: 1) large molecular weight (5.8 kDa); 2) short half-life (3–10 min); 3) solubility and partition coefficient; 4) hydrophilicity; 5) colloidal aggregation; 6) enzymatic cleavage (e.g. by pepsin, elastase, lipase, carboxypeptidases, trypsin, chymotrypsin, brush border endopeptidase, exopeptidase and cytosolic lysozyme); 7) poor oral absorption; 8) low diffusion rate across mucin barrier; 9) poor stability at different pH; 10) limited permeation through gastrointestinal membranes; and 11) first-pass elimination leads to a low therapeutic index, low bioavailability (< 2%) and, in turn, ineffective in controlling the blood glucose levels [62]. Hence, developing an effective technique enhancing the physicochemical properties of insulin and providing protection against various barriers encountered during oral administration is becoming imperative. In this thesis, insulin will serve as the primary target biomolecule for developing keratin-based nanocarriers.

1.3 Nanocarriers

1.3.1 Overview of nanotechnology

Nanotechnology has been taken as a crucial tool for creating promising nanostructures in potential biomolecule delivery systems [63]. Various nanotechnology-based delivery systems have been developed and validated, such as nanoparticles, micelles, liposomes, dendrimers, nano-emulsions, nanotubes and nanogels (**Figure 1.2**) [64, 65]. Nanoparticles are minute objects with at least one

dimension between 1 and 100 nm in diameter, exhibiting improved physicochemical and physiological properties owing to their small size and large surface area [66]. A recent review noted that the size of nanoparticles can be extended up to 1000 nm [67]. Typical advantages include improved solubility/dispersibility, colloidal stability and surface reactivity, prolonged gastrointestinal retention via mucoadhesion and enhanced permeability [68, 69]. Nanoparticles can encapsulate biomolecules within the matrix or core, protecting against harsh conditions, enzyme degradation and other barriers in the GI tract. The small sizes are beneficial for increasing nanoparticle mobility across a heterogeneous viscoelastic network of mucus, which has been reported with an average mesh size from 10 to 200 nm [70]. Their internalization by epithelial cells or M cells within Peyer's patches could also promote intestinal absorption [71]. Additionally, nanoparticles can improve lengthening circulatory half-life, targeted delivery and controlled release [72]. Nanoparticles have been widely applied in food, nutraceutical and pharmaceutical areas, exhibiting remarkable capability for delivering biomolecules within the precise dosage range prescribed [48, 73]. This leads to enhanced biomolecule bioavailability and reduced side effects and facilitates greater patient compliance.

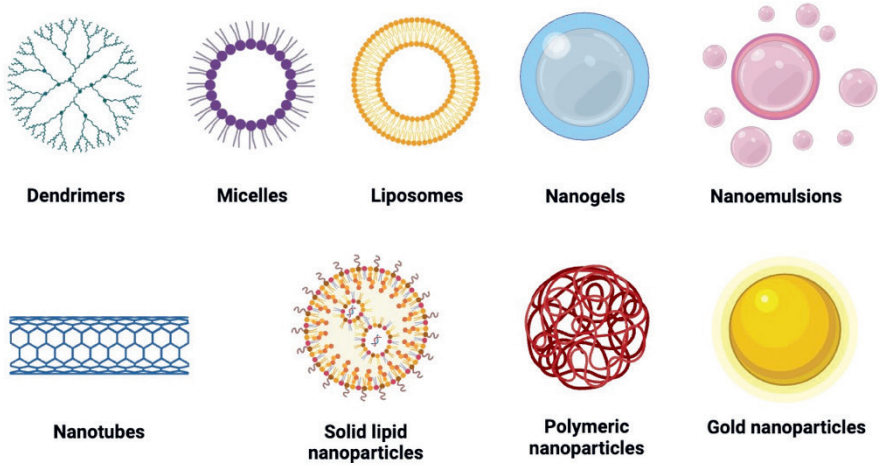

Figure 1.2. Representative formulations of nanocarriers [64, 74].

1.3.2 Classification of nanoparticles

Researchers have categorized nanoparticles into three types based on materials: lipid-based, inorganic and polymeric nanoparticles [71], demonstrating sound oral delivery effects. Polymeric nanoparticles are broadly classified into two major

groups: synthetic and natural polymeric nanoparticles. Especially, natural and synthetic biodegradable polymers derived from bio-based materials have promoted the development of safe and targeted nanocarrier systems, due to benefits such as biocompatibility, biodegradability, low toxicity, sustained release properties, inherent immune regulation, biocompatibility, mucosal adhesion, etc. [75]. Nevertheless, despite the vast potential of synthetic biopolymers, their global production is still a minor fraction, necessitating extensive research for cost-effective, large-scale production and confirming environmental compliance [76]. Conversely, natural polymers show greater promise for applications in nanocarrier systems.

1.3.3 Natural polymeric nanoparticles

Natural polymeric nanoparticles are sourced from natural polymers, such as proteins and polysaccharides derived from plants, animals and microorganisms [48]. Due to their excellent biodegradability, biocompatibility and low toxicity, they have been widely applied in nano-delivery systems and taken as the best choice for encapsulating and delivering drugs [77]. The ideal characteristics for natural polymers in oral delivery systems encompass biocompatibility, bio-adhesion, biodegradability, renewability, cost-effectiveness, non-toxicity, hydrophilicity, surface modifiability and derivation from renewable sources [78]. The most common natural polymers, including alginate [79], chitosan/chitin [80], pectin [81], gelatin [82], collagen [83], zein [84], rice protein [85], whey protein [86], soy protein [40], casein [87], albumin [88], keratin [89], etc. have been reported for extensive application to deliver macromolecules, proteins and drugs. They are prominent for their economic feasibility, ease of preparation and stability in biological fluids, and some even exhibit superior cell proliferation, adhesion and efficient targeting, making them ideal for various applications [90]. Natural polymers are relatively safer than synthetic polymers and demonstrate the potential for more suitable drug delivery [78, 91].

1.3.4 Protein-based nanoparticles and main preparation techniques

Recently, protein-based polymers, such as zein, whey protein and soy protein mentioned above, have been widely applied to nanoparticles for orally delivering biomolecules due to various merits. These protein-based polymers can bear positive or negative charges at pH values below or above their isoelectric points, respectively, thus enabling the loading of biomolecules [92-95]. They can undergo site-selective modifications through amino acid mutagenesis, allowing the conjugation of

biomolecules into the protein backbone. The hydrophobic domains within protein molecular structures are able to attract hydrophobic therapeutics, such as water-insoluble drugs [96]. Despite significant improvements in biomolecule delivery, certain deficiencies of protein-based nanoparticles are still worth improving. For example, some protein nanoparticles are prone to aggregation and exhibit instability in diverse aqueous environments, leading to a shortened shelf life [96]. The poor permeability through the mucus layer and the intestinal epithelium is also a critical problem needing improvement [97]. Thus, more suitable polymers and enhanced formulations will be required to overcome the shortcomings associated with nano-delivery systems.

Nowadays, the techniques for preparing protein-based nanoparticles have been well developed and mainly classified into natural self-assembly, physical, chemical and enzymatic types based on the physical and chemical differences [98]. The existing advantages and drawbacks of the most common techniques are summarized in **Table 1.1**. Despite significant progress, shortcomings have been exposed, such as residual chemicals, energy consumption and high cost. Therefore, developing a more sustainable technique for preparing protein-based nanoparticles with high performance from both economic and environmental viewpoints is meaningful.

Table 1.1. The most common techniques for preparing protein nanoparticles as summarized in the previous review [98].

Classification	Techniques	Advantages	Limitations
Natural self-assembly techniques		Simple operation, low cost and no chemicals	Depending on environmental conditions, e.g. pH
Physical techniques	Isoelectric point	Simple operation, low cost and no chemicals	pH reliance
	pH-cycle	Simple operation, low cost, no organic chemicals and suitability for industrial scale	Laborious requirement and time consumption
	Antisolvent precipitation/ solvent evaporation	Simple operation process, low cost and wide suitability	Residual organic solvents
	Heat-induced aggregation	Shape diversity, simple operation process, low cost and suitability for industrial scale	Energy consumption
	Non-electrostatic complexation	Simple, mild, economic and feasible process; avoidance of organic solvents, vigorous mechanical shearing and high energy	Only for ingredients forming non-electrostatic interactions
	Mechanical top-down	Widely applicability, avoidance of organic chemicals, intact protein structure and suitability for industrial scale	Energy consumption
Chemical techniques	Ionic crosslinking	Simple, mild, economic and feasible process; avoidance of organic solvents, vigorous mechanical shearing and high energy input	
	Heat-induced disulfide crosslinking	Simple operation, low cost, no new chemicals and high stability	Large particle size and energy consumption
	Aldehyde-induced covalent crosslinking	Low surface hydrophobicity, high surface charges and nanoparticle internal integrity	Large particle size and residual solvents
	Genipin-induced covalent crosslinking	High stability and low toxicity	Time consumption
Enzymatic techniques		High specificity of enzymatic catalysis, mild reaction condition and sustainable enzymes	High cost and time consumption

1.4 Oral delivery system

1.4.1 Overview of oral delivery system

Millions of patients have been reported to avoid their medications because of needle phobia and accompanying pain, thus oral delivery stands out as the favorable medication over injections [99]. Oral delivery is becoming a widely applied and popular medication pathway due to its convenience, painlessness, cost-effectiveness, high compliance, and sustained and controlled delivery [100, 101]. The large intestinal surface area (300-400 m^2), coated with a viscous mucosal layer, can facilitate drug attachment and subsequent absorption [102]. The abundance of enterocytes distributed throughout various parts of the intestine, particularly the microfold cells (M cells) that cover Peyer's patches and the lymphoid segment of the small intestine, will also contribute to the absorptive capacity of the human intestinal epithelium [103]. It is particularly favored for self-medication and facilitating adherence to a prescribed medication regimen [104]. So far, researchers have made significant achievements in developing oral nano-delivery systems, such as self-emulsifying delivery systems [105], polymer conjugation [106], encapsulation [107] and nanoparticle vesicles [108].

1.4.2 Barriers to the oral delivery system

Despite the progress of nano-delivery systems, barriers along the GI tract, such as physiological, biochemical and formulation-based barriers [71, 101], remain a big challenge for biomolecule bioaccessibility. Physiological and biochemical barriers mainly include saliva solutions, harsh gastric pH, enzymatic degradation, mucus layer, epithelium cells with tight junctions, bioconversion by gut microbiota, efflux mechanism and hepatic metabolism [48, 97] (**Figure 1.3**).

Saliva fluid is the first barrier during mouth containing proline-rich glycoprotein and antimicrobial compounds, which can potentially cause degradation of antioxidant molecules (e.g. polyphenols and β-carotene) [109, 110]. The second barrier involved hash luminal pH, its variation and luminal enzymes during the GI tract. The luminal pH varies from 1.2-3.0 (stomach) to 6.5-8.0 (intestine), which can induce deamination and oxidation of biomolecules [111]. Various luminal enzymes, such as pepsin, pancreatic and colonic bacterial enzymes, can induce biomolecule degradation [112, 113]. The third barrier is mucus, which covers all inner surfaces of the GI tract with a pore size of about 200 nm, comprised of mucin, glycoproteins,

electrolytes, and so on. It prevents large molecules and pathogens into the systemic circulation [97, 114, 115]. After that is the epithelial barrier, comprised of epithelial cells (enterocytes, goblet cells, Paneth cells and Microfold cells) interconnected through tight junctions, adherent junctions and desmosomes [116]. It is challenging to transport biomolecules with a bulky nature and hydrophilicity across the intestinal epithelium is challenging [71]. Additionally, the microbiota-mediated metabolism may affect the bioactivity, bioavailability and toxicity of biomolecules, involving processes such as ester hydrolysis, deglycosylation, decarboxylation, deconjugation, dehydroxylation, demethylation, oxidation, reduction, racemization, ring fission and ring breakage [48]. In addition to that, the authors also summarized the risks from hepatic metabolism and efflux mechanism. Hence, it is crucial to consider the mentioned challenges regarding oral delivery when developing new delivery systems.

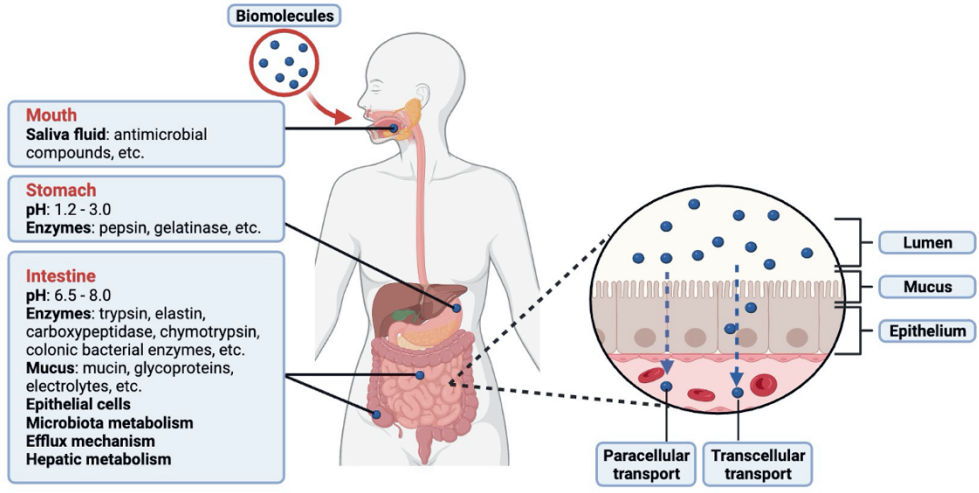

Figure 1.3. Physiological and biochemical barriers in the GI tract [48, 78].

Beyond physiological barriers, the formulations also encounter challenges for orally delivering biomolecules [72]. Key strategies addressing formulation barriers include overcoming obstacles in the GI tract, where approaches such as enzyme inhibitor, modification and carriers (micro/nanoparticles, micelles, liposomes, hydrogel, etc.) can be potentially applied [101]. Herein, it is crucial to understand the biomolecules-excipient interactions for a better design of stable formulations. The design of carriers for facilitating the oral delivery of biomolecules should consider the abovementioned obstacles, including but not limited to an acidic environment,

enzymes, residence time, microbiome and permeability across mucus and the intestinal epithelium.

1.5 Thesis outline

Over the past decade, significant efforts have been devoted to enhancing the utilization and valorization of residual keratin materials. Despite notable progress in disposal techniques, a need for an alternative, more sustainable, cost-effective and efficient strategy remains. Prior research has provided insights into the physicochemical and biological properties of keratin, leading to the development of several highly-valued products. However, there are fewer reports on the bioactivity of hydrolyzed keratin and its potential application in nanoparticles for delivering biomolecules. Considering the above, this thesis aims to 1) explore alternative and highly efficient strategies for reusing feather keratin with sustainability in mind; 2) delve into the potential antimicrobial and cell-penetrating capabilities of hydrolyzed keratin; 3) develop keratin-based nanoparticles for delivering biomolecules, where insulin was applied as the target biomolecule.

In **Chapter 2**, we proposed a strategy combining ultrasound and Cys-reduction to extract keratin from chicken feather waste. The effect of ultrasound on the physicochemical properties of keratin was investigated, and the process with optimal conditions was obtained via Box-Behnken Design. As enzymatic hydrolysis is effective for preparing bioactive peptides, the potential bioactivity of keratin hydrolysate was delved into in **Chapters 3** and **4.** In **Chapter 3**, the instant catapult steam explosion (ICSE) technique assisted with enzymatic hydrolysis was applied to prepare keratin peptides (KEP). The study involved the effect of ICSE treatment on feather pre-deconstruction, followed by an assessment of different enzymes on feather further deconstruction. The resulting keratin hydrolysates were then investigated for their antimicrobial activity, revealing their potential application in antimicrobial products. Antimicrobial peptides (AMPs) and cell-penetrating peptides (CPPs) often share common physicochemical characteristics with functional similarity, based on which we hypothesize that KEP might possess cell-penetrating ability. The hypothesis was verified in **Chapter 4**, employing fluorescein-labeled insulin (FITC-INS) as the target intracellular molecule for investigating its cellular uptake into Caco2 cells delivered by KEP. In addition, the cytotoxicity, cellular uptake mechanism and physicochemical characterization of

KEP were investigated, which might provide insights into their action mechanism. **Chapter 5** focused on preparing self-assembled keratin nanoparticles (KNPs) through partial hydrolysis and pH-shifting method. This chapter delved into the impact of different degrees of hydrolysis (DH) on the physicochemical properties of KNPs, e.g. solubility, microstructure, aggregation behavior and digestibility. Additionally, the restructuring of KNPs by shifting pH between 2.0 to 7.0 was investigated. Allied to this, **Chapter 6** endeavored to develop a novel formulation incorporating KNP and sodium alginate (ALG) with enhanced stability. In this section, the double-coated nanoparticles (ALG-KNP-INS) were prepared via gelation based on the process of partial hydrolysis and pH-shifting mentioned in **Chapter 5**. The assessment involved physicochemical properties (e.g. FTIR, re-dispersibility and microstructure), environmental stability (e.g. heating and storage), and physiological stability in the GI tract with/without enzymes. Finally, in **Chapter 7**, the results obtained in this thesis are presented and discussed in a broader context. Future recommendations and perspectives regarding the valorization and application of keratin materials are discussed.

1.6 References

1. M. Pakdel, Z. Moosavi-Nejad, R.K. Kermanshahi, H. Hosano, Self-assembled uniform keratin nanoparticles as building blocks for nanofibrils and nanolayers derived from industrial feather waste, Journal of Cleaner Production, 335 (2022).
2. S. Feroz, N. Muhammad, J. Ranayake, G. Dias, Keratin - Based materials for biomedical applications, Bioact Mater, 5 (2020) 496-509.
3. T.K. Kumawat, A. Sharma, V. Sharma, S. Chandra, Keratin waste: the biodegradable polymers, in: Keratin, IntechOpen, 2018.
4. L. Guo, L. Lu, M. Yin, R. Yang, Z. Zhang, W. Zhao, Valorization of refractory keratinous waste using a new and sustainable bio-catalysis, Chemical Engineering Journal, 397 (2020).
5. A. Thornton, This is how many animals we eat each year, in: World Economic Forum, 2019.
6. B. Mu, F. Hassan, Y. Yang, Controlled assembly of secondary keratin structures for continuous and scalable production of tough fibers from chicken feathers, Green Chemistry, 22 (2020) 1726-1734.
7. A. Ullah, T. Vasanthan, D. Bressler, A.L. Elias, J. Wu, Bioplastics from Feather Quill, Biomacromolecules, (2011).
8. S. Alahyaribeik, A. Ullah, Methods of keratin extraction from poultry feathers and their effects on antioxidant activity of extracted keratin, Int J Biol Macromol, 148 (2020) 449-456.
9. W. Ye, M. Qin, R. Qiu, J. Li, Keratin-based wound dressings: From waste to wealth, International Journal of Biological Macromolecules, 211 (2022) 183-197.
10. A. Ullah, T. Vasanthan, D. Bressler, A.L. Elias, J. Wu, Bioplastics from feather quill, Biomacromolecules, 12 (2011) 3826-3832.
11. X. Han, R. Yang, X. Wan, J. Dou, J. Yuan, B. Chi, J. Shen, Antioxidant and multi-sensitive PNIPAAm/keratin double network gels for self-stripping wound dressing application, Journal of Materials Chemistry B, 9 (2021) 6212-6225.
12. L. Wang, Y. Shang, J. Zhang, J. Yuan, J. Shen, Recent advances in keratin for biomedical applications, Advances in Colloid and Interface Science, (2023) 103012.
13. J.G. Rouse, M.E. Van Dyke, A review of keratin-based biomaterials for biomedical applications, Materials, 3 (2010) 999-1014.
14. J. Wang, S. Hao, T. Luo, Z. Cheng, W. Li, F. Gao, T. Guo, Y. Gong, B. Wang, Feather keratin hydrogel for wound repair: Preparation, healing effect and biocompatibility evaluation, Colloids Surf B Biointerfaces, 149 (2017) 341-350.
15. A. Sarma, Biological importance and pharmaceutical significance of keratin: A review, International Journal of Biological Macromolecules, (2022).
16. P. Kshetri, P.L. Singh, S.B. Chanu, T.S. Singh, C. Rajiv, K. Tamreihao, H.N. Singh, T. Chongtham, A.K. Devi, S.K. Sharma, Biological activity of peptides isolated from feather keratin waste through microbial and enzymatic hydrolysis, Electronic Journal of Biotechnology, 60 (2022) 11-18.
17. C. Yamauchi, W. Okazaki, T. Yoshida, A. Karasawa, Enzymatic degradation of keratin films and keratin fibers prepared from human hair, Biological and Pharmaceutical Bulletin, 31 (2008) 994-997.
18. K. Yamauchi, A. Yamauchi, T. Kusunoki, A. Kohda, Y. Konishi, Preparation of stable aqueous solution of keratins, and physiochemical and biodegradational properties of films, Journal of Biomedical Materials Research: An Official Journal of The Society for Biomaterials and The Japanese Society for Biomaterials, 31 (1996) 439-444.
19. P. Hill, H. Brantley, M. Van Dyke, Some properties of keratin biomaterials: kerateines, Biomaterials,

31 (2010) 585-593.
20. H. Xu, S. Cai, L. Xu, Y. Yang, Water-stable three-dimensional ultrafine fibrous scaffolds from keratin for cartilage tissue engineering, Langmuir, 30 (2014) 8461-8470.
21. K. Callegaro, A. Brandelli, D.J. Daroit, Beyond plucking: feathers bioprocessing into valuable protein hydrolysates, Waste management, 95 (2019) 399-415.
22. A. Shavandi, T.H. Silva, A.A. Bekhit, A.E.A. Bekhit, Keratin: dissolution, extraction and biomedical application, Biomater Sci, 5 (2017) 1699-1735.
23. I. Sinkiewicz, A. Śliwińska, H. Staroszczyk, I. Kołodziejska, Alternative Methods of Preparation of Soluble Keratin from Chicken Feathers, Waste and Biomass Valorization, 8 (2016) 1043-1048.
24. Y. Zhang, R. Yang, W. Zhao, Improving digestibility of feather meal by steam flash explosion, J Agric Food Chem, 62 (2014) 2745-2751.
25. Y. Zhang, W. Zhao, R. Yang, Steam Flash Explosion Assisted Dissolution of Keratin from Feathers, ACS Sustainable Chemistry & Engineering, 3 (2015) 2036-2042.
26. A.M. Woodin, Molecular size, shape and aggregation of soluble feather keratin, Biochemical Journal, 57 (1954) 99.
27. P. Schrooyen, P.J. Dijkstra, R. Oberthür, A.A. Bantjes, J. Feijen, Partially carboxymethylated feather keratins. 1. Properties in aqueous systems, Journal of Agricultural & Food Chemistry, 48 (2000) 4326-4334.
28. A. Shavandi, T.H. Silva, A.A. Bekhit, E.D.A. Bekhit, Keratin: dissolution, extraction and biomedical application, Biomaterials Science, 5 (2017).
29. G. Toennies, R.P. Homiller, The Oxidation of Amino Acids by Hydrogen Peroxide in Formic Acid, Journal of the American Chemical Society, 64 (1942) 3054-3056.
30. Y. Zhang, W. Zhao, R. Yang, Steam Flash Explosion Assisted Dissolution of Keratin from Feathers, Acs Sustainable Chemistry & Engineering, 3 (2015) 150717112248006.
31. I. Sinkiewicz, A. Śliwińska, H. Staroszczyk, I. Kołodziejska, Alternative Methods of Preparation of Soluble Keratin from Chicken Feathers, Waste & Biomass Valorization, 8 (2016) 1-6.
32. Y. Zhang, R. Yang, Z. Wei, Improving Digestibility of Feather Meal by Steam Flash Explosion, Journal of Agricultural and Food Chemistry, 62 (2014) 2745-2751.
33. N.A. Azmi, A. Idris, N.S.M. Yusof, Ultrasonic technology for value added products from feather keratin, Ultrason Sonochem, 47 (2018) 99-107.
34. Y.X. Wang, X.J. Cao, Extracting keratin from chicken feathers by using a hydrophobic ionic liquid, Process Biochemistry, 47 (2012) 896-899.
35. N. Eslahi, F. Dadashian, N.H. Nejad, An investigation on keratin extraction from wool and feather waste by enzymatic hydrolysis, Preparative Biochemistry and Biotechnology, 43 (2013) 624-648.
36. A. Brandelli, Bacterial keratinases: useful enzymes for bioprocessing agroindustrial wastes and beyond, Food and Bioprocess Technology, 1 (2008) 105-116.
37. A. Brandelli, Bacterial Keratinases: Useful Enzymes for Bioprocessing Agroindustrial Wastes and Beyond, Food and Bioprocess Technology, 1 (2007) 105-116.
38. H. Cui, M.J. Webber, S.I. Stupp, Self-assembly of peptide amphiphiles: From molecules to nanostructures to biomaterials, Peptide Science: Original Research on Biomolecules, 94 (2010) 1-18.
39. D. Mandal, A.N. Shirazi, K. Parang, Self-assembly of peptides to nanostructures, Organic & biomolecular chemistry, 12 (2014) 3544-3561.
40. D. Yuan, F. Zhou, P. Shen, Y. Zhang, L. Lin, M. Zhao, Self-assembled soy protein nanoparticles by

partial enzymatic hydrolysis for pH-Driven Encapsulation and Delivery of Hydrophobic Cargo Curcumin, Food Hydrocolloids, 120 (2021).

41. M. Hadidi, C. Tan, E. Assadpour, M.S. Kharazmi, S.M. Jafari, Emerging plant proteins as nanocarriers of bioactive compounds, Journal of Controlled Release, 355 (2023) 327-342.
42. D.J. González-Serrano, M. Hadidi, M. Varcheh, A.Z. Jelyani, A. Moreno, J.M. Lorenzo, Bioactive peptide fractions from collagen hydrolysate of common carp fish byproduct: Antioxidant and functional properties, Antioxidants, 11 (2022) 509.
43. M.T. Bazana, C.F. Codevilla, C.R. de Menezes, Nanoencapsulation of bioactive compounds: Challenges and perspectives, Current opinion in food science, 26 (2019) 47-56.
44. B. Zheng, D.J. McClements, Formulation of more efficacious curcumin delivery systems using colloid science: enhanced solubility, stability, and bioavailability, Molecules, 25 (2020) 2791.
45. B. Tian, J. Liu, Resveratrol: A review of plant sources, synthesis, stability, modification and food application, Journal of the Science of Food and Agriculture, 100 (2020) 1392-1404.
46. S. Sun, N. Liang, H. Yamamoto, Y. Kawashima, F. Cui, P. Yan, pH-sensitive poly(lactide-co-glycolide) nanoparticle composite microcapsules for oral delivery of insulin, Int J Nanomedicine, 10 (2015) 3489-3498.
47. S.A. Siddiqui, M.Q.U. Farooqi, S. Bhowmik, Z. Zahra, M.C. Mahmud, E. Assadpour, R.-Y. Gan, M.S. Kharazmi, S.M. Jafari, Application of micro/nano-fluidics for encapsulation of food bioactive compounds-principles, applications, and challenges, Trends in Food Science & Technology, (2023).
48. H. Nsairat, Z. Lafi, M. Al-Sulaibi, L. Gharaibeh, W. Alshaer, Impact of Nanotechnology on the Oral Delivery of Phyto-bioactive Compounds, Food Chemistry, (2023) 136438.
49. R. Vásquez-Villanueva, M. Plaza, M.C. García, M.L. Marina, Recovery and determination of cholesterol-lowering compounds from Olea europaea seeds employing pressurized liquid extraction and gas chromatography-mass spectrometry, Microchemical Journal, 156 (2020) 104812.
50. S. Afrin, I. Jahan, A. Hasan, K. Deepa, Novel approaches of herbal drug delivery, Journal of Pharmaceutical Research International, 21 (2018) 1-11.
51. S. Bhattacharya, Phytosomes: the new technology for enhancement of bioavailability of botanicals and nutraceuticals, International Journal of Health Research, 2 (2009) 225-232.
52. M. Singh, S. Devi, V.S. Rana, B.B. Mishra, J. Kumar, V. Ahluwalia, Delivery of phytochemicals by liposome cargos: Recent progress, challenges and opportunities, Journal of microencapsulation, 36 (2019) 215-235.
53. P. Dey, Gut microbiota in phytopharmacology: A comprehensive overview of concepts, reciprocal interactions, biotransformations and mode of actions, Pharmacological research, 147 (2019) 104367.
54. S.S. Imam, S. Alshehri, M.M. Ghoneim, A. Zafar, O.A. Alsaidan, N.K. Alruwaili, S.J. Gilani, M. Rizwanullah, Recent advancement in chitosan-based nanoparticles for improved oral bioavailability and bioactivity of phytochemicals: Challenges and perspectives, Polymers, 13 (2021) 4036.
55. F. Aqil, R. Munagala, J. Jeyabalan, M.V. Vadhanam, Bioavailability of phytochemicals and its enhancement by drug delivery systems, Cancer letters, 334 (2013) 133-141.
56. P. Błazińska, A. Sykuła, Application and properties of selected flavanones, Biotechnology and Food Science, 82 (2018) 61-74.
57. M. Gunawan, V. Boonkanokwong, Current applications of solid lipid nanoparticles and nanostructured lipid carriers as vehicles in oral delivery systems for antioxidant nutraceuticals: A

review, Colloids and Surfaces B: Biointerfaces, (2023) 113608.
58. A. Taheri, S.M. Jafari, Gum-based nanocarriers for the protection and delivery of food bioactive compounds, Advances in colloid and interface science, 269 (2019) 277-295.
59. N. Malekjani, S.M. Jafari, Modeling the release of food bioactive ingredients from carriers/nanocarriers by the empirical, semiempirical, and mechanistic models, Comprehensive Reviews in Food Science and Food Safety, 20 (2021) 3-47.
60. N. Malekjani, S.M. Jafari, Intelligent and probabilistic models for evaluating the release of food bioactive ingredients from carriers/nanocarriers, Food and Bioprocess Technology, 15 (2022) 1495-1516.
61. M. Peyrot, R.R. Rubin, D.F. Kruger, L.B. Travis, Correlates of insulin injection omission, Diabetes care, 33 (2010) 240-245.
62. M.S. Chellathurai, C.L. Yong, Z.M. Sofian, S. Sahudin, N.B.M. Hasim, S. Mahmood, Self-assembled chitosan-insulin oral nanoparticles—A critical perspective review, International journal of biological macromolecules, (2023) 125125.
63. M. Martínez-Ballesta, Á. Gil-Izquierdo, C. García-Viguera, R. Domínguez-Perles, Nanoparticles and controlled delivery for bioactive compounds: Outlining challenges for new "smart-foods" for health, Foods, 7 (2018) 72.
64. S. Ashique, A. Upadhyay, N. Kumar, S. Chauhan, N. Mishra, Metabolic syndromes responsible for cervical cancer and advancement of nanocarriers for efficient targeted drug delivery-A review, Advances in Cancer Biology-Metastasis, 4 (2022) 100041.
65. S. Ashique, M. Faiyazuddin, O. Afzal, S. Gowri, A. Hussain, N. Mishra, A. Garg, S. Maqsood, M.S. Akhtar, A.S. Altamimi, Advanced nanoparticles, the hallmark of targeted drug delivery for osteosarcoma-an updated review, Journal of Drug Delivery Science and Technology, (2023) 104753.
66. M.S. Kamal, A.A. Adewunmi, A.S. Sultan, M.F. Al-Hamad, U. Mehmood, Recent advances in nanoparticles enhanced oil recovery: rheology, interfacial tension, oil recovery, and wettability alteration, Journal of Nanomaterials, 2017 (2017).
67. K. Mahajan, N. Thakur, M. Goswami, I. Arora, Polymer based nanoparticles for BCS class II drugs-"A mini Review", Materials Today: Proceedings, (2022).
68. X. Lang, T. Wang, M. Sun, X. Chen, Y. Liu, Advances and applications of chitosan-based nanomaterials as oral delivery carriers: A review, Int J Biol Macromol, 154 (2020) 433-445.
69. T. Zhang, L. Li, S. Chunta, W. Wu, Z. Chen, Y. Lu, Enhanced oral bioavailability from food protein nanoparticles: A mini review, Journal of Controlled Release, 354 (2023) 146-154.
70. H.M. Yildiz, C.A. McKelvey, P.J. Marsac, R.L. Carrier, Size selectivity of intestinal mucus to diffusing particulates is dependent on surface chemistry and exposure to lipids, Journal of drug targeting, 23 (2015) 768-774.
71. Q. Zhu, Z. Chen, P.K. Paul, Y. Lu, W. Wu, J. Qi, Oral delivery of proteins and peptides: Challenges, status quo and future perspectives, Acta Pharm Sin B, 11 (2021) 2416-2448.
72. S.R. Pamshong, D. Bhatane, S. Sarnaik, A. Alexander, Mesoporous silica nanoparticles: An emerging approach in overcoming the challenges with oral delivery of PPs, Colloids and Surfaces B: Biointerfaces, (2023) 113613.
73. S. Afolalu, O. Ikumapayi, T. Ogedengbe, J. Kayode, A. Ogundipe, T. Jen, A review on emerging trends in the scientific application of nano-coatings and nanoparticle synthesis, Materials Today: Proceedings, (2023).

74. X. Wang, H. Sun, T. Mu, Materials and structure of polysaccharide-based delivery carriers for oral insulin: A review, Carbohydrate Polymers, (2023) 121364.
75. P. Jana, M. Shyam, S. Singh, V. Jayaprakash, A. Dev, Biodegradable polymers in drug delivery and oral vaccination, European Polymer Journal, 142 (2021).
76. M. Rahman, M.R. Hasan, Synthetic Biopolymers, in: M.A. Jafar Mazumder, H. Sheardown, A. Al-Ahmed (Eds.) Functional Biopolymers, Springer International Publishing, Cham, 2019, pp. 1-43.
77. H. Idrees, S.Z.J. Zaidi, A. Sabir, R.U. Khan, X. Zhang, S.-u. Hassan, A review of biodegradable natural polymer-based nanoparticles for drug delivery applications, Nanomaterials, 10 (2020) 1970.
78. S.S. Shetty, P. Halagali, A.P. Johnson, K.A. Spandana, H. Gangadharappa, Oral insulin delivery: Barriers, strategies, and formulation approaches: A comprehensive review, International Journal of Biological Macromolecules, (2023) 125114.
79. N.H. AbdelAllah, Y. Gaber, M.E. Rashed, A.F. Azmy, H.A. Abou-Taleb, S. AbdelGhani, Alginate-coated chitosan nanoparticles act as effective adjuvant for hepatitis A vaccine in mice, Int J Biol Macromol, 152 (2020) 904-912.
80. M. Yanat, K. Schroën, Advances in chitin-based nanoparticle use in biodegradable polymers: A review, Carbohydrate Polymers, (2023) 120789.
81. C. Hua, W. Yu, M. Yang, Q. Cai, T. Gao, S. Zhang, H. Xu, H. He, N. Peng, Y. Liu, Casein-pectin nanocomplexes as a potential oral delivery system for improving stability and bioactivity of curcumin, Colloid and Polymer Science, 299 (2021) 1557-1566.
82. T.G. Shutava, S.S. Balkundi, P. Vangala, J.J. Steffan, R.L. Bigelow, J.A. Cardelli, D.P. O'Neal, Y.M. Lvov, Layer-by-layer-coated gelatin nanoparticles as a vehicle for delivery of natural polyphenols, ACS nano, 3 (2009) 1877-1885.
83. A. Arun, P. Malrautu, A. Laha, H. Luo, S. Ramakrishna, Collagen nanoparticles in drug delivery systems and tissue engineering, Applied Sciences, 11 (2021) 11369.
84. C. Liu, B. Xu, D.J. McClements, X. Xu, S. Cui, L. Gao, L. Zhou, L. Xiong, Q. Sun, L. Dai, Properties of curcumin-loaded zein-tea saponin nanoparticles prepared by antisolvent co-precipitation and precipitation, Food Chemistry, 391 (2022) 133224.
85. P. Xu, Y. Qian, R. Wang, Z. Chen, T. Wang, Entrapping curcumin in the hydrophobic reservoir of rice proteins toward stable antioxidant nanoparticles, Food Chem, 387 (2022) 132906.
86. S. Zhou, L. Han, K. Lu, B. Qi, X. Du, G. Liu, Y. Tang, S. Zhang, Y. Li, Whey protein isolate-phytosterols nanoparticles: Preparation, characterization, and stabilized food-grade pickering emulsions, Food Chem, 384 (2022) 132486.
87. Z.x. Yuan, S. Deng, L. Chen, Y. Hu, J. Gu, L. He, pH-driven entrapment of enrofloxacin in casein-based nanoparticles for the enhancement of oral bioavailability, Food Science & Nutrition, 9 (2021) 4057-4067.
88. A. Jithan, K. Madhavi, M. Madhavi, K. Prabhakar, Preparation and characterization of albumin nanoparticles encapsulating curcumin intended for the treatment of breast cancer, International journal of pharmaceutical investigation, 1 (2011) 119.
89. P. Liu, Q. Wu, Y. Li, P. Li, J. Yuan, X. Meng, Y. Xiao, DOX-Conjugated keratin nanoparticles for pH-Sensitive drug delivery, Colloids Surf B Biointerfaces, 181 (2019) 1012-1018.
90. V. Pande, Studies on the characteristics of zaltoprofen loaded gelatin nanoparticles by nanoprecipitation, Inventi Rapid NDDS, 3 (2015) 1-7.
91. A. Barfar, H. Alizadeh, S. Masoomzadeh, Y. Javadzadeh, Oral Insulin Delivery: A Review On

Recent Advancements and Novel Strategies, Current Drug Delivery, (2024).
92. A.O. Elzoghby, W. El-Fotoh, N.A. Elgindy, Casein-based formulations as promising controlled release drug delivery systems, Journal of Controlled Release, 153 (2011) 206-216.
93. A. Raza, U. Hayat, M. Bilal, H. Iqbal, J.Y. Wang, Zein-based micro- and nano-constructs and biologically therapeutic cues with multi-functionalities for oral drug delivery systems, Journal of Drug Delivery Science and Technology, 58 (2020) 101818.
94. L. Dai, R. Li, Y. Wei, C. Sun, L. Mao, Y. Gao, Fabrication of zein and rhamnolipid complex nanoparticles to enhance the stability and invitro release of curcumin, Food Hydrocolloids, (2018) 617-628.
95. P.R. Sarika, N.R. James, Polyelectrolyte complex nanoparticles from cationised gelatin and sodium alginate for curcumin delivery, Carbohydrate Polymers, 148 (2016) 354-361.
96. H. Xu, Z. Shi, N. Reddy, Y. Yang, Intrinsically water-stable keratin nanoparticles and their in vivo biodistribution for targeted delivery, J Agric Food Chem, 62 (2014) 9145-9150.
97. C. Milián-Guimerá, R. McCabe, L.H.E. Thamdrup, M. Ghavami, A. Boisen, Smart pills and drug delivery devices enabling next generation oral dosage forms, Journal of Controlled Release, 364 (2023) 227-245.
98. T. Zhang, J. Xu, J. Chen, Z. Wang, J. Zhong, Protein nanoparticles for Pickering emulsions: A comprehensive review on their shapes, preparation methods, and modification methods, Trends in Food Science & Technology, 113 (2021).
99. M.A. Mumuni, F.C. Kenechukwu, O.C. Ernest, A.M. Oluseun, B. Abdulmumin, D.C. Youngson, O.C. Kenneth, A.A. Anthony, Surface-modified mucoadhesive microparticles as a controlled release system for oral delivery of insulin, Heliyon, 5 (2019) e02366.
100. C. Li, L. Yuan, X. Zhang, A. Zhang, Y. Pan, Y. Wang, W. Qu, H. Hao, S.A. Algharib, D. Chen, Core-shell nanosystems designed for effective oral delivery of polypeptide drugs, Journal of Controlled Release, 352 (2022) 540-555.
101. B. Homayun, X. Lin, H.-J. Choi, Challenges and recent progress in oral drug delivery systems for biopharmaceuticals, Pharmaceutics, 11 (2019) 129.
102. M. Schenk, C. Mueller, The mucosal immune system at the gastrointestinal barrier, Best Practice & Research Clinical Gastroenterology, 22 (2008) 391-409.
103. P. Mukhopadhyay, S. Maity, S. Mandal, A.S. Chakraborti, A.K. Prajapati, P.P. Kundu, Preparation, characterization and in vivo evaluation of pH sensitive, safe quercetin-succinylated chitosan-alginate core-shell-corona nanoparticle for diabetes treatment, Carbohydr Polym, 182 (2018) 42-51.
104. R.M. Gilhotra, M. Ikram, S. Srivastava, N. Gilhotra, A clinical perspective on mucoadhesive buccal drug delivery systems, Journal of biomedical research, 28 (2014) 81.
105. W.T. Aung, V. Boonkanokwong, Preparation, optimization using a mixture design, and characterization of a novel astaxanthin-loaded rice bran oil self-microemulsifying delivery system formulation, Journal of Dispersion Science and Technology, 44 (2023) 1336-1349.
106. M. Huerta-Madronal, J. Caro-Leon, E. Espinosa-Cano, M.R. Aguilar, B. Vázquez-Lasa, Chitosan–Rosmarinic acid conjugates with antioxidant, anti-inflammatory and photoprotective properties, Carbohydrate Polymers, 273 (2021) 118619.
107. P. Nalawade, A. Gajjar, Optimization of astaxanthin microencapsulation in hydrophilic carriers using response surface methodology, Archives of Pharmacal Research, (2015) 1-17.
108. S. Castellani, A. Trapani, A. Spagnoletta, L. Di Toma, T. Magrone, S. Di Gioia, D. Mandracchia, G.

Trapani, E. Jirillo, M. Conese, Nanoparticle delivery of grape seed-derived proanthocyanidins to airway epithelial cells dampens oxidative stress and inflammation, Journal of translational medicine, 16 (2018) 1-15.

109. T. Vila, A.M. Rizk, A.S. Sultan, M.A. Jabra-Rizk, The power of saliva: Antimicrobial and beyond, PLoS pathogens, 15 (2019) e1008058.
110. O. Baker, M. Edgerton, J. Kramer, S. Ruhl, Saliva-microbe interactions and salivary gland dysfunction, Advances in dental research, 26 (2014) 7-14.
111. A. Sood, R. Panchagnula, Peroral route: an opportunity for protein and peptide drug delivery, Chemical Reviews, 101 (2001) 3275-3304.
112. J. Sanchón, S. Fernández-Tomé, B. Miralles, B. Hernández-Ledesma, D. Tomé, C. Gaudichon, I. Recio, Protein degradation and peptide release from milk proteins in human jejunum. Comparison with in vitro gastrointestinal simulation, Food Chemistry, 239 (2018) 486-494.
113. G. Patel, A. Misra, Oral delivery of proteins and peptides: concepts and applications, Challenges in delivery of therapeutic genomics and proteomics, (2011) 481-529.
114. M. Abdulkarim, N. Agulló, B. Cattoz, P. Griffiths, A. Bernkop-Schnürch, S.G. Borros, M. Gumbleton, Nanoparticle diffusion within intestinal mucus: Three-dimensional response analysis dissecting the impact of particle surface charge, size and heterogeneity across polyelectrolyte, pegylated and viral particles, European Journal of Pharmaceutics and Biopharmaceutics, 97 (2015) 230-238.
115. M.E. Johansson, H. Sjövall, G.C. Hansson, The gastrointestinal mucus system in health and disease, Nature reviews Gastroenterology & hepatology, 10 (2013) 352-361.
116. C. Zihni, C. Mills, K. Matter, M.S. Balda, Tight junctions: from simple barriers to multifunctional molecular gates, Nature reviews Molecular cell biology, 17 (2016) 564-580.


2

CHAPTER 2

Effect of ultrasound on keratin valorization from chicken feather waste: process optimization and keratin characterization

Published as: Xiaojie Qin, Chuan Yang, Yujie Guo, Jiqian Liu, Johannes H. Bitter, Elinor L. Scott, Chunhui Zhang (2023). Effect of ultrasound on keratin valorization from chicken feather waste: Process optimization and keratin characterization. *Ultrasonics Sonochemistry*, 93, 106297.

Abstract

Chicken feather (CF) has been deemed as one of the main poultry byproducts with a large amount produced globally. However, the robust chemical nature of chicken feathers has been limiting in its wide-scale utilization and valorization. The study proposed a strategy of keratin extraction from chicken feathers combining ultrasound and Cysteine (Cys)-reduction. First, the ultrasonic effect on feather deconstruction and keratin properties was investigated based on Cys-reduction. The results show that the feather dissolution was significantly improved by increasing both ultrasonic time and power, and the former had a greater impact on keratin yield. However, the treating time > 4 h led to a decrease in keratin yield, producing a large amount of small soluble peptides. Meanwhile, prolonging time led to decreased thermal stability and amino acid loss (e.g. Ser, Pro and Gly) of keratin. Conversely, solely by increasing ultrasonic power caused insignificant damage to chemical structure and thermal stability but enhanced the keratin solubility. Compared to the control, the keratin extracted under optimal conditions (130 W, 2.7 h and 15% of Cys) exhibited better solubility without damage in chemical structure, thermal stability and amino acids composition. The findings illustrate that ultrasound physically improved CF deconstruction and keratin solubility without nature damage. The study provides an alternative for keratin extraction involving no toxic reagent, holding promise in the utilization and valorization of feather waste.

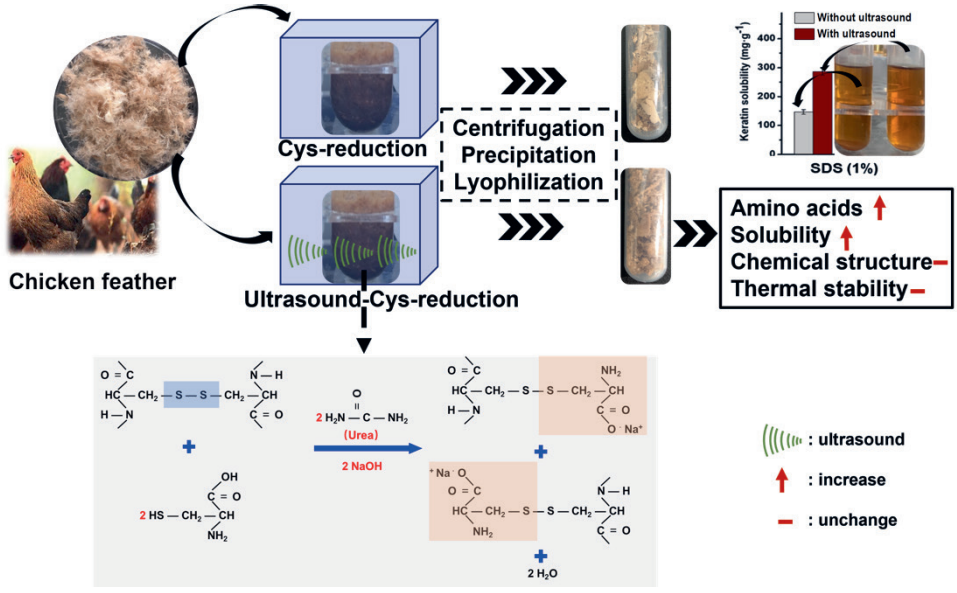

2.1 Introduction

With a great demand for chicken meat and eggs, there are about 50 billion chickens raised globally every year, with a large amount of feather waste produced [1]. Feather waste is a renewable resource containing more than 90% of keratin [2], rich in Cys, Gly, Pro and Ser [3]. Feather keratin has potential to be a highly applicable biopolymer with a molecular weight of around 10500 Da resulting in good biocompatibility, absorbability, biodegradability and non-toxicity [4, 5]. Some feather waste has been processed into animal feeds, fertilizers, as well as biomaterials, including hydrogels, nanoparticles, sponges, biofilms and biomedical materials [6-11]. For example, Wang et al. have extracted chicken feather into keratin nanoparticles and applied them to hemostasis [12]. Despite extensive research devoted to keratin regeneration, the highly stable and resistant nature of feather keratin caused by abundant disulfide cross-link in high content of cystine (~ 7 mol %), hydrogen bonds and hydrophobic interactions has limited its utilization on a large scale [4, 13, 14]. The majority of feather waste end up in landfills leading to both environmental problems and resource waste. Therefore, it is desirable and important to develop an efficient and more eco-friendly way for reusing feather waste into available materials.

There are several ways for keratin extraction from keratin-rich materials, including oxidation, alkaline hydrolysis, reduction, microwave irradiation, steam explosion, sulfitolysis, ionic liquids and enzymatic hydrolysis [15]. Although chemical hydrolysis possesses high efficiency in solubilizing keratin, most of the current methods can produce chemical residues (e.g. sodium dodecyl sulfate, SDS), which limits the application in food and pharmaceutical areas, even with toxic chemicals (e.g. mercaptoethanol, MEC), resulting in environmental problems. Additionally, the methods of oxidation, alkaline and sufitolysis have been reported to own the risk of damaging protein backbone and amino acid residue (e.g. Trp and Met) [16-18], while thermal hydrolysis may result in severe degradation and chemical modification though with less requirement of reagents [19]. The methods with microwave, ionic liquids (IL) and enzymes are more eco-friendly compared to other methods, however, exhibit drawbacks as well, such as time-consuming, low yield and high cost [20, 21]. For instance, the feather-degradation rate only reached about 47.56% via keratinase enzymatic hydrolysis after 1220 min [22], while there was feather keratin with a maximum yield of 21.5% was extracted through the ionic liquid of 1-hydroxyethyl-3methylimidazolium bis (trifluoromethanesulfonyl) amide

([HOEMIm][NTf2]) after 4 h [23]. Hence, it is a pressing issue to find a more suitable method to regenerate feather keratin with minimal usage of chemicals and with high efficiency at a low cost.

Reduction hydrolysis under alkaline conditions is the most common way for keratin extraction through which the product quality can be controlled via different solvents, reaction time and other parameters [24, 25]. The use of reducing reagents like thiols has lots of disadvantages, such as being expensive and harmful to both humans and the environment. Xu. et al. have proposed a reduction way using Cys as reducing reagent and urea as protein denaturant instead of MEC for keratin extraction, with which the disulfide bonds were broken down controllably [26]. The amino acid Cys exhibits strong reducibility owing to the thiol group, and more importantly, it can be commercially produced via fermentation, thus being an environmentally friendly agent [27]. Also, urea could be recycled from extraction solutions showing sustainability [28].

Besides, ultrasound has been widely applied in various areas, such as food, biomedicine and cosmetics. On the one hand, the mechanical vibration effect can promote the contact between material and medium, thus facilitating the reaction process. On the other hand, destruction often occurs with acoustic cavitation through a sonication medium. Generally, the acoustic streaming of mechanical vibration effect can enhance mass transfer and finally result in productivities in industrials. For example, it has been reported that the yield of collagen Ⅱ (3.37 g) from chicken sternal cartiage was greatly increased by treating with ultrasound for 36 min compared with non-ultrasound group (1.73 g), with an improvement of functional properties, such as foaming and emulsifying properties [29]. In the study of regenerating keratin from feather using (1-butyl-3-methylimidazolium chloride, [BMIM]Cl) assisted with ultrasound, ultrasonic irradiation significantly improved keratin dissolution compared with the conventional method and shortened process time from 2 h to less than 20 min [21]. Taken together, it is a promising way to combine ultrasound and Cys reduction for keratin extraction.

The main purpose of this study was to develop an efficient and sustainable process combining Cys-reduction and ultrasound for feather waste valorization. Firstly, the effect of ultrasonic power and time on the yield and physical properties (e.g. feather dissolubility, keratin yield, chemical structure and crystallinity) of regenerated keratin was investigated based on the Cys-reduction method. Then, the process

optimization of Cys-reduction assisted with ultrasound was conducted using Box-Behnken Design. Finally, feather keratin was prepared under optimal conditions, the physicochemical characterization, including chemical structure, crystallinity, thermal stability, amino acids composition and keratin solubility, of which was also assayed taking keratin untreated with ultrasound as control. The study systematically explored the potential application of ultrasound in feather deconstruction and might be meaningful in providing an alternative strategy for utilizing feather waste.

2.2 Materials and methods

2.2.1 Materials and chemicals

Chicken feather was supplied by the Institute of Animal Sciences of Chinese Academy of Agricultural Sciences (CAAS). Feathers were cleaned with detergent and distilled water and then were dried at 50 °C in an oven for 48 h. Subsequently, the dried feathers were milled into a cotton shape for keratin extraction. Reagents including urea, Cys, etc. were of analytical grade and purchased from Sinopharm Chemical Reagent Co., Ltd (China). HPLC grade acetonitrile (ACN) was supplied by Thermo Fisher Scientific (Waltham, USA). The deionized water was obtained via Milli-Q 50 system (Millipore Corp., Milford, MA, USA).

2.2.2 Keratin extraction using Cys reduction assisted with ultrasound

2 g of milled feather were mixed with 20 mL of a solution containing 8 M urea and 15% Cys, which has been adjusted to pH 10.5. The mixture was treated with ultrasound at various power (100-600 W) for varying times (2-10 h) at 70 °C using an ultrasonic instrument at the frequency of 40 kHz (YQ1001C, Yijing Ultrasonic Instrument Co., Ltd, Shanghai, China). Then, the mixture was centrifuged at 8000 rpm for 20 min thus obtaining supernatant. The keratin was further precipitated by adjusting the supernatant to pH 4 with hydrochloric acid and then was washed three times with distilled water under centrifugation of 8000 rpm for 20 min. Finally, the regenerated keratin was lyophilized and weighed. The effect of both ultrasonic power and time on keratin yield was analyzed by linear regression modeling. The yield (Y) of regenerated keratin was calculated with equation (1):

$$Y(\%) = \frac{m_0}{m_1} \times 100 \qquad (1)$$

Where m_0 represents the weight of dried keratin, and m_1 represents the weight of

introduced chicken feathers on a dry base.

2.2.3 The morphology of chicken feather

The uncrushed feathers were treated by ultrasound-assisted Cys-reduction under conditions as **section 2.2.2** described for various times (2 to 10 h) with ultrasonic power of 200 W. The treated feathers were washed three times with distilled water, and then were stored in 4% paraformaldehyde at 4 °C. The feathers were observed using an inverted microscope (Zeiss Axio Vert.A1, Zeiss, Germany) at 2-3 cm from the thick end with a magnification of ×100.

2.2.4 Characterization of regenerated keratin

The keratin extracted under conditions as **section 2.2.2** described (200 W for 2 to 10 h and 100 to 600 W for 4 h) was characterized with raw chicken feather as control. For chemical structure, the samples were determined referring to previous study [30]. Keratin samples were ground with potassium bromide (KBr) under dried air, and then the mixture was pressed into a 1 mm pellet and scanned in a frequency from 4000 to 400 cm^{-1} using Fourier transform infrared spectroscopy (FTIR) spectrometer (Model Nicolet Nexus 470, Thermo Fisher Scientific, Waltham, MA, USA).

For thermogravimetric analysis (TGA) and derivative thermogravimetric analysis (DTG), the samples were analyzed via Thermogravimetric Analyzer (Pyris Diamond TG/DTA, PerkinElmer, USA) in a flowing nitrogen atmosphere. The samples were loaded in aluminum pans and equilibrated, and then were heated from 30 °C to 500 °C with a heating scan rate of 10 °C·min^{-1}.

For crystallinity analysis, X-ray diffraction (XRD) study was performed using a Panalytical Empyrean powder diffractometer (Ultima IV, Rigaku, Japan) at 25 °C. The CuKα1 radiation (λ = 1.54 Å) was produced at 40 kV and 40 mA. Diffraction intensities were recorded with 2θ ranging from 5° to 80° with a step size of 0.02° 2θ at a scan speed of 5°/min. The crystallinity index (CI) was calculated with equation (2) [31]:

$$CI\ (\%)=\frac{A_{crystal}}{A_{total}}\times 100 \qquad (2)$$

Where A_{total} is the total area under the diffraction curve from 5 to 60 °, and A_{cystal} is the area below the crystal diffraction peaks.

2.2.5 Content of soluble protein and peptides

2 g of milled feather mixed with 20 mL of the buffer as **section 2.2.2** mentioned were treated with ultrasound at 200 W for different times (2, 4, 6, 8 and 10 h) and with varying ultrasound (100 to 600W) at 70 °C. The supernatant was obtained by centrifuging the mixture at 8000 rpm for 20 min and then was diluted 100 times using distilled water for assaying soluble protein and peptides according to the method as Lowry et al. mentioned [32], using bovine serum albumin as a standard.

For soluble protein determining, briefly, 20 μL of the diluted supernatant and 200 μL of reagents were added into 96-well plates, and the mixture was then stood for 30 min at 37 °C. After that, the absorbance was detected via a microplate reader (Synergy H1, BioTek, USA) at 660 nm.

In order to determine soluble peptides, 0.25 mL of diluted supernatant was fully mixed with an equal volume of trichloroacetic acid (TCA) solution (10%) and stood for 60 min at room temperature. After that, the final supernatant was prepared by centrifuging the mixture at 10000 ×g for 20 min. Subsequently, the procedure for peptides detection was the same as that of protein measurement above.

2.2.6 Distribution of molecular weight of peptides

The molecular weight (M_w) of soluble peptides in extraction supernatant obtained as **section 2.2.5** described was assayed using Agilent liquid chromatograph 1200 with a UV detector (Agilent, CA, USA) [33]. The TSK gel filtration column (G2000 SWXL 300 mm × 7.8 mm, Tosoh Co., Tokyo, Japan) was adopted, and the mobile phase was composed of water/acetonitrile/trifluoroacetic acid (55/45/0.1, v/v/v). The flow rate of the mobile phase was 0.5 mL /min with column thermo-stated at 40 °C. The injection volume of the sample was 10 μL, and the absorbance was monitored at 220 nm. The standards used for M_W calibration curve included Gly-Sar (146.15 Da), tetrapeptide Gly-Gly-Tyr-Arg (451 Da), bacitracin (1423 Da), aprotinin (6511 Da), cytochrome C (12355 Da) (Sigma Aldrich, St. Louis, MO, USA). The data were analyzed via gel permeation chromatography software.

2.2.7 Amino acids analysis

The amino acids composition in regenerated keratin were analyzed using peroxidation and acid hydrolysis method [34]. Briefly, the accurately weighted samples (~10 mg) were slowly dispersed in 2 mL ice-cold performic acid solution

(hydrogen peroxide: formic acid = 1:9) which has been freshly prepared. The mixture was incubated in fridge for 16 h, and then 0.3 mL ice-cold hydrobromic acid was added and stood for another 30 min on ice. The mixture was dried with nitrogen blowing device at 50 °C, after which 10 mL of HCl (6 M) containing 0.1% phenol were added for 24-h hydrolysis at 110 °C. The hydrolysate was filtered and transferred into a volumetric flask (50 mL). After that, 1 mL of filtered hydrolysate was dried via nitrogen blowing device at 37 °C and then redissolved with 1 mL of HCl (0.02 M). The sample solution was further filtrated through 0.22 μm membrane, and pre-derivatized with OPA before HPLC (Thermo Fisher Ultrimate 3000, USA) analysis. The method can determine most amino acids except for Tyr and Trp. Especially, Cys could be quantified via oxidizing into cysteic acid.

2.2.8 Optimization of keratin extraction via Box-Behnken experiment

For the single-factor experiment, urea (8 M), pH (10.5), and temperature (70 °C) were constant in the three groups, while the "Ultrasonic time," "Ultrasonic power," "Solid-liquid ratio," and "Cys fraction" were separately served as the variation in three control groups, with the other three factors serving as a fixed factor. Briefly, the milled chicken feather was firstly fully mixed with buffer containing 8 M urea and various fractions of Cys (5, 10, 15, 20 and 25%) at a solid-liquid ratio of 1: 10 to 1:30, the pH of which was adjusted to 10.5 using NaOH (6 M). Then, the mixtures were treated with ultrasound at varying powers (100, 200, 300, 400, 500 and 600 W) for a certain time (2, 4, 6, 8 and 10 h). After that, the mixtures were centrifuged at 8000 rpm for 20 min to precipitate undissolved residues. The supernatant was adjusted to pH 4 to precipitate keratin. After washing three times with distilled water, the regenerated keratin was freeze-dried and weighed to calculate the yield using equation (1).

The Box-Behnken experiment was designed based on the effect of three independent variables of "Ultrasonic time," "Ultrasonic power," and "Cys fraction" on keratin yield, and three levels of each factor were shown in **Table S2.1**. The "Solid-liquid ratio" was kept at 1:10 because a lower ratio led to less keratin due to the buoyancy effect. The results were analyzed by multiple regression fitting analysis using Design Expert 8.0 software. Finally, the verification test was conducted under optimized conditions (130 W, 2.7 h, 15% Cys). Analysis of FTIR, TGA, XRD and amino acids composition of keratin from verification test was conducted, taking the keratin extracted without ultrasonic treatment (2.7 h, 15% Cys) as control. The methods were

the same as those in **sections 2.2.4 and 2.2.7**.

2.2.9 Keratin solubility in different solvents

The solubility of regenerated keratin assisted with or without ultrasound in different solvents was investigated, referring to a previous study with some modifications [35]. In this study, four kinds of solvents were prepared: SDS (1%), NaOH (0.1 M), Na_3PO_4 (0.01 M, pH 7.5) and Na_3PO_4 (0.01 M, pH 7.5, 2% urea). Briefly, 100 mg of samples were dispersed in 5 mL of various solvents and incubated at room temperature for 60 min. Then, the mixtures were centrifuged at 3000 ×g for 15 min. The supernatant was diluted 10 times to detect the soluble protein content using the method as **section 2.2.5** described.

2.2.10 Statistical analysis

Statistical analysis was conducted via SPSS 17.0 software. The figures were made by Origin8.5 software. Differences among mean values were established using the Duncan multiple range test at $P < 0.05$. All analyses were carried out in triplicate samples, and the results are presented as the mean values ± standard deviation (SD).

2.3 Results and discussion

2.3.1 Effect of ultrasound on feather deconstruction

2.3.1.1 Feather dissolubility and keratin yield treated with ultrasound

This part was conducted to explore the effect of varying ultrasonic power (100-600 W) and time (2-10 h) on both feather dissolubility and keratin yield based on the Cys reduction method. Chicken feather was firstly swelled by urea, in light of which keratin dissolution was processed by disulfide bonds breakage with the thiol group consisting in Cys. **Figure 2.1A** showed that feathers were dissolved sharply when the ultrasonic time increased from 2 h to 4 h at low ultrasonic power (e.g. 100 and 200 W), and then were gradually promoted with the increase of both ultrasonic power and time. The feather dissolubility reached about 79.1% and 80.7% at 200 W-10 h and 600 W-10 h, respectively, exhibiting no significant difference ($P > 0.05$). There was about 20% of feather undissolved, possibly resulting from the floating on buffer surface.

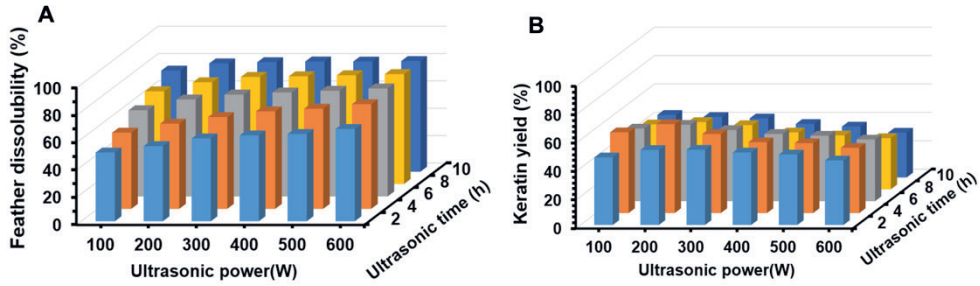

Figure 2.1. (A) Feather dissolubility (%), and (B) yield (%) from chicken feather treated with various ultrasonic power for different time. The ultrasonic power changed from 100 to 600 W, and the time was from 2 to 10 h. The results are presented as the mean values, n = 3. The linear regression model of keratin yield was $Y = 63.736 - 0.02X_{power} - 1.67X_{time}$ ($R^2 = 0.751$, $P < 0.001$).

Figure 2.1B showed that keratin yield increased at first and then fell with time and power increasing, with the maximum value of 62.65% under the condition of 200 W-4 h. Ultrasound might facilitate the production of free amino acids and peptides with small Mw with the combined effect of mechanical vibration and acoustic cavitation, and stronger ultrasound might result in over-degradation of keratin [21, 36]. Despite a relatively lower keratin yield compared to previous methods where MEC, thiourea and thioglycolic acid were adopted as reducing agents (with keratin yield of 67-91%) [15], the present study avoided the use and residue of toxic chemicals while taking a shorter time. The potential of the Cys reduction method assisted with ultrasound in solubilizing feather waste is still worthy of exploring. Through linear regression analysis, ultrasonic time was found to be more influential on keratin yield, while ultrasonic power had less influence (**Figure 2.1B**). The feather morphology, soluble protein composition and physicochemical properties of extracted keratin would be further determined to investigate the effect of ultrasound and Cys reduction on chicken feather.

2.3.1.2 Morphological changes of feather treated by ultrasound

The effect of various ultrasonic power and time on feather morphology was visually assayed by treating unmilling feather with ultrasound for a certain time. **Figure 2.2** showed that the barb ridges of feather were obviously dissolved with time and power increasing. The feather branches were totally solubilized when treated at 200 W for 6 h and 300 W for 4 h, indicating a positive effect of ultrasound. The feather shaft was significantly broken with a rough surface (e.g. 400 W-4 h), possibly caused by the combined action of ultrasound and reagents. The shaft was thinner with a

hollow part that clearly emerged when the process lasted for 8 h at 200 W and increased to 500 W for 4 h. Unlike the transverse cracks and cavities on the surface given by steam explosion treatment [19], the feather fibers were longitudinally dissolved layer by layer with ultrasonic treatment. In general, ultrasound could positively improve feather dissolution.

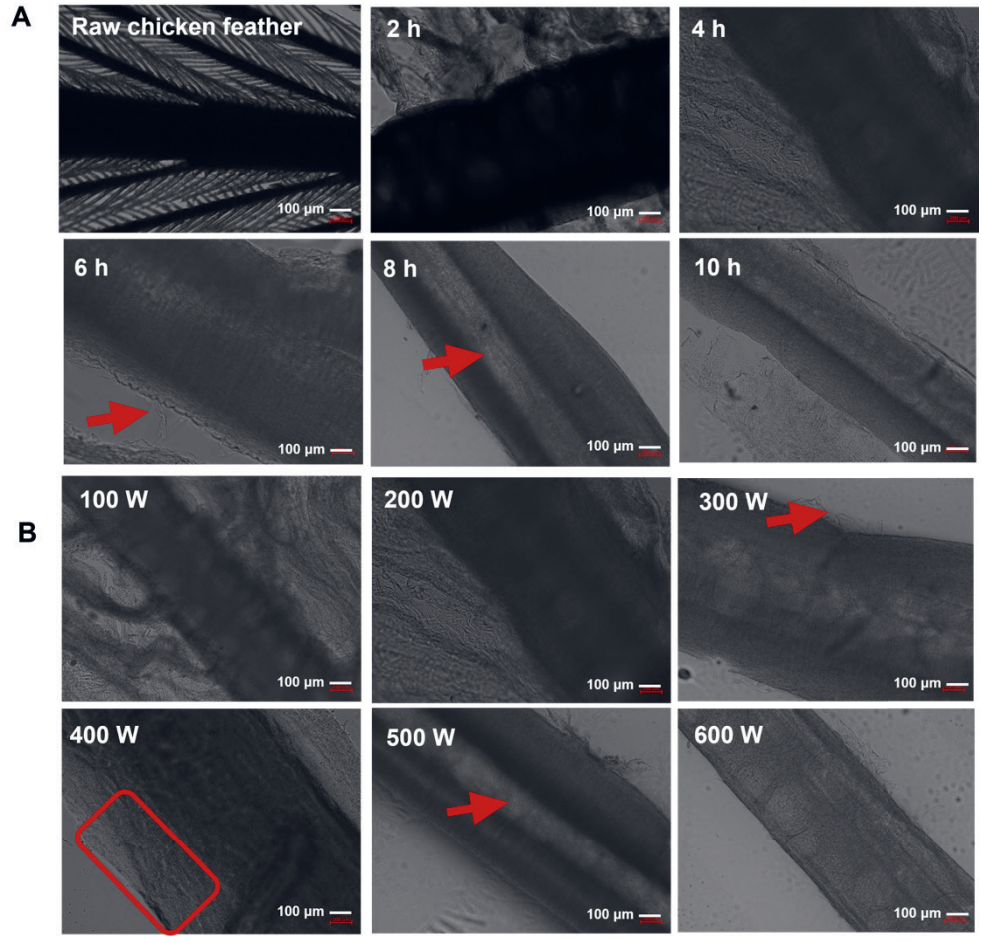

Figure 2.2. (A) The apparent structure of chicken feather treated without or with ultrasound at 200 W for various time (from 2 to 10 h), and (B) treated with varying ultrasonic power (from 100 to 600 W) for 4 h. The feathers were photographed at 2-3 cm from the thick end with a magnification of ×100.

2.3.1.3 Analysis of soluble peptides in feather hydrolysate

The effect of different ultrasonic times and power on feather hydrolysis was evaluated by assaying soluble peptides (**Figure 2.3A&B**). The result showed that ultrasonic time significantly improved peptide content growing from about 29

mg·mL^{-1} at 2 h to 389 mg·mL^{-1} at 10 h, while ultrasonic power made less effect with peptide content growing from about 207 mg·mL^{-1} at 100 W to 283 mg·mL^{-1} at 600 W for 4 h. **Figure 2.3A** indicated that there was about 47% of them with Mw less than 3 kDa at 2 h while the peptides < 0.5 kDa was about 8.7%. As processing time was prolonged to 10 h, around 65% of peptides < 3 kDa were produced, among which about 20% were smaller than 0.5 kDa. Similarly, power rising also resulted in the proportion increase of smaller peptides, which contributed to feather dissolution (**Figure 2.3B**). The result illustrated that this process effectively facilitated the breakage of feather keratin. Despite the beneficial effect of ultrasound on feather deconstruction, the quality of regenerated keratin should also be concerned. The influence of various ultrasonic power and time on keratin properties solubility and amino acids composition will be further discussed.

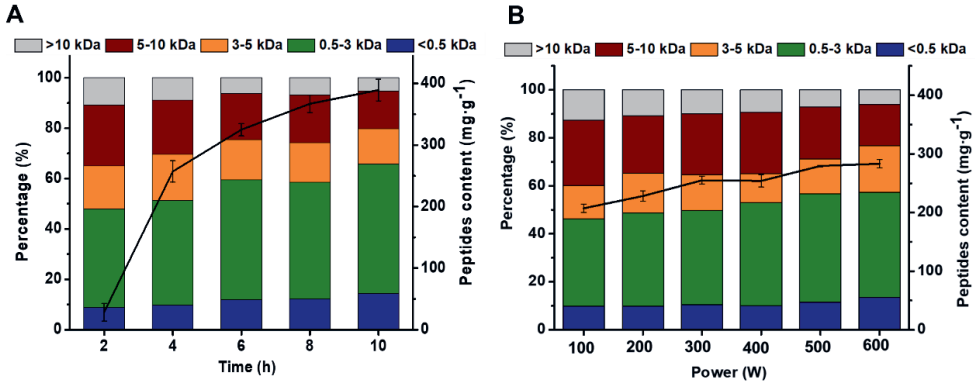

Figure 2.3. (A) Effect of various ultrasonic time (2-10 h, 200 W) and (B) ultrasonic power (100-600 W, 4 h) on the content and Mw distribution of soluble peptides in extracting solution. The results are presented as the mean values ± SD, n = 3.

2.3.2 Characterization of regenerated keratin treated by ultrasound

2.3.2.1 Chemical structure analysis

FTIR measurement was used to assess the effect of ultrasound on structural changes in keratin. The FTIR spectrum indicated that various regenerated keratin exhibited similar bands compared to raw chicken feathers (**Figure 2.4A&B**). The absorption bands at about 3292 cm^{-1} were observed known as the Amide A vibrations regarding the N–H stretching [37], and the peak at around 2932 cm^{-1} was related to the asymmetrical stretch of CH_2, CH_3 and C–H [38, 39]. The strong bands that appeared at 1657 cm^{-1} mainly resulted from the C=O stretching of Amide I in α-helix structures,

while the peak at 1535 cm^{-1} assigned to the C–N stretching of Amide II coupled with N–H bending vibration [29]. At about 1396 cm^{-1} and 1234 cm^{-1}, the bands were mainly related to C–N and C–C stretching, N–H plane bending and C=O bending vibration of Amide III [21]. As result presented, the increase of ultrasonic power and treating time would not distinctly change the characteristic chemical groups or produce new functional groups in regenerated keratin.

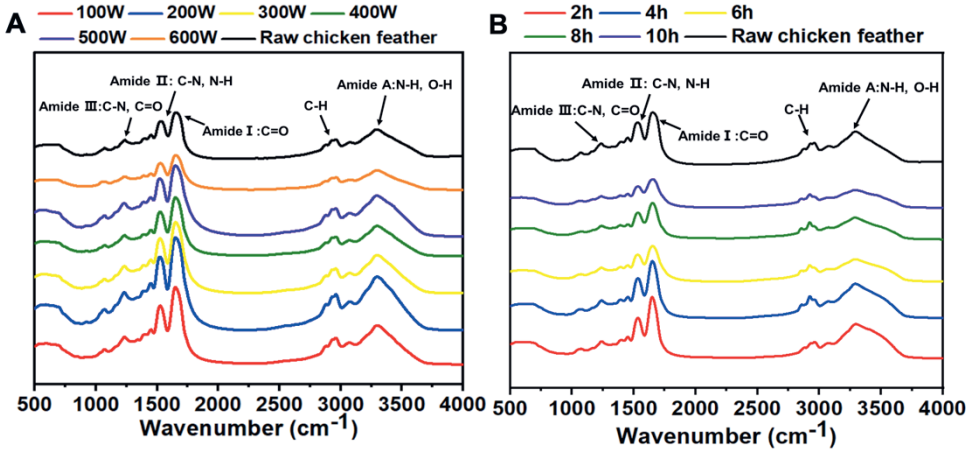

Figure 2.4. FTIR spectrogram of regenerated feather keratin treated for 2 to 10 h at 200 W (A) and treated from 100 to 600 W for 4 h (B).

2.3.2.2 Thermal stability analysis

The effect of ultrasound on the thermal stability of feather keratin was assayed by TGA. **Figure 2.5A&B** showed that treating time was found to have an obvious influence on keratin weight loss instead of ultrasonic power compared to raw chicken feathers. Raw chicken feathers exhibited two phases of weight loss, while regenerated keratin treated over 6 h lost weight in three steps. The result showed that there were about 5.4% of weight loss happened in raw chicken feather at 100.32 °C, and the keratin treated with ultrasound for 2 to 10 h had weight loss of 3.2-4.6%. This step was caused by moisture evaporation, and the difference between raw chicken feathers and extracted keratin was mainly due to different moisture content [40]. Subsequently, the weight of raw chicken feather dropped to 39.4% from 200 to 400 °C due to the escape of hydrogen sulfides and sulfur dioxides resulting from disulfide bonds damage [41-43]. Similarly, the second weight loss of extracted keratin happened when heating to 180 °C around, followed by a further loss at about 260 °C. For regenerated keratin, the second phase was possibly attributed to the

breakage of α-keratin fibers and smaller particle size, while the final weight loss was induced by the deconstructing of β-sheet consisting of disulfide bonds and polypeptide chains and larger particle size [40, 44]. Importantly, longer ultrasonic time led to a sharper decline of keratin weight in the second phase, specially treated for over 6 h. Meanwhile, the keratin treated with longer-time ultrasound had weight loss at a lower temperature. It indicated that long-time ultrasound potentially promoted the cleavage of keratin fibers and reduced disulfide-bond content, thus leading to relatively poorer thermal stability. When changing ultrasonic power, no significant difference was found between various samples, except for keratin at 600 W losing weight remarkably which might result from higher bonding moisture. The result indicated that the thermal stability of regenerated keratin might be potentially reduced by combined action of Cys and ultrasound for over 6 h, while solely improving ultrasonic power showed no obvious effect.

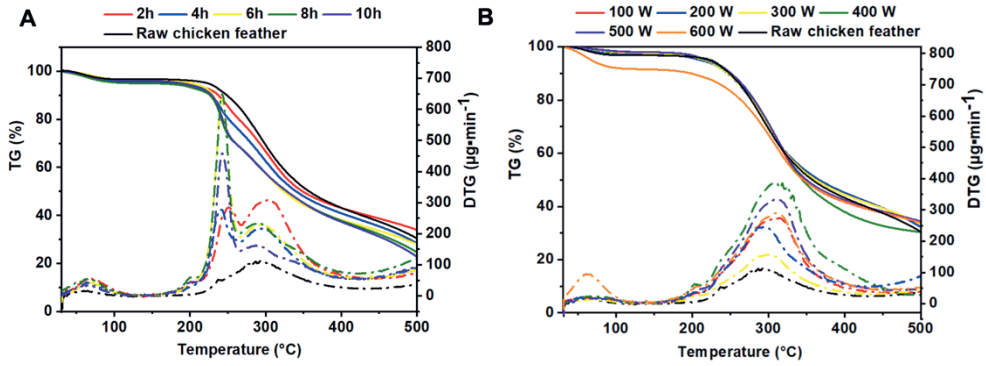

Figure 2.5. TGA traces of regenerated feather keratin treated for 2 to 10 h at 200 W (A) and treated from 100 to 600 W for 4 h (B).

2.3.2.3 Crystallinity analysis

Figure 2.6A&B presented the XRD result of raw chicken feather and regenerated keratin to evaluate their secondary structure and crystallinity. Similar to the previous study, two notable 2θ peaks appeared at about 9.8° and 20° for each keratin material [12, 22]. The 2θ peak at about 9.8° was related to both α-helix and β-sheet, while 20° was also a typical peak value of β-sheet structure [45]. Compared to raw chicken feather, regenerated keratin exhibited lower intensity of peak at about 9.8°. It indicated that the combined treatment of Cys and ultrasound might deconstruct α-helix and β-sheet structure in raw chicken feather resulting in a decreasing crystallinity of regenerated keratin. Nevertheless, the peak at about 9.8° became

smaller with ultrasonic time rising while showing no notable changes with the power increase. These changes were consistent with the result of thermal stability, where there was a sharp decline in the second weight loss phase. Additionally, broader peaks at about 20° were observed in ultrasound-treated samples, which might be attributed to the overlap of the β-sheet and β-turn peaks [21]. Keratin has been reported to own a CI of about 63.6%, with a mixture of crystal and amorphous structure [46, 47]. Some treatments have been found to remarkably change the keratin CI. For example, the keratin extracted using 2 ME had a CI of 30.46% [31]. In this study, the regenerated keratin showed a decrease in crystallinity rate at about 62% compared to raw chicken feather (66.27%), and different conditions made no remarkable change in CI (**Table S2.2**).

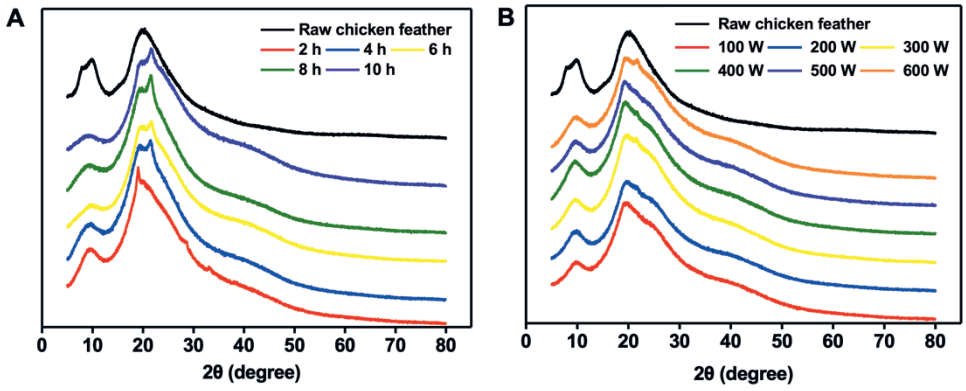

Figure 2.6. X-ray diffraction spectrogram of regenerated feather keratin treated for 2 to 10 h at 200 W (A) and treated from 100 to 600 W for 4 h (B).

Overall, ultrasound facilitated feather dissolution based on the Cys reduction method without changing the main chemical structure of extracted keratin. However, the thermal stability of extracted keratin would be reduced by long-time treatment (> 6 h). In our study, the solubility of regenerated keratin in different solvents would be further explored, which was closely related to chemical structure and crystallinity [35].

2.3.2.4 Keratin solubility in different solvents

Abundant covalent and non-covalent bonds have resulted in poor solubility of feather keratin. However, proper solubility is the prerequisite for further utilization of keratin widely. The effect of ultrasound on keratin solubility in various solvents were studied. **Figure 2.7** indicated that 0.1 M NaOH owned the best ability in

dissolving keratin, followed by 1% SDS solution, while the solutions of Na_3PO_4 (0.01 M, pH 7.5) and Na_3PO_4 (0.01 M, pH 7.5, 2% urea) dissolved keratin limitedly. Generally, the exposed hydrophobic residues during denaturation are considered as the major reason of protein aggregation [48], and the protein solubility will be increased when the electrostatic repulsion is dominant compared to the hydrophobic interaction [48, 49]. In this study, the high pH value was crucial to keratin solubility by changing the electrostatic interactions, and SDS presented a good capacity of dissolving keratin by disrupting the hydrophobic interactions. Nevertheless, urea did not obviously improve keratin dissolution, indicating a relatively weak force from hydrogen bonds in extracted keratin. Additionally, it should be noted that keratin solubility showed a growing trend with the increasing of ultrasonic time and power, possibly caused by the physical changes of intermolecular crosslinks. Previously, it has also been concluded that sonication mainly produced a physical effect on keratin with minimal effect on the chemical structure, which would not affect the backbone structure [21]. In our case, the increasing ultrasonic intensity likely weakened the degree of physical crosslinking of extracted keratin, and thus improved its solubility in aqueous solutions.

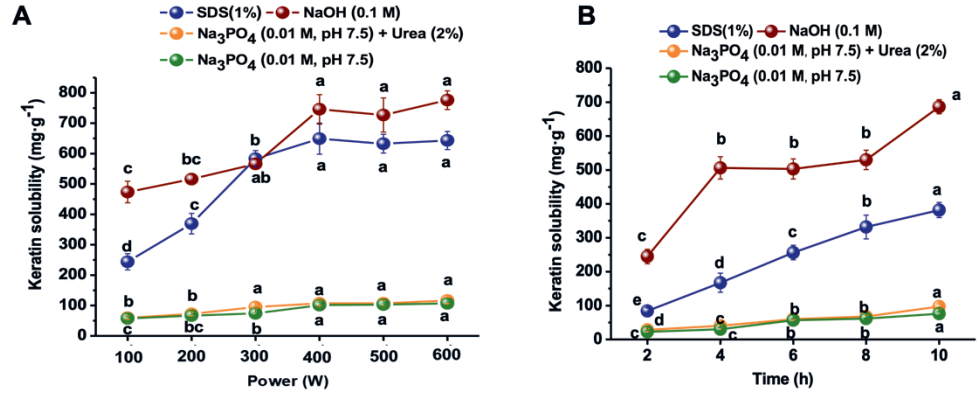

Figure 2.7. (A) Effect of various ultrasonic time (2-10 h, 200 W) and (B) ultrasonic power (100-600 W, 4 h) on the solubility of extracted keratin in different solvents. The results are presented as mean values ± SD, n = 3. The lowercase letters "a-e" indicate the significant difference in soluble protein content between different ultrasonic conditions ($P < 0.05$).

2.3.2.5 Analysis of amino acids in regenerated keratin

Considering the significant effect of treating time on the thermal stability and solubility of extracted keratin, the amino acids composition was assayed which might be a key factor. The result showed that most amino acids became less with

treating time increasing from 4 to 10 h, such as Gly, Ala, Ser, Pro, Val, Ile, Phe and so on (**Figure 2.8**). Long-time treatment resulted in a high hydrolysis degree and serious amino acids loss. Also, the cystine content presented a decrease with time prolonging, which might be due to the growing reduction degree via Cys. As reported, cystine was quite sensitive in alkaline solutions [15], the disulfide bonds of which were easily cut with the presence of sulfhydryl. However, longer processing time also led to an obvious Cys loss. Conversely, an increase of Asp and Lys was observed when prolonging treating time. Similar to previous study, serious loss of Thr, Ser and Cys was found when treating feather with 0.1 M NaOH at 90 °C, while Lys increased [50]. The amino acids composition change resulted from long-time processing might closely relate to the keratin solubility, and the process time should be controlled to avoid keratin over-degradation.

Taken together, Cys reduction assisted with ultrasound was an effective way to dissolve feather waste. Ultrasonic assistance could potentially improve keratin extracting without obvious chemical deconstruction. However, a long processing time would result in decreased thermal stability and serious loss of amino acids from extracting keratin. Therefore, it is still necessary to find an optimal condition that can endow extracted keratin with good stability and solubility without over-degradation while consuming less energy and time.

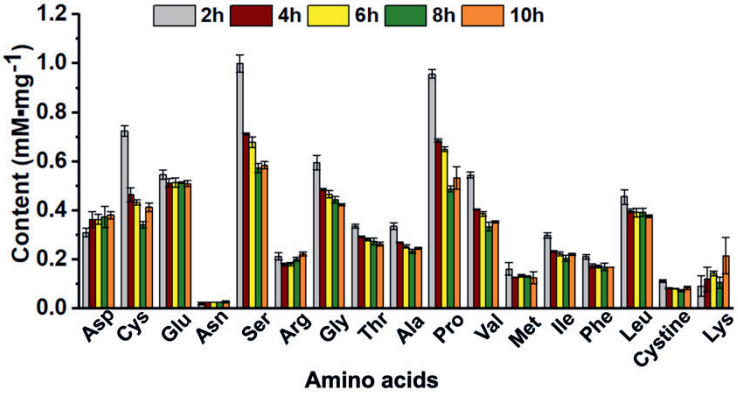

Figure 2.8. Content of 17 kinds of amino acids in extracted keratin treated for 2 to 10 h. The results are presented as the mean values ± SD, n = 3.

2.3.3 Optimization of keratin extraction via Box-Behnken design

2.3.3.1 Single-factor experiment and Box-Behnken design

Effect of factors including ultrasonic time, ultrasonic power, Cys fraction and the ratio of feather to buffer on keratin yield were preliminarily investigated (**Figure 2.9A-D**). By treating feather with varying ultrasonic power and time, the extraction yields showed peak values at 200 W and 4 h, respectively, which were significantly higher than others ($P < 0.05$) (**Figure 2.9A&B**). Higher ultrasonic power and longer treating time might lead to excessive degradation of keratin, producing more smaller peptides which has been discussed in **section 2.3.1.3**. **Figure 2.9C** indicated that the keratin yield reached the highest point when adding 15% of Cys ($P < 0.05$). The decrease of keratin yield with higher Cys fraction might be caused by buffer dilution since more NaOH solution was needed for pH adjusting with increasing Cys. Due to the buoyancy of feather on the buffer surface, a high solid-liquid ratio was found to result in less deconstruction (**Figure 2.9D**). Therefore, the ratio of 1:10 was chosen as constant viable in process optimization. Finally, the optimal conditions of 200 W, 4 h and 15% were chosen as central points for the Box-Behnken design.

Seventeen groups of trials were designed for optimizing keratin extraction based on three variables, and the results were analyzed by multiple regression fitting analysis using Design Expert 8.0 software (**Table S2.3**). A quadratic regression equation model was obtained as follows: $R_1 = 623.50 – 19.36*A – 46.76*B + 22.18*C – 6.64*AB – 5.95*AC – 11.71*BC – 25.55*A^2 – 48.55*B^2 – 27.20 *C^2$. The result showed that the model coefficient (R^2) was 0.9585 with significant deference ($P < 0.001$), and the lack of fit was with an insignificant difference ($P > 0.0688$), indicating that this model fitted well and correctly reflected the relationship of three factors and keratin extraction yield (**Table S2.3**). Generally, the effect of different factors on response value can be reflected by contour density and response surface slope. In the present study, ultrasonic time was found to be the most important factor affecting keratin extraction, followed by Cys fraction and ultrasonic power in sequence, which was also consistent with the ANOVA result ($P < 0.001$) (**Figure 2.9E-J** & **Table S2.3**). In order to achieve a maximum keratin yield with low energy and time-consumption, the optimal conditions were screened and finally determined as 132.40 W, 2.71 h and 15.07% of Cys, under which the theoretical yield was 632.537 mg/g. Considering the practical operability, 130 W, 2.7 h and 15% were chosen as the optimal conditions to

extract keratin. By verification, a final keratin yield of 640.27 ± 9.50 mg/g was obtained, the relative error of which was 1.22%. The quality of regenerated keratin would be further explored compared to the keratin without ultrasonic disposal.

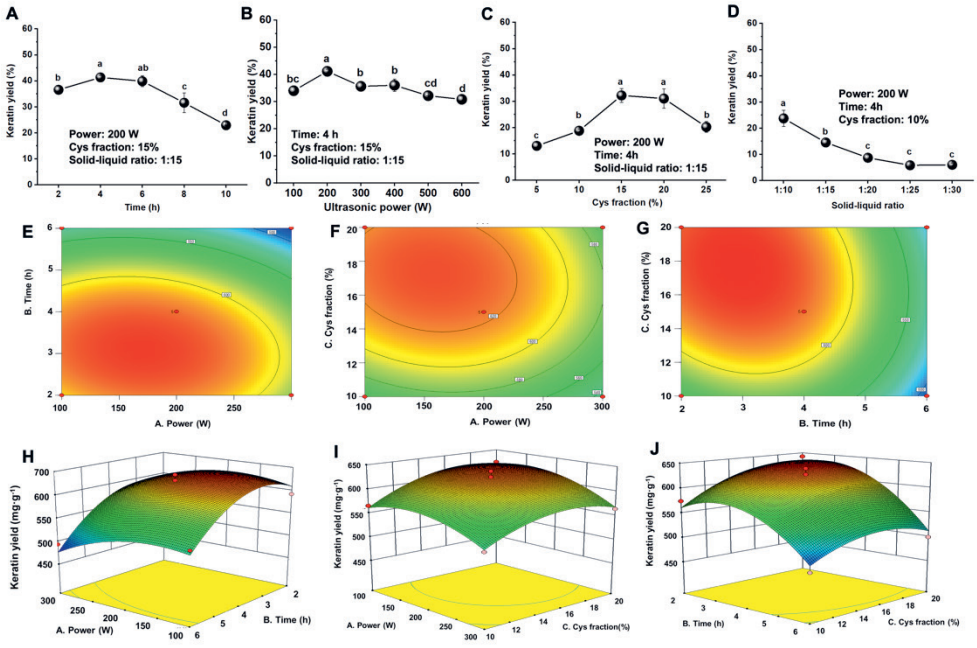

Figure 2.9. (A) Effect of different ultrasonic time, (B) ultrasonic power, (C) Cys fraction and (D) ratio of feather to buffer on keratin yield. (E-G) contour plots and (H-J) response surface plots (3D) showing the effect of various ultrasonic time, power and Cys fraction on keratin yield. The results are presented as the mean values ± SD, n = 3. Different lowercase letters (a-d) indicate a significant difference ($P < 0.05$) among the samples under different conditions.

2.3.3.2 Analysis of chemical structure, thermal stability and crystallinity of regenerated keratin under optimal conditions

The physical properties of regenerated keratin via the ultrasound-Cys-reduction method were analyzed, taking keratin obtained via Cys-reduction and raw chicken feather as control groups. **Figure 2.10A** showed no significant difference between three groups in main chemical groups, including Amide Ⅰ, Ⅱ, Ⅲ, A and B. The process within 2.7 h did no remarkable changes in main chemical bonds. By further analyzing the XRD spectrum, both extracted keratins with and without ultrasound exhibited lower intensity of 2θ peak at about 9.8° than the raw chicken feather, indicating lower content of tightly packed crystals (**Figure 2.10B**). The CI of ultrasound-treated and ultrasound-untreated keratin were 61.98% and 62.19%,

respectively, indicating no obvious difference in crystallinity. For thermal stability, three kinds of keratin materials presented two main steps of weight loss from about 40-100 °C and 200-400 °C, respectively, attributing to the evaporation of bonding moisture and the rupture of both helical conformation and disulfide bonds [21] (**Figure 2.10C**). The result further proved that ultrasonic assistance would not significantly affect the chemical structure, crystallinity and thermal stability of extracted feather keratin, and the optimal conditions were feasible for keratin generation.

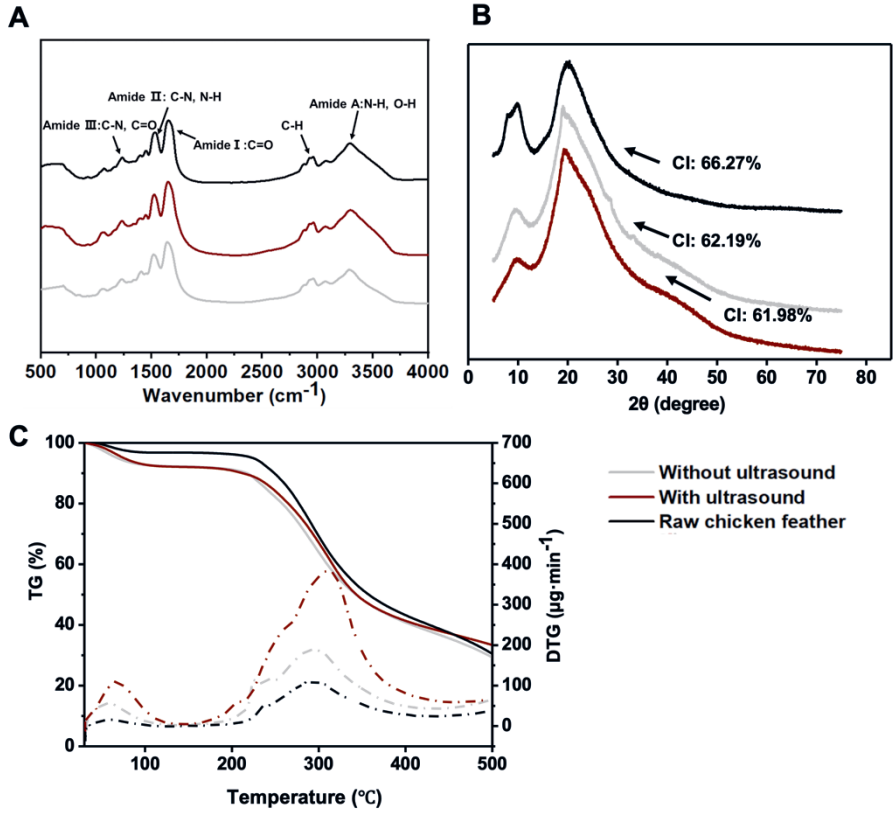

Figure 2.10. (A) FT-IR spectrogram, (B) X-ray diffraction spectrogram, (C) TGA and DTG traces. The keratin treated with ultrasound was regenerated under optimized conditions (130 W, 2.7 h, 15% Cys, 70 °C, pH 10.5, 8 M urea, 1:10 solid-liquid ratio), while the other was obtained under the same conditions except for ultrasonic treatment.

2.3.3.3 Analysis of amino acids and solubility in different solvents

The effect of ultrasonic treatment under optimized condition on amino acids composition of keratin was investigated compared to the ultrasound-untreated

group (**Figure 2.11A**). The result showed that most of amino acids were richer in ultrasound-treated keratin than ultrasound-untreated group, such as Ser, Gly, Ala, Pro, Val, Phe and Leu. Different form the serious amino acids loss at higher temperature (> 100 °C), 75 °C treatment would not result in keratin over-degradation [51]. In this study, the ultrasound-treatment improved the total amino acids content (7.45 mM/mg) which was significantly higher than the control group (6.81 mM/mg) (P > 0.05). However, ultrasound has resulted in a lower Cys content in extracted keratin while no significant difference was found in cystine content. It indicated that Cys was more susceptible and easily degraded under ultrasonic condition. Consistent with previous studies, the regenerated keratin in the present study contained abundant Pro, Ser, Glu, Val and Leu [12, 35].

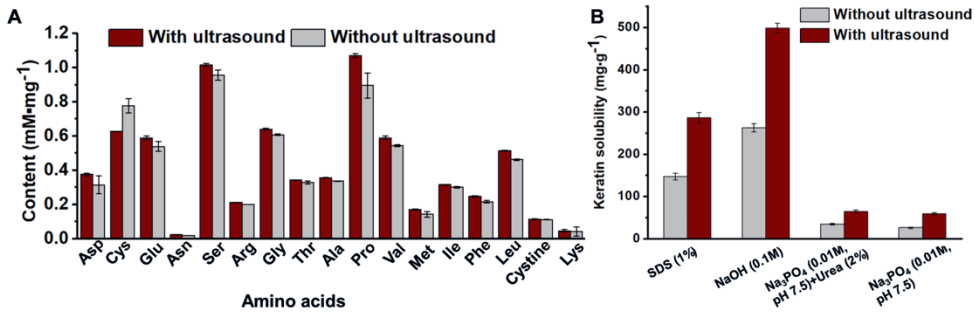

Figure 2.11. (A) Content of 17 kinds of amino acids and (B) keratin solubility in various solvents. The keratin treated with ultrasound was regenerated under optimized conditions (130 W, 2.7 h, 15% Cys, 70 °C, pH 10.5, 8 M urea, 1:10 solid-liquid ratio), while the other was obtained under the same conditions except for ultrasonic treatment. The results are presented as the mean values ± SD, n = 3.

Similar to the result in **section 2.3.2.4**, NaOH solution owned the best capacity of dissolving regenerated keratin, which was followed by 1% SDS solution, while there was less keratin dissolved in Na_3PO_4 solution with or without urea at pH 7.5 (**Figure 2.11B**), further suggesting the strong hydrophobic and electrostatic interactions in keratin and relatively weaker hydrogen bonding. Obviously, the ultrasound-treated keratin possessed higher solubility in various aqueous solutions than the ultrasound-untreated group. Considering no significant difference in chemical structure, crystallinity and thermal stability has been found between those two groups, it was further verified that ultrasound potentially reduced non-covalent bonds, such as hydrogen bonds, hydrophobic interaction and Van der Waals force, thus leading to better solubility of extracted keratin.

Taken together, the optimal conditions of 130 W, 2.7 h and 15% of Cys were practical for keratin extraction from feather waste, under which the product reserved complete chemical structure while possessing good stability and solubility. The process realized feather extracting in time-saving way without toxic chemicals, which might be promising in reusing keratin materials in various areas.

2.4 Conclusion

To conclude, ultrasound could improve feather deconstruction based on the Cys reduction method by physically destroying crosslinking interactions while still retaining the protein backbone structure. However, the long processing time resulted in feather over-degradation producing a large number of peptides with small molecular weight, and the keratin product exhibited low thermal stability and serious amino acids loss. Under the optimal conditions (130 W, 2.7 h and 15% Cys) obtained via Box-Behnken design, keratin exhibited better solubility in various solvents than the control group, while without serious amino acids loss and obvious damage on chemical structure and thermal stability. The optimal process reserved the structural integrity of keratin and endowed it with good thermal stability and solubility, thus was potential in generating high-performance keratin materials from chicken feather. The study investigated the ultrasonic effect on feather keratin systemically and proposed a green alternative strategy for keratin extraction, which might be meaningful for utilizing and valorizing feather waste.

2.5 References

1. Compassion in world farming. https://www.ciwf.org.uk/farm-animals/chickens/
2. P. Kshetri, T. Surchandra, B. Shamjetshabam, S.S. Roy, K. Tamreihao, Valorization of chicken feather waste into bioactive keratin hydrolysate by a newly purified keratinase from Bacillus sp. RCM-SSR-102, Journal of Environmental Management, 273 (2020). https://doi.org/10.1016/j.jenvman.2020.111195
3. T. Korniłłowicz-Kowalska, J. Bohacz, Biodegradation of keratin waste: Theory and practical aspects, Waste Management, 31 (2011) 1689-1701. https://doi.org/10.1016/j.wasman.2011.03.024
4. A. Ullah, T. Vasanthan, D. Bressler, A.L. Elias, J. Wu, Bioplastics from Feather Quill, Biomacromolecules, (2011). https://doi.org/10.1021/bm201112n
5. J.G. Rouse, M.V. Dyke, A Review of Keratin-Based Biomaterials for Biomedical Applications, Materials, 3 (2010) 999-1014. DOI: 10.3390/ma3020999
6. Sharma, S., & Gupta, A. (2016). Sustainable Management of Keratin Waste Biomass: Applications and Future Perspectives. Brazilian Archives of Biology and Technology, 59(0). doi:10.1590/1678-4324-2016150684
7. N. Ramakrishnan, S. Sharma, A. Gupta, B.Y. Alashwal, Keratin based bioplastic film from chicken feathers and its characterization, International Journal of Biological Macromolecules, (2018) 352-358. DOI:10.1016/j.ijbiomac.2018.01.037
8. H. Xu, Z. Shi, N. Reddy, Y. Yang, Intrinsically water-stable keratin nanoparticles and their in vivo biodistribution for targeted delivery, Journal of Agricultural & Food Chemistry, 62 (2015) 9145-9150. https://doi.org/10.1021/jf502242h
9. H. Zhang, M. Pei, P. Liu, pH-Activated surface charge-reversal double-crosslinked hyaluronic acid nanogels with feather keratin as multifunctional crosslinker for tumor-targeting DOX delivery, International Journal of Biological Macromolecules, 150 (2020) 1104-1112. https://doi.org/10.1016/j.ijbiomac.2019.10.116
10. Yussef, Esparza, Nandika, Bandara, Aman, Ullah, Jianping, Wu, Hydrogels from feather keratin show higher viscoelastic properties and cell proliferation than those from hair and wool keratins, Materials Science & Engineering C, (2018). https://doi.org/10.1016/j.msec.2018.04.067
11. H. Xu, S. Cai, L. Xu, Y. Yang, Water-stable three-dimensional ultrafine fibrous scaffolds from keratin for cartilage tissue engineering, Langmuir, 30 (2014) 8461-8470. https://doi.org/10.1021/la500768b
12. W. Ju, S. Hao, T. Luo, Y. Qian, B. Wang, Development of feather keratin nanoparticles and investigation of their hemostatic efficacy, Mater Sci Eng C Mater Biol Appl, 68 (2016) 768-773. https://doi.org/10.1016/j.msec.2016.07.035
13. S. Agrahari, N. Wadhwa, Degradation of Chicken Feather a Poultry Waste Product by Keratinolytic Bacteria Isolated from Dumping Site at Ghazipur Poultry Processing Plant, International Journal of Poultry Science, 9 (2010). DOI: 10.3923/ijps.2010.482.489
14. T. Paul, S.K. Halder, A. Das, S. Bera, C. Maity, A. Mandal, P.S. Das, P. Mohapatra, B.R. Pati, K.C. Mondal, Exploitation of chicken feather waste as a plant growth promoting agent using keratinase producing novel isolate Paenibacillus woosongensis TKB2, Biocatalysis & Agricultural Biotechnology, 2 (2013) 50-57. https://doi.org/10.1016/j.bcab.2012.10.001
15. A. Shavandi, T.H. Silva, A.A. Bekhit, E.D.A. Bekhit, Keratin: dissolution, extraction and biomedical application, Biomaterials Science, 5 (2017). DOI: 10.1039/C7BM00411G
16. G. Toennies, R.P. Homiller, The Oxidation of Amino Acids by Hydrogen Peroxide in Formic Acid,

Journal of the American Chemical Society, 64 (1942) 3054-3056. https://doi.org/10.1021/ja01264a518

17. Y. Zhang, W. Zhao, R. Yang, Steam Flash Explosion Assisted Dissolution of Keratin from Feathers, Acs Sustainable Chemistry & Engineering, 3 (2015) 150717112248006. https://doi.org/10.1021/acssuschemeng.5b00310
18. I. Sinkiewicz, A. Śliwińska, H. Staroszczyk, I. Kołodziejska, Alternative Methods of Preparation of Soluble Keratin from Chicken Feathers, Waste & Biomass Valorization, 8 (2016) 1-6. DOI: 10.1007/s12649-016-9678-y
19. Y. Zhang, R. Yang, Z. Wei, Improving Digestibility of Feather Meal by Steam Flash Explosion, Journal of Agricultural and Food Chemistry, 62 (2014) 2745-2751. https://doi.org/10.1021/jf405498k
20. A. Ghosh, S. Clerens, S. Deb-Choudhury, J.M. Dyer, Thermal effects of ionic liquid dissolution on the structures and properties of regenerated wool keratin, Polymer Degradation & Stability, 108 (2014) 108-115. https://doi.org/10.1016/j.polymdegradstab.2014.06.007
21. N.A. Azmi, A. Idris, N.S.M. Yusof, Ultrasonic technology for value added products from feather keratin, Ultrason Sonochem, 47 (2018) 99-107. https://doi.org/10.1016/j.ultsonch.2018.04.016
22. L. Guo, L. Lu, M. Yin, R. Yang, W. Zhao, Valorization of refractory keratinous waste using a new and sustainable bio-catalysis, Chemical Engineering Journal, 397 (2020). https://doi.org/10.1016/j.cej.2020.125420
23. Y.X. Wang, X.J. Cao, Extracting keratin from chicken feathers by using a hydrophobic ionic liquid, Process Biochemistry, 47 (2012) 896-899. https://doi.org/10.1016/j.procbio.2012.02.013
24. A.J. Poole, R.E. Lyons, J.S. Church, Dissolving Feather Keratin Using Sodium Sulfide for Bio-Polymer Applications, Journal of Polymers and the Environment, 19 (2011) 995-1004. DOI: 10.1007/s10924-011-0365-6
25. O.D. Fagbemi, B. Sithole, T. Tesfaye, Optimization of keratin protein extraction from waste chicken feathers using hybrid pre-treatment techniques, Sustainable Chemistry and Pharmacy, 17 (2020) 100267. https://doi.org/10.1016/j.scp.2020.100267
26. H. Xu, Y. Yang, Controlled De-Cross-Linking and Disentanglement of Feather Keratin for Fiber Preparation via a Novel Process, ACS Sustainable Chemistry & Engineering, 2 (2014) 1404-1410. https://doi.org/10.1021/sc400461d
27. M. Wada, H. Takagi, Metabolic pathways and biotechnological production of L-cysteine, Applied Microbiology & Biotechnology, 73 (2006) 48-54. DOI: 10.1007/s00253-006-0587-z
28. J. Behrendt, E. Arevalo, H. Gulyas, J. Niederstehollenberg, A. Niemiec, J. Zhou, R. Otterpohl, Production of value-added products from separately collected urine, Water Science & Technology A Journal of the International Association on Water Pollution Research, 46 (2002) 341. DOI: 10.1029/2001WR000769
29. A.N. Akram, C. Zhang, Extraction of collagen-II with pepsin and ultrasound treatment from chicken sternal cartilage; physicochemical and functional properties, Ultrasonics Sonochemistry, 64 (2020) 105053. https://doi.org/10.1016/j.ultsonch.2020.105053
30. Y. Sun, M. Zhong, M. Kang, Y. Liao, Z. Wang, Y. Li, B. Qi, Novel core-shell nanoparticles: Encapsulation and delivery of curcumin using guanidine hydrochloride-induced oleosome protein self-assembly, LWT - Food Science and Technology, (2023). https://doi.org/10.1016/j.lwt.2022.114352
31. M. Pakdel, Z. Moosavi-Nejad, R.K. Kermanshahi, H. Hosano, Self-assembled uniform keratin nanoparticles as building blocks for nanofibrils and nanolayers derived from industrial feather

waste, Journal of cleaner production, (2022). https://doi.org/10.1016/j.jclepro.2021.130331

32. O.H. Lowry, H.J. Rosebrough, A. Farr, R.J. Randall, Protein measurement with the pholin phenol reagent, Journal of Biological Chemistry, 193 (1951) 265.
33. G.B. Irvine, C. Shaw, High-performance gel permeation chromatography of proteins and peptides on columns of TSK-G2000-SW and TSK-G3000-SW: A volatile solvent giving separation based on charge and size of polypeptides, Analytical Biochemistry, 155 (1986) 141-148. https://doi.org/10.1016/0003-2697(86)90239-3
34. A. Masuda, N. Dohmae, Amino Acid Analysis, Analytical & Bioanalytical Chemistry, 82 (2019) 8939-8945.
35. W. Zhao, R. Yang, Y. Zhang, W. L, Sustainable and practical utilization of feather keratin by an innovative physicochemical pretreatment: high density steam flash-explosion, Green Chemistry, (2012). DOI: 10.1039/c2gc36243k
36. R. Manasseh, P. Tho, A. Ooi, K. Petkovic-Duran, Y. Zhu, Cavitation microstreaming and material transport around microbubbles, Physics Procedia, 3 (2010) 427-432. https://doi.org/10.1016/j.phpro.2010.01.056
37. J.H. Muyonga, C. Cole, K.G. Duodu, Characterisation of acid soluble collagen from skins of young and adult Nile perch (Lates niloticus), Food Chemistry, 85 (2004) 81-89. https://doi.org/10.1016/j.foodchem.2003.06.006
38. B.L. Hsu, Y.M. Weng, Y.H. Liao, W. Chen, Structural investigation of edible zein films/coatings and directly determining their thickness by FT-Raman spectroscopy, Journal of Agricultural & Food Chemistry, 53 (2005) 5089-5095. https://doi.org/10.1021/jf0501490
39. K.J. Payne, A. Veis, Fourier transform ir spectroscopy of collagen and gelatin solutions: Deconvolution of the amide I band for conformational studies, Biopolymers, 27 (1988) 1749. DOI: 10.1002/bip.360271105
40. S. Alahyaribeik, A. Ullah, Methods of keratin extraction from poultry feathers and their effects on antioxidant activity of extracted keratin, International Journal of Biological Macromolecules, 148 (2020). https://doi.org/10.1016/j.ijbiomac.2020.01.144
41. K. Wang, R. Li, J.H. Ma, Y.K. Jian, J.N. Che, Extracting keratin from wool by using L-cysteine, Green Chemistry, 18 (2016). DOI: 10.1039/c5gc01254f
42. A. Idris, R. Vijayaraghavan, U.A. Rana, A.F. Patti, D.R. Macfarlane, Dissolution and regeneration of wool keratin in ionic liquids, Green Chemistry, 16 (2014). DOI: 10.1039/c4gc00213j
43. G. Guidotti, M. Soccio, T. Posati, G. Sotgiu, A. Aluigi, Regenerated wool keratin-polybutylene succinate nanofibrous mats for drug delivery and cells culture, Polymer Degradation and Stability, 179 (2020) 109272. https://doi.org/10.1016/j.polymdegradstab.2020.109272
44. A. Vasconcelos, G. Freddi, A. Cavaco-Paulo, Biodegradable Materials Based on Silk Fibroin and Keratin, Macromolecules, 9 (2008) 1299–1305. https://doi.org/10.1021/bm7012789
45. M.A. Xiang, L.B. Wei, C. Hx, B. Bm, C.A. Yue, E. Yybd, Transferring feather wastes to ductile keratin filaments towards a sustainable poultry industry - ScienceDirect, Waste Management, 115 (2020) 65-73. https://doi.org/10.1016/j.wasman.2020.07.022
46. Z.P. Rad, H. Tavanai, A.R. Moradi, Production of feather keratin nanopowder through electrospraying, Journal of Aerosol ence, 51 (2012) 49–56. https://doi.org/10.1016/j.jaerosci.2012.04.007
47. R. Fraser, D. Parry, The structural basis of the filament-matrix texture in the avian/reptilian group

of hard β-keratins, Journal of Structural Biology, 173 (2011) 391-405. https://doi.org/10.1016/j.jsb.2010.09.020

48. J.L. Cleland, M.F. Powell, S.J. Shire, The development of stable protein formulations: A close look at protein aggregation, deamidation, and oxidation, Critical Reviews in Therapeutic Drug Carrier Systems, 10 (1993) 307. PMID: 8124728
49. J.F. Zayas, Solubility of Proteins, Springer Berlin Heidelberg, (1997). DOI: 10.1007/978-3-642-59116-7_2
50. Y. Nagai, T. Nishikawa, Alkali Solubilization of Chichken Feather Keratin, Agricultural and biological chemistry, 34 (1970) 16-22. DOI: 10.1271/bbb1961.34.16
51. V.S. Chang, F.K. Agbogbo, M.T. Holtzapple], Lime treatment of keratinous materials for the generation of highly digestible animal feed: 1. Chicken feathers, Bioresource Technology, (2006). https://doi.org/10.1016/j.biortech.2005.05.021

2.6 Supplementary materials

Table S2.1. Conditions of Box-Behnken experiment design.

Factors	Levels		
	-1	0	1
Ultrasonic power (A/W)	100	200	300
Ultrasonic time (B/h)	2	4	6
Cys fraction (C/%)	10	15	20

Note: The optimal conditions of the single-factor experiment were 200 W, 4 h and 15% of Cys.

Table S2.2. The crystallinity index of regenerated keratin.

Time (h)	2	4	6	8	10	
CI (%)	61.93	61.92	61.61	61.67	63.16	
Power (W)	100	200	300	400	500	600
CI (%)	62.27	62.77	62.71	61.91	62.09	61.54

Table S2.3. ANOVA analysis for response surface quadratic model of variance.

Sources of variance	Sum of squares	df	Mean square	*F* value	*P* value (*P* > *F*)
Model	42577.31	9	4730.81	17.97	0.0005**
A	2997.70	1	2997.70	11.39	0.0118*
B	17491.05	1	17491.05	66.45	0.0001**
C	3936.95	1	3936.95	14.96	0.0062*
AB	176.36	1	176.36	0.67	0.4400
AC	141.85	1	141.85	0.54	0.4867
BC	548.26	1	548.26	2.08	0.1922
A^2	2749.02	1	2749.02	10.44	0.0144*
B^2	9804.10	1	9804.10	37.25	0.0005*
C^2	3114.94	1	3114.94	11.83	0.0108*
Residual	1842.53	7	263.22		
Lack of fit	1476.66	3	492.22	5.38	0.0688

Pure error	365.86	4	91.47
Cor total	44419.84	16	
Coefficient	R^2 = 0.9585 Adj R^2 = 0.9052	Pre R^2 = 0.4552	Adeq precision = 12.196

Note: A represents ultrasonic power, B represents ultrasonic time, and C represents Cys fraction.


3

CHAPTER 3

A sustainable and efficient recycling strategy of feather waste into keratin peptides with antimicrobial activity

Published as: Xiaojie Qin, Xiong Xu, Yujie Guo, Qingshan Shen, Jiqian Liu, Chuan Yang, Elinor L. Scott, Johannes H. Bitter, Chunhui Zhang (2022). A sustainable and efficient recycling strategy of feather waste into keratin peptides with antimicrobial activity. *Waste Management*, 144, 421-430.

Abstract

The study aimed to propose an efficient and eco-friendly strategy to improve the utilization of feather waste and converting it into high-valued antimicrobial products. Under the synergistic effect of instant catapult steam explosion (ICSE) (1.5 MPa-120 s), over 90% of chicken feather powder (CFP) was degraded into soluble peptides via keratinolysis within 3 h, about 90% of which were smaller than 3 kDa, indicating an overwhelming advantage than general proteolysis. Importantly, the keratinolysis hydrolysate of CFP was able to inhibit *E. coli* growth, among which the fraction < 3 kDa exhibited highest antimicrobial activity with a minimal inhibitory concentration of 30 mg/mL. Compared to other fractions, the fraction < 3 kDa contained higher content of hydrophobic amino acids (364.11 mg/g), in which about 79% of peptides had more than 60% hydrophobic ratio, potentially contributing to its antimicrobial activity. ICSE-keratinolysis process holds potential in reducing both protein resource waste and environmental pollution by valorizing feathers into antimicrobial product.

3.1 Introduction

Annually, 2-5 million tons of feathers become available from the meat processing industry [1, 2], which has been taken as a huge keratinous resource. Keratin is the main component of chicken feather (≥ 90%) containing some essential amino acids such as threonine, valine and leucine, and it can be seen as a potential protein resource. However, it is still challenging to recycle feathers. Keratin is composed of abundant disulfide bonds and cross-linkages which folds into β-sheets and stacked and twisted into helical structure [3]. The inherent intact structure of keratin renders it high stability and resistance to most of proteases and reagents. Thus, chicken feather has been only utilized in a small scale with low-value products, such as animal feeds, fertilizer, biocomposites [4]. As reported, most of feather wastes were still handled by landfill and incineration [5], resulting in serious environment pollution and protein resource waste. Proposing a strategy for efficiently reusing feather wastes as high-valued product is growingly drawing considerable attention.

In recent years, antimicrobial peptides (AMPs) gradually became a research focus for their potential in substituting antibiotics which would severely disrupt microecological balance of animal intestines and led to bacterial antibiotic resistance [6]. So far, more than 2000 kinds of AMPs have been obtained from natural protein resource, such as fish gelatin, bitter beans, goat whey and crab crustin, serving as innovative green antimicrobial drug [6-10]. The antimicrobial activity of peptides mainly depends on their amino acid composition, electric charge, hydrophobicity, amphiphilicity, conformation, etc. [11]. Most AMPs were identified as small cationic peptides with hydrophobic properties [12], such as porcine myeloid antimicrobial peptide-36 which contained up to 36% of cationic amino acids [13]. Especially, some AMPs were reported to be rich in cysteine. Crustin has been universally accepted as antimicrobial peptides, owning a cationic region at the carboxyl terminus consisting of twelve cysteine residues and a whey acidic protein domain where were eight cysteine residues at defined sites forming a four intracellular disulfide core [14]. Plant defensins, a representative group of plant antimicrobial peptides, are composed of 45-54 amino acids including eight conserved cysteine residues forming four disulfide bonds [15]. The bacteriostatic mechanism of AMPs is to penetrate cell plasma membrane with ion channels forming through charge attraction, thus causing destruction of cell membrane structure and intracellular materials outflowing [6]. Compared to antibiotics, it is unlikely to produce resistant strain such as the

persister cell. Thus, natural protein resource is a promising alternative for producing antimicrobial peptides.

Keratin is a potential natural biomass owning various properties including biocompatibility, low-toxicity, biodegradability, showing promise in biological applications. There was over 7% of cysteine in keratin amino acids composition, contributing to a higher stability than other proteins [4]. What is important is that the tripeptides of "Arg-Gly-Asp" and "Leu-Asp-Val" existing in keratin have been concluded to own ability of binding with cell surface ligands and thus promoting cell adhesion [16]. Xu et al. have found that keratin nanoparticles possessed remarkable water stability under varying pH values (pH 2.0-7.0) and temperatures (4-37 ºC), and keratin nanoparticles successfully penetrated into kidney and liver cells exhibiting positive ability in attachment and proliferation [17]. In addition, keratin was supposed to be cut and finely tuned to incorporate with various hydrophilic and hydrophobic tails due to its amino acid composition [18, 19]. In a study of catalyzing feather keratin, some peptides with N-terminal hydrophobic amino acids (e.g. Leu and Val) emerged [20], which can potentially enhance the accessibility to hydrophobic substances such as phospholipid. Overall, the high cysteine content, special tripeptide structure and hydrophobic residues may provide keratin peptides with potential penetrating ability of bacterial. However, less study regarding the antimicrobial activity of keratin hydrolysates obtained via different conventional proteases and keratinase was reported.

The existing methods for degrading keratin include chemical treatment (e.g. strong acid-base and oxidation-reduction treatment), physicochemical treatment (e.g. hydrothermal and superheated water treatments) and biocatalysis (e.g. keratinases) [4]. Nevertheless, there were unwanted effects during these processes, such as environmental pollution resulting from various reagents, excessive degradation, low efficiency via proteases. As reported, there was only 47.56% of raw chicken feather degraded after 1220 min by keratinase which has been taken as the only group of enzymes for hydrolyzing keratin material [20], even though enzymatic hydrolysis is a relatively mild and green method with lower energy consumption. Instant catapult steam-explosion (ICSE) is an adiabatic expansion process involving the transformation of thermal energy into mechanical energy without using chemicals. The steam can fully penetrate organic tissue structure with a powerful seepage force, and then a severe disruption of internal structure in biomass would

be introduced by the mechanical shearing force when given a rapid decompression. In our previous work, ICSE technology has been adopted for liquefying chicken sternal cartilage and bovine bone [21, 22]. Additionally, steam explosion was found to be effective for destabilizing β-sheets crystals and disulfide bonds in feathers, which was beneficial to keratin extraction and digestibility improvement of feather meal [23-25]. It is worth mentioning that the feather substrate pretreated by steam explosion was found to be effectively degraded by conventional proteases (e.g. alcalase, pepsin, papain and neutrase) [20]. Undoubtably, ICSE is an eco-friendly and effective pretreating way to help preliminarily disrupt stiff feather waste and further enzymatically hydrolyze them into active keratin peptides. However, a mild ICSE condition that can appropriately deconstruct chicken feather without over-degradation need to be optimized, after which chicken feather will be more accessible to enzymes.

The overall purpose of the study was to optimize a mild ICSE condition for destructing chicken feather into chicken feather powder (CFP) without severe degradation, as well as to explore the potential anti-*Escherichia coli* (*E. coli*) activity of CFP hydrolysates cleaved via conventional proteolysis and keratinolysis. It was achieved through 1) determining an optimal ICSE condition via systematically analyzing the changes of disulfide bonds, released soluble peptides and free amino acids; 2) investigating the *E. coli*-inhibitory ability of CFP hydrolysates that enzymatically hydrolyzed with different enzymes (keratinase, alcalase, papain, trypsin, neutrase, protamex and flavourzyme); 3) analyzing the difference of antimicrobial activity affected by molecular weights (< 3 kDa, 3-5 kDa, 5-10 kDa and > 10 kDa) of keratinolysis hydrolysate (with highest antimicrobial ability) via focusing on their amino acid composition and sequence. The proposed strategy combining ICSE and keratinolysis would be meaningful for greenly and efficiently recycling feather waste into value-added antimicrobial products, which would also contribute to reducing environmental pollution and valorizing feather waste.

3.2 Materials and methods

3.2.1 Materials and chemicals

White chicken feather was collected from a poultry industry (Protil Biological Technology Co. Ltd., Henan province, China). Feathers were washed with distilled water then dried in an oven at 50 °C for 48 h. The enzymes, including papain,

keratinase, trypsin, protamex, neutrase, alcalase and flavourzyme, were supplied by Solaibao Biological Technology Co., Ltd (Shanghai, China). HPLC grade acetonitrile (ACN) was purchased from Thermo Fisher Scientific (Waltham, USA). Other reagents including ethylenediaminetetraacetic acid (EDTA), sodium dodecyl sulfate (SDS), Tris−HCl, 5,5′-dithiobis (2-nitrobenzoic acid) (DTNB), urea and Na_2SO_3 supplied by Sinopharm Chemical Reagent Co., Ltd (China) were of analytical grade. The deionized water was prepared via Milli-Q 50 system (Millipore Corp., Milford, MA, USA).

3.2.2 Preparation of chicken feather powder via ICSE treatment

ICSE experiments were performed via the ICSE apparatus (QBS-80 SE, Gentle Bioenergy Co. Ltd., Hebi, Henan province, China) referring to previous study [24]. Briefly, 20 g of cleaned feather was loaded in an apparatus chamber pressurized at 0.5, 1.0, 1.5, 2.0 and 2.5 MPa. Each pressure was maintained for 15, 30, 60, 90 and 120 s. Afterward, the chamber was depressurized instantly, leading to an intense explosion. Treated samples were lyophilized and ground into chicken feather powder (CFP).

3.2.3 The yield and morphology of ICSE feather

The yield (Y) of CFP were calculated using equation (1) based on dry basis.

$$Y(\%) = \frac{m_0}{m_1} \times 100 \qquad (1)$$

Where m_0 represents the weight of dried CFP, and m_1 represents the initial dry weight of introduced chicken feather.

The feather treated with ICSE at different conditions were photographed using Cannon camera.

3.2.4 Soluble peptides in ICSE CFP

1 g of CFP was dispersed in 10 mL of distilled water and stood for 1 h at room temperature. Then the samples were centrifuged at 10000 ×g for 15 min to obtain supernatant for soluble peptides and free amino acids (FAA) analysis. For peptides determination, 0.25 mL of sample supernatant was mixed with equal volume of 10% TCA firstly, and the final supernatant was obtained after 20 min centrifuging at 10000 ×g, 4 °C. Then, 20 μL of the final supernatant obtained above were measured using the method from Lowry et al., with bovine serum albumin as a standard [26].

The absorbance of samples was detected using microplate reader (Synergy H1, BioTek, USA) at 650 nm.

3.2.5 Distribution of polypeptides molecular weight (PMW) and analysis of amino acids (AA)

The molecular weight (Mw) of polypeptides in samples (ICSE CFP and enzymatic hydrolysates as **section 3.2.7** described) was determined by Agilent liquid chromatograph 1200 with a UV detector performed at 220 nm (Agilent, CA, USA) [27]. The TSK gel filtration column (G2000 SWXL 300 mm × 7.8 mm, Tosoh Co., Tokyo, Japan) was employed, and the flow rate of mobile phase composed of water/acetonitrile/trifluoroacetic acid (70/30/0.1, v/v/v) was 0.5 mL /min. The column was thermo-stated at 40 °C and samples were injected into the high-performance liquid chromatography system in a volume of 10 μL. The standards including tripeptide GGG (189 Da), tetrapeptide GGYR (451 Da), aprotinin (6511 Da), cytochrome C (12355 Da) and bovine serum albumin (66446 Da) (Sigma Aldrich, St. Louis, MO, USA) were used for MW calibration curve. The data were analyzed via gel permeation chromatography software.

For analyzing FAA in ICSE CFP, 1 mL of supernatant sample, obtained as **section 3.2.4** described, was mixed with 1 mL of sulfosalicylic acid (8%) and incubated for 120 min at 4 °C. The suspension was obtained by centrifugation at 10000 ×g for 15 min. Subsequently, it was dried with nitrogen, and 1 mL of HCl (0.02 M) was added to dissolve the sample for analysis. 20 μL of the prepared sample were injected to L8900 AA auto-analyzer for amino acids assay. In order to analyze the AA composition of keratin peptides via keratinolysis (4 fractions obtained as **section 3.2.9** described), about 50 mg of sample were hydrolyzed by 10 mL of HCl (6 M) at 110 °C for 24 h, and then were filtered and transferred into volumetric flask with volume of 50 mL. After that, 1 mL of hydrolysate was dried with nitrogen and redissolved in 5 mL of HCl (0.02 M) for further determination with a L8900 AA auto-analyzer.

3.2.6 Content of disulfide and free sulfhydryl

Disulfide and free sulfhydryl content were detected with method mentioned by Chan et al. with some modifications [28]. For free sulfhydryl assay, 15 mg of CFP was suspended in 800 μL of buffer 1 (8 M urea, 3 mM EDTA, 1% SDS and Tris−HCl (0.2 M, pH 8.0)). The mixture was shaken at 100 rpm for 2.5 h at room temperature. After that, 200 μL of buffer 2 (10 mM DTNB in Tris−HCl (0.2 M, pH 8.0)) was added and

kept shaking for another 1 h, and then the reaction mixture was centrifuged at 12000 ×g for 15 min at 25 °C. The supernatant absorbance was determined at 412 nm. The extinction coefficient was 13600 $M^{-1}cm^{-1}$ for calculating thiol groups.

The detection procedure of total sulfhydryl was performed as described above except for using different reagents. Buffer 1 was replaced with buffer 3 containing 8 M urea, 3 mM EDTA, 1% SDS, 0.2 M Tris−HCl (pH 9.5), 0.1 M Na_2SO_3 and 50 mM 2-nitro-5-thio-sulfobenzoic acid ($NTSB^{2-}$) synthesized by DTNB [29]. The disulfide content was calculated as the difference between the thiol group content before and after reduction of disulfide bonds with sulfite.

3.2.7 Enzymatic hydrolysis of CFP with different enzymes

Alcalase, papain, neutrase, trypsin, keratinase, flavourzyme and protamex were used for enzymatic hydrolysis with concentration of 6000 U/g, the conditions of which are shown in **Table 3.1**, referring to both producer instructions and previous studies with some modifications [20, 30]. 1 g of CFP obtained via ICSE at 1.5 MPa for 120 s was dispersed in 50 mL of phosphate buffer and preheated to designed temperature in water bath, and then mixed with enzymes. The mixture was stirred at 200 rpm for 3 h. The reaction was stopped by boiling for 10 min to inactivate the enzyme. The mixture was centrifuged at 12000 ×g for 10 min at 4 °C and then the hydrolysate was filtrated through 0.45 μm of filter membrane. After that, the hydrolysate was dialyzed (cutoff Mw 100 Da) for 3 days in distilled water at 4 °C. Part of hydrolysate was used to analyze soluble protein and polypeptides, and the dialyzed hydrolysate was lyophilized.

Table 3.1. Enzymatic hydrolysis conditions of different enzymes.

Enzyme	Alcalase	Papain	Neutrase	Trypsin	Keratinase	Flavourzyme	Protamex
pH	8	7	7	7	8.5	7	7
Temp. (°C)	50	45	50	40	55	50	55
Time (min)	180	180	180	180	180	180	180

3.2.8 Antimicrobial activity

The antimicrobial activity was explored according to the following procedure [31]. Briefly, *E. coli* (MG1655) was provided by the Department of Food Science, Henan Institute of Science and Technology (Xinxiang, Henan, China), and it was cultured to the exponential phase in Luria-Bertani (LB) broth medium, then diluted to OD_{600}

= 0.1. The lyophilized feather hydrolysates were diluted in 0.9% saline with different concentrations (5, 10, 50, 100, 150 and 200 mg/mL). 40 μL of hydrolysate dilution at varying concentrations and 160 μL of the bacterial dilution were added into the 96-well plates and then incubated for 12-24 h at 37 °C with shaking at 170 rpm. Positive control was to add 40 μL of mixed solution composed of penicillin (100 U/mL) and streptomycin (0.1 mg/mL), and negative control was adding the same volume of saline. Three duplicates were conducted, and the antimicrobial experiments were repeated at least twice. The bacterial growth was monitored by determining the absorbance at 600 nm with microplate reader (Synergy H1, BioTek, USA). The minimum inhibitory concentration (MIC) referred to the lowest peptide concentration at which no bacterial growth was observed.

3.2.9 Fractionation of feather hydrolysate obtained via keratinase

The lyophilized hydrolysate via keratinase was dissolved in distilled water (10 mg/mL) and fractionated by ultrafiltration. The fractions were collected separately by their different molecular weights (Mw: < 3 kDa, 3-5 kDa, 5-10 kDa and > 10 kDa) and lyophilized. The antimicrobial activity of different fractions with various concentrations was investigated as **section 3.2.8** described.

3.2.10 Nano-HPLC-MS/MS analysis

The fraction < 3 kDa acquired via keratinolysis were analyzed by online nano flow liquid chromatography tandem mass spectrometry via EASY-nanoLC 1200 system (Thermo Fisher Scientific, MA, USA) which was connected to Q Exactive™ Plus mass spectrometer (Thermo Fisher Scientific, MA, USA). Acclaim PepMap C18 (75 μm ×25 cm) as equilibrated with solvent A (A: 0.1% formic acid in water) and solvent B (B: 0.1% formic acid in ACN). 3 μL of sample was loaded and separated with 60 min-gradient at flow rate of 300 nL/min. The column temperature and electrospray voltage were 40 °C and 2 kV, respectively. The mass spectrometer was run under data dependent acquisition mode which was automatically switched between MS and MS/MS mode. The survey of full scan MS spectra (m/z 100-1500) was acquired in the Orbitrap with 70000 resolutions. The maximum injection time was 50 ms, and the top 20 most intense precursor ions were selected into collision cell for fragmentation by higher-energy collision dissociation, with collection energy of 28. The MS/MS resolution at 17500, the automatic gain control target at $1e^5$, the maximum injection time of 45 ms, isolation window of 2 m/z, and dynamic exclusion

of 30 s were set.

The tandem mass spectra obtained above were further processed by PEAKS Studio version X+ (Bioinformatics Solutions Inc., Waterloo, Canada). PEAKS DB was set up to search the Gallus gallus (version 201907, entries 18124) database. PEAKS DB were searched with a fragment ion mass tolerance of 0.02 Da and a parent ion tolerance of 7 ppm. Oxidation and Deamidation were specified as the variable modifications. The peptides with -10lgP ≥ 20 and the proteins with -10lgP ≥ 0 and containing at least 1 unique peptide were filtered. The hydrophobic ratio (HPR, %) of each peptide was obtained by calculating the proportion of hydrophobic amino acids.

3.2.11 Statistical analysis

Statistical analysis was performed using SPSS 17.0 software. Difference among mean values was established using the Duncan multiple range test (DMRT) at $P < 0.05$. All analyses were carried out in triplicate samples and the data are presented as mean ± standard deviation (SD).

3.3 Results and discussion

3.3.1 Effects of ICSE treatment on chicken feather

3.3.1.1 The recovery of ICSE chicken feather and disulfide analysis

ICSE technology, developed from traditional steam explosion, has been widely applied in biomass deconstruction. The saturated steam can penetrate organic tissue with powerful seepage force, and then seriously disrupt the internal structure by mechanical shearing force when given an instant decompression. Previously, it was found that the cracks and holes of feather enabled by steam explosion were conductive to the enzyme attack [20]. Therefore, it is meaningful to find an appropriate ICSE condition assisting with enzyme hydrolysis for antimicrobial-peptide production.

In the present study, chicken feather was gradually broken and became muddy and granular with the increase of pressure and maintaining time (**Figure 3.1A**). Under the conditions of 2.0 MPa-120 s and 2.5 MPa-120 s, the feather was almost liquified. In the study on improving digestibility of feather meal, the original structure of feather was found to be destroyed with lots of cracks and cavities emerging at 1.8 MPa-1 min [24]. With pressure and maintaining time increasing, the ICSE feather varied from white to dark yellow. The color change might result from the presence

of chromophores originating from the aromatic amino acids, such as tyrosine, phenylalanine and tryptophan [32]. The result showed that the yield decreased obviously with the liquefaction aggravation of feathers (**Figure 3.1B**). Similarly, about 17.9% of the initial wool mass was found to be lost via steam explosion treatment at 220 °C-10 min, which was probably result from the presence of non-proteinous materials and the incomplete recovery process [32]. To discharge pressure instantaneously, the cylinder was totally opened on a flat surface which was hard to collect small particles and liquid.

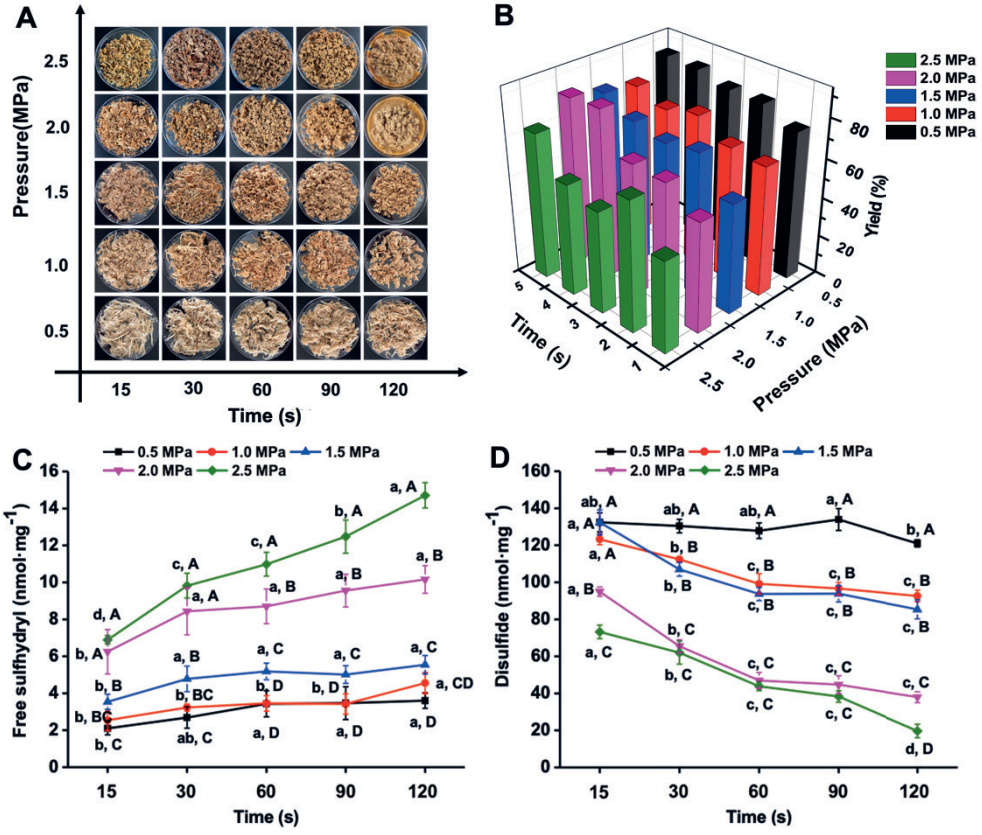

Figure 3.1. (A) Morphology of ICSE chicken feather, (B) recovery of chicken feather treated by ICSE at different pressures and times, (C) free sulfhydryl, and (D) disulfide content. The results are presented as the mean values ± SD, n = 3. The regression models of free sulfhydryl content and disulfide content were $Y = 4.215X_{pressure} + 0.028X_{time} - 1.874$ ($R^2_{adj} = 0.836$) and $Y = 172.401 - 42.025X_{pressure} - 0.337X_{time}$ ($R^2_{adj} = 0.872$), respectively. Different lowercase letters (a-d) indicate significant difference ($P < 0.05$) among ICSE samples treated at the same pressure with different times; different uppercase letters (A-E) indicate significant difference ($P < 0.05$) among ICSE samples treated at different pressures with the same time.

The massive disulfide bond cross-linking and the tight packing β-sheet in the polypeptide chain endowed feather keratin with high stability [25]. To further explore the effect of ICSE strength on feather structure, the contents of both disulfide and free sulfhydryl of CFP were assayed (**Figure 3.1C&D**). As result showed, the increase of pressure and maintaining time significantly increased the content of free sulfhydryl while decreased that of disulfide. Based on the liner regression analysis, pressure was found to be the main influence factor while the maintaining time made less effect. Taken together, ICSE treatment could effectively disrupt the structure of chicken feather. However, an appropriate condition needs to be determined which could moderately loosen keratin structure while without excessive degradation.

3.3.1.2 Analysis of soluble peptides and free amino acids

Keratin possesses plenty of intramolecular and intermolecular cystine cross-links, forming filamentous structures made of polypeptide chains folded into β-sheets which are stacked and twisted to form a helical structure [3]. This special structure endows feather keratin with insolubility and resistance to most proteolytic enzymes. In this study, peptides and FAA were determined to investigate the damage degree of ICSE to feather. The soluble peptide content showed an obvious upward trend with pressure and maintaining time increasing (**Figure 3.2A**). It was indicated that the increase in ICSE strength led to keratin cracking. By analyzing PMW, it was found that there were less solubilized peptides under 0.5 MPa, most of which might be susceptible fragments and amino acids with small size. The relative content of peptides from 2 to 5 kDa went up remarkably as the maintaining time was prolonged with pressure increasing from 1.0 MPa to 1.5 MPa. The reason possibly was that part of resistant and stable crosslinks, such as disulfide bonds and other covalent bonds, were deconstructed with relatively more large molecules producing. As we can see, there were more peptides from 2 to 5 kDa produced with pressure increased from 1 to 1.5 MPa. Under the conditions of 1.0 MPa-60/90/120 s and 1.5 MPa-30/60/90/120 s, more than 50% peptides over 2 kDa were produced. However, when the pressure further increased from 2 to 2.5 MPa, there were more small peptides from 0.5 to 2 kDa produced, indicating that severe conditions deconstructed keratin into smaller peptides. An ICSE condition under which keratin would not suffer from over-degradation should be chosen for peptides production.

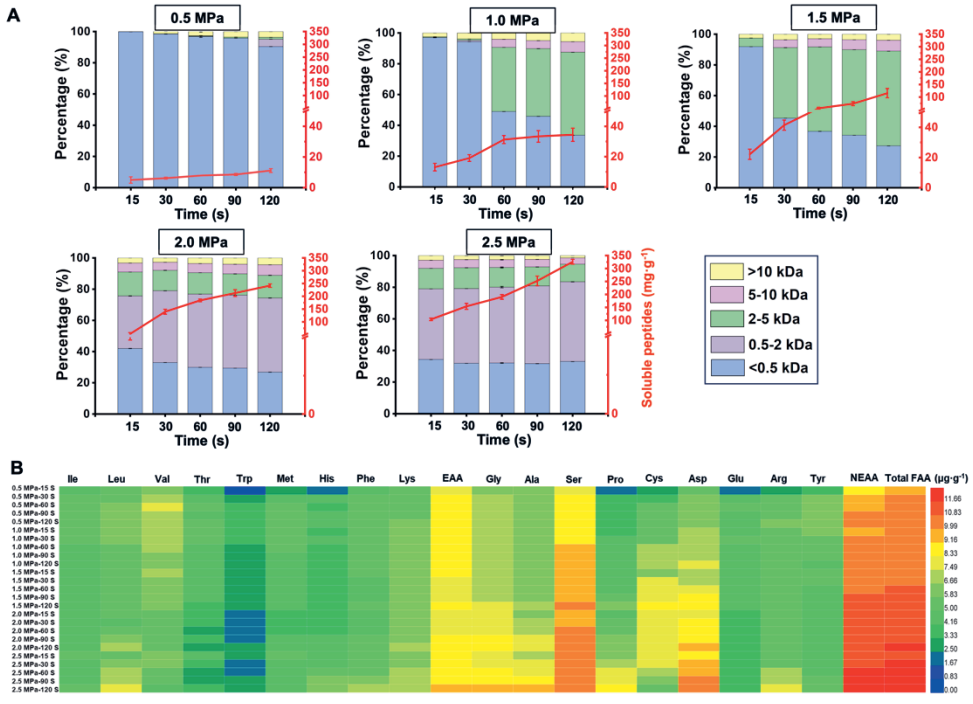

Figure 3.2. (A) The contents of soluble peptides and the relative distribution of peptides molecular weight, and (B) the contents of free amino acids in different ICSE samples. "EAA" represents the sum of Ile, Leu, Val, Thr, Trp, Met, His, Phe and Lys, while "NEAA" represents the sum of the rest amino acids. Values are normalized based on logarithm (log 2.0). The results are presented as the mean values ± SD, n = 3.

The increase of ICSE strength exhibited growing effect on producing FAA content in CFP (**Figure 3.2B**). When the ICSE pressure was over 2.0 MPa-60 s, there was more than 3000 ug·g^{-1} of FAA generated indicating a severe degradation. When the ICSE condition was 2.5 MPa-120 s, the FAA content reached 5754.71 ug·g^{-1} which was 8.5 times more than that at 0.5 MPa-15 s. In our study, most essential amino acids (EAA) in keratin were found to be less released by ICSE (varying from 238.98 to 618.35 ug·g^{-1}), while non-essential amino acids (NEAA) were much easier to be released from feather keratin (increased from 438.32 to 5136.37 ug·g^{-1}). Among EAA, free Leu and Lys improved slightly when increasing ICSE conditions, while free Thr, Trp and Val showed a slight descending which might result from thermal destruction [33]. Obviously, Ser, Asp, Gly, Cys and Pro were growingly released from feather keratin with ICSE conditions rising, becoming the main components of FAA, among which Ser, Asp and Gly were found to be easiest dissociated from feather keratin.

AMPs are majorly small cationic molecules and most of them (86%) are composed

of 11-50 amino acids [34-37]. That way, the ICSE condition should be selected based on the premise that feather keratin structure was loosened with less FAA and small peptides (< 2 kDa) produced, which might be helpful for enhancing the hydrolysate antimicrobial activity. With a view to soluble peptides and FAA, 1.5 MPa-120 s was chosen as the optimal condition for feather pretreatment.

3.3.2 Enzymatic hydrolysis of ICSE-CFP via different enzymes

The high stability and durability of keratin are attributed to its vast cross-linking with disulfide bonds, salt linkages, hydrogen bonds and so forth, and thus being resistant to common enzymes [33]. Keratinases were reported to be the only group of proteases that could attack and completely degrade highly intricate keratins [38]. However, the feather-degradation rate via keratinase only reached 47.56% after 1220 min [20]. In the present study, the hydrolysis capacity of keratinase and conventional proteases including protamex, alcalase, neutrase, papain, trypsin and flavourzyme were investigated based on ICSE pretreatment. The results showed that keratinase owned the best ability for feather deconstruction, following which were papain and alcalase, and the flavourzyme had weakest hydrolysis ability for feather keratin (**Figure 3.3A**). Based on the disruption of ICSE on feather structure, keratinase hydrolysis resulted in more than 90% of peptides dissolved within 3 h, and there were more than 90% of peptides with molecular weight less than 3 kDa, among which were about 60% of peptides below 500 Da (**Figure 3.3B**).

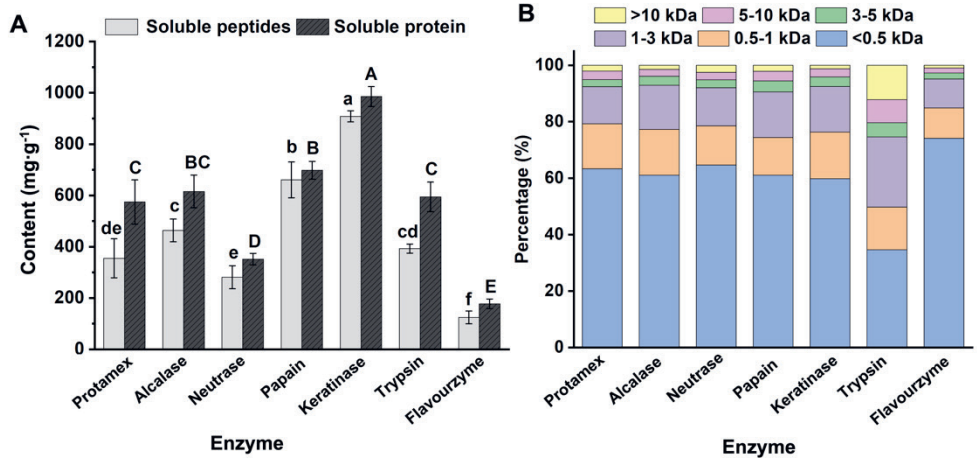

Figure 3.3. (A) Content of soluble peptides and protein, and (B) distribution of peptide molecular weight in different hydrolysates after ICSE treatment. The results are presented as the mean values ± SD, n = 3.

Different lowercase letters (a-f) indicate significant difference ($P < 0.05$) of soluble peptides among different hydrolysates by different enzymes; different uppercase letters (A-E) indicate significant difference ($P < 0.05$) of soluble protein among different hydrolysates via different enzymes.

Significantly, ICSE pretreatment facilitated hydrolysis of feather keratin. Most likely, the specific hydrophobic residues in raw feather were previously cleaved and thus making active sites accessible to keratinase. Similarly, in despite of lower deconstruction rate, the proteolysis via conventional proteases was also improved by ICSE. Two possible reasons for the low hydrolysis ability of conventional proteases, especially for flavourzyme, neutrase, protamex and trypsin, were the hinder of crosslinkings of disulfides and dominate hydrophobic residues in CFP. Yamamura et al. have proposed that keratinolysis involved a synergistic action of disulfide sulfitolysis and proteolysis [39], while most of conventional protease owned none process of disulfide reducing. The cross-linkages of keratin by disulfide bonds hindered its deconstruction by proteases. The hydrophilic Lys and Arg which were the sites at which conventional enzymes (e.g. trypsin) act were inaccessible in native keratin [40]. Especially for trypsin, large peptides were more observable than small peptides in hydrolysate, indicating a weakest keratin cleavage ability. Above all, ICSE treatment greatly improved the keratinolysis of chicken feather, and ICSE-keartinolysis process exhibited overwhelming advantage than conventional proteolysis for keratin peptides preparation.

3.3.3 The antimicrobial activity and the minimal inhabitation concentration of feather hydrolysates

Different cleavage sites might endow feather hydrolysate with promising antimicrobial activity based on the potential structure and sequence of feather keratin. Thus, the antimicrobial activity of different hydrolysate was explored. The result showed that the hydrolysate obtained via keratinase hydrolysis exhibited antimicrobial activity against *E. coli* (**Figure 3.4A**), while other hydrolysates could not inhibit *E. coli* growth. The difference between various enzymes might result from different cutting sites related to antimicrobial properties. Molecular weight, amino acid sequence, structural features like peptide helicity, hydrophobicity and combination of specific amino acids such as His, Arg, Ala, Val and Leu, were considered as the key factors for antimicrobial activity of peptides [41]. It has been reported that most of AMPs were cationic and hydrophobic amino acids [12, 42]. Typically, HKABF by Pichia pastoris, a kind of cationic peptide containing eight

cysteines engaged in four intramolecular disulfide bridges, was found to exhibit strong resistance against Staphylococcus aureus and Staphylococcus saprophyticus [43]. Keratinase possesses high specificity for hydrophobic residues (Met, Ala, Phe, Trp and Leu) and hydrophilic His which was absent in feather keratin though.

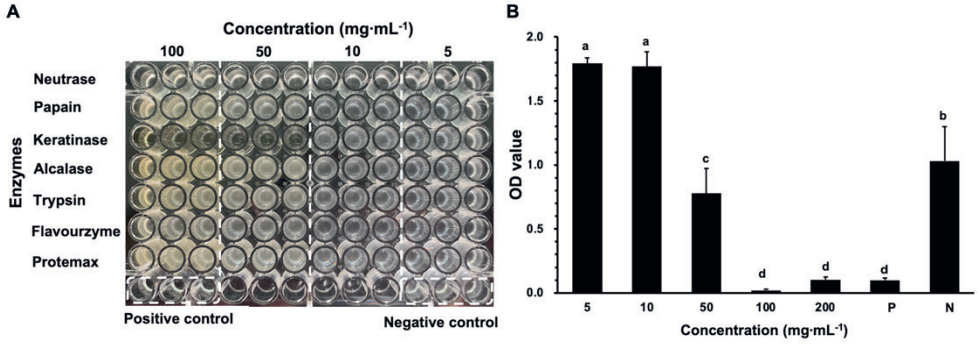

Figure 3.4. (A) The growth image of *E. coli* exposed to varying concentrations of keratin hydrolysates, and (B) the OD value of *E. coli* exposed to varying concentrations of keratin hydrolysates at 600 nm. The bacteria was cultured for 22 h, and the positive control was adding penicillin (100 U/mL) and streptomycin (0.1 mg/mL), while the negative control was adding same volume of saline. The results are presented as the mean values ± SD, n = 3. Different lowercase letters (a-d) indicate the significant difference ($P < 0.05$).

On the contrary, other common proteases could act on hydrophilic residues including Lys and Cly except for some hydrophobic residues [20]. In addition to abundant cationic Arg and special β-sheet fortified by Cys, the higher hydrophobicity of keratinase hydrolysate might be another key reason for its antimicrobial activity. The cationic peptide would interact with negatively charged components, such as lipoteichoic acids present on the bacteria cell membrane. The peptides-lipid interaction would further give rise to the formation of separation channel and disorganization of lipid bilayers, and then resulting in bacteria death. By exploring antimicrobial activity of keratinase hydrolysate at concentrations ranging from 5 to 200 mg/mL, it was found that the minimal inhabitation concentrate was 50 mg/mL (**Figure 3.4B**). Conversely, the limited effective cleavage of feather keratin by conventional proteases and the exposed hydrophilic residues were not conductive to inhibiting bacteria growth. Nevertheless, keratinase was promising for feather keratin hydrolysis and AMPs preparation.

In some previous studies, it has been found that the hydrolysates with molecular weight < 3 kDa expressed stronger activity against bacteria than larger hydrolysates,

such as the hydrolysate from fish waste and barred mackerel gelatin [10, 44]. Therefore, the keratinase hydrolysate would be separated into several fractions according to their molecular weight (< 3 kDa, 3-5 kDa, 5-10 kDa and > 10 kDa) to explore the antimicrobial mechanism.

3.3.4 Antimicrobial activity of keratin peptides with different molecular weight obtained via keratinase

To improve the purity of effective peptides and focus on the potential antimicrobial peptides, four fractions with different molecular weights were obtained by ultrafiltration. As expected, the peptides with molecular weight less than 3 kDa showed better inhibitory activity of *E. coli* than that of larger molecular weight (**Figure 3.5A**&**B**).

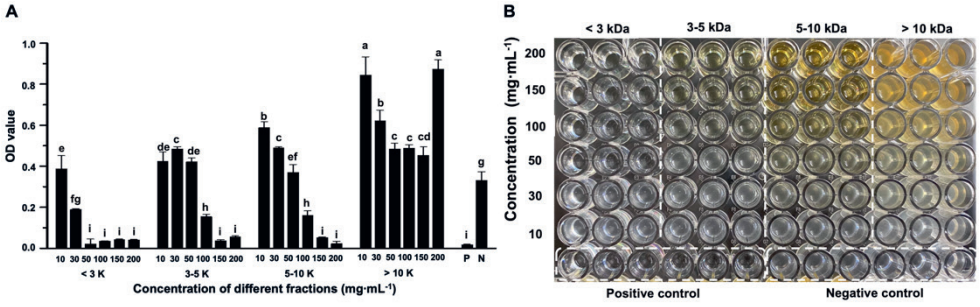

Figure 3.5. The inhibitory effect of keratin peptides on *E. coli*. (A) the OD value of *E. coli* exposed to varying concentrations of keratin peptides at 600 nm, and (B) the growth image of *E. coli* exposed to varying concentrations of keratin peptides. The keratin peptides were obtained by keratinase hydrolysis. The bacterial was cultured for 16 h, and the positive control was adding penicillin (100 U/mL) and streptomycin (0.1 mg/mL), while the negative control was adding same volume of saline. The results are presented as the mean values ± SD, n = 3. "a-i" indicate the significant difference ($P < 0.05$) in *E. coli* growth with different fractions at various concentrations.

Similarly, the most active AMPs of fish waste hydrolysate also emerged in the fraction smaller than 3 kDa, which has been proved to contain more hydrophobic amino acids compared to other fractions [44]. In the study on investigating the antimicrobial activity of peptides isolated from green juice alfalfa, the molecular weight of identified AMPs was distributed from 378-1220 Da, and the activity was presumably attributed to their specific amino acid composition, hydrophobicity and secondary structure [45]. The general characteristics of antimicrobial peptides include the load, structural diversity hydrophobicity and specific amino acid composition, such as His, Arg, Pro, Cys and Gly [46]. Previously, Nedjar-Arroume et al. have

illustrated that most of the active peptides in peptic hemoglobin hydrolysate were the shortest ones and perhaps acted with mechanism closer to parabens involving terminal tyrosyl group instead of by classical mechanism of antimicrobial peptides [41]. Nevertheless, the amino acids composition and sequence of keratin peptides < 3 kDa would be further studied to clarify their potential mechanism against *E.coli*.

What is more, the hydrolysate fraction from 3 to10 kDa also expressed antimicrobial activity at concentrations higher than 100 mg/mL. It might result from the presence of the peptide fragment with antimicrobial characteristics. The MIC of fraction < 3 kDa of CFP hydrolysate was 30 mg/mL and was higher than that of other hydrolysate (e.g. 0.5 mg/mL) reported in previous studies [10, 44]. There might be inactive peptides, other than AMPs, produced via ICSE treatment.

3.3.5 Amino acid composition of keratin peptides obtained via keratinase and distribution of peptides with different hydrophobic ratios in fraction < 3 kDa

By analyzing the composition of amino acids in four fractions, highest content of hydrophobic amino acids including Ala, Val, Ile, Leu, Phe etc. was found in the fraction < 3 kDa (**Figure 3.6A)**, and the total content of hydrophobic amino acids reached about 364.11 mg/g, which might contribute to its outstanding *E. coli* inhibitory ability as Pezeshk et al. have concluded, where a higher content of hydrophobic amino acids emerged in antimicrobial hydrolysate compared to non-antimicrobial fractions [44]. Additionally, the content of negatively charged amino acids, e.g. Asp and Glu, in fraction < 3 kDa (157.91 mg/g in total) was significantly lower than that in others ($P < 0.05$), while the positively charged amino acids were more. Specially, the contents of Cys, Gly, Phe and Leu in fraction < 3 kDa were significantly higher than other groups ($P < 0.05$). As reported, some peptides rich in Cys (e.g. insect defensin and drosomycin) and Gly (e.g. attacin and gloverin) owned significant antimicrobial capacity, while there were also Leu-rich AMPs (e.g. GLLSLLSLLGKLL) and Phe-rich peptide of FFFLSRIF that exihbited remarkable ability against bacteria, possibly owing to a highly hydropobic sequence [47, 48].

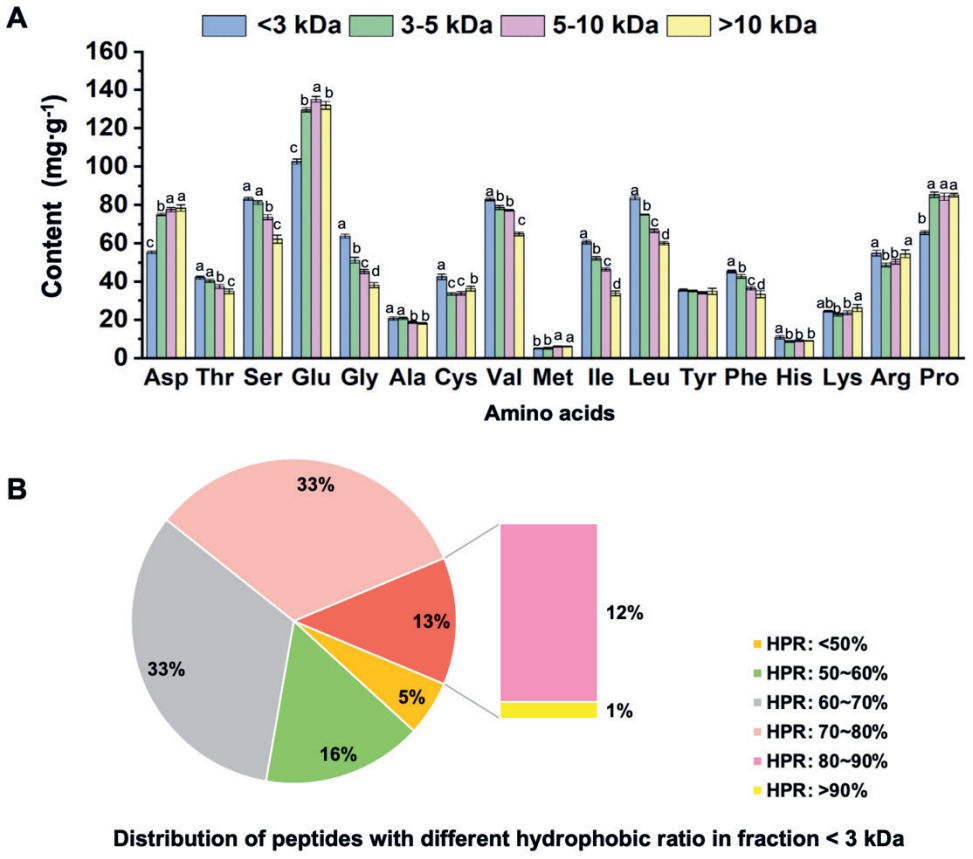

Figure 3.6. (A) Amino acid composition of different fractions, and (B) distribution of peptides with different hydrophobic ratio (HPR) in fraction < 3 kDa. The keratin peptides were obtained by keratinase hydrolysis. The results are presented as the mean values ± SD, n = 3. "a-d" indicate the significant difference ($P < 0.05$) in amino acid content among four fractions.

There were 182 of peptides identified in fraction < 3 kDa in total, with molecular weight ranging from 366.15 to 2516.44 (**Table S3.1**). Result showed that about 13% of peptides owned more than 80% hydrophobic residues (**Figure 3.6B**), among which the Pro-Val-Val-Val peptide with high hydrophobicity emerged. 79% of peptides were with HPR higher than 60%, such as Val-Val-Val-Thr-Leu-Pro-Gly-Pro-Ile-Leu, Val-Val-Thr-Leu-Pro-Gly-Pro-Ile-Leu, Pro-Ser-Pro-Val-Val-Val and so on. Manny AMPs are composed of abundant hydrophobic residues, 1-2 of which frequently appear in every 3-4 residues [49]. In the study on the antimicrobial activity of pepetides from Green Juice Alfalfa, most antimicrobial peptides were found to possess about 50% of hydrophobic residues [45]. In the present study, the better

antimicrobial activity of keratin peptides < 3 kDa could presumably be attributed to the high proportion of hydrophobic segments, which were probably inserted into the cell membrane of the bacteria, thus destabilizing water inlet and causing cell lysis.

Taken together, keratin hydrolysate via keratinolysis was found to be potential AMPs against *E.coli,* and the better antimicrobial activity, especially of peptides < 3 kDa, most likely result from the high hydrophobic ratio. In a future study, the antimicrobial activity action mechanism in which peptides are involved can be clarified after further separation, purification and identification. By comprehensively considering the resistance of feather keratin to enzymes and the efficiency of ICSE technology, the ICSE-keratinolysis process was promising for preparing AMPs against *E. coli*.

3.4 Conclusion

The present study demonstrated that feather structure was effectively damaged by ICSE treatment with lots of soluble peptides and FAA dissolved, and the ICSE condition at 1.5 MPa-120s could moderately destruct chicken feather without severe degradation. Assisted with ICSE pretreatment, keratinolysis greatly improved feather deconstruction, and its hydrolysate product exhibited remarkable inhibitory activity against *E. coli*, while the hydrolysates via conventional proteolysis showed no obvious anti-*E.coli* effect. Additionally, the fraction < 3 kDa in keratinolysis hydrolysate possessed best antimicrobial activity, probably owing to their high proportion of hydrophobic residues. The study provided an ICSE process for moderately destructing chicken feather in a short time involving no chemicals, and the keratin hydrolysate via keratinolysis could serve as a new alternative anti-*E.coli* product. Consequently, ICSE-keratinolysis process could be performed as an effective and eco-friendly way for converting renewable feather waste into value-added antimicrobial product, holding potential in improving economic value while reducing resource waste and environment pollution.

3.5 References

1. N.C. Barman, F.T. Zohora, K.C. Das, M.G. Mowla, N.A. Banu, M. Salimullah, A. Hashem, Production, partial optimization and characterization of keratinase enzyme by Arthrobacter sp. NFH5 isolated from soil samples, AMB Express, 7 (2017) 181.
2. K. Tamreihao, S. Mukherjee, R. Khunjamayum, L.J. Devi, R.S. Asem, D.S. Ningthoujam, Feather degradation by keratinolytic bacteria and biofertilizing potential for sustainable agricultural production, J Basic Microbiol, 59 (2019) 4-13.
3. R.B. Fraser, D.A. Parry, The structural basis of the filament-matrix texture in the avian/reptilian group of hard β-keratins, Journal of structural biology, 173 (2011) 391-405.
4. A. Shavandi, T.H. Silva, A.A. Bekhit, A.E.A. Bekhit, Keratin: dissolution, extraction and biomedical application, Biomater Sci, 5 (2017) 1699-1735.
5. M. Kaur, M. Arshad, A. Ullah, In-situ nanoreinforced green bionanomaterials from natural keratin and montmorillonite (MMT)/cellulose nanocrystals (CNC), ACS Sustainable Chemistry & Engineering, 6 (2018) 1977-1987.
6. Z. Xie, Q. Zhao, H. Wang, L. Wen, W. Li, X. Zhang, W. Lin, H. Li, Q. Xie, Y. Wang, Effects of antibacterial peptide combinations on growth performance, intestinal health, and immune function of broiler chickens, Poult Sci, 99 (2020) 6481-6492.
7. B.J. Muhialdin, N.F. Abdul Rani, A.S. Meor Hussin, Identification of antioxidant and antibacterial activities for the bioactive peptides generated from bitter beans (Parkia speciosa) via boiling and fermentation processes, Lwt, 131 (2020).
8. A. Osman, H.A. Goda, M. Abdel-Hamid, S.M. Badran, J. Otte, Antibacterial peptides generated by Alcalase hydrolysis of goat whey, LWT - Food Science and Technology, 65 (2016) 480-486.
9. R. Rekha, B. Vaseeharan, R. Ishwarya, M. Anjugam, S.A. N, S. Kadaikunnan, J.M. Khaled, M.N. Al-Anbr, M. Govindarajan, Searching for crab-borne antimicrobial peptides: Crustin from Portunus pelagicus triggers biofilm inhibition and immune responses of Artemia salina against GFP tagged Vibrio parahaemolyticus Dahv2, Mol Immunol, 101 (2018) 396-408.
10. A. Mirzapour-Kouhdasht, M. Moosavi-Nasab, Y.M. Kim, J.B. Eun, Antioxidant mechanism, antibacterial activity, and functional characterization of peptide fractions obtained from barred mackerel gelatin with a focus on application in carbonated beverages, Food Chem, 342 (2021) 128339.
11. Q.Q. Gu, S.W. He, L.H. Liu, G.H. Wang, D.F. Hao, H.M. Liu, C.B. Wang, C. Li, M. Zhang, N.Q. Li, A teleost bactericidal permeability-increasing protein-derived peptide that possesses a broad antibacterial spectrum and inhibits bacterial infection as well as human colon cancer cells growth, Dev Comp Immunol, 118 (2021) 103995.
12. K.L. Brown, R.E. Hancock, Cationic host defense (antimicrobial) peptides, Current opinion in immunology, 18 (2006) 24-30.
13. M. Scocchi, I. Zelezetsky, M. Benincasa, R. Gennaro, A. Mazzoli, A. Tossi, Structural aspects and biological properties of the cathelicidin PMAP-36, The FEBS journal, 272 (2005) 4398-4406.
14. V.J. Smith, J.M. Fernandes, G.D. Kemp, C. Hauton, Crustins: enigmatic WAP domain-containing antibacterial proteins from crustaceans, Developmental & Comparative Immunology, 32 (2008) 758-772.
15. A.F. Lacerda, É.A. Vasconcelos, P.B. Pelegrini, M.F. Grossi de Sa, Antifungal defensins and their role in plant defense, Frontiers in microbiology, 5 (2014) 116.

16. H. Xu, S. Cai, L. Xu, Y. Yang, Water-stable three-dimensional ultrafine fibrous scaffolds from keratin for cartilage tissue engineering, Langmuir, 30 (2014) 8461-8470.
17. H. Xu, Z. Shi, N. Reddy, Y. Yang, Intrinsically water-stable keratin nanoparticles and their in vivo biodistribution for targeted delivery, J Agric Food Chem, 62 (2014) 9145-9150.
18. R. Nakata, Y. Osumi, S. Miyagawa, A. Tachibana, T. Tanabe, Preparation of keratin and chemically modified keratin hydrogels and their evaluation as cell substrate with drug releasing ability, J Biosci Bioeng, 120 (2015) 111-116.
19. S. Han, T.R. Ham, S. Haque, J.L. Sparks, J.M. Saul, Alkylation of human hair keratin for tunable hydrogel erosion and drug delivery in tissue engineering applications, Acta Biomater, 23 (2015) 201-213.
20. L. Guo, L. Lu, M. Yin, R. Yang, Z. Zhang, W. Zhao, Valorization of refractory keratinous waste using a new and sustainable bio-catalysis, Chemical Engineering Journal, 397 (2020).
21. Q. Shen, C. Zhang, W. Jia, X. Qin, X. Xu, M. Ye, H. Mo, A. Richel, Liquefaction of chicken sternal cartilage by steam explosion to isolate chondroitin sulfate, Carbohydrate polymers, 215 (2019) 73-81.
22. X. Qin, Q. Shen, Y. Guo, J. Liu, H. Zhang, W. Jia, X. Xu, C. Zhang, An advanced strategy for efficient recycling of bovine bone: Preparing high-valued bone powder via instant catapult steam-explosion, Food Chem, 374 (2022) 131614.
23. W. Zhao, R. Yang, Y. Zhang, L. Wu, Sustainable and practical utilization of feather keratin by an innovative physicochemical pretreatment: high density steam flash-explosion, Green Chemistry, 14 (2012).
24. Y. Zhang, R. Yang, W. Zhao, Improving digestibility of feather meal by steam flash explosion, J Agric Food Chem, 62 (2014) 2745-2751.
25. Y. Zhang, W. Zhao, R. Yang, Steam Flash Explosion Assisted Dissolution of Keratin from Feathers, ACS Sustainable Chemistry & Engineering, 3 (2015) 2036-2042.
26. O.H. Lowry, N.J. Rosebrough, A.L. Farr, R.J. Randall, Protein measurement with the Folin phenol reagent, Journal of biological chemistry, 193 (1951) 265-275.
27. G.B. Irvine, C. Shaw, High-performance gel permeation chromatography of proteins and peptides on columns of TSK-G2000-SW and TSK-G3000-SW: a volatile solvent giving separation based on charge and size of polypeptides, Analytical biochemistry, 155 (1986) 141-148.
28. K.Y. Chan, B.P. Wasserman, Direct Colorimetric Assay of Free Thiol Groups and Disulfide Bonds in Suspensions of Solubilized and Particulate Cereal Proteins, Cereal Chemistry, 70 (1993) 22-26.
29. Thannhauser, T. W.; Konishi, Y., Scheraga, H.A., Analysis for disulfide bonds in peptides and proteins. Disulfide Bonds in Peptides and Proteins, 143 (1987) 115-119.
30. M. Ye, W. Jia, C. Zhang, Q. Shen, L. Zhu, L. Wang, Preparation, identification and molecular docking study of novel osteoblast proliferation-promoting peptides from yak (Bos grunniens) bones, RSC advances, 9 (2019) 14627-14637.
31. Z. Li, Y. Yuan, S. Li, B. Deng, Y. Wang, Antibacterial activity of a scorpion-derived peptide and its derivatives in vitro and in vivo, Toxicon, 186 (2020) 35-41.
32. Tonin, C.; Zoccola, M., Aluigi, A., Varesano, A., Montarsolo, A., Vineis, C., Zimbardi, F., Study on the conversion of wool keratin by steam explosion. Biomacromolecules, 7 (2006) 3499-3504.
33. R. Sharma, S. Devi, Versatility and commercial status of microbial keratinases: a review, Reviews in Environmental Science and Bio/Technology, 17 (2017) 19-45.

34. G. Wang, Database-Guided Discovery of Potent Peptides to Combat HIV-1 or Superbugs, Pharmaceuticals (Basel), 6 (2013) 728-758.
35. D. Pisuttharachai, F.F. Fagutao, M. Yasuike, H. Aono, Y. Yano, K. Murakami, H. Kondo, T. Aoki, I. Hirono, Characterization of crustin antimicrobial proteins from Japanese spiny lobster Panulirus japonicus, Dev Comp Immunol, 33 (2009) 1049-1054.
36. T. Li, Q. Liu, H. Chen, J. Li, Antibacterial activity and mechanism of the cell-penetrating peptide CF-14 on the gram-negative bacteria, Escherichia coli, Fish Shellfish Immunol, 100 (2020) 489-495.
37. J.Y. Niu, I.X. Yin, W.K.K. Wu, Q.L. Li, M.L. Mei, C.H. Chu, Antimicrobial peptides for the prevention and treatment of dental caries: A concise review, Arch Oral Biol, 122 (2021) 105022.
38. R. Gupta, P. Ramnani, Microbial keratinases and their prospective applications: an overview, Appl Microbiol Biotechnol, 70 (2006) 21-33.
39. S. Yamamura, Y. Morita, Q. Hasan, K. Yokoyama, E. Tamiya, Keratin degradation: a cooperative action of two enzymes from Stenotrophomonas sp, Biochemical and Biophysical Research Communications, 294 (2002) 1138-1143.
40. P. Ramnani, R. Gupta, Keratinases vis-à-vis conventional proteases and feather degradation, World Journal of Microbiology and Biotechnology, 23 (2007) 1537-1540.
41. N. Nedjar-Arroume, V. Dubois-Delval, E.Y. Adje, J. Traisnel, F. Krier, P. Mary, M. Kouach, G. Briand, D. Guillochon, Bovine hemoglobin: an attractive source of antibacterial peptides, Peptides, 29 (2008) 969-977.
42. P. Bulet, R. Stöcklin, L. Menin, Anti-microbial peptides: from invertebrates to vertebrates, Immunological reviews, 198 (2004) 169-184.
43. L. Wang, C.-e. Lai, Q. Wu, J. Liu, M. Zhou, Z. Ren, D. Sun, S. Chen, A. Xu, Production and characterization of a novel antimicrobial peptide HKABF by Pichia pastoris, Process Biochemistry, 43 (2008) 1124-1131.
44. S. Pezeshk, S.M. Ojagh, M. Rezaei, B. Shabanpour, Fractionation of Protein Hydrolysates of Fish Waste Using Membrane Ultrafiltration: Investigation of Antibacterial and Antioxidant Activities, Probiotics Antimicrob Proteins, 11 (2019) 1015-1022.
45. S. Kobbi, R. Balti, A. Bougatef, G. Le Flem, L. Firdaous, M. Bigan, G. Chataigné, S. Chaabouni, P. Dhulster, N. Nedjar, Antibacterial activity of novel peptides isolated from protein hydrolysates of RuBisCO purified from green juice alfalfa, Journal of Functional Foods, 18 (2015) 703-713.
46. D. Andreu, L. Rivas, Animal antimicrobial peptides: an overview, Peptide Science, 47 (1998) 415-433.
47. B. Mishra, G. Wang, Ab initio design of potent anti-MRSA peptides based on database filtering technology, Journal of the American Chemical Society, 134 (2012) 12426-12429.
48. F. Abbassi, O. Lequin, C. Piesse, N. Goasdoue, T. Foulon, P. Nicolas, A. Ladram, Temporin-SHf, a new type of phe-rich and hydrophobic ultrashort antimicrobial peptide, J Biol Chem, 285 (2010) 16880-16892.
49. A. Schmidtchen, M. Pasupuleti, M. Malmsten, Effect of hydrophobic modifications in antimicrobial peptides, Adv Colloid Interface Sci, 205 (2014) 265-274.

3.6 Supplementary materials

Table S3.1. The sequence description of keratin peptides in fraction < 3 kDa derived from feather keratin.

No.	Sequence	Length	Mass	hydrophobic ratio (%)
1	V.GSIL.S	4	388.23	75.00
2	P.VVVT.L	4	416.26	75.00
3	S.PVVV.T	4	412.27	100.00
4	R.FSGR.R	4	465.23	50.00
5	S.SGGF.G	4	366.15	75.00
6	V.PISSG.G	5	459.23	60.00
7	P.SPVVV.T	5	499.30	80.00
8	F.GISGL.G	5	445.25	80.00
9	A.AVGSI.L	5	445.25	80.00
10	P.GPILS.S	5	485.28	80.00
11	T.LPGPI.L	5	495.31	80.00
12	S.PVVVT.L	5	513.32	80.00
13	L.PGPILS.S	6	564.33	83.33
14	S.RVVIQP.S	6	710.44	66.67
15	C.QDSRVV.I	6	702.37	33.33
16	I.LSSFPQ.N	6	734.36	50.00
17	G.FGISGL.G	6	592.32	83.33
18	E.EGVPIS.S	6	600.31	66.67
19	P.ISSGGF.G	6	566.27	33.33
20	S.RVVIQP.S	6	709.46	66.67
21	Q.PSPVVV.T	6	596.35	83.33
22	L.GSRFSG.R	6	609.29	50.00
23	S.SGGFGI.S	6	536.26	83.33
24	L.PGPILS.S	6	582.34	83.33
25	R.VVIQPS.P	6	641.37	66.67
26	V.PISSGGF.G	7	663.32	71.43
27	L.GSRFSGR.R	7	765.39	42.86
28	D.SRVVIQP.S	7	796.49	57.14
29	E.GVPISSG.G	7	615.32	71.43
30	F.GISGLGS.R	7	589.31	71.43
31	T.LPGPILS.S	7	695.42	85.71
32	V.TLPGPIL.S	7	708.45	71.43
33	V.TLPGPIL.S	7	709.44	71.43
34	S.RVVIQPS.P	7	797.48	57.14
35	S.STSAAVG.S	7	591.29	57.14
36	L.SEEGVPI.S	7	729.35	57.14
37	R.VVIQPSPV.V	8	836.51	75.00
38	V.IQPSPVVV.T	8	894.52	75.00

39	S.RVVIQPSP.V	8	876.52	62.50
40	V.IQPSPVVV.T	8	908.53	75.00
41	T.LPGPILSS.F	8	839.48	75.00
42	V.TLPGPILS.S	8	796.47	75.00
43	F.GISGLGSR.F	8	745.41	62.50
44	V.IQPSPVVV.T	8	837.50	75.00
45	D.SRVVIQPS.P	8	884.51	50.00
46	R.VVIQPSPV.V	8	837.50	75.00
47	L.SEEGVPIS.S	8	816.39	50.00
48	V.TLPGPILS.S	8	795.49	75.00
49	I.SSGGFGIS.G	8	710.32	62.50
50	G.PILSSFPQ.N	8	887.48	62.50
51	C.QDSRVVIQ.P	8	943.51	37.50
52	S.GLGSRFSGR.R	9	935.49	55.56
53	S.RVVIQPSPV.V	9	975.59	66.67
54	S.RVVIQPSPV.V	9	993.60	66.67
55	L.SEEGVPISS.G	9	903.42	44.44
56	P.GPILSSFPQ.N	9	944.50	66.67
57	V.VTLPGPILS.S	9	938.54	77.78
58	D.SRVVIQPSP.V	9	963.55	55.56
59	V.VTLPGPILS.S	9	952.56	77.78
60	S.RVVIQPSPV.V	9	1050.62	66.67
61	S.RVVIQPSPV.V	9	1036.60	66.67
62	F.GISGLGSRF.S	9	891.49	66.67
63	V.VTLPGPILS.S	9	966.58	77.78
64	S.TSAAVGSIL.S	9	817.45	66.67
65	V.TLPGPILSS.F	9	883.50	66.67
66	R.VVIQPSPVV.V	9	936.56	77.78
67	E.GVPISSGGF.G	9	819.41	77.78
68	V.VVTLPGPIL.S	9	907.57	88.89
69	D.SRVVIQPSP.V	9	981.56	55.56
70	F.GISGLGSRF.S	9	892.48	66.67
71	V.IQPSPVVVT.L	9	938.54	77.78
72	V.VTLPGPILS.S	9	895.54	77.78
73	S.RVVIQPSPVV.V	10	1092.67	70.00
74	R.VVIQPSPVVV.T	10	1035.63	80.00
75	L.PGPILSSFPQ.N	10	1041.55	70.00
76	I.SGLGSRFSGR.R	10	1022.53	50.00
77	D.SRVVIQPSPV.V	10	1080.63	60.00
78	G.GFGISGLGSR.F	10	949.50	70.00
79	C.VRQCQDSRVV.I	10	1242.61	30.00
80	S.STSAAVGSIL.S	10	904.49	60.00
81	D.SRVVIQPSPV.V	10	1062.62	60.00

82	V.VVTLPGPILS.S	10	1065.64	80.00
83	V.VVTLPGPILS.S	10	994.61	80.00
84	R.VVIQPSPVVV.T	10	1017.62	80.00
85	D.SRVVIQPSPV.V	10	1079.65	60.00
86	P.VVVTLPGPIL.S	10	988.63	90.00
87	S.RVVIQPSPVVV.T	11	1191.73	72.73
88	S.RVVIQPSPVVV.T	11	1234.74	72.73
89	S.GGFGISGLGSR.F	11	1006.52	72.73
90	S.RVVIQPSPVVV.T	11	1223.72	72.73
91	P.VVVTLPGPILS.S	11	1093.67	81.82
92	S.RVVIQPSPVVV.T	11	1262.77	72.73
93	S.RVVIQPSPVVV.T	11	1223.72	72.73
94	V.VVTLPGPILSS.F	11	1081.64	72.73
95	T.LPGPILSSFPQ.N	11	1154.63	72.73
96	R.VVIQPSPVVVT.L	11	1136.68	72.73
97	S.RVVIQPSPVVV.T	11	1173.72	72.73
98	A.CVRQCQDSRVV.I	11	1274.59	27.27
99	S.RVVIQPSPVVV.T	11	1219.73	72.73
100	S.RVVIQPSPVVV.T	11	1175.74	72.73
101	S.RVVIQPSPVVV.T	11	1248.76	72.73
102	T.LPGPILSSFPQ.N	11	1392.86	72.73
103	S.RVVIQPSPVVV.T	11	1161.72	72.73
104	V.VTLPGPILSSF.P	11	1128.65	72.73
105	V.VVTLPGPILSS.F	11	1065.64	72.73
106	S.RVVIQPSPVVV.T	11	1190.75	72.73
107	S.RVVIQPSPVVV.T	11	1233.74	72.73
108	D.SRVVIQPSPVV.V	11	1179.70	63.64
109	A.CVRQCQDSRVV.I	11	1257.62	27.27
110	S.RVVIQPSPVVV.T	11	1205.71	72.73
111	D.SRVVIQPSPVVV.T	12	1278.77	66.67
112	D.SRVVIQPSPVVV.T	12	1260.76	66.67
113	D.SRVVIQPSPVVV.T	12	1321.77	66.67
114	L.SEEGVPISSGGF.G	12	1164.53	50.00
115	D.SRVVIQPSPVVV.T	12	1320.78	66.67
116	T.LPGPILSSFPQN.T	12	1268.68	66.67
117	S.GGFGISGLGSRF.S	12	1153.59	75.00
118	P.VVVTLPGPILSS.F	12	1180.71	75.00
119	F.GISGLGSRFSGR.R	12	1192.63	58.33
120	D.SRVVIQPSPVVV.T	12	1335.79	66.67
121	D.SRVVIQPSPVVV.T	12	1306.76	66.67
122	D.SRVVIQPSPVVV.T	12	1306.80	66.67
123	S.PVVVTLPGPILS.S	12	1190.73	83.33
124	S.RVVIQPSPVVVT.L	12	1349.80	66.67

125	D.SRVVIQPSPVVV.T	12	1310.76	66.67
126	D.SRVVIQPSPVVV.T	12	1292.78	66.67
127	D.SRVVIQPSPVVV.T	12	1248.76	66.67
128	S.RVVIQPSPVVVT.L	12	1292.78	66.67
129	C.QDSRVVIQPSPV.V	12	1323.71	50.00
130	S.RVVIQPSPVVVT.L	12	1406.82	66.67
131	D.SRVVIQPSPVVV.T	12	1276.75	66.67
132	P.SPVVVTLPGPIL.S	12	1190.73	83.33
133	D.SRVVIQPSPVVV.T	12	1292.75	66.67
134	C.QDSRVVIQPSPV.V	12	1306.69	50.00
135	D.SRVVIQPSPVVV.T	12	1260.76	66.67
136	G.GFGISGLGSRFS.G	12	1240.62	66.67
137	C.FDLCRPCGPTPL.A	12	1527.82	58.33
138	V.TLPGPILSSFPQ.N	12	1255.68	66.67
139	V.TLPGPILSSFPQ.N	12	1237.67	66.67
140	C.QDSRVVIQPSPV.V	12	1380.74	50.00
141	G.SILSEEGVPISS.G	12	1216.62	50.00
142	Q.DSRVVIQPSPVVV.T	13	1393.79	61.54
143	V.VTLPGPILSSFPQ.N	13	1354.75	69.23
144	Q.DSRVVIQPSPVVV.T	13	1464.83	61.54
145	D.SRVVIQPSPVVVT.L	13	1379.81	61.54
146	P.SPVVVTLPGPILS.S	13	1277.76	76.92
147	Q.DSRVVIQPSPVVV.T	13	1450.81	61.54
148	L.PGPILSSFPQNTL.V	13	1369.72	61.54
149	S.RVVIQPSPVVVTL.P	13	1389.87	69.23
150	L.PGPILSSFPQNTL.V	13	1386.75	61.54
151	Q.PSPVVVTLPGPILS.S	14	1374.81	78.57
152	C.QDSRVVIQPSPVVV.T	14	1578.87	57.14
153	D.SRVVIQPSPVVVTL.P	14	1492.90	64.29
154	C.QDSRVVIQPSPVVV.T	14	1503.84	57.14
155	C.QDSRVVIQPSPVVV.T	14	1521.85	57.14
156	C.QDSRVVIQPSPVVV.T	14	1504.83	57.14
157	D.SRVVIQPSPVVVTL.P	14	1609.90	64.29
158	V.VVTLPGPILSSFPQ.N	14	1453.82	71.43
159	Q.DSRVVIQPSPVVVT.L	14	1494.84	57.14
160	G.GFGISGLGSRFSGR.R	14	1396.72	64.29
161	D.SRVVIQPSPVVVTL.P	14	1476.90	64.29
162	Q.CQDSRVVIQPSPVVV.T	15	1649.86	53.33
163	S.GGFGISGLGSRFSGR.R	15	1453.74	66.67
164	D.SRVVIQPSPVVVTLP.G	15	1595.96	66.67
165	V.IQPSPVVVTLPGPIL.S	15	1528.92	80.00
166	S.RVVIQPSPVVVTLPG.P	15	1559.94	73.33
167	D.SRVVIQPSPVVVTLPG.P	16	1646.97	68.75

168	R.QCQDSRVVIQPSPVVV.T	16	1718.93	50.00
169	V.IQPSPVVVTLPGPILS.S	16	1615.95	75.00
170	V.VIQPSPVVVTLPGPILS.S	17	1715.02	76.47
171	R.VVIQPSPVVVTLPGPILS.S	18	1814.09	77.78
172	S.RVVIQPSPVVVTLPGPIL.S	18	1883.16	77.78
173	S.RVVIQPSPVVVTLPGPIL.S	18	1882.18	77.78
174	S.RVVIQPSPVVVTLPGPILS.S	19	1970.19	73.68
175	A.CVRQCQDSRVVIQPSPVVV.T	19	2094.07	47.37
176	A.CVRQCQDSRVVIQPSPVVV.T	19	2077.11	47.37
177	D.SRVVIQPSPVVVTLPGPILS.S	20	2057.22	70.00
178	D.SRVVIQPSPVVVTLPGPILS.S	20	2039.21	70.00
179	L.SEEGVPISSGGFGISGLGSRF.S	21	2201.05	61.90
180	L.SEEGVPISSGGFGISGLGSRFS.G	22	2126.03	59.09
181	D.SRVVIQPSPVVVTLPGPILSSFPQ.N	24	2516.44	66.67
182	L.SEEGVPISSGGFGISGLGSRFSGRR.C	25	2495.25	56.00

4

CHAPTER 4

Enhanced delivery of biomolecules into Caco2 cells based on the cell-penetrating ability of keratin peptides

Submitted as: Xiaojie Qin, Ruilin Li, Yujie Guo, Johannes H. Bitter, Elinor L. Scott, Chunhui Zhang (2024). Enhanced delivery of biomolecules into Caco2 cells based on the cell-penetrating ability of keratin peptides.

Abstract

Keratin, as a promising bioresource, possesses significant potential for diverse biological applications due to its favorable biocompatibility, low toxicity, biodegradability and cell-adhesion ability. However, there are few studies on the cell-penetrating ability of keratin peptides (KEP) for biomolecule delivery. Therefore, this study explored the cell-penetrating ability of KEP with different molecular weights (Mw) on Caco2 cells using fluorescein-labeled insulin (FITC-INS) as the target intracellular biomolecule. The potential cell-penetrating mechanism was elaborated by combining cellular investigation with the physicochemical characterization of KEP. The result shows that the KEP < 3 kDa (KEP1) exhibited the highest cell-penetrating ability at 2 mg/mL, allowing efficient delivery of FITC-INS into Caco2 cells without covalent bonding. The cellular uptake mechanism was energy-dependent, mainly involving macropinocytosis. The further fractionation of KEP1 reveals that the most effective components consisted of 8-19 amino acids, including specific hydrophobic peptides (e.g. RVVIEPSPVVV and IIIQPSPVVV), PP Ⅱ amphipathic peptides (e.g. PPPVVVTFP and FIQPPPVVV) and Cys-rich peptides (e.g. LCAPTPCGPTPL and CLPCRPCGPTPL). Additionally, analysis of the secondary and tertiary structure and amino acid composition illustrated that KEP1 exhibited rich hydrophobic residues and disulfide bonds which probably contributed to its cell-penetrating ability, as opposed to its small particle size and electrostatic interactions. This study reveals the cell-penetrating ability of keratin peptides, thus highlighting their potential as vehicles for delivering biomolecules in a non-covalent way.

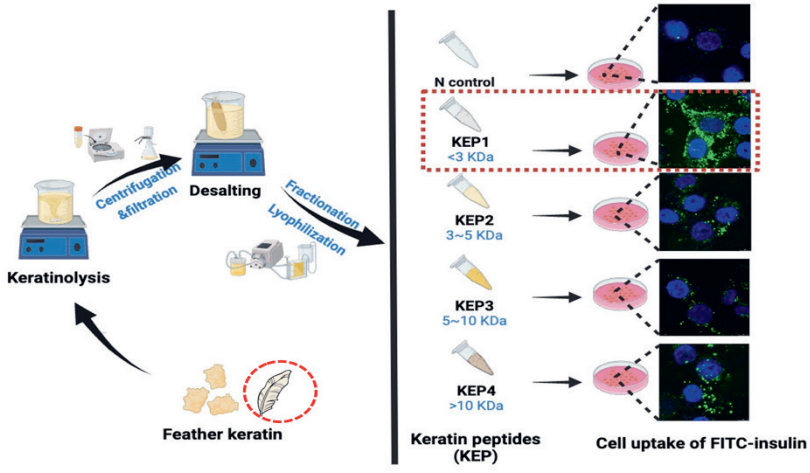

4.1 Introduction

The development and production of new therapeutic proteins and peptides have been on the rise due to recent breakthroughs in biotechnology and molecular engineering. However, significant challenges exist in achieving efficient delivery of proteinaceous molecules through the biological membrane or into cells due to their non- lipophilicity resulting in low permeation [1]. The current techniques for enhancing biomolecule delivery, such as viral vectors and membrane perturbation, have been reported with high toxicity, immunogenicity and low-efficiency [2]. In recent years, several novel approaches have emerged for improving the delivery penetration and efficiency of biomolecules, including chemical modification, combining with cell-penetrating peptides (CPPs), loading by polymeric or mucoadhesive vehicles as reviews by Rehmani and Dixon [1]. Over the last two decades, over 100 CPPs have been discovered and recognized as potent transepithelial vectors for transporting biomolecules across biological membranes [1], receiving growing attention from researchers.

CPPs, also known as protein transduction domains, are relatively small functional carrier peptides generally comprised of 5-30 amino acids that can penetrate biological membranes and transport diverse molecules into cells [2]. CPPs could be categorized into three classes based on physicochemical properties: cationic, amphipathic and hydrophobic [3-5]. Cationic CPPs are often rich in positively charged amino acid residues (e.g. Arg and Lys), demonstrating good cytoplastic membrane affinity that can bind to negatively charged glycoproteins on the membrane surface by electrostatic interactions, such as transcription activator protein (Tat) and octa-arginine R8 [6, 7]. Amphipathic CPPs often contain both a non-polar region enriched with hydrophobic amino acids and a cationic, anionic or polar region, such as GALA (WEAALAEALAEALAEHLAEALAEALEALAA) and P28 (LSTAADM-QGVVTDGMASGLDKDYLKPDD) [8, 9]. Hydrophobic CPPs are mainly constructed of a larger number of hydrophobic residues in their structure which are possibly responsible for both a low net charge and high cell membrane affinity. When biomolecules are attached to the CPP, they can penetrate intact and subsequently become internalized into cells [10, 11]. There are two ways of conjugating biomolecules to CPPs: non-covalent and covalent binding. The first approach mainly depends on electrostatic interactions between CPPs and biomolecules, which has been widely applied due to its high flexibility [12]. The co-administration of CPPs and insulin as a

physical mixture without intermolecular crosslinking has been found to enhance intestinal insulin absorption [13]. Their non-invasive ability to enter cells without disrupting cell membrane integrity sets them apart from traditional techniques like microinjection and electroporation [14], making them a safe and highly efficient option. Therefore, CPPs are promising vehicles for non-covalently delivering biomolecules into cells.

Keratin is a natural biomass that holds great potential for use in biological applications, because of its biocompatibility, low toxicity and biodegradability. An earlier study has suggested that the tripeptides structure of "Arg-Gly-Asp" and "Leu-Asp-Val" presented in keratin could bind to cell surface ligands, thereby promoting cell adhesion [15]. Subsequently, keratin nanoparticles were found to successfully penetrate into kidney and liver cells, demonstrating a positive capability for attachment and proliferation [16]. In a previous investigation, we found that the keratin hydrolysates produced through keratinolysis with instant catapult steam explosion (ICSE) displayed an antimicrobial effect [17]. This effectiveness was attributed to the high presence of hydrophobic residues and certain peptides (e.g. Leu-rich peptides). The antimicrobial peptides (AMPs) and CPPs often share common physicochemical characteristics, including cationic residues, hydrophobicity and amphipathicity [18, 19]. Due to the functional similarity between CPPs and AMPs, it was demonstrated that CPPs could act as antimicrobial peptides, e.g. Tat and TP10 [20, 21], and AMPs can serve as drug delivery vehicles, e.g. Buforin and Tachyplesin [22, 23]. Thus, we hypothesize that keratin hydrolysates may possess the ability to alter cellular permeability, which could improve the delivery of biomolecules into cells, known as cell-penetrating ability.

This study aims 1) to verify our hypothesis that keratin peptides (KEP) may possess the cell-penetrating ability, thereby altering cell membrane permeability and improving delivering intracellular molecules into cells; 2) to clarify the possible cell-penetrating mechanism through a combination of cell experiments and physicochemical characterization. Here, fluorescein-labeled insulin (FITC-INS) was used as the target intracellular molecule for investigating the cell-penetrating ability of KEP. First, the cytotoxicity and cellular uptake of FITC-INS delivered by KEP with different molecular weights were investigated. Then, the physicochemical properties of KEP, such as peptide identification, chemical structure, secondary structure, tertiary structure and amino acid composition, were comprehensively

investigated, which may provide insights into their ability to penetrate cell membranes.

4.2 Materials and methods

4.2.1 Materials and chemicals

Chicken feathers were supplied by the Institute of Animal Science of the Chinese Academy of Agricultural Science (Beijing, China). Feathers were completely cleaned with food-grade detergent and distilled water, then dried at 50 °C for 48 h. Keratinase was provided by Shanghai Yuanye Bio-Technology Co., Ltd (Shanghai, China). Fluorescein isothiocyanate labelled insulin (FITC-INS, 95%) Insulin was supplied by Taigu Biotechnology Co., Ltd (Nanjing, China). Other chemicals, including chlorpromazine, colchicine, amiloride hydrochloride and methyl-beta-cyclodextrin (M-β-CD), acetonitrile (ACN) and so on, were of analytical grade supplied by Beijing Solarbio Science & Technology Co., Ltd (Beijing, China).

4.2.2 Preparation of keratin peptides with different molecular weights

Feather keratin was extracted using the cysteine reduction method assisted with ultrasonic as described in our previous study [24]. Keratin was enzymatically hydrolyzed with keratinase at 6000 units/g, pH 8.5, 55 °C. The keratin hydrolysate was obtained by centrifugation at 8000 ×g for 30 min and further filtration through 0.45 μm filters. Then, the obtained supernatant was dialyzed with a molecular weight cutoff (MwCO, 100 Da) for 48 h in distilled water at 4 °C. Keratin peptides (KEP) with molecular weight of < 3 kDa, 3-5 kDa, 5-10 kDa and > 10 kDa were further obtained via ultrafiltration and lyophilization, named as KEP1, KEP2, KEP3 and KEP4, respectively.

The KEP1 exhibiting the highest cell-penetrating ability was subjected to a Sephadex G-25 column (26 mm × 780 mm) for further fractionation and purification (fraction1, 2, 3 and 4). The column was equilibrated and eluted with ultrapure water at a flow rate of 0.5 mL/min and monitored at 220 nm via a UV detector (HD-97-1, Shanghai Jiapeng Technology Co., Ltd., China).

4.2.3 Cell-penetrating ability of KEP

4.2.3.1 Cell culture

In this study, Caco-2 cells were used for investigating the insulin uptake intervened by KEP. Caco-2 cells were purchased from iCell Bioscience Inc., (Shanghai, China) and cultured in T-25 flasks with Dulbecco's Modified Eagle's Medium (DMEM) in an incubator at 37 °C under 5% CO_2. The DMEM was supplemented with 10% fetal bovine serum [25]. The following steps were performed when the cells filled the flask.

4.2.3.2 Cytotoxicity

The cytotoxicity of KEP on Caco-2 cells was evaluated by CCK-8 assay. Briefly, the cells were seeded in a 96-well plate (4×10^3 cells/well) and cultured at 37 °C under 5% CO_2 overnight. Subsequently, the culture medium was replaced by fresh media including KEP samples at various concentrations (0, 0.1, 0.5, 1, 2, 5 and 8 mg/mL). After 2 h incubation, the cells were washed three times with HBSS and refilled with 100 μL of fresh DMEM. 10 μL of CCK-8 reagent was added and the cells were further incubated for another 3 h. Finally, the absorbance (A_{sample}) was measured at 450 nm via a microplate reader (SPARK10M TECAN, Switzerland). The blank was the absorbance (A_{blank}) of cells treated without KEP. The relative cell viability was then calculated with the following formula (1):

$$\text{Cell viability (\%)} = A_{sample}/A_{blank} \times 100 \qquad (1)$$

4.2.3.3 Cellular uptake

After washing by HBSS and digestion by 0.25% trypsin, the Caco-2 cells obtained from **section 4.2.3.1** were seeded onto 96-well plates at a density of 4×10^3 cells/well and cultured overnight. The culture medium was replaced with 200 μL fresh culture medium containing KEP samples (KEP1, KEP2, KEP3 and KEP4) at different concentrations (0, 0.1, 0.5, 1, 2 and 5 mg/ml) and 50 μg/mL of FITC-INS. Meanwhile, the N-control treated without KEP was conducted. After incubation at 37 °C for 2 h, cells were washed with HBSS three times and resuspended. The fluorescence intensity of cells was measured at λ_{ex} 495 nm and λ_{em} 519 nm by a fluorescence microplate reader (SPARK10M TECAN, Switzerland).

To further test the FITC-INS uptake, Caco-2 cells were seeded into a glass-bottomed cell dish (5×10^5 cells/well) and cultured under the same conditions as described above. Then, the cells were immediately fixed by adding paraformaldehyde (4%)

and then stained with Hoechst33342 (10 μg/mL) for 15 min. The cells were washed three times using HBSS. Finally, the cellular uptake was imaged by confocal laser scanning microscopy (CLSM, FV1200 Olympus, Japan) at 100× magnification.

4.2.3.4 Cellular uptake mechanism

The physical and pharmacological inhibitors, including low temperature (4 °C), chlorpromazine (10 ug/mL), colchicine (5 ug/mL), amiloride hydrochloride (0.3 mg/mL) and methyl-β-cyclodextrin (M-β-CD, 5 mg/mL), were applied to investigate the cellular uptake mechanism of insulin delivered by KEP. The cells were seeded onto 96-well plates at a density of 4×10^3 cells/well and cultured overnight. The cells were treated with each inhibitor for 1 h and then were washed with HBSS three times. After that, fresh DMEM containing KEP (2 mg/mL) and FITC-INS (50 μg/mL) were added and the cells were further incubated for 2 h. After the washing steps, the fluorescence intensity of the cells was measured as **section 4.2.3.2** mentioned. Caco-2 cells were cultured at a temperature of 4 °C for 1 h to treat the low-temperature group. They were then incubated with KEP at 4 °C for 2 h. The control group, which did not involve any inhibitors, was incubated with KEP and FITC-INS at a temperature of 37 °C. The N-control group, on the other hand, was only incubated with FITC-INS at 37 °C.

4.2.4 KEP characterization

The chemical structure was analyzed via a Fourier transform infrared spectroscopy (FTIR, Vertex 70, Bruker Inc., U.S.). KEP were ground with dried potassium bromide and pressed into a 1 mm pellet. Then it was scanned from 400 to 4000 cm^{-1} with a resolution of 4 cm^{-1}.

The intrinsic fluorescence was measured through a Cary Eclipse Fluorimeter (Agilent Technologies, Inc., U.S.). KEP was diluted to 0.25 mg/mL with PBS buffer (pH 7.0, 10 mM). The excitation wavelength was 280 nm to excite tryptophan. The emission spectra were obtained by scanning samples from 290 nm to 450 nm at a speed of 240 nm/min. The excitation and emission slits were set at 5 nm. Each spectrum was the average of three scans and corrected with blank.

The secondary structure was assessed through circular dichroism (CD, Jasco J-815, Jasco Inc., Japan). KEP were dispersed in PBS buffer (pH 7.0, 10 mM) with a concentration of 0.25 mg/mL. Ten scans were recorded and averaged with

wavelengths ranging from 185nm to 260 nm at scanning speed of 50 nm/min at 20 °C. The blank PBS buffer was performed for baseline subtraction. The CD fitting software, BeStSel, was used for calculating the secondary structure contents, including β-sheet, α-helix and β-turns [26].

Particle size was measured using dynamic light scattering (Nano ZetasSizer, Malvern Instruments, UK). KEP were dispersed in distilled water at concentration of 0.1 mg/mL and detected at 25 °C.

4.2.5 Analysis of amino acids composition

The composition of total amino acids in KEP was assessed via peroxidation and acid hydrolysis method as described in our previous study [24]. Briefly, KEP was accurately weighted and dispersed in 2 mL of ice-cold performic acid solution. The mixture was stored in the fridge at 4 °C for 16 h, and the 0.3 mL ice-cold hydrobromic acid was added. After 30 min ice-incubation, the mixture was dried with a nitrogen blowing device, and then was hydrolyzed with 10 mL of HCl (6 M, containing 0.1% phenol) at 110 °C for 24 h. Subsequently, the hydrolysate was filtered and diluted to 50 mL, after which 1 mL of diluted hydrolysate was dried via nitrogen at 37 °C. The dried samples were then redissolved in 0.02 M HCl and filtered using 0.22 μm filters. Finally, the samples were determined through HPLC (Thermo Fisher Ultrimate 3000, USA), after pre-derivatization.

4.2.6 Nano-HPLC-MS/MS analysis

The fraction 1 presenting the highest cell-penetrating capacity was further analyzed by online nanoflow liquid chromatography tandem mass spectrometry using a EASY-NANOLC 1200 system (Thermo Fisher Scientific, MA, USA) which was connected to Q Exactive™ Plus mass spectrometer (Thermo Fisher Scientific, MA, USA) according to our previous method [17]. The solvent A (A: 0.1% formic acid in water) and solvent B (B: 0.1% formic acid in ACN) were used for equilibrating acclaim PepMap C18 (75 μm ×25 cm). The column temperature, electrospray voltage and flow rate were set as 40 °C, 2 kV, and 300 nL/min, respectively. The mass spectrometer was run under data dependent acquisition (DDA) mode, and automatically switched between MS and MS/MS mode. The Orbitrap was used to obtain full-scan MS spectra with a resolution of 70000 in the m/z range of 100-1500. Precursor ions with the top 20 highest intensities were selected for fragmentation by higher-energy collision dissociation in the collision cell, with a collection energy of

28 and a maximum injection time of 50 ms. MS/MS spectra were acquired with a resolution of 17500, an automatic gain control target of $1e^5$, a maximum injection time of 45 ms, an isolation window of 2 m/z, and dynamic exclusion of 30 s.

The tandem mass spectra acquired previously underwent further processing using PEAKS Studio version X+ (Bioinformatics Solutions Inc., Waterloo, Canada). The PEAKS DB search was configured to look into the Gallus gallus database (version 201907, entries 18124) with a fragment ion mass tolerance of 0.02 Da and a parent ion tolerance of 7 ppm. Variable modifications specified were oxidation and deamidation. Peptides with -10lgP ≥ 20 and proteins with -10lgP ≥ 0 and at least one unique peptide were filtered.

4.2.7 Statistics

SPSS 17.0 software was utilized for statistical analysis. The Duncan multiple range test (DMRT) at $P < 0.05$ was conducted to determine differences among mean values. The analysis was performed on triplicate samples and the results are presented as mean values ± standard deviation (SD).

4.3 Results and discussion

4.3.1 Cytotoxicity and cell-penetrating ability of keratin peptides

In this study, FITC-INS was applied as the target biomolecule for investigating the cell-penetrating ability of KEP. The initial step was to investigate the cell toxicity of KEP with different molecular weights to assess their applicability to drug delivery. The cell viability of KEP at varying concentrations from 0.1 to 8 mg/mL was demonstrated in **Figure 4.1A**. Four KEP samples at concentrations ≤ 2 mg/mL showed cell viability higher than 90%, indicating a low cytotoxicity. As the KEP concentration increased over 5 mg/mL, the cell viability dropped below 90%, among which KEP1 led to significantly lower cell viability < 80% than other groups. In short, KEP presented low cytotoxicity at concentrations ≤ 2 mg/mL, indicating their applicability at low concentrations, while high concentration (> 5 mg/mL) should be avoided.

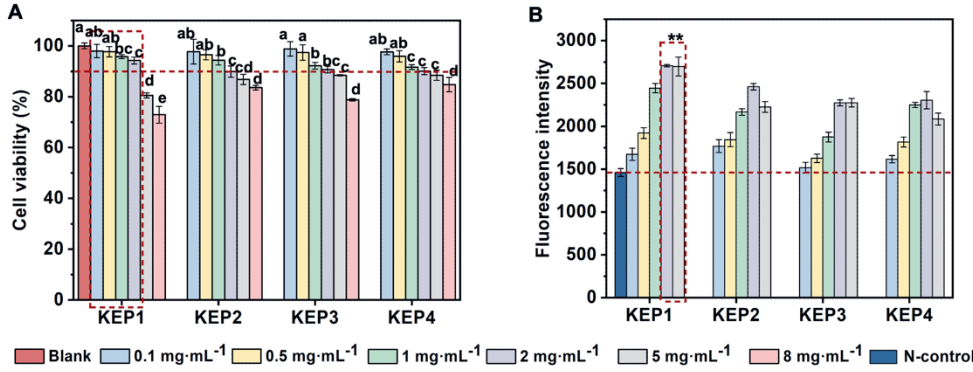

Figure 4.1. (A)The cytotoxicity of KEP at varying concentrations (0.1-8 mg/mL), and (B) the uptake efficiency of FITC-INS into Caco2 cells delivered by different KEP at varying concentrations (0.1-5 mg/mL). KEP includes KEP1 (< 3 kDa), KEP2 (3-5 kDa), KEP3 (5-10 kDa) and KEP4 (>10 kDa). The results are presented as the mean values ± SD, n = 3. "a-e" indicate the significance in cell viability between different concentrations for each KEP ($P < 0.05$), and "**" indicates the significance in fluorescence intensity with N-control ($P < 0.001$). N-control represents the treating with FITC-INS without adding KEP.

Based on the cytotoxicity result above, the effectiveness of KEP in delivering FITC-INS into cells was explored at concentrations from 0.1 to 5 mg/mL. As depicted in **Figure 4.1B**, the fluorescence intensities of treatments with KEP were higher than that of N-control, and the concentrations ≥ 1 mg/mL led to significant increases. It indicates that four KEP samples can improve FITC-INS cellular uptake compared to the N-control group, especially at high concentrations ≥ 1 mg/mL. Among the four samples, KEP1 presented relatively higher fluorescence intensity than other groups, which reached the peak at 2 mg/mL. It indicates the higher efficiency of KEP1 in improving FITC-INS cellular uptake. Additionally, CLSM was applied to visualize the cellular uptake of FITC-INS, which are shown in **Figure 4.2&4.3**. As illustrated in **Figure 4.2**, four KEP groups presented higher fluorescence density than N-control, and those of KEP1 treatments were more obvious. It indicates that FITC-INS cellular uptake was obviously improved by KEP, and KEP1 had a better capability. By the concentration investigation of KEP1 (**Figure 4.3**), an increase in FITC-INS density was found at higher concentrations of KEP1, which was consistent with the result of **Figure 4.1B**.

In brief, KEP was proven to have low cytotoxicity and a positive effect on delivering FITC-INS into cells, among which KEP1 was the most effective and had the potential in altering cellular permeability.

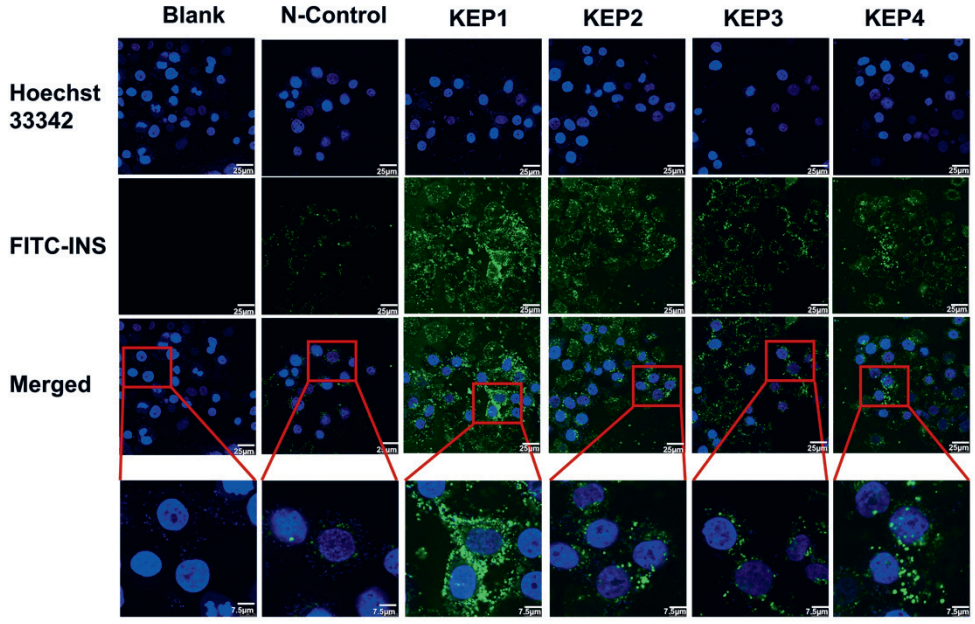

Figure 4.2. CLSM images of the translocation of FITC-INS into Caco2 cells. The cells were incubated for 2 h at 37 °C with KEP1 (< 3 kDa), KEP2 (3-5 kDa), KEP3 (5-10 kDa) and KEP4 (> 10 kDa) at 2 mg/mL.

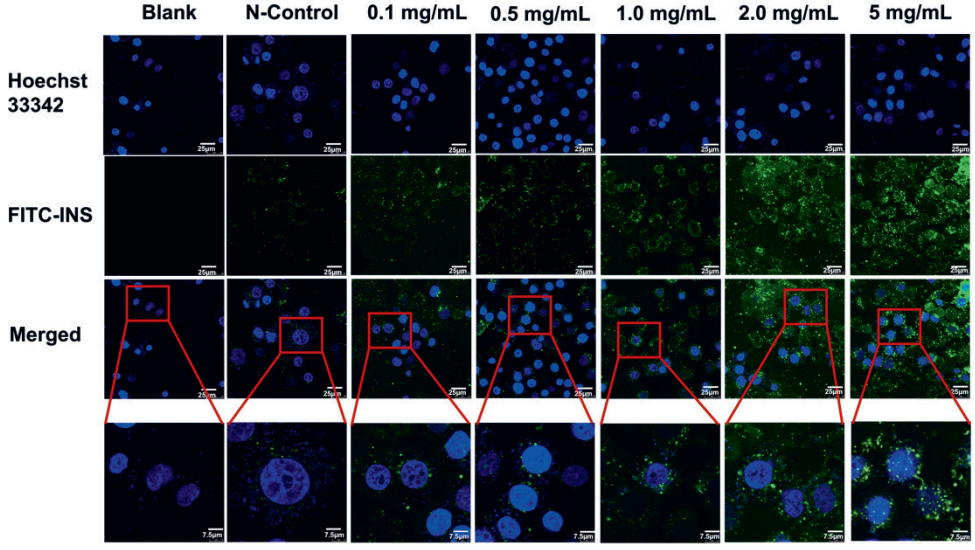

Figure 4.3. CLSM images of the translocation of FITC-INS into Caco2 cells. The cells were incubated for 2 h at 37 °C with KEP1 (< 3 kDa) at various concentrations (0.1, 0.5, 1.0, 2.0 and 5.0 mg/mL).

4.3.2 Cellular uptake mechanism

As reported, there are three possible mechanisms for CPPs internalization: endocytosis, direct penetration and translocation through forming a transitory structure [2]. According to previous literatures [27, 28], exposure to low temperature (4 °C) can cause a reduction in membrane fluidity and depletion of energy. Chlorpromazine is effective in inhibiting clathrin-mediated endocytosis, while colchicine could hinder pinocytosis. Amiloride hydrochloride is another inhibitor for macropinocytosis, and M-β-CD is often utilized to block caveolae/lipid-raft-mediated endocytosis. To explore the cellular internalization pathway of KEP, the cellular uptake of FITC-INS in the presence of those endocytosis inhibitors was conducted.

The results depicting FITC-INS uptake by KEP delivery under various treatments are presented in **Figure 4.4A-D**. Among four KEP samples, the treatments with colchicine, amiloride hydrochloride, M-β-CD and low temperature decreased the fluorescence intensity compared to control. It indicates the similar cellular paths of four KEP samples. Low-temperature treatment was the most effective in decreasing fluorescence intensity, which was even lower than the N-control group ($P < 0.05$). It means that the cellular uptake of FITC-INS delivered by KEP is energy-dependent. The decrease in FITC-INS uptake by colchicine and amiloride hydrochloride indicates a macropinocytosis penetration mechanism. For KEP1 (**Figure 4.4A**), the fluorescence intensity treated with M-β-CD was significantly lower than the control, implying an inhibitory effect on FITC-INS cellular uptake through cavernous-dependent endocytosis by disrupting lipid rafts [29]. However, chlorpromazine, as the inhibitor of clathrin-mediated endocytosis, showed no significant effect on FITC-INS cellular uptake ($P > 0.05$). It has been reported that the endocytosis pathway was the dominant mechanism of CPP internalization, which is not probable for highly cationic CPPs [30]. The results illustrate that KEP possibly contains a great number of amphiphilic or hydrophobic CPPs.

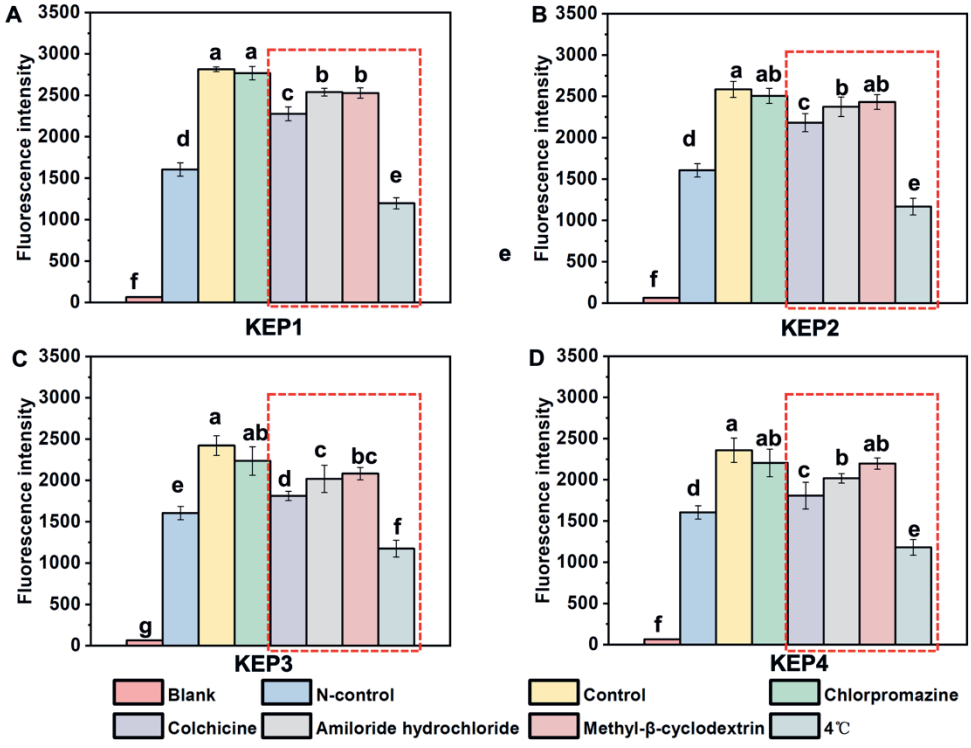

Figure 4.4. Cellular uptake of FITC-INS delivered by (A) KEP1 (< 3 kDa), (B) KEP2 (3-5 kDa), (C) KEP3 (5-10 kDa) and (D) (> 10 kDa) under different inhibitors. The results are presented as the mean values ± SD, n = 3. The lowercase letters "a-g" indicate the significant difference between samples treated with various inhibitors ($P < 0.05$).

Thus, the mechanism of KEP in delivering insulin is energy-dependent mainly involving macropinocytosis, which is probably attributed to the amphiphilic and hydrophobic composition.

4.3.3 Fractionation and identification of KEP1

Here we focus on further characterization of the most bioactive molecules from KEP1 where fractionation and peptide characterization of KEP1 was performed to provide insight to elucidate reasons for bioactivity. KEP1 was fractionated into 4 separate fractions (**Figure S4.1**). The cytotoxicity and cellular uptake of FITC-INS of the 4 fractions are shown in **Figure 4.5A&B**. As depicted in **Figure 4.5B**, fraction1 presented significantly higher fluorescence intensity than other groups at concentrations ≥ 0.8 mg/mL, indicating a superior capacity in delivering FITC-INS into cells. Meanwhile, the cell viability of fraction 1 at concentrations ranging from

0.1 to 1 mg/mL was higher than 90% (**Figure 4.5A**), implying its applicability. The results reveal that the effective peptides/domains mainly exist in fraction1 with relatively large molecular weight and exhibit low cytotoxicity.

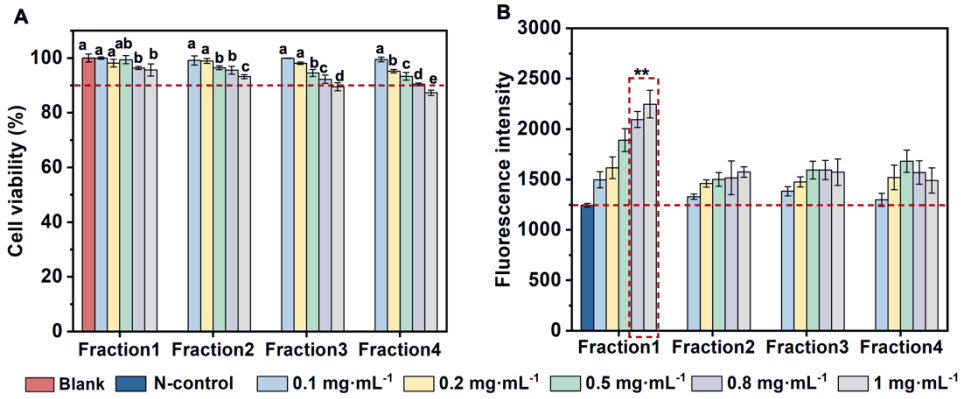

Figure 4.5. (A)The cytotoxicity and (B) the uptake efficiency of FITC-INS into Caco2 cells delivered by four fractions from KEP1 at varying concentrations (0.1-1 mg/mL). The results are presented as the mean values ± SD, n = 3. "a-e" indicate the significance in cell viability between different concentrations for each fraction ($P < 0.05$), and "**" indicates the significance in fluorescence intensity with N-control ($P < 0.001$). N-control represents the treatment with FITC-INS without adding KEP.

The peptides composition and sequences of fraction1 were further analyzed and are shown in **Table 4.1**. 24 kinds of peptides derived from chicken feather keratin were identified with molecular weights ranging from 837.40 to 2003.89 consisting of 8-19 amino acids (**Table 4.1**). These peptide lengths fall within the previously reported range of 5 to 30 amino acids, which are known to exhibit cell-penetrating property [2]. As inferred in **section 4.3.2**, the majority of the identified peptides were found to be amphipathic and hydrophobic in nature. These peptides are primarily composed of fewer positively charged amino acid residues such as Arg (R), His (H), and Lys (K). Amphipathic CPPs include both anionic and cationic peptides and are further categorized into 4 classifications: 1) primary amphipathic peptides with defined hydrophobic and cationic domains; 2) secondary amphipathic peptides forming α-helix with one hydrophobic face and one hydrophilic face; 3) amphipathic β-sheet peptides owning a hydrophobic stretch and a hydrophilic stretch; 4) Pro-rich amphipathic peptides containing polyproline Ⅱ (PP Ⅱ) structures [31-33]. Hydrophobic CPPs contain mainly hydrophobic residues or have a notable hydrophobic stretch, which might contribute to a low net charge and high cell membrane affinity.

Table 4.1. The sequences of peptides identified from fraction1 of KEP1 by Nano-HPLC-MS/MS.

No.	Sequence	Length	Mass	Hydrophobic ratio (%)
1	F.DLSGFGSR.Y	8	837.40	25.0
2	Q.PPPVVVTFP.G	9	951.54	88.89
3	A.FIQPPPVVV.T	9	994.59	88.89
4	R.VVIQPSSVVV.T	10	1025.61	70.00
5	T.IVIEPSPVVV.T	10	1050.63	80.00
6	T.IIIQPSPVVV.T	10	1064.65	80.00
7	V.PISSGGFGGFGL.S	12	1094.54	41.67
8	F.PGPILSSCPQE.S	11	1127.52	45.45
9	L.STAGVPISSGGSL.G	13	1131.58	38.46
10	S.TVVIQPSPVVV.T	11	1137.66	72.73
11	Q.VVIQPSTVVVT.L	11	1140.68	63.64
12	**D.LCAPTPCGPTPL.A**	12	1168.56	58.33
13	V.PISSGGFGLSGFG.S	13	1181.57	38.46
14	C.VPSPCGASGPTPL.A	13	1181.58	53.85
15	S.RVVIEPSPVVV.T	11	1192.72	72.73
16	Q.GPGPERDYSPY.Y	11	1236.54	27.27
17	L.PGPILSSYPQST.T	12	1246.61	41.67
18	**Q.CLPCRPCGPTPL.A**	12	1255.59	50.00
19	V.GSILSQEGVPISS.G	13	1272.66	38.46
20	S.RVVIQPSSVVVT.L	12	1282.76	58.33
21	F.PGPILSSFPQNAV.V	13	1326.68	61.54
22	L.PGPILSSFPQNTA.V	13	1327.68	53.85
23	F.PGPILSSSPQYAAV.G	14	1386.70	57.14
24	**C.GPTPLANSCNELCVRQCQA.S**	19	2003.89	36.84

As shown in **Table 4.1**, various peptides exhibiting typical characteristics of CPPs were discovered. Several amphipathic peptides with a combination of cationic Arg residues and hydrophobic domains were identified, including RVVIEPSPVVV and RVVIQPSSVVVT (in blue text in **Table 4.1**). The PP Ⅱ amphipathic peptides, namely PPPVVVTFP and FIQPPPVVV (in green text in **Table 4.1**), were also observed with abundant hydrophobic residues. Many peptides with a high ratio of hydrophobic residues included Val, Ile and Pro, such as VVIQPSSVVV, IVIEPSPVVV, IIIQPSPVVV, TVVIQPSPVVV and VVIQPSTVVVT (in red text in **Table 4.1**). These might hold potential for affecting cellular permeability. As interfacial active peptides, these hydrophobic and amphipathic peptides possibly perturb the membrane structure at the contact interface by selectively activating small GTPases, leading to actin network reconstruction and lamellipodia formation [34].

Additionally, the presence of abundant disulfide bonds has been identified as a crucial factor in the cell-penetrating ability of peptides. Previous studies have found that the disulfide-rich and anionic peptide rT7 (CVSSGIVDACSECCEPDKCIIMLPTWPPRYVCSV) derived from Hibiscus sabdariffa could penetrate cells [35]. This ability was attributed to the "inside-out" feature caused by the cystine scaffold formed via Cys connections, forcing the hydrophobic side chains to point outwards. Moreover, the presence of Pro residues further enhanced the penetrating ability of rT7. In this study, Cys-rich peptides LCAPTPCGPTPL, CLPCRPCGPTPL and GPTPLANSCNELCVRQCQA (in **bold** font in **Table 4.1**) were also observed, which likely played a combined role in enhancing the cell penetrating ability of KEP1.

Overall, the specific composition of amphipathic and hydrophobic peptides probably endowed KEP1 with promising cell-penetrating ability which further led to a higher insulin delivery ability into Caco2 cells.

4.3.4 Physicochemical characterization of KEP

4.3.4.1 Particle size and intrinsic fluorescence

The physicochemical properties of KEP were investigated to clarify their possible effect on cell-penetrating ability. KEP with different molecular weights were assessed mainly with particle size, chemical structure, secondary structure, tertiary structure and amino acids composition. These would assist in a more comprehensively understanding of the cell-penetrating ability of KEP1.

Particle size has been taken as a critical factor affecting the bioavailability of drug vehicles following oral exposure, as larger particles may encounter steric barriers within the mucosal network leading to reduced efficacy. Therefore, optimizing particle size is often necessary to achieve higher efficacy of drug delivery [36]. Nanoparticles have been reported to possess excellent biological interactions, including biodistribution, permeation, cellular uptake and so on, resulting from the properties of small size, large surface area, shape modulation and high surface functionality [37-41]. The result of particle size analysis is presented in **Figure 4.6A**. As shown in the figure, KEP4 exhibited the smallest average particle size at approximately 132 nm, while KEP3 had the largest size at around 849 nm. KEP1 and KEP2 showed similar average particle sizes, measuring 376 and 397 nm, respectively. Additionally, KEP1, KEP2 and KEP3 tended to aggregate, with the peaks shifting

towards the right. KEP3 displayed a significant peak at around 1000 nm, indicating a higher level of aggregation or crosslinking. Despite the smaller particle size of KEP4, it was not found to have higher cell-penetrating ability compared to other KEPs as discussed in **section 4.3.1**. Hence, there was no observed correlation between smaller particle size and increased cell-penetrating ability in KEP.

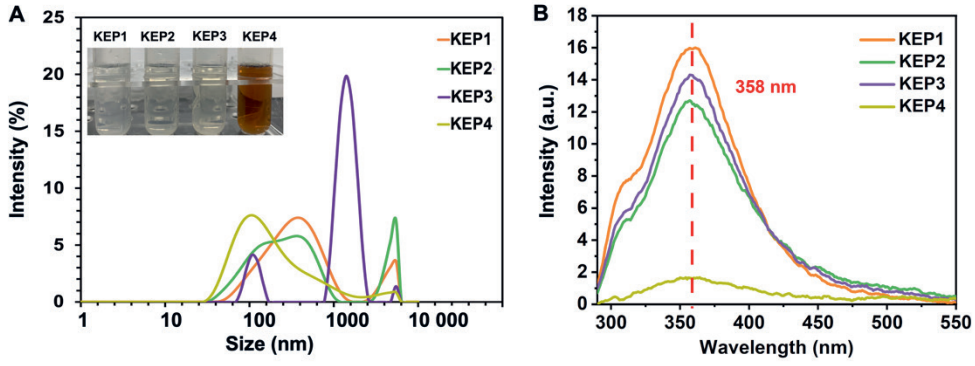

Figure 4.6. (A) Particle size distribution and (B) intrinsic fluorescence spectrum of KEP1 (< 3 kDa), KEP2 (3-5 kDa), KEP3 (5-10 kDa) and KEP4 (>10 kDa).

Analysis of the tertiary structure was performed using the intrinsic fluorescence spectrum, which is closely associated with the Trp residue. The result is shown in **Figure 4.6B**. The findings reveal that all four KEP samples exhibited similar characteristic fluorescence at 358 nm without significant variation. However, there was a notable difference in the intensity of fluorescence. The fluorescence intensity of KEP2 and KEP3 was considerably lower compared to KEP1. In a study on the noncovalent conjugation of phytosterols with bovine serum albumin (BSA), it was found that hydrogen bonds and hydrophobic forces played a crucial role in quenching the fluorescence of BSA [42]. The reduced fluorescence intensity observed in KEP2 and KEP3 was proposed to be due to an increase in hydrophobic interactions, which resulted in the quenching of Trp fluorescence. Such an effect has been observed in a study on pea protein which found that the aggregates formed by hydrophobic residues led to the reburying of Trp, presenting decreased fluorescence intensity [43]. Here, the higher aggregation degree of KEP2 and KEP3, which has been observed in **Figure 4.6A**, could be another reason resulting in the shielding effect on Trp fluorescence. KEP4 exhibited a dark brown color because of abundant pigments that could absorb blue and green color or covered chromophoric groups, leading to an inconspicuous fluorescence absorption. Therefore, KEP with varying molecular

weights presented different tertiary conformations because of different inter or intra-molecule forces.

4.3.4.2 Chemical structure and secondary structure

The main chemical groups in KEP were assessed by FTIR, and the result is shown in **Figure 4.7A**. The peak at 3288 cm^{-1} is about N-H and O-H stretching vibration, probably regarding the hydrogen bonds attributed to the interactions between the amide groups [44]. The peak of KEP1 at 3288 cm^{-1} was broader than others, indicating the forming of more hydrogen bonds and some changes in the secondary structure [45]. However, no obvious difference was found in other chemical groups among KEP samples. The absorption peak at about 1650 cm^{-1} was about amide Ⅰ bands related to the stretching vibrations of C=O groups, while the peak of 1545 cm^{-1} indicates the C-N and N-H groups of amide Ⅱ bands [46]. The other absorption bands that appeared at 1450 cm^{-1} and 1250 cm^{-1} were attributed to C-N and C-O of amide Ⅲ [47, 48]. Although comprised of different molecular compositions, the KEP samples exhibited similar chemical structures.

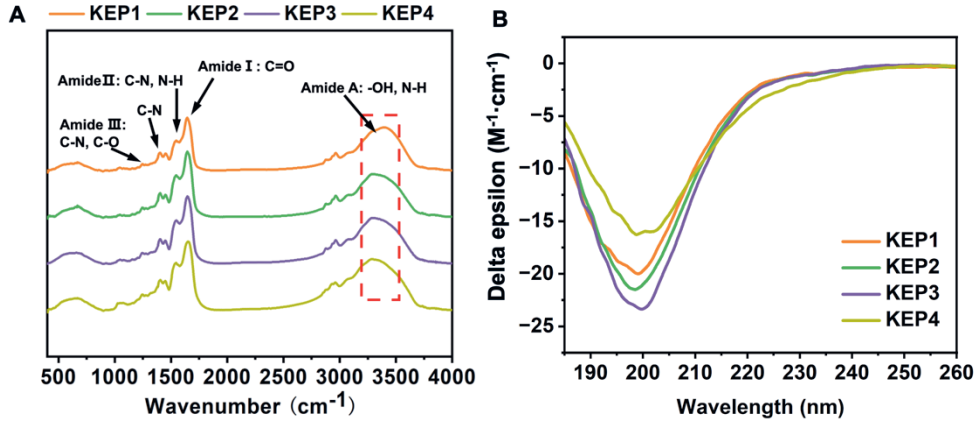

Figure 4.7. (A) FTIR spectrum and (B) CD spectrum of KEP1 (< 3 kDa), KEP2 (3-5 kDa), KEP3 (5-10 kDa) and KEP4 (> 10 kDa).

The possible changes in the secondary structure of KEP are shown in **Figure 4.7B** and **Table 4.2**. In CD spectra, the peaks at 192 nm and the negative peaks at around 208 nm and 222 nm are related to α-helix [49], while the positive peak at about 195 nm and negative peak at 215 represent β-sheet [50]. By analysis using BeStSel (**Table 4.2**), it was found that the β-sheet content of KEP4 was about 47.1%, while the other groups owned over 60% of β-sheet among which KEP3 reached the highest of 65.7%.

Conversely, KEP4 contained the richest α-helix structure, reaching about 20.2%, while there were 12.9%, 13.2% and 14.1% in KEP1, KEP2 and KEP4, respectively. In a study on the solubility of pea protein isolates, the result also presented higher β-sheet content and lower α-helix content in soluble aggregates [43]. The α-helix structure might be deconstructed and rearranged into β-sheets. It has been speculated that the decrease in α-helix and the increase in β-sheet structures might correlate with the formation of soluble aggregates due to exposure of hydrophobic regions [51]. As depicted in **Figure 4.6A**, it was observed that KEP3 exhibited the highest proportion of large particles compared to the other samples, whereas KEP4 had the lowest proportion. The molecular interaction forces, such as hydrogen bonds and hydrophobic interactions, have been reported to induce the variation of protein secondary structure [52].

Table 4.2. Secondary structure fractions of KEP.

Fractions	KEP1	KEP2	KEP3	KEP4
α-helix (%)	12.9	13.2	14.1	20.2
β-sheet (%)	62.5	63.5	65.7	47.1
Turn (%)	--	--	--	--
Others (%)	24.6	23.3	20.2	32.7

4.3.4.3 Composition of amino acids

The potential difference in amino acids composition of KEP was assessed which might be a key factor on their cell penetration ability. The result is presented in **Figure 4.8**. As the figure showed, the KEP with a smaller molecular weight contained a higher proportion of hydrophobic amino acids, such as Pro, Val and Leu. KEP1 exhibited the highest concentration of hydrophobic amino acids, reaching approximately 3.80 mM/mg, while KEP4 had a lower concentration of around 2.39 mM/mg. KEP1 had significantly higher levels of Gly, Pro, Val, Ile and Leu compared to the other groups. Notably, KEP1 exhibited a significantly higher presence of cystine than other samples ($P < 0.05$). It has been reported that the presence of the disulfide scaffold in cystine likely contribute to an "inside-out" feature with exposed hydrophobic regions, leading to increased interaction with the cell membrane [35]. However, the positively charged amino acids Lys and Arg in KEP1 (0.31 mM/mg) did not demonstrate a substantial advantage over KEP4 (0.36 mM/mg). As inferred in **section 4.3.2**, the amino acid composition results further suggest that the cell-penetrating ability of KEP1 is not primarily reliant on the electrostatic interaction

mechanism from cationic CPPs, but rather on its amphiphilic or hydrophobic properties.

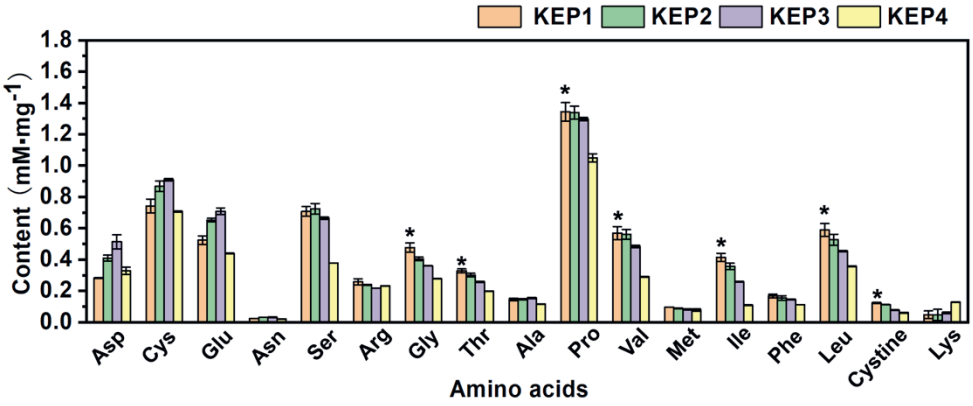

Figure 4.8. Amino acids composition of KEP samples. The results are presented as the mean values ± SD, n = 3. "*" indicates the significant difference between different KEP samples ($P < 0.05$).

In summary, the KEP samples, despite having different molecular compositions, exhibited similar chemical structures. However, variations were observed in their amino acids composition, secondary and tertiary structures, which potentially impacted the maintaining force and size of particles. KEP with a lower molecular weight possessed richer hydrophobic amino acids and β-sheet structures. It potentially led to increased exposure of hydrophobic regions and consequently large aggregations. It is important to note that the smallest particle size of KEP4 did not necessarily correspond to its cell-penetration ability. The higher content of disulfide scaffold, β-sheet and hydrophobic tertiary structures in KEP1 might have a more pronounced influence on the cell-penetrating ability.

4.4 Conclusion

The investigation on cytotoxicity of KEP elucidated KEP1 with low cytotoxicity, indicating their potential for diverse applications. As expected, these peptides also possessed the ability to penetrate cells, allowing efficient delivery of FITC-INS into Caco2 cells through a non-covalent mechanism. The identification of the most effective peptides and domains reveals that these sequences consisted of 8-19 amino acids, with a notable presence of hydrophobic residues. Certain peptides enriched in Pro, Leu, and Cys were also discovered, potentially serving as the crucial components that presented cell-penetrating properties. The findings related to the

secondary and tertiary structure, and amino acid composition provide validation for the significant features observed in KEP1, including rich hydrophobic interactions and disulfide bonds. Conversely, the impact of small particle size and electrostatic interactions on cell-penetrating ability was found to be less significant. Overall, this research confirmed the cell-penetrating ability of KEP, highlighting their tremendous potential as vehicles for non-covalently delivering biomolecules, with promising applications across various fields, such as the food and pharmaceutical industries.

4.5 References

1. S. Rehmani, J.E. Dixon, Oral delivery of anti-diabetes therapeutics using cell penetrating and transcytosing peptide strategies, Peptides, 100 (2018) 24-35.
2. H. Derakhshankhah, S. Jafari, Cell penetrating peptides: A concise review with emphasis on biomedical applications, Biomed Pharmacother, 108 (2018) 1090-1096.
3. H. Kim, M. Kitamatsu, T. Ohtsuki, Enhanced intracellular peptide delivery by multivalent cell-penetrating peptide with bioreducible linkage, Bioorg Med Chem Lett, 28 (2018) 378-381.
4. M. Pooga, M. Hällbrink, M. Zorko, Ü. Langel, Cell penetration by transportan, The FASEB Journal, 12 (1998) 67-77.
5. T. Wang, C. Wang, S. Zheng, G. Qu, Z. Feng, J. Shang, Y. Cheng, N. He, Insight into the Mechanism of Internalization of the Cell-Penetrating Carrier Peptide Pep-1 by Conformational Analysis, Journal of biomedical nanotechnology, 16 (2020) 1135-1143.
6. P.A. Wender, D.J. Mitchell, K. Pattabiraman, E.T. Pelkey, L. Steinman, J.B. Rothbard, The design, synthesis, and evaluation of molecules that enable or enhance cellular uptake: peptoid molecular transporters, Proceedings of the National Academy of Sciences, 97 (2000) 13003-13008.
7. L.M. van Oppen, J. Pille, C. Stuut, M. van Stevendaal, L.N. van der Vorm, J.A. Smeitink, W.J. Koopman, P.H. Willems, J.C. van Hest, R. Brock, Octa-arginine boosts the penetration of elastin-like polypeptide nanoparticles in 3D cancer models, European Journal of Pharmaceutics and Biopharmaceutics, 137 (2019) 175-184.
8. D.K. Schach, W. Rock, J. Franz, M. Bonn, S.H. Parekh, T. Weidner, Reversible activation of a cell-penetrating peptide in a membrane environment, Journal of the American Chemical Society, 137 (2015) 12199-12202.
9. S. Shahbazi, A. Bolhassani, Comparison of six cell penetrating peptides with different properties for in vitro and in vivo delivery of HPV16 E7 antigen in therapeutic vaccines, International Immunopharmacology, 62 (2018) 170-180.
10. G. Guidotti, L. Brambilla, D. Rossi, Cell-penetrating peptides: from basic research to clinics, Trends in pharmacological sciences, 38 (2017) 406-424.
11. J.-H. Kang, M.-Y. Jung, X. Yin, M. Andrianifahanana, D.M. Hernandez, E.B. Leof, Cell-penetrating peptides selectively targeting SMAD3 inhibit profibrotic TGF-β signaling, The Journal of clinical investigation, 127 (2017) 2541-2554.
12. A. Bolhassani, B.S. Jafarzade, G. Mardani, In vitro and in vivo delivery of therapeutic proteins using cell penetrating peptides, Peptides, 87 (2017) 50-63.
13. L. Li, L. Yang, M. Li, L. Zhang, A cell-penetrating peptide mediated chitosan nanocarriers for improving intestinal insulin delivery, Carbohydr Polym, 174 (2017) 182-189.
14. D. Zhang, J. Wang, D. Xu, Cell-penetrating peptides as noninvasive transmembrane vectors for the development of novel multifunctional drug-delivery systems, Journal of controlled release, 229 (2016) 130-139.
15. H. Xu, S. Cai, L. Xu, Y. Yang, Water-stable three-dimensional ultrafine fibrous scaffolds from keratin for cartilage tissue engineering, Langmuir, 30 (2014) 8461-8470.
16. H. Xu, Z. Shi, N. Reddy, Y. Yang, Intrinsically water-stable keratin nanoparticles and their in vivo biodistribution for targeted delivery, J Agric Food Chem, 62 (2014) 9145-9150.
17. X. Qin, X. Xu, Y. Guo, Q. Shen, J. Liu, C. Yang, E. Scott, H. Bitter, C. Zhang, A sustainable and efficient recycling strategy of feather waste into keratin peptides with antimicrobial activity, Waste

Manag, 144 (2022) 421-430.
18. Z. Guo, H. Peng, J. Kang, D. Sun, Cell-penetrating peptides: Possible transduction mechanisms and therapeutic applications, Biomedical reports, 4 (2016) 528-534.
19. K. Splith, I. Neundorf, Antimicrobial peptides with cell-penetrating peptide properties and vice versa, European Biophysics Journal, 40 (2011) 387-397.
20. H.-J. Jung, K.-S. Jeong, D.-G. Lee, Effective antibacterial action of tat (47-58) by increased uptake into bacterial cells in the presence of trypsin, Journal of microbiology and biotechnology, 18 (2008) 990-996.
21. J. Xie, Y. Gou, Q. Zhao, S. Li, W. Zhang, J. Song, L. Mou, J. Li, K. Wang, B. Zhang, Antimicrobial activities and action mechanism studies of transportan 10 and its analogues against multidrug-resistant bacteria, Journal of Peptide Science, 21 (2015) 599-607.
22. A. Jain, B.K. Yadav, A. Chugh, Marine antimicrobial peptide tachyplesin as an efficient nanocarrier for macromolecule delivery in plant and mammalian cells, The FEBS Journal, 282 (2015) 732-745.
23. C.B. Park, K.-S. Yi, K. Matsuzaki, M.S. Kim, S.C. Kim, Structure–activity analysis of buforin II, a histone H2A-derived antimicrobial peptide: the proline hinge is responsible for the cell-penetrating ability of buforin II, Proceedings of the National Academy of Sciences, 97 (2000) 8245-8250.
24. X. Qin, C. Yang, Y. Guo, J. Liu, J.H. Bitter, E.L. Scott, C. Zhang, Effect of ultrasound on keratin valorization from chicken feather waste: process optimization and keratin characterization, Ultrasonics Sonochemistry, (2023) 106297.
25. L. Yang, M. Li, Y. Sun, L. Zhang, A cell-penetrating peptide conjugated carboxymethyl-beta-cyclodextrin to improve intestinal absorption of insulin, Int J Biol Macromol, 111 (2018) 685-695.
26. A. Micsonai, F. Wien, É. Bulyáki, J. Kun, É. Moussong, Y.-H. Lee, Y. Goto, M. Réfrégiers, J. Kardos, BeStSel: a web server for accurate protein secondary structure prediction and fold recognition from the circular dichroism spectra, Nucleic acids research, 46 (2018) W315-W322.
27. B. Wu, M. Li, K. Li, W. Hong, Q. Lv, Y. Li, S. Xie, J. Han, B. Tian, Cell penetrating peptide TAT-functionalized liposomes for efficient ophthalmic delivery of flurbiprofen: Penetration and its underlying mechanism, retention, anti-inflammation and biocompatibility, Int J Pharm, 598 (2021) 120405.
28. S.E. Chong, J.H. Oh, K. Min, S. Park, S. Choi, J.H. Ahn, D. Chun, H.H. Lee, J. Yu, Y. Lee, Intracellular delivery of immunoglobulin G at nanomolar concentrations with domain Z-fused multimeric alpha-helical cell penetrating peptides, J Control Release, 330 (2021) 161-172.
29. Y. Sun, J. Lu, D. Yan, L. Shen, H. Hu, D. Chen, Cellular uptake mechanism and clearance kinetics of fluorescence-labeled glycyrrhetinic acid and glycyrrhetinic acid–modified liposome in hepatocellular carcinoma cells, Environmental Toxicology and Pharmacology, 53 (2017) 46-56.
30. A. Mishra, G.H. Lai, N.W. Schmidt, V.Z. Sun, A.R. Rodriguez, R. Tong, L. Tang, J. Cheng, T.J. Deming, D.T. Kamei, Translocation of HIV TAT peptide and analogues induced by multiplexed membrane and cytoskeletal interactions, Proceedings of the National Academy of Sciences, 108 (2011) 16883-16888.
31. J.L. Zaro, W.-C. Shen, Cationic and amphipathic cell-penetrating peptides (CPPs): Their structures and in vivo studies in drug delivery, Frontiers of Chemical Science and Engineering, 9 (2015) 407-427.
32. F. Milletti, Cell-penetrating peptides: classes, origin, and current landscape, Drug discovery today, 17 (2012) 850-860.

33. L.M. Reid, C.S. Verma, J.W. Essex, The role of molecular simulations in understanding the mechanisms of cell-penetrating peptides, Drug Discov Today, 24 (2019) 1821-1835.
34. A. Borrelli, A.L. Tornesello, M.L. Tornesello, F.M. Buonaguro, Cell penetrating peptides as molecular carriers for anti-cancer agents, Molecules, 23 (2018) 295.
35. A. Kam, S. Loo, J.-S. Fan, S.K. Sze, D. Yang, J.P. Tam, Roseltide rT7 is a disulfide-rich, anionic, and cell-penetrating peptide that inhibits proteasomal degradation, Journal of Biological Chemistry, 294 (2019) 19604-19615.
36. Y. Han, Z. Gao, L. Chen, L. Kang, W. Huang, M. Jin, Q. Wang, Y.H. Bae, Multifunctional oral delivery systems for enhanced bioavailability of therapeutic peptides/proteins, Acta Pharm Sin B, 9 (2019) 902-922.
37. M. Naeem, U.A. Awan, F. Subhan, J. Cao, S.P. Hlaing, J. Lee, E. Im, Y. Jung, J.-W. Yoo, Advances in colon-targeted nano-drug delivery systems: challenges and solutions, Archives of pharmacal research, 43 (2020) 153-169.
38. M. Zeeshan, H. Ali, S. Khan, S.A. Khan, B. Weigmann, Advances in orally-delivered pH-sensitive nanocarrier systems; an optimistic approach for the treatment of inflammatory bowel disease, International journal of pharmaceutics, 558 (2019) 201-214.
39. M.C. García, Nano-and microparticles as drug carriers, in: Engineering Drug Delivery Systems, Elsevier, 2020, pp. 71-110.
40. A.E. Nel, L. Mädler, D. Velegol, T. Xia, E.M. Hoek, P. Somasundaran, F. Klaessig, V. Castranova, M. Thompson, Understanding biophysicochemical interactions at the nano–bio interface, Nature materials, 8 (2009) 543-557.
41. A. Banerjee, J. Qi, R. Gogoi, J. Wong, S. Mitragotri, Role of nanoparticle size, shape and surface chemistry in oral drug delivery, Journal of Controlled Release, 238 (2016) 176-185.
42. R. Sobhy, F. Zhan, E. Mekawi, I. Khalifa, H. Liang, B. Li, The noncovalent conjugations of bovine serum albumin with three structurally different phytosterols exerted antiglycation effects: a study with AGEs-inhibition, multispectral, and docking investigations, Bioorganic chemistry, 94 (2020) 103478.
43. K. Gao, J. Rao, B. Chen, Unraveling the mechanism by which high intensity ultrasound improves the solubility of commercial pea protein isolates, Food Hydrocolloids, 131 (2022).
44. A. Khan, C. Wang, X. Sun, A. Killpartrick, M. Guo, Preparation and characterization of whey protein isolate–DIM nanoparticles, International Journal of Molecular Sciences, 20 (2019) 3917.
45. L. Han, K. Lu, S. Zhou, S. Zhang, F. Xie, B. Qi, Y. Li, Development of an oil-in-water emulsion stabilized by a black bean protein-based nanocomplex for co-delivery of quercetin and perilla oil, Lwt, 138 (2021) 110644.
46. G. Han, Y. Li, Q. Liu, Q. Chen, H. Liu, B. Kong, Improved water solubility of myofibrillar proteins by ultrasound combined with glycation: A study of myosin molecular behavior, Ultrason Sonochem, 89 (2022) 106140.
47. F. Pourjavaheri, S. Ostovar Pour, O.A.H. Jones, P.M. Smooker, R. Brkljača, F. Sherkat, E.W. Blanch, A. Gupta, R.A. Shanks, Extraction of keratin from waste chicken feathers using sodium sulfide and l-cysteine, Process Biochemistry, 82 (2019) 205-214.
48. D. Wang, W. Li, Y. Wang, H. Yin, Y. Ding, J. Ji, B. Wang, S. Hao, Fabrication of an expandable keratin sponge for improved hemostasis in a penetrating trauma, Colloids Surf B Biointerfaces, 182 (2019) 110367.

49. F. Wu, X. Shi, H. Zou, T. Zhang, X. Dong, R. Zhu, C. Yu, Effects of high-pressure homogenization on physicochemical, rheological and emulsifying properties of myofibrillar protein, Journal of food engineering, 263 (2019) 272-279.
50. D.M. Rogers, S.B. Jasim, N.T. Dyer, F. Auvray, M. Réfrégiers, J.D. Hirst, Electronic circular dichroism spectroscopy of proteins, Chem, 5 (2019) 2751-2774.
51. X. Sun, W. Zhang, L. Zhang, S. Tian, F. Chen, Effect of ultrasound-assisted extraction on the structure and emulsifying properties of peanut protein isolate, Journal of the Science of Food and Agriculture, 101 (2021) 1150-1160.
52. K. Liu, X.-Q. Zha, Q.-M. Li, L.-H. Pan, J.-P. Luo, Hydrophobic interaction and hydrogen bonding driving the self-assembling of quinoa protein and flavonoids, Food Hydrocolloids, 118 (2021).

4.6 Supplementary materials

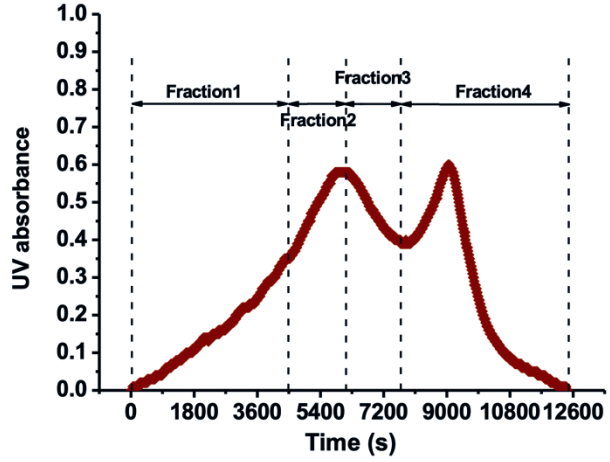

Figure S4.1. Four fractions of KEP1 via sephadex column.

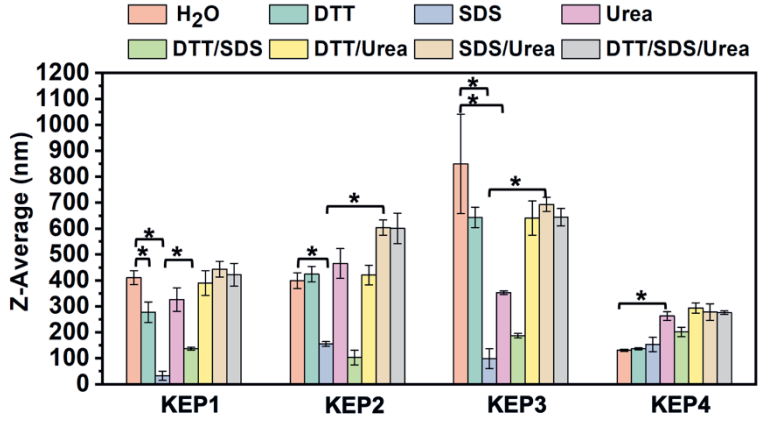

Figure S4.2. The average size of KEP samples dispersed in different denaturants (H_2O, DTT, SDS, Urea, DTT/SDS, DTT/Urea, SDS/Urea and DTT/SDS/Urea). The data are presented as the mean values ± SD, n = 3. "*" indicates the significant difference between samples treated with different denaturants ($P < 0.05$).

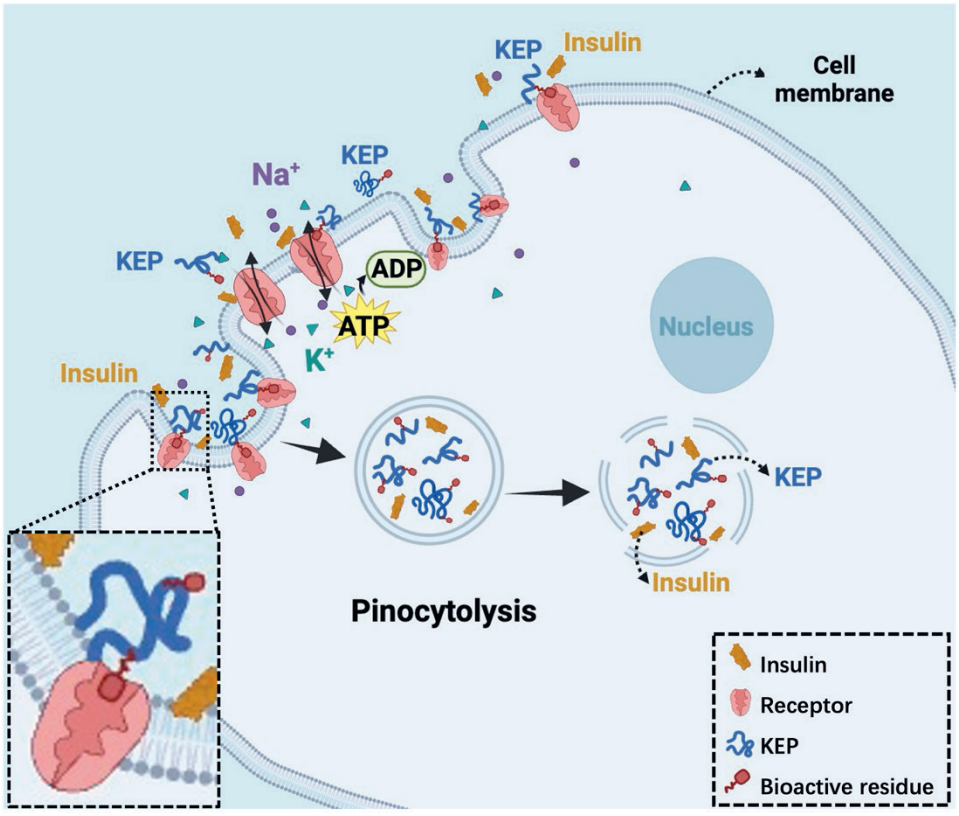

Figure S4.3. Hypothesis of the cell-penetrating mechanism of KEP.


5

CHAPTER 5

Preparing keratin nanoparticles via partial hydrolysis and pH-shifting

Authors: Xiaojie Qin, Johannes H. Bitter, Chunhui Zhang, Elinor L. Scott

Abstract

Keratin, an abundant natural biopolymer in animal by-products, has significant potential for nanoparticle applications. It has merits such as biocompatibility, biodegradability, low toxicity and cell adhesion. However, keratin encounters limited utilization due to its inherent stability resulting from disulfide (S-S) bonds. Here we show an effective strategy for preparing keratin nanoparticles (KNPs) via partial hydrolysis and pH-shifting. We found that the partial hydrolysis at a 5% degree of hydrolysis (DH) produced self-assembled spherical keratin nanoparticles (KNPs). The KNPs exhibited significantly reduced particle size (~123 nm) and improved water solubility (94.5%) compared to raw keratin, whose size is at a micrometer level with 8.5% of water solubility. They demonstrated size stability (< 180 nm) and resistance to enzymatic digestion in the gastrointestinal tract. Moreover, the pH-shifting from 2.0 to 7.0 revealed the reversible "open-close" structure of KNPs, presenting high loading efficiency (LE, > 94%) of biomolecules (insulin and resveratrol). Nevertheless, higher DH (≥ 10%) resulted in more β-sheets and exposed hydrophobic residues of KNPs, producing more aggregation and denser clusters. They showed inferior structural transformation reacting to pH-shifting, along with lower LE of biomolecules. Our results highlight the potential of KNPs (5% DH) as nanocarriers for biomolecule encapsulation. This study sheds light on the transformative potential of keratin, providing valuable insights for its utilization in nutrients, nanomedicine and drug delivery systems.

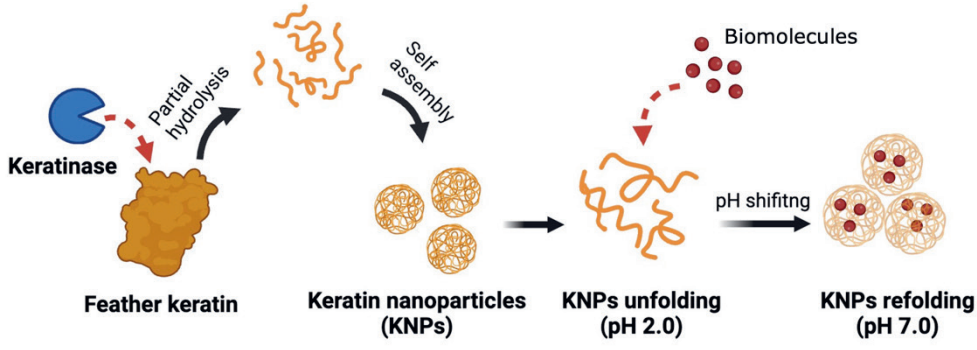

5.1 Introduction

Numerous bioactive molecules (biomolecules) have recently garnered interest among researchers owing to their physiological functions. They demonstrate broad applications in preserving human health and treating diseases i.e. act as a therapeutic. For example, resveratrol and curcumin exhibited potent antioxidant, anti-inflammatory and anti-cancer effects [1, 2]; insulin and carvedilol were recognized to be efficient for diabetes and hypertension, respectively [3, 4]. However, due to their non-polar or peptide structures, most biomolecules exhibit unfavorable physicochemical properties such as limited water solubility, instability towards enzymatic degradability, low cell permeability and environmental instability in response to heat, light and extreme pH [5]. These drawbacks can result in low bioavailability, which is a major concern for various therapeutic molecules. Hence, multiple formulations have been developed for enhancing the performance of biomolecules. Especially nanoparticles have shown great promise, owing to their high surface area, prolonged duration, etc. [6].

The emergence of nanoparticles (1-1000 nm) represents a significant development due to their numerous advantages in delivering biomolecules [7]. Nanoparticles exhibit merits including solubility in aqueous media, less aggregation, protection of biomolecules from harsh environments, controlled release and ability to penetrate biological membranes [8-11]. The increase in surface area and high exposure of surface atoms can improve interfacial properties (e.g. surface charge and dissolubility), further influencing the biological interactions of nanoparticles with cells, tissues and organs [12]. Typically, nanoparticles < 200 nm exhibit advantages in bioaccesibility, attributed to their high permeation across the mucosa and prolonged circulation in the bloodstream [12-14]. Thus, nanoparticles < 200 nm are a promising formulation for effectively delivering biomolecules. Especially nanoparticles constructed by natural polymers present merits, such as biodegradability, biocompatibility, low toxicity, etc. [6].

Natural polymers derived from plants, animals or microorganisms, such as chitosan, alginate, zein, gelatin and casein, have shown positive prospects as biomaterials. They exhibit advantages of low toxicity, biocompatibility, biodegradability and attractive costs [15, 16]. Notably, natural proteins display significant potential as promising contenders due to their diverse functional groups, including hydroxyl,

carboxyl and amino groups. This inherent property allows them to interact effectively with biomolecules. Despite their advantages, certain protein biomasses have shown insufficient stability in aqueous environments or under physiological temperatures [17], limiting their potential for biomedical applications. A more suitable alternative material will be required. Keratin, an abundant component in feather waste, is particularly notable for its inherent stability.

Keratin, consisting over 90% of feathers, is a highly applicable biopolymer known for its good biocompatibility, biodegradability and low toxicity. The abundance of disulfide bonds, largely attributed to its high cysteine content (~7 mol%), provides keratin with stability and resistance to conventional proteases [18, 19]. Keratin nanoparticles (KNPs) were found to have water stability under varying pH values and temperatures (pH 2.0-7.0, 4-37 °C) [20]. Allied to this, they were able to penetrate kidney and liver cells, displaying a favourable capacity for attachment and proliferation. Subsequently, KNPs were applied for doxorubicin delivery [21, 22], exhibiting controlled release capability and compatibility with blood. Thus, feather keratin is an appealing alternative biomaterial for fabricating biomolecule-loaded nanoparticles. However, abundant disulfide bonds lead to a low dissolubility of keratin in aqueous solution, and the self-aggregation often happens due to crosslinking by the formation of disulfide bonds, hydrogen bonds and hydrophobic interactions [17]. This would limit its practical application. Therefore, developing methods for producing KNPs with enhanced solubility and dispersibility becomes significant.

Recently, a range of novel technologies have been developed for nanoparticle preparation accompanied by reduced environmental pollution and product toxicity. The techniques such as ionic gelation [23], spray drying [24], coacervation [25], anti-solvent precipitation [26] and pH-shifting method (from pH 12.0 to pH 7.0) [27] were often employed. Currently, the popular approach to forming protein nanoparticles, named pH shifting, has drawn people's attention. In that process protein unfolding, i.e. changing of the tertiary and quaternary structure, by incubation in acidic (pH 1.5 to 3.5) or alkaline (pH 10.0 to 12.0) solutions followed by refolding at pH 7.0 [28] is applied. Earlier study reveal that the soy protein particles prepared by pH shifting had core-shell structures with average sizes from 100 to 250 nm [29]. Besides, researchers have combined partial enzymatic hydrolysis and pH-shifting to prepare soy protein nanoparticles for curcumin encapsulation [30]. The resulting

nanoparticles presented homogeneous size distribution and spherical shape, with enhanced solubility, stability and encapsulation efficiency. Given the above, the combination of partial enzymatic hydrolysis and pH-shifting is a potential strategy for preparing high-performance keratin nanoparticles. However, the impact of partial hydrolysis at different degrees of hydrolysis (DHs) on keratin reactivity and restructuring remains unknown, as does their behavior under pH shifting.

This study aims to investigate the impact of partial hydrolysis and pH-shifting on keratin reactivity and restructuring, thus fabricating KNPs for biomolecule encapsulation. The following approaches were applied to reach that aim. First, the self-assembled KNPs were prepared through partial enzymatic hydrolysis (DH: 5-20%) using keratinase. The physicochemical properties of KNPs were then assessed, involving water solubility, aggregation behavior, secondary/tertiary structure, thermal stability, inter- and intra-particle forces, digestibility, etc. which might be interrelated. Subsequently, the restructuring of KNPs was investigated by shifting pH from 2.0 to 7.0, followed by the fabrication of biomolecule-loaded KNPs. Here insulin and resveratrol were chosen as the target biomolecules.

5.2 Materials and methods

5.2.1 Materials and chemicals

Feather keratin was extracted using our previous method [31], with chicken feathers supplied by the Institute of Animal Science of the Chinese Academy of Agricultural Science (Beijing, China). The bovine insulin (27 U/mg, 5733.49 Da) was supplied by Yuanye Bio-Technology Co., Ltd (Shanghai, China). Acetonitrile (ACN) and methanol (MeOH) were of HPLC gradient grade supplied by Actu-All chemicals. The other chemicals were of analytical grade and provided by Sigma.

5.2.2 Preparation of KNPs

Raw keratin (RK) was dispersed in phosphorate buffer (PB, pH 7.0, 10 mM) at a concentration of 5% (w/v) and equilibrated overnight to get complete hydration. After that, the pH of the keratin dispersion was adjusted to pH 8.5 and treated with keratinase (6000 U/g) at 55 °C for different times (0.5-5 h) to reach various degrees of hydrolysis. Then, the mixture was boiled at 95 °C for 3 min to inactivate enzymes, after which the pH was adjusted to 7.0. The supernatant was collected and centrifuged (8000 ×g, 4 °C) for 20 min. The resultant hydrolysates were then

lyophilized. Finally, the self-assembly KNPs with varying DHs of 5%, 10%, 15% and 20% were obtained and grouped as K5, K10, K15 and K20, respectively. The DH was analyzed with the OPA method [32].

5.2.3 Solubility of KNPs

The solubility of KNPs in Milli-Q (MQ) water, 80% ethanol and 96% ethanol were investigated. Briefly, KNPs were dispersed in the solvents above at a concentration of 2 mg/mL and stood for 1h at room temperature. The mixture was centrifuged at 3000 ×g for 15 min. The supernatant was diluted four times and the soluble protein content was determined with BCA reagents following the previous method [33]. The absorbance at 562 nm was read using a microplate reader (Spark, Tecan, Switzerland).

5.2.4 Characterization and morphology of KNPs

Particle size analysis was performed using dynamic light scattering (DLS) (ZetasSizer, Malvern Instruments, UK). KNPs were dispersed in MQ water at a concentration of 0.1 mg/mL and then were determined at 25 °C.

The morphology of KNPs was assessed with transmission electron microscopy (TEM, JEM 1400Plus, JEOL Ltd., USA). Briefly, KNPs were dispersed in PB (pH 7.0, 10 mM) at a concentration of 0.1 mg/mL. 5 μL of KNPs dispersion was added on a formvar/carbon grid and kept for 2 min. After removing the excess, the grid was washed with a drop of MQ water. Then, 5 μL of phosphotungstic acid (1%, w/v) was added on the grid for negative staining. After removing the excess and drying, the grid was observed using TEM.

5.2.5 Chemical functionality, secondary structure and thermogravimetric (TG) analysis

The chemical functionality of KNPs was analyzed via a Fourier transform infrared spectroscopy (FTIR, Vertex 70, Bruker Inc., U.S.). Briefly, KNPs were ground with dried potassium bromide and pressed into a 1 mm pellet. Then, it was scanned from 400 to 4000 cm^{-1} with a resolution of 4 cm^{-1}.

The secondary structure was assessed using circular dichroism (CD, Jasco J-815, Jasco Inc., Japan). Briefly, KNPs were dispersed in PB (pH 7.0, 10 mM) at 0.25 mg/mL. Ten scans were recorded and averaged with wavelengths ranging from 185 nm to 260 nm at a scanning speed of 50 nm/min at 20 °C. The blank PB buffer was performed for baseline subtraction. The CD fitting software, BeStSel, was used for

calculating the secondary structure contents, including β-sheet, α-helix and β-turns [34].

Analysis of thermogravimetric (TGA) and derivative thermogravimetry (DTGA) was performed on a thermogravimetric analyzer (METTLER TOLEDO™ TGA/DSC, ThermoFisher, US). The samples weighed about 8 mg and the gas consumption rate was set as 120 mL/min. Then, the samples were heated from 25 °C to 500 °C at a heating rate of 10 °C/min under nitrogen atmosphere.

5.2.6 Disulfide bond content of KNPs

The sulfhydryl content was assessed using the previous method [35]. The disulfide content was calculated using total sulfhydryl content to subtract the free sulfhydryl content. For the free sulfhydryl assay, 2 mg of KNPs was suspended in 800 μL of buffer A (8 M urea, 3 mM EDTA, 1% SDS and Tris−HCl (0.2 M, pH 8.0)). The mixture was shaken at 100 rpm for 2.5 h at room temperature. After that, 200 μL of buffer B (10 mM DTNB in Tris−HCl (0.2 M, pH 8.0)) was added and kept shaking for another 1 h, and then the reaction mixture was centrifuged at 12000 ×g for 15 min at 25 °C. The supernatant absorbance was determined at 412 nm using UV spectrophotometer (UV-1600PC, VWR).

The total sulfhydryl was determined following the similar procedure described above, using different chemicals. To be detailed, 2 mg of KNPs was suspended in 1mL of buffer containing 8 M urea, 3 mM EDTA, 1% SDS, 0.2 M Tris−HCl (pH 9.5), 0.1 M Na_2SO_3 and 50 mM 2-nitro-5-thio-sulfobenzoic acid ($NTSB^{2-}$) which synthesized by DTNB [36]. After shaking at 100 rpm for 2.5 h at room temperature, the reaction mixture was centrifuged at 12000 ×g for 15 min at 25 °C, and then the supernatant was measured at 412 nm. The extinction coefficient was 13600 $M^{-1}cm^{-1}$ for calculating thiol groups.

5.2.7 Surface hydrophobicity

The surface hydrophobicity of KNPs was assessed using the fluorescence probe method [37]. The reagent 1-anilino-8-naphthalenesulfonate (ANS) was applied for assessing protein hydrophobicity. Briefly, KNPs were diluted to different concentrations (0-2 mg/mL) using PB buffer (pH 7.0, 10 mM). 4 mL of KNPs dilution was mixed with 20 μL of ANS (8 mM in 10 mM PB, pH 7.0). After standing for 20 min in the dark, the fluorescence intensity was detected at λ_{ex} 370 nm and λ_{em} 465

nm using a fluorescence microplate reader (SPARK10M TECAN, Switzerland). The slope of the linear regression line between fluorescence intensity and protein concentration was utilized to express the surface hydrophobicity.

5.2.8 Pattern of inter- and intra-particle forces

The inter- and intra-particle forces of KNPs were assessed by evaluating the particle size changes under various additives. These include urea (6 M), sodium lauryl sulfate solution (SDS, 0.5%) and dithiothreitol (DTT, 30 mM), either alone or in combination. Briefly, KNPs were dispersed in the additives above at a concentration of 0.5 mg/mL. There were seven treatments for each KNPs sample, grouped as DTT, SDS, Urea, DTT/SDS, DTT/Urea, SDS/Urea and DTT/SDS/Urea. MQ water was taken as control, named H_2O.The dispersions were kept for 30 min and then subjected to ZetaSizer for size analysis.

5.2.9 Digestibility in the gastrointestinal tract

The digestibility of KNPs was investigated by simulating the gastrointestinal (GI) tract. The simulated gastric fluid (SGF) was prepared using 0.7 mL of HCl (37 %) and 0.2 g NaCl dissolved in 100 mL of MQ water, adjusting the pH to 1.2. Pepsin was added to SGF at the final concentration of 3.2 mg/mL. KNPs (6 mg/ml) were mixed with SGF at a ratio of 1:1 (v/v). The pH of the mixture was adjusted to 2.0, then transferred to a 37 °C water bath and incubated with agitation at 250 rpm for 1 h. The hydrolysis was stopped by adjusting the pH to 7.0 and cooling with an ice bath. The digesta was centrifuged at 8000 ×g, 4 °C. The content of free amino acids (FAA) was determined using the OPA method [32].

As to the simulated intestinal fluid (SIF), the pH of the mixture from the gastric phase was adjusted to 7.0 using 1 M NaOH. Then they were mixed with a solution containing bile salt, pancreatin, $CaCl_2$ and NaCl, the final concentrations of which reached 5 mg/ml, 5 mg/ml, 4.4 mg/ml and 0.52 mg/ml, respectively. The mixture was kept in a 37 °C water bath and incubated with continuous agitation at 250 rpm for 2 h. Finally, the hydrolysis was stopped, and supernatant was obtained, as described above. The content of FAA was assessed using the OPA method, named $FAA_{KNPs(enzyme)}$. Blank was conducted without KNPs named FAA_{enzyme}, and controls were performed without adding enzymes named $FAA_{KNPs(no\ enzyme)}$. The digestibility of KNPs was calculated by the following equation (1):

$$\text{Digestibility (\%)}=\frac{\text{FAA}_{KNPs(enzyme)}-\text{FAA}_{KNPs(no\ enzyme)}-\text{FAA}_{enzyme}}{\text{TAA}_{KNPs}}\times 100 \qquad (1)$$

Where TAA_{KNPs} represents the total content of amino acids in KNPs.

5.2.10 Loading efficiency of insulin and resveratrol via pH-shifting method

The biomolecule loading ability of KNPs was investigated based on two different types of biomolecules: insulin and resveratrol. Briefly, 20 mg of KNPs were dispersed in 2 ml of PB (10 mM, pH 2.0) and stirred at 700 rpm for 1 h. Then, 2 ml of insulin (5 mg/mL) dissolved in 0.01 N HCl were added and continued with agitation for 1 h. After that, the pH was adjusted to 7.0 and the mixture was stirred for another 2 h. Finally, the samples were dialyzed with a molecular weight cutoff (MwCO: 7 kDa) for 36 h to remove free insulin and volume to 25 mL. The insulin content was measured using HPLC, referring to the previous method [38]. The samples after dialysis were designated as K5-Ins, K10-Ins, K15-Ins and K20-Ins, and lyophilized before storage at -20 °C.

For resveratrol loading, 80 μL of resveratrol (10 mg/mL) dissolved in ethanol was added into 2 mL of KNPs solution (PB, 10 mM, pH 2.0). Resveratrol-loaded KNPs were prepared following the same procedure mentioned above. For resveratrol measurement, the free resveratrol was removed by centrifuging at 8000 ×g for 20 min, and then the supernatant was measured at 305 nm using a UV spectrophotometer (UV-1600PC, VWR). The supernatants were designated as K5-Res, K10-Res, K15-Res and K20-Res, and finally lyophilized before storage at -20 °C.

The loading efficiency (LE) of insulin and resveratrol was calculated using the following formula (2):

$$\text{LE (\%)} = \frac{\text{Amount of molecules in supernatant}}{\text{Total amount of molecules}} \times 100 \qquad (2)$$

The average particle sizes of insulin- and resveratrol-loaded nanoparticles were analyzed using ZetaSizer.

5.2.11 Statistics

SPSS 17.0 software was utilized for statistical analysis. The Duncan multiple range test (DMRT) at $P < 0.05$ was conducted to determine differences among mean values. The analysis was performed on triplicate samples and the results are presented as the mean values ± standard deviation (SD).

5.3 Results and discussion

5.3.1 Preparation and characterization of KNPs

5.3.1.1 Solubility, particle size and microstructure

Here, the effect of various DHs on KNPs solubility, particle size and microstructure were investigated. The result of KNPs solubility in MQ water and ethanol is depicted in **Figure 5.1**. As shown, there was over 90% of KNPs dissolved in MQ water, while only about 8.5% of RK dissolved. It indicates that partial hydrolysis significantly improved the dissolubility of KNPs compared to RK. Additionally, about 40% of KNPs were dissolved in 80% ethanol, while it reduced below 16% in 96% ethanol. It implies that KNPs are water soluble with polar residues and that the high purity of ethanol could potentially separate KNPs. Nevertheless, there was no significant difference in KNPs solubility among varying DHs. The water solubility will potentially expand the application of KNPs.

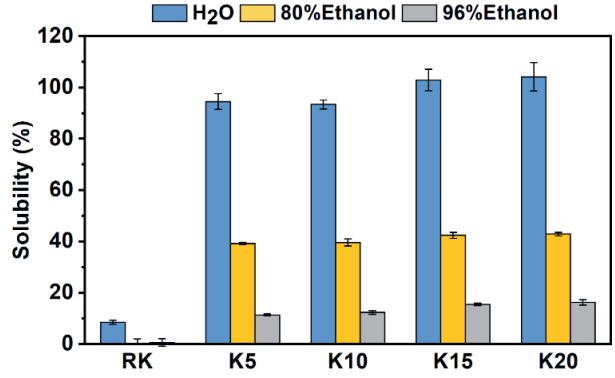

Figure 5.1. Solubility of RK and KNPs (K5, K10, K15 and K20) in MQ water, 80% and 96 % ethanol. The data are presented as the mean values ± SD (n = 3).

The result of the particle size and morphology of KNPs dispersed in an aqueous solution is presented in **Table S5.1** and **Figure 5.2A-F**, respectively. DLS analysis shows that the average particle size of KNPs with varying DHs (5-20%) ranged from 123 ± 7.0 to 157 ± 10.5 nm (**Table S5.1**). Different DHs did not result in significant changes in average particle size. However, the TEM images indicated that the size of KNPs was obviously decreased than RK (**Figure 5.2**). RK exhibited a larger and more tightly packed structure (**Figure 5.2A&B**). In contrast, KNPs exhibited decreased size with regularly spherical shapes (**Figure 5.2C-F**). Besides, KNPs tended to aggregate and form more compact clusters with increased DH (**Figure**

5.2E&F). It might result from the changes in keratin structure, e.g. secondary and tertiary structure, resulting from hydrolysis.

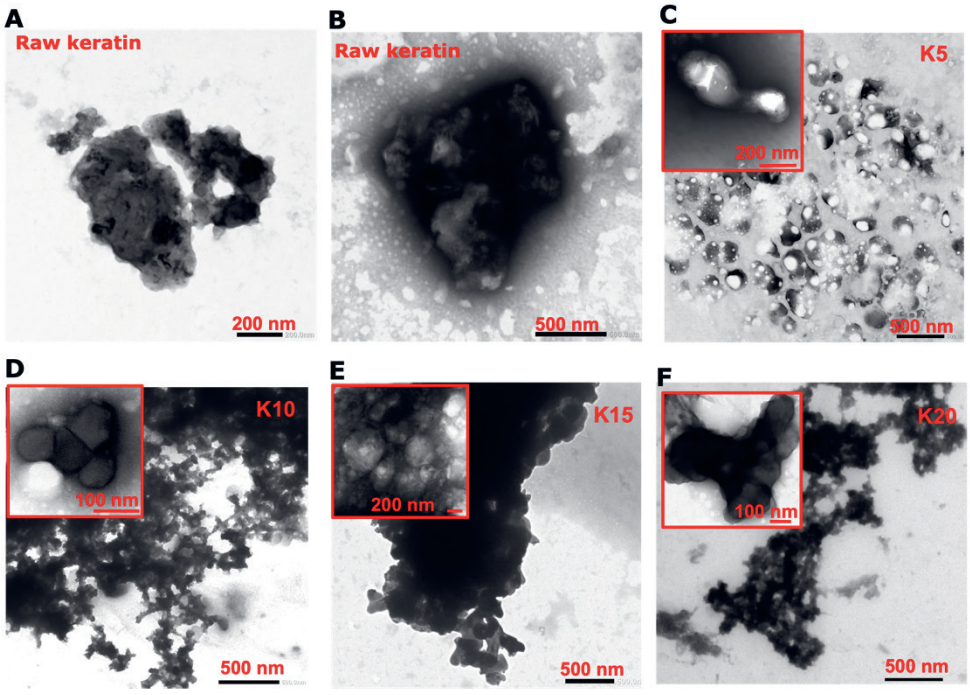

Figure 5.2. TEM images of RK (A&B) and KNPs (C-F).

It has been shown that partial hydrolysis was effective in improving KNPs solubility and reducing particle size compared to RK. KNPs (5% DH) were evenly dispersed with spherical shapes. Conversely, the increasing DH resulted in more and tighter aggregations. Subsequent steps would involve further analysis of the physicochemical properties of KNPs.

5.3.1.2 Chemical functionality

This study investigated the difference of varying DHs in the primary chemical functionalities and secondary and tertiary structures, as it may influence KNPs properties such as thermal stability, hydrophobicity and aggregation behavior.

Analysis of chemical functionalities from FTIR spectrum is shown in **Figure 5.3**. The result reveals the main absorption peaks of KNPs at amide A (N-H and O-H, 3200-3500 cm^{-1}), amide I (C=O, 1600-1700 cm^{-1}), amide II (C-N and N-H, 1480-1580 cm^{-1}) and amide III (C-N and C-O, 1220-1300 cm^{-1}) [39-43]. Here, the peaks of KNPs falling

at 3280 cm^{-1} were broader than that of RK, suggesting hydrogen bonding between amide groups after hydrolysis. Additionally, the peaks at around 1540 cm^{-1} and 1645 cm^{-1} in KNPs exhibited different relative intensity compared to RK, probably resulting from the changes in C-N and C=O of amide. Earlier, the peaks at 1522 cm^{-1} and 1632 cm^{-1} were reported to relate to the β-sheet structure and a combination of α-helix and β-sheet, respectively [44]. Hence the changes in relative intensity at this region indicated the different secondary structures of KNPs, which would be further assessed with CD spectrum. Besides, peaks at about 1400 cm^{-1} likely resulted from COOH [45]. The peaks between 1000 and 1200 cm^{-1} suggested the presence of cysteine-S-sulfonated residues (S=O stretching vibrations) and cross-linked residues, while that at about 540 cm^{-1} was associated with the disulfide group involving both reformed and unbroken bonds [45, 46]. The result confirms that various KNPs showed similar basic chemical groups, while there were potential changes in secondary structure and hydrogen bonds compared to RK.

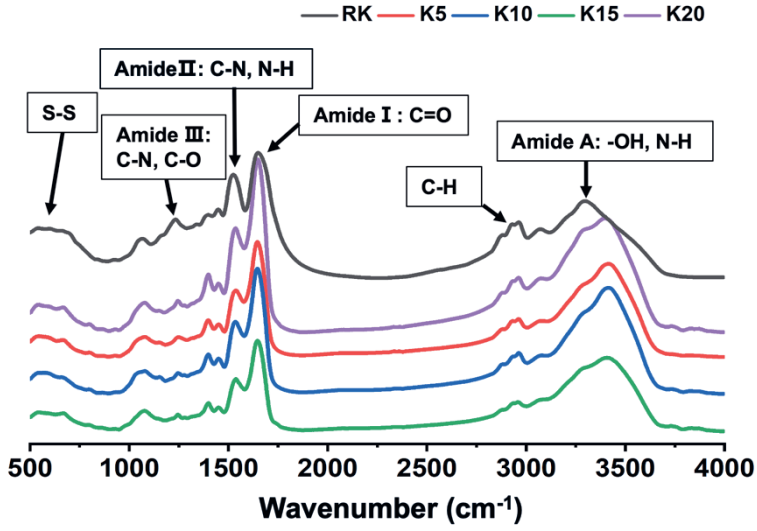

Figure 5.3. FTIR spectra of RK and KNPs (K5, K10, K15 and K20).

5.3.1.3 Secondary structure

The CD spectra were assessed to confirm the changes in the secondary structure composition of KNPs. The resulting data is presented in **Table 5.1**. Here, about 12.8% of α-helix, 22.5% of β-sheet and over 64.7% of other structures were determined in RK. Nevertheless, the β-sheet content of KNPs significantly increased over 63.4% as the dominant structure, while α-helix made a small contribution below 14.2%.

Previously, the β-sheet structure was found to increase as the dominant secondary structure (~45.6%) after forming keratin nanoparticle, with a small proportion of α-helix (~15.0%) [17]. The reason might be that keratinolysis caused bonds within the keratin molecule to cleavage, and then the molecules rearranged and formed different structures. Additionally, the increase in DH (5-20%) improved the β-sheet (63.4-70.5%) in KNPs. In the study of forming soy protein nanoparticles through Alcalse hydrolysis [37], there was also significant increase in β-sheet content with DH going up. It was deduced that the increasing β-sheet possibly resulted from the transformation from α-helix and random coil structures related to the degradation of subunits. However, α-helix content was not found to decrease in KNPs. Thus, the increasing β-sheet most likely resulted from random coil transformation. Besides, there has been speculation that the increase in β-sheet structures could be associated with the formation of soluble aggregates due to high exposure of hydrophobic regions [47]. Given the above, we deduce that a higher DH could generate more β-sheet structures, which further resulted in aggregation. Actually, more pronounced aggregation in KNPs with higher DH has been observed in **Figure 5.2C-F**.

Table 5.1. Composition of the secondary structure of KNPs.

	α-helix (%)	**β-sheet (%)**	**β-turn (%)**	**Others (%)**
RK	12.8	22.5	17	47.7
K5	9.0	63.4	--	27.6
K10	10.1	64.9	--	24.9
K15	14.2	70.5	--	15.4
K20	11.9	69.2	1.1	17.7

5.3.1.4 Tertiary structure

Fluorescence spectroscopy is a critical tool for analyzing tertiary structures of biomolecule studies. The intrinsic fluorescence of Trp residues is frequently applied for tracking protein conformation by analysis of changes in emission wavelength, intensity, absorption maxima, etc. [48]. The result of the fluorescence spectra of KNPs is shown in **Figure 5.4**.

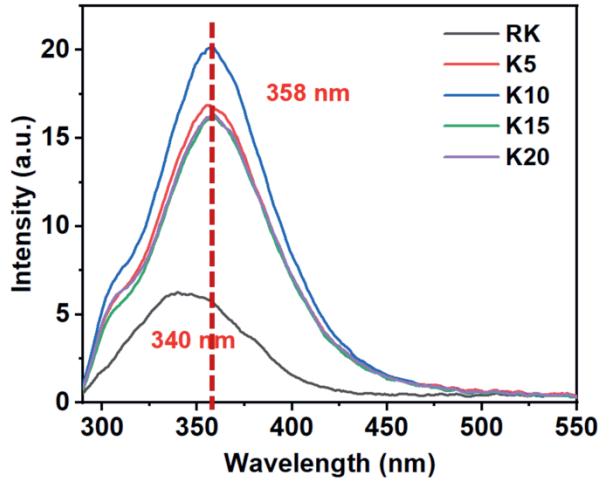

Figure 5.4. Fluorescence intensity of RK and KNPs (K5, K10, K15 and K20).

As indicated, KNPs exhibited strong absorption at 358 nm, shifting 18 nm to the right compared to RK. It was probably attributed to the increase of polarity of Trp exposed to an aqueous solution with the loosened structure of KNPs. The positively charged residues near the benzene end or negative charges near the pyrrole end of the Trp ring would produce a red shift due to the electric field imposed by protein and solvent [49]. Additionally, the fluorescence intensity of KNPs was obviously higher than RK. The dense and robust aggregation of RK might increase the shielding effect on Trp residues. The disulfide bonds have been reported as one of the strongest quenchers of Trp fluorescence [50]. As to KNPs, the fluorescence intensity first increased and then dropped with DH increasing. The low DH (≤ 10%) probably loosened the tight keratin aggregation and reduced the shielding effect on Trp, thus leading to increasing intensity. However, the higher DH (≥ 15%) resulted in more exposure of Trp buried in hydrophobic regions of KNPs. The more Trp exposed to polar microenvironment displayed a decreased fluorescence intensity. Meanwhile, a partial loss of hydrophobic groups, due to over-degradation and the reaggregation by hydrophobic residues, could also contribute to the decreasing fluorescence intensity [30, 51].

Given the above, partial hydrolysis with varying DHs did not influence the main chemical functionalities of KNPs, but changed the secondary and tertiary structure to some extent. The key reasons were probably the breakage and reformation of various inter- and intra-particle interactions, such as disulfide bonds, hydrophobic

interactions and hydrogen bonds.

5.3.1.5 Content of disulfide bonds

As reported, keratin extracted via the reduction technique possessed chain entanglements and free thiol groups that could spontaneously form disulfide crosslinking [52]. The changes in disulfide bonds in KNPs are closely related to KNPs conformation and behavior. Hence, disulfide bonds in various samples were quantified. As shown in **Figure 5.5**, RK contains the highest number of disulfide bonds, which might be formed when removing chemicals during extraction. After partial hydrolysis, the content of disulfide bonds significantly decreased and reached its lowest at 10% DH. More disulfide bonds were reformed when further hydrolyzing (DH ≥ 15%). The higher DH might cleave more disulfide bonds, producing growing thiol groups. They probably further reformed into disulfide crosslinking when forming nanoparticles. The increased disulfide bonds in K15 and K20 aptly accounted for the quenching effect on Trp fluorescence, as discussed in **section 5.3.1.4**.

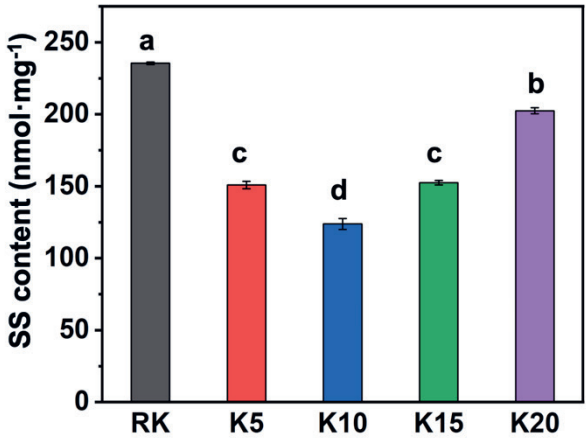

Figure 5.5. Disulfide bond content of RK and KNPs (K5, K10, K15 and K20). The data are presented as the mean values ± SD (n = 3). "a-d" indicate the significant difference between various samples ($P < 0.05$).

5.3.1.6 Analysis of surface hydrophobicity

The abovementioned changes in disulfide bonds, secondary and tertiary structures, probably influence the surface hydrophobicity of KNPs. Thus, the impact of various DHs on KNPs surface hydrophobicity was assessed. The result is shown in **Figure 5.6**. As indicated, the surface hydrophobicity dramatically decreased when the DH

increased from 5% to 10%. It might result from the preference for disulfide bond cleavage, with relatively higher production of hydrophilic residues. Previously, it has been interpreted that the disulfide bonds in keratin would be firstly attacked by disulfide sulfitolysis, yielding a partially cleaved protein that would be further degraded through the second phase of proteolysis [53]. Similarly, the surface hydrophobicity of soy protein nanoparticles was also found to decrease with DH increasing from 3% to 11%, leaving fractions with higher hydrophilicity in the supernatant [37].

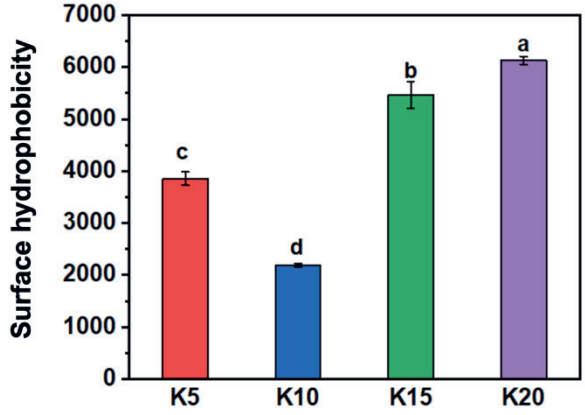

Figure 5.6. Surface hydrophobicity KNPs (K5, K10, K15 and K20). The data are presented as the mean values ± SD (n = 3), and "a-d" indicate the significant difference between different KNPs ($P < 0.05$).

Further hydrolysis from 15% to 20% led to an increasing surface hydrophobicity of KNPs. The higher DH resulted in a high unfolding of keratin and exposure of hydrophobic groups buried in the keratin structure. In alignment with this, **Figure 5.4** shows that more hydrophobic residues were exposed to the aqueous environment with DH increasing. Moreover, the reformed disulfide bonds would form an "inside-out" scaffold, which might also facilitate the hydrophobic groups to point outwards [54].

5.3.1.7 Thermogravimetric analysis (TGA) and derivative thermogravimetry analysis (DTGA)

TGA and DTGA were conducted to investigate the patterns of KNPs degradation and their thermal stability, possibly affecting their application. The result is illustrated in **Figure 5.7**.

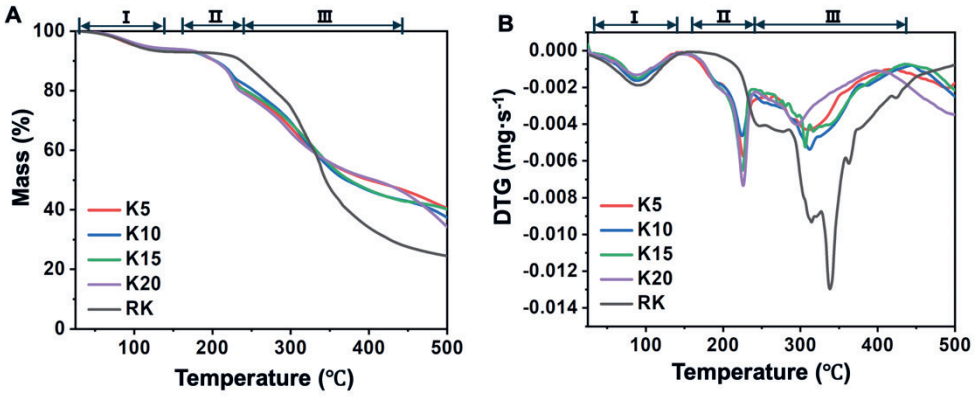

Figure 5.7. Thermogravimetric analysis (TGA) and derivative thermogravimetry analysis (DTGA) of RK and KNPs (K5, K10, K15 and K20). Areas labeled as "Ⅰ", "Ⅱ" and "Ⅲ" correspond to temperature ranges of "30-140 °C", "160-240 °C" and "240-440 °C", respectively.

KNPs were found to present three steps of weight loss when heating (areas Ⅰ, Ⅱ and Ⅲ), while RK had two main steps (areas Ⅰ and Ⅲ). The first weight loss phase happened from 30 to 140 °C (area Ⅰ), where various samples showed no obvious difference. This weight loss phase was attributed to moisture evaporation [55]. The second weight loss of KNPs occurred from 160 to 240 °C (area Ⅱ), where fewer changes happened to RK. It could be ascribed to the deconstruction of secondary structures, especially α-helix degradation, along with less tightly packed arrangement of molecules compared to RK [46, 56, 57]. Area Ⅲ (240-440 °C) is the last common weight loss for KNPs and RK, likely resulting from the deconstruction of disulfide bonds and polypeptide chains [58]. K5 and K10 showed similar characteristic temperatures (312 °C) for the final weight loss, while the characteristic temperature descended to 296 °C at DH 20% with promoted pyrolysis. It suggests that DHs ≥ 15% would result in poorer thermal stability of KNPs due to over-degradation.

5.3.1.8 Inter- and intra-particle forces

This part was conducted to elucidate the pattern of inter- and intra-particle forces maintaining KNP structures. The additives urea, SDS and DTT can break hydrogen bonds, hydrophobic interactions and disulfide bonds, respectively [37, 59]. The effect of different additives of altering protein interactions on size changes of KNPs is shown in **Figure 5.8**.

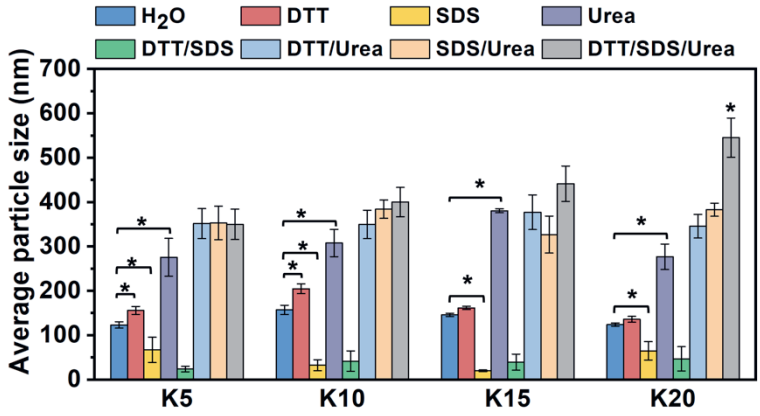

Figure 5.8. Average particle size of KNPs (K5, K10, K15 and K20) dispersed in various additives or combinations (H_2O, DTT, SDS, Urea, DTT/SDS, DTT/Urea, SDS/Urea and DTT/SDS/Urea). The data are presented as the mean values ± SD (n = 3), and "*" represents the significant difference between different additives ($P < 0.05$).

As **Figure 5.8** indicated, SDS and urea effectively changed the particle size of KNPs with varying DHs. It implies the roles of hydrophobic interactions and hydrogen bonds in maintaining KNPs structure. Additionally, K5 and K10 were significantly affected by DTT. They demonstrated an obvious increase in particle size from about 123 to 155 nm and 157 to 204 nm, respectively. In contrast, K15 and K20 were less affected by DTT. The result indicates that the intramolecular disulfide bonds might be dominant in K5 and K10, the breakage of which led to KNPs unfolding. The disulfide bond reforming at DH of 15% and 20% probably mainly happened between molecules. Moreover, the combination of additives obviously influenced the particle sizes of KNPs at higher DH. It suggests a synergistic and protective effect between different particle forces. The study demonstrates that hydrophobic interactions and hydrogen bonds played a leading role in maintaining the external structure of all KNPs. In contrast, disulfide bonds were potentially involved in maintaining internal structure at lower DH (≤ 10%). With DH increasing (DH ≥ 15%), the synergistic and protective effect of various particle forces would happen.

5.3.1.9 Anti-digestion ability of KNPs

The anti-digestion ability is critical for orally delivering systems, which could protect loaded biomolecules from harsh GI environments. Here, the changes in particle size and enzymatic degradation of KNPs during the GI tract were investigated. The results are shown in **Figure 5.9**.

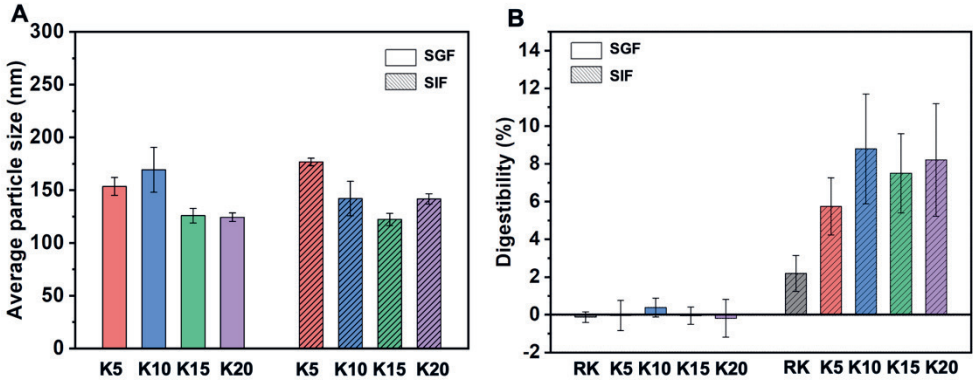

Figure 5.9. (A) Changes in average particle size of KNPs during the GI tract without enzyme and (B) digestibility of RK and KNPs during the GI tract with enzymes. The GI tract includes SGF and SIF, representing simulated gastric and intestinal fluids, respectively. The data are presented as the mean values ± SD (n = 3).

As observed in **Figure 5.9A**, K5 and K10 dispersed in SGF exhibited larger average particle sizes (~150 nm) than K15 and K20 (~125 nm). When transferring into SIF, the average particle size of four KNPs remained below 180 nm, exhibiting insignificant changes. From **Figure 5.9B**, the digestibility of KNPs remained similar to RK in the SGF phase, showing resistance to pepsin. When transited to the SIF phase, approximately 5.7-8.8 % of KNPs were degraded by enzymes, with a slight increase compared to RK (~2.19 %). The results indicate that KNPs demonstrated a relatively stable size under pH variations and resistance to enzymatic degradation in the GI tract, with the majority remaining undegraded. Moreover, variations in DH did not significantly affect KNPs digestibility. The stability could be attributed to the reformation of disulfide bonds, hydrophobic interactions and hydrogen bonds during KNPs self-assembly.

In summary, partial hydrolysis enhanced KNPs solubility and reduced their particle size to the nanoscale. Varying DHs did not alter the primary chemical functionalities but influenced the reformation of S-S bonds and keratin conformation. Higher DH resulted in increased β-structures and exposure of hydrophobic residues. These further contributed to improved surface hydrophobicity and more aggregation, albeit with reduced thermal stability. Hydrophobic interactions and hydrogen bonds were effective in maintaining the external structure of KNPs, while S-S bonds had an impact on the internal structure of KNPs at lower DH. Additionally, KNPs demonstrated stability in the GI tract, displaying minimal changes in particle size

and degradation. In brief, KNPs at lower DH are potential for orally delivering biomolecules.

5.3.2 Reversible structure via pH-shifting

Here the impact of pH-shifting on KNPs reactivity and restructuring was investigated. The transition of KNPs appearance from pH 2.0 to 7.0 was observed with TEM and presented in **Figure 5.10A-H**.

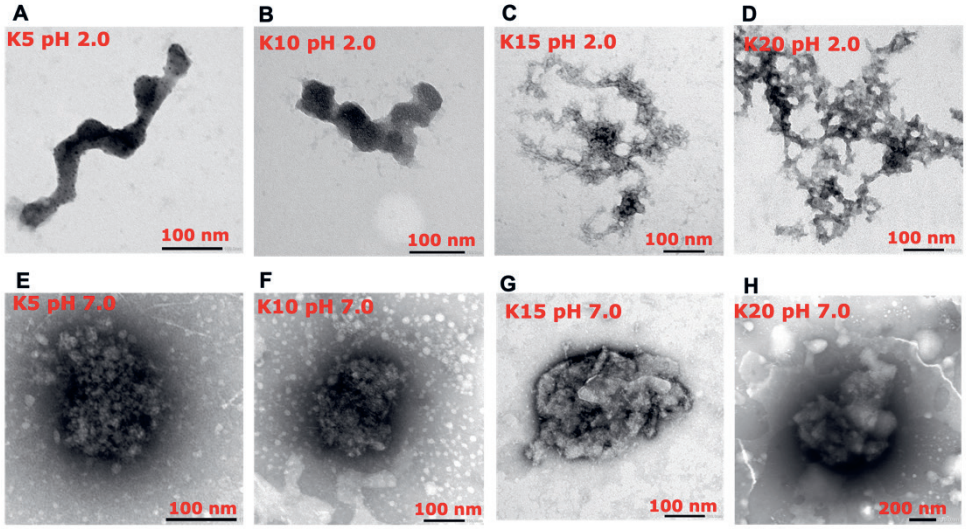

Figure 5.10. (A-D) Morphology of KNPs at pH 2.0 (PB 10 mM) and (E-H) Morphology of KNPs switched from pH 2.0 to pH 7.0. The samples were observed with TEM.

As depicted in **Figure 5.10A-D**, the acidic treatment at pH 2.0 efficiently unraveled the original spatial structure of KNPs at various DHs. K5 and K10 were unfolded and stretched into chain-like structures at pH 2.0, while unfolded K15 and K20 were interconnected due to exposed hydrophobic residues. After adjusting the pH to 7.0, the unfolded keratin molecules refolded into compact particles (**Figure 5.10E-H**), showing a potential reversible "open-close" structure. Specifically, the extended molecules of K5 and K10 were refolded into small tight particles with sizes below 200 nm, whereas the refolded particles from K15 and K20 were larger (> 300 nm) exhibiting irregular shapes. When turning from extremely acidic to neutral environment, the overexposed hydrophobic residues in K15 and K20 might easily interact and form larger clusters. Therefore, KNPs with DH ≤ 10% had a regularly reversible "open-close" structure by pH-shifting, showing potential in encapsulating biomolecules as carriers. Next, the loading efficiency of different

biomolecules will be investigated.

5.3.3 Particle size and loading efficiency of insulin- and resveratrol-loaded KNPs

This part delved into the biomolecule loading ability of KNPs with varying DHs based on their reversible "open-close" structure. Proteins and polyphenols, specifically insulin (Ins) and resveratrol (Res), were utilized for the investigation to gain deeper insights. The LE of insulin and resveratrol using KNPs is summarized in **Table 5.2**, along with the result of average particle size.

Table 5.2. Average particle size and loading efficiency of insulin- and resveratrol-loaded KNPs.

	Particle size (nm)	LE of Ins (%)		Particle size (nm)	LE of Res (%)
K5-Ins	141.2 ± 12.5	94.12 ± 5.31	**K5-Res**	131.9 ± 3.3	99.61 ± 0.44
K10-Ins	136.6 ± 19.7	77.04 ± 4.77	**K10-Res**	131.6 ± 1.3	92.48 ± 1.46
K15-Ins	308.1 ± 5.2	76.42 ± 4.60	**K15-Res**	168.7 ± 16.8	92.07 ± 0.59
K20-Ins	282.4 ± 14.3	73.42 ± 6.47	**K20-Res**	251.0 ± 33.6	87.41 ± 2.78

Note: Ins and Res represent insulin and resveratrol, respectively. LE represents the loading efficiency of biomolecules by KNPs, obtained as described in **section 5.2.10**. The data are presented as the mean values ± SD, n = 3.

As **Table 5.2** indicated, the average particle size of K5-Ins/Res and K10-Ins/Res ranged from approximately 132 nm to 141 nm that are smaller than K15 and K20 (168-308 nm). This result is consistent with the pictures observed in **Figure 5.10G-H**. The LE of Ins and Res by K5 was about 94% and 99%, respectively. Conversely, the increasing DH resulted in decreasing LE of Ins and Res, which dropped to about 73% and 87% by K20, respectively. This can be attributed to the higher production of smaller fragments as DH increased, leading to fewer refolded particles. Additionally, the abundance of hydrophobic residues in K15 and K20 might result in self-crosslinking, as observed in **section 5.3.2**. Thus, K5 demonstrated the highest capability in loading biomolecules due to its reversible structure facilitated by pH-shifting, making it a promising material for nanocarrier applications.

5.4 Conclusion

This study proposed an efficient strategy for preparing high-performance KNPs by combining partial hydrolysis and pH-shifting. Our study reveals the impact of DH on keratin reactivity and restructuring, along with the reversible "open-close" structure under pH shifting. The findings demonstrate that partial hydrolysis (5% DH) is beneficial for fabricating KNPs with nanoscale particle size in spherical shapes. They exhibited improved water solubility, anti-digestion stability, favorable "open-close" structure and high biomolecule loading efficiency. Combining partial hydrolysis and pH-shifting overcomes the limitations of keratin's robust chemical structure, making KNPs promising candidates for encapsulating biomolecules. Nevertheless, the stability of biomolecules under acidic conditions needs attention during encapsulation by KNPs. This study provides insights into the potential applications of KNPs (5% DH) in the field of biomolecule encapsulation and delivery, offering a novel and efficient platform for various nutritional, pharmaceutical and biomedical applications. Future studies on biomolecule release and fortification under specific targeted environments can be conducted.

5.5 References

1. X. Huang, X. Huang, Y. Gong, H. Xiao, D.J. McClements, K. Hu, Enhancement of curcumin water dispersibility and antioxidant activity using core–shell protein–polysaccharide nanoparticles, Food Research International, 87 (2016) 1-9.
2. B. Tian, J. Liu, Resveratrol: A review of plant sources, synthesis, stability, modification and food application, Journal of the Science of Food and Agriculture, 100 (2020) 1392-1404.
3. F. Jaberifard, N. Arsalani, M. Ghorbani, H. Mostafavi, Incorporating halloysite nanotube/carvedilol nanohybrids into gelatin microsphere as a novel oral pH-sensitive drug delivery system, Colloids and Surfaces A: Physicochemical and Engineering Aspects, 637 (2022).
4. J. Tuomilehto, J. Lindström, J.G. Eriksson, T.T. Valle, H. Hämäläinen, P. Ilanne-Parikka, S. Keinänen-Kiukaanniemi, M. Laakso, A. Louheranta, M. Rastas, Prevention of type 2 diabetes mellitus by changes in lifestyle among subjects with impaired glucose tolerance, New England Journal of Medicine, 344 (2001) 1343-1350.
5. Y. Yuan, M. Ma, Y. Xu, D. Wang, Surface coating of zein nanoparticles to improve the application of bioactive compounds: A review, Trends in Food Science & Technology, 120 (2022) 1-15.
6. S.S. Shetty, P. Halagali, A.P. Johnson, K.A. Spandana, H. Gangadharappa, Oral insulin delivery: Barriers, strategies, and formulation approaches: A comprehensive review, International Journal of Biological Macromolecules, (2023) 125114.
7. K. Mahajan, N. Thakur, M. Goswami, I. Arora, Polymer based nanoparticles for BCS class II drugs-"A mini Review", Materials Today: Proceedings, (2022).
8. J. Wu, Z. Zhu, W. Liu, Y. Zhang, Y. Kang, J. Liu, C. Hu, R. Wang, M. Zhang, L. Chen, How nanoparticles open the paracellular route of biological barriers: mechanisms, applications, and prospects, ACS nano, 16 (2022) 15627-15652.
9. D.A. Subramanian, R. Langer, G. Traverso, Mucus interaction to improve gastrointestinal retention and pharmacokinetics of orally administered nano-drug delivery systems, Journal of Nanobiotechnology, 20 (2022) 1-23.
10. S. Haddadzadegan, F. Dorkoosh, A. Bernkop-Schnurch, Oral delivery of therapeutic peptides and proteins: Technology landscape of lipid-based nanocarriers, Adv Drug Deliv Rev, 182 (2022) 114097.
11. N. Kato, U. Hasegawa, N. Morimoto, Y. Saita, K. Nakashima, Y. Ezura, H. Kurosawa, K. Akiyoshi, M. Noda, Nanogel-based delivery system enhances PGE2 effects on bone formation, Journal of cellular biochemistry, 101 (2007) 1063-1070.
12. A.E. Nel, L. Mädler, D. Velegol, T. Xia, E.M. Hoek, P. Somasundaran, F. Klaessig, V. Castranova, M. Thompson, Understanding biophysicochemical interactions at the nano–bio interface, Nature materials, 8 (2009) 543-557.
13. K. Maisel, L. Ensign, M. Reddy, R. Cone, J. Hanes, Effect of surface chemistry on nanoparticle interaction with gastrointestinal mucus and distribution in the gastrointestinal tract following oral and rectal administration in the mouse, Journal of Controlled Release, 197 (2015) 48-57.
14. K. Maruyama, Intracellular targeting delivery of liposomal drugs to solid tumors based on EPR effects, Advanced drug delivery reviews, 63 (2011) 161-169.
15. P. Jana, M. Shyam, S. Singh, V. Jayaprakash, A. Dev, Biodegradable polymers in drug delivery and oral vaccination, European Polymer Journal, 142 (2021).
16. T. Zhang, L. Li, S. Chunta, W. Wu, Z. Chen, Y. Lu, Enhanced oral bioavailability from food protein nanoparticles: A mini review, Journal of Controlled Release, 354 (2023) 146-154.

17. M. Pakdel, Z. Moosavi-Nejad, R.K. Kermanshahi, H. Hosano, Self-assembled uniform keratin nanoparticles as building blocks for nanofibrils and nanolayers derived from industrial feather waste, Journal of Cleaner Production, 335 (2022).
18. A.J. Poole, R.E. Lyons, J.S. Church, Dissolving Feather Keratin Using Sodium Sulfide for Bio-Polymer Applications, Journal of Polymers and the Environment, 19 (2011) 995-1004.
19. A. Ullah, T. Vasanthan, D. Bressler, A.L. Elias, J. Wu, Bioplastics from feather quill, Biomacromolecules, 12 (2011) 3826-3832.
20. H. Xu, Z. Shi, N. Reddy, Y. Yang, Intrinsically water-stable keratin nanoparticles and their in vivo biodistribution for targeted delivery, Journal of Agricultural & Food Chemistry, 62 (2015) 9145-9150.
21. A. Aluigi, M. Ballestri, A. Guerrini, G. Sotgiu, C. Ferroni, F. Corticelli, M.B. Gariboldi, E. Monti, G. Varchi, Organic solvent-free preparation of keratin nanoparticles as doxorubicin carriers for antitumour activity, Mater Sci Eng C Mater Biol Appl, 90 (2018) 476-484.
22. J. Lin, X. Zhi, P. Li, X. Jiang, Y. Jiang, Triple stimuli-responsive keratin nanoparticles as carriers for drug and potential nitric oxide release, Materials Science and Engineering: C, (2018).
23. S. Racoviță, S. Vasiliu, M. Popa, C. Luca, Polysaccharides based on micro-and nanoparticles obtained by ionic gelation and their applications as drug delivery systems, Revue Roumaine de Chimie, 54 (2009) 709-718.
24. C. Arpagaus, PLA/PLGA nanoparticles prepared by nano spray drying, Journal of Pharmaceutical Investigation, 49 (2019) 405-426.
25. R. Peñalva, I. Esparza, J. Morales-Gracia, C.J. González-Navarro, E. Larrañeta, J.M. Irache, Casein nanoparticles in combination with 2-hydroxypropyl-β-cyclodextrin improves the oral bioavailability of quercetin, International journal of pharmaceutics, 570 (2019) 118652.
26. C. Liu, B. Xu, D.J. McClements, X. Xu, S. Cui, L. Gao, L. Zhou, L. Xiong, Q. Sun, L. Dai, Properties of curcumin-loaded zein-tea saponin nanoparticles prepared by antisolvent co-precipitation and precipitation, Food Chemistry, 391 (2022) 133224.
27. L. Dai, H. Zhou, Y. Wei, Y. Gao, D.J. McClements, Curcumin encapsulation in zein-rhamnolipid composite nanoparticles using a pH-driven method, Food Hydrocolloids, 93 (2019) 342-350.
28. J. Jiang, Y.L. Xiong, J. Chen, Role of β-conglycinin and glycinin subunits in the ph-shifting-induced structural and physicochemical changes of soy protein isolate, Journal of food science, 76 (2011) C293-C302.
29. Y. Yang, S. He, Y. Ye, X. Cao, H. Liu, Z. Wu, J. Yue, H. Sun, Enhanced hydrophobicity of soybean protein isolate by low-pH shifting treatment for the sub-micron gel particles preparation, Industrial Crops and Products, 151 (2020).
30. D. Yuan, F. Zhou, P. Shen, Y. Zhang, L. Lin, M. Zhao, Self-assembled soy protein nanoparticles by partial enzymatic hydrolysis for pH-Driven Encapsulation and Delivery of Hydrophobic Cargo Curcumin, Food Hydrocolloids, 120 (2021).
31. X. Qin, C. Yang, Y. Guo, J. Liu, J.H. Bitter, E.L. Scott, C. Zhang, Effect of ultrasound on keratin valorization from chicken feather waste: process optimization and keratin characterization, Ultrasonics Sonochemistry, (2023) 106297.
32. P. Nielsen, D. Petersen, C. Dambmann, Improved method for determining food protein degree of hydrolysis, Journal of food science, 66 (2001) 642-646.
33. O.H. Lowry, N.J. Rosebrough, A.L. Farr, R.J. Randall, Protein measurement with the Folin phenol reagent, Journal of biological chemistry, 193 (1951) 265-275.

34. A. Micsonai, F. Wien, É. Bulyáki, J. Kun, É. Moussong, Y.-H. Lee, Y. Goto, M. Réfrégiers, J. Kardos, BeStSel: a web server for accurate protein secondary structure prediction and fold recognition from the circular dichroism spectra, Nucleic acids research, 46 (2018) W315-W322.
35. K.Y. Chan, B.P. Wasserman, Direct Colorimetric Assay of Free Thiol Groups and Disulfide Bonds in Suspensions of Solubilized and Particulate Cereal Proteins, Cereal Chemistry, 70 (1993) 22-26.
36. Thannhauser, T. W., Konishi, Y., Scheraga, H. A., Analysis for disulfide bonds in peptides and proteins. Methods in Enzymology. Academic Press, 143 (1987) 115-119.
37. P. Shen, F. Zhou, Y. Zhang, D. Yuan, Q. Zhao, M. Zhao, Formation and characterization of soy protein nanoparticles by controlled partial enzymatic hydrolysis, Food Hydrocolloids, 105 (2020).
38. A. Najjar, M. Alawi, N. AbuHeshmeh, A. Sallam, A rapid, isocratic HPLC method for determination of insulin and its degradation product, Advances in Pharmaceutics, 2014 (2014).
39. D. Pavia, G. Lampman, G. Kriz, J. Vyvyan, Introduction to Spectroscopy (p. 38), Belmont: Brooks/Cole, Cengage Learning, (2008).
40. S. Sharma, A. Gupta, S.M.S.B.T. Chik, C.Y.G. Kee, P.K. Poddar, Dissolution and characterization of biofunctional keratin particles extracted from chicken feathers, in: IOP conference series: materials science and engineering, IOP Publishing, 2017, pp. 012013.
41. D. Wang, W. Li, Y. Wang, H. Yin, Y. Ding, J. Ji, B. Wang, S. Hao, Fabrication of an expandable keratin sponge for improved hemostasis in a penetrating trauma, Colloids Surf B Biointerfaces, 182 (2019) 110367.
42. F. Pourjavaheri, S. Ostovar Pour, O.A.H. Jones, P.M. Smooker, R. Brkljača, F. Sherkat, E.W. Blanch, A. Gupta, R.A. Shanks, Extraction of keratin from waste chicken feathers using sodium sulfide and l-cysteine, Process Biochemistry, 82 (2019) 205-214.
43. G. Han, Y. Li, Q. Liu, Q. Chen, H. Liu, B. Kong, Improved water solubility of myofibrillar proteins by ultrasound combined with glycation: A study of myosin molecular behavior, Ultrason Sonochem, 89 (2022) 106140.
44. B. Ma, Q. Sun, J. Yang, J. Wizi, X. Hou, Y. Yang, Degradation and regeneration of feather keratin in NMMO solution, Environ Sci Pollut Res Int, 24 (2017) 17711-17718.
45. P. Kakkar, S. Verma, I. Manjubala, B. Madhan, Development of keratin–chitosan–gelatin composite scaffold for soft tissue engineering, Materials Science and Engineering: C, 45 (2014) 343-347.
46. S. Alahyaribeik, A. Ullah, Methods of keratin extraction from poultry feathers and their effects on antioxidant activity of extracted keratin, Int J Biol Macromol, 148 (2020) 449-456.
47. X. Sun, W. Zhang, L. Zhang, S. Tian, F. Chen, Effect of ultrasound-assisted extraction on the structure and emulsifying properties of peanut protein isolate, Journal of the Science of Food and Agriculture, 101 (2021) 1150-1160.
48. A.B. Ghisaidoobe, S.J. Chung, Intrinsic tryptophan fluorescence in the detection and analysis of proteins: a focus on Förster resonance energy transfer techniques, International journal of molecular sciences, 15 (2014) 22518-22538.
49. J.T. Vivian, P.R. Callis, Mechanisms of tryptophan fluorescence shifts in proteins, Biophysical journal, 80 (2001) 2093-2109.
50. A.S. Ladokhin, Fluorescence spectroscopy in peptide and protein analysis, Encyclopedia of analytical chemistry, (2000) 5762-5779.
51. K. Gao, J. Rao, B. Chen, Unraveling the mechanism by which high intensity ultrasound improves the solubility of commercial pea protein isolates, Food Hydrocolloids, 131 (2022).

52. S. Han, T.R. Ham, S. Haque, J.L. Sparks, J.M. Saul, Alkylation of human hair keratin for tunable hydrogel erosion and drug delivery in tissue engineering applications, Acta Biomater, 23 (2015) 201-213.
53. S. Yamamura, Y. Morita, Q. Hasan, K. Yokoyama, E. Tamiya, Keratin degradation: a cooperative action of two enzymes from Stenotrophomonas sp, Biochemical and Biophysical Research Communications, 294 (2002) 1138-1143.
54. A. Kam, S. Loo, J.-S. Fan, S.K. Sze, D. Yang, J.P. Tam, Roseltide rT7 is a disulfide-rich, anionic, and cell-penetrating peptide that inhibits proteasomal degradation, Journal of Biological Chemistry, 294 (2019) 19604-19615.
55. A. Higuchi, T. Iijima, DSC investigation of the states of water in poly (vinyl alcohol) membranes, Polymer, 26 (1985) 1207-1211.
56. P. Milczarek, M. Zielinski, M. Garcia, The mechanism and stability of thermal transitions in hair keratin, Colloid and Polymer Science, 270 (1992) 1106-1115.
57. G. Guidotti, M. Soccio, T. Posati, G. Sotgiu, M. Tiboni, M. Barbalinardo, F. Valle, L. Casettari, R. Zamboni, N. Lotti, A. Aluigi, Regenerated wool keratin-polybutylene succinate nanofibrous mats for drug delivery and cells culture, Polymer Degradation and Stability, 179 (2020).
58. A. Vasconcelos, G. Freddi, A. Cavaco-Paulo, Biodegradable materials based on silk fibroin and keratin, Biomacromolecules, 9 (2008) 1299-1305.
59. D. Yuan, F. Zhou, Z. Niu, P. Shen, M. Zhao, Formation of mucus-permeable nanoparticles from soy protein isolate by partial enzymatic hydrolysis coupled with thermal and pH-shifting treatment, Food Chem, 398 (2023) 133851.

5.6 Supplementary materials

Table S5.1. Degree of hydrolysis (DH) and average particle size of KNPs.

	DH (%)	Average particle size (nm)	Polydispersity index (PDI)
K5	5 ± 0.54	123.1 ± 7.0	0.46 ± 0.02
K10	10 ± 0.52	157.1 ± 10.5	0.60 ± 0.18
K15	15 ± 0.51	137.9 ± 8.1	0.40 ± 0.03
K20	20 ± 0.37	124.2 ± 4.3	0.37 ± 0.01

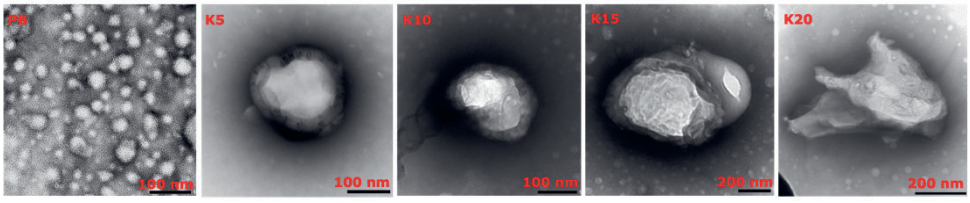

Figure S5.1. TEM of PB (pH 7.0, 10 mM) reference and KNPs (K5, K10, K15 and K20).

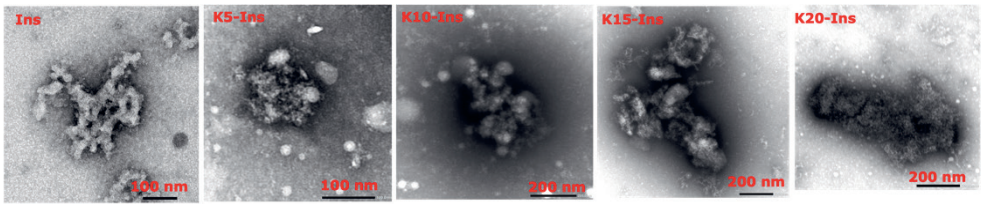

Figure S5.2. TEM of insulin and insulin-loaded KNPs.

6

CHAPTER 6

Preparation and evaluation of double-coated nanoparticles incorporating keratin and sodium alginate for enhanced stability

Authors: Xiaojie Qin, Johannes H. Bitter, Chunhui Zhang, Elinor L. Scott

Abstract

Protein-based nanoparticles are becoming a favorable formulation for orally delivering biomolecules. They can provide biomolecules with improved water solubility, less aggregation, protection from harsh pH and enzymatic degradation. However, some of them exhibit inadequate stability in various environments, resulting in premature degradation and low bioavailability. Here we show a novel insulin (INS)-loaded formulation constructed from keratin nanoparticles (KNP) and sodium alginate (ALG) with enhanced performance. We found that double-coating nanoparticles (ALG-KNP-INS) via a gelation technique displayed a small average particle size (~173 nm) with regular spherical shapes alongside good re-dispersibility. The ALG-KNP coating demonstrated a positive effect on stabilizing size (< 200 nm) during heating (80 °C) with enhanced insulin stability (> 83% undegraded). Likewise, enhanced stability in size (< 270 nm) and insulin (> 77% undegraded) was observed during storage at 4 °C for 4 weeks. Moreover, ALG-KNP-INS presented size changes in the gastrointestinal tract, potentially protecting insulin against enzymatic degradation. Our findings indicate ALG-KNP coating as a stability-enhanced formulation, exhibiting small spherical shapes and uniform distribution. We anticipate our study to give a competitive alternative formulation for biomolecule encapsulation and delivery. The ALG-KNP coating holds potential for enhancing the performance and bioavailability of various biomolecules in the fields of food, nutraceuticals and pharmaceuticals.

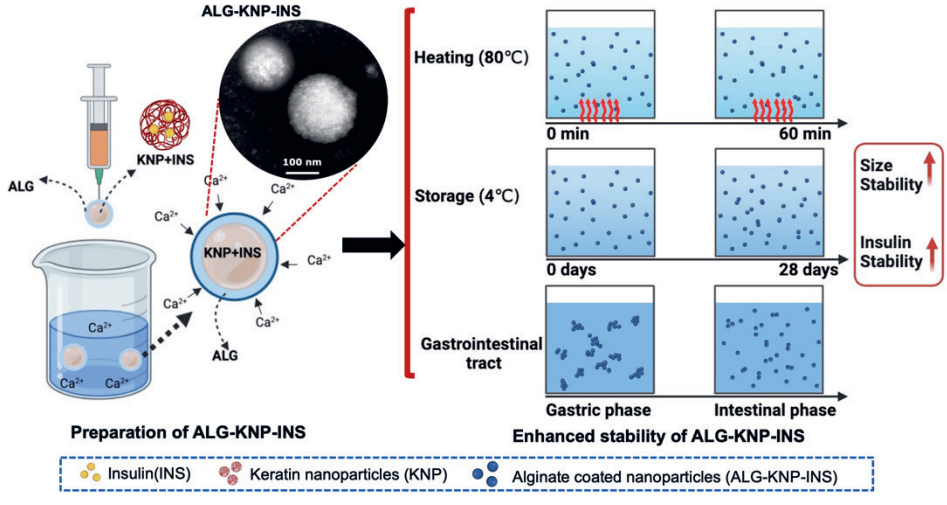

6.1 Introduction

Recent advances in *in-vitro* screening methods have given rise to numerous biomolecules with diverse biological activities, showing potential in pharmaceutical and food areas [1]. For example, the biomolecules quercetin and curcumin provide effectiveness against oxidation, cancer and inflammation [2, 3]. Oral administration is preferred owing to its simplicity, convenience and high patient compliance [4]. Despite their appealing bioactivities, most of them exhibit poor physicochemical properties, such as poor water solubility, susceptibility to harsh pH and enzymes and low biomembrane permeability [5, 6]. For example, quercetin and curcumin exhibited poor solubility and physicochemical stability in aqueous media and low oral bioavailability [2, 7]. Insulin (INS), another example, also encounters challenges under varying environmental and physiological conditions, such as low water solubility, instability at high temperatures and harsh pH, enzymatic degradation, etc. [8, 9]. In this regard, their bioavailability and applications are often restricted. Therefore, an effective technique to enhance the physicochemical properties of biomolecules and provide protection against various barriers is becoming imperative.

Researchers have attempted to develop protein-based nanoparticles for orally delivering biomolecules, such as soy protein and zein nanoparticles [10, 11]. Besides the low toxicity, biocompatibility and biodegradability, natural proteins exhibit a wide array of functional groups, such as hydroxyl, carboxyl and amino groups. These functional groups enable chemical modifications and effective interactions with biomolecules [12, 13]. Nanoparticles become favorable because of their appealing merits, such as enhanced solubility in aqueous media, less aggregation, protection of biomolecules from harsh environments, controlled release and ability to penetrate biological membranes, etc. [12]. Hence, protein nanoparticles are a promising formulation for oral delivery systems. Nevertheless, some proteins exhibited inadequate stability in aqueous environments and physiological temperatures [14]. The loaded biomolecules often encounter challenges such as premature leakage and degradation, restricted loading capacity and release limitations [6]. Therefore, a stability-enhanced formulation constructed by more stable protein material is required. Among these, keratin, a protein with intrinsic water stability, holds particular promise for nanoparticle fabrication [13].

Keratin is an abundant natural protein resource in animal by-products, which consists over 90% in chicken feathers [15]. Literature has reported the potential of keratin as a carrier due to its attributes of biocompatibility, biodegradability, low toxicity, water stability and resistance to conventional enzymes [13, 16]. It has been upcycled into diverse biomaterials, e.g. nanoparticles, microparticles and hydrogels [14, 17, 18]. Earlier, researchers elucidated the positive impact of keratin nanoparticles (KNP) on cell attachment and proliferation and the ability to penetrate into kidney and liver cells [13]. Our previous investigations have also demonstrated the potential of keratin peptides to alter cell membrane permeability since they were able to inhibit *E.coli* and improve insulin delivery into Caco2 cells [15]. Furthermore, an approach combining partial hydrolysis and pH-shifting techniques was found to be effective for preparing biomolecule-loaded KNP in our previous study (**Chapter 5**). The resultant KNP exhibited potential for oral delivery systems. However, a protective coating will be essential to shield KNP from potential deconstruction under pH variations in the gastrointestinal (GI) tract. Polysaccharides are taken as versatile biopolymers capable of modification, functionalization and coating to meet oral delivery requirements [19]. Among these, sodium alginate (ALG) provides a promising coating option due to its efficient properties.

ALG exhibits biocompatibility, biodegradability, non-toxicity and gelatinization, thus being widely applied in dietetic, biotechnology, cosmetic and pharmaceutical areas [4]. The gel-forming and mucosal adhesion properties of ALG render it a viable excipient for enhancing drug delivery dosage forms [20]. ALG can form a swollen polymer matrix by cross-linking. It is able to shrink at acidic pH and swell at neutral or basic pH, along with its exceptional muco adhesion properties [21-23]. ALG has been recognized for its potential in modulating molecule delivery within the intestinal tract. It has been employed in various formulations, including nanoparticles, liposomes, capsules, tablets, hydrogels, beads and microspheres [3, 22, 24]. Given the above, ALG stands out as a prime candidate for shielding biomolecules-loaded KNP from harsh pH and enzymatic degradation in the GI tract.

This study aims to develop stability-enhanced nanoparticles incorporating ALG and KNP for biomolecule encapsulation and delivery. Allied to it, the effect of ALG-KNP coating on the physicochemical properties and stability of nanoparticles will be assessed. Here insulin will be applied as the target biomolecule for evaluating nanoparticle performance. To reach that aim, the following approaches were applied.

First, three techniques including covalent crosslinking, gelation and inverse gelation were evaluated and screened. Then ALG-KNP-INS and ALG-INS were prepared, taking KNP-INS and INS as controls. Subsequently, the physicochemical characterization of various nanoparticles was conducted, involving particle size, FTIR, re-dispersibility and microstructure. After that, the environmental stability (e.g. thermal and storage stability) and the physiological stability in the GI tract with/without enzymes were investigated.

6.2 Materials and methods

6.2.1 Materials and chemicals

Feather keratin was extracted using Cys-reduction assisted with ultrasound, as described in our previous study [25]. Chicken feathers were supplied by the Institute of Animal Science of the Chinese Academy of Agricultural Science (Beijing, China). The chemicals, including sodium alginate (medium viscosity, A2033), N-(3-Dimethylaminopropyl)-N′-ethylcarbodiimide hydrochloride (EDC), N-Hydroxysuccinimide (NHS), pepsin and pancreatin, were of analytical grade and provided by Sigma. The bovine insulin (27 U/mg, 5733.49 Da) was supplied by Yuanye Bio-Technology Co., Ltd. Acetonitrile (ACN) and methanol (MeOH) were of HPLC gradient grade supplied by Actu-All chemicals.

6.2.2 Preparation of insulin-loaded keratin nanoparticles

KNP was prepared according to our previous method (**Chapter 5**). Briefly, keratin was hydrolyzed to a degree of hydrolysis (DH, 5%) using keratinase (6000 U/g) under conditions of 55 °C, pH 8.5. The enzymes were inactivated by heating at 95 °C for 3 min, and the mixture was adjusted to pH 7.0. After centrifugation at 8000 ×g, 4 °C for 20 min, the supernatant was collected and lyophilized. The self-assembled KNP was obtained and lyophilized.

KNP-INS were formed based on the pH-shifting method (**Chapter 5**). Briefly, 20 mg KNP was unfolded by dispersing in 2 mL of phosphate buffer (PB, 10 mM, pH 2.0) and stirring at 700 rpm for 1 h. Then, 2 mL of insulin stock (5 mg/mL, 0.01 M HCl) was added and stirred for another 1 h. The pH of the mixture was subsequently adjusted to 7.0 using NaOH (1 M). After 1h agitation, the refolded particles were formed. Free insulin was removed by dialysis with a molecular weight cutoff (MwCO: 7 kDa). Finally, KNP-INS were collected and lyophilized.

6.2.3 Preparation of alginate-coated nanoparticles and covalently crosslinked nanoparticles

KNP-INS were coated with ALG by inverse gelation and gelation methods, grouped as IAKI and GAKI, respectively. The procedures are shown in **Figure 6.1**. First, the concentrations of $CaCl_2$ (final: 0-10 mM) and ALG (final: 0.1-2 mg/mL) were optimized based on the particle size changes. After that, KNP-INS were formed according to the procedure above (**section 6.2.2**) by adding a certain volume of $CaCl_2$ (1 M). The mixture was subsequently added dropwise to an equal volume of ALG (1 mg/mL) at 2.5 mL/h using a syringe pump (NE-1600, SyringeSIX, New Era Instruments, USA). The mixture was continually stirred at 700 rpm for 1 h to form IAKI. After removing free insulin via dialysis (MwCO: 7 kDa), IAKI was obtained.

For GAKI preparation, the concentrations of $CaCl_2$ (final: 2-8 mM) and ALG (final: 0.1-2 mg/mL) were optimized initially. The dispersion of KNP-INS, formed according to **section 6.2.2**, was added dropwise to an equal volume of ALG (1 mg/mL) at the speed of 2.5 mL/h. After 1h of continual agitation, the mixture was dropped dropwise to an equal volume of $CaCl_2$ solution (8 mM). After stirring for another 1 h, GAKI was formed. Free insulin was removed by dialysis (MwCO: 7 kDa). The control was prepared using the same procedure without KNP, named ALG-INS.

As shown in **Figure 6.1**, covalent crosslinking nanoparticles were fabricated using the previous method with minor modifications [26, 27]. The pH of KNP-INS dispersion (formed from **section 6.2.2**) was adjusted to 4.7 and then was mixed with EDC (24 mg) and NHS (28.8 mg). The mixture was stirred for 1 h, followed by a stand at 4 °C for 24 h. Subsequently, the pH of the mixture was switched to 7.4 and continued with 1 h agitation. After an additional placement at 4 °C for 24 h, the mixture was finally dialyzed to remove free insulin (MwCO: 7 kDa). The formed particles were named as K=I.

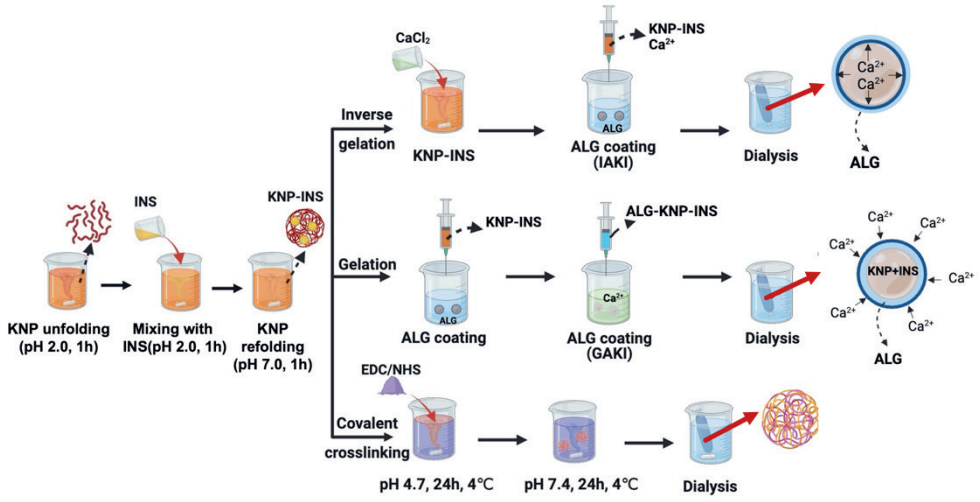

Figure 6.1. Scheme of inverse gelation, gelation and covalent crosslinking for nanoparticle preparation.

The insulin amount in the nanoparticle solution obtained above was quantified using the HPLC method. IAKI, IAI, GAKI and GAI were finally lyophilized and stored at -20 °C for further analysis, including particle size, polydispersity index (PDI), re-dispersibility and microstructure.

6.2.4 Insulin quantification

The method for insulin measurement was modified according to the previous method [28]. Briefly, the obtained samples were diluted with PB (pH 7.4, 20 mM) and then subjected to Acquity UPLC BEH C18 column (2.1 mm × 150 mm, Waters). They were detected using a variable wavelength detector at 214 nm (Thermo Fisher Ultrimate 3000, Thermo Fisher Scientific, USA). The mobile phase was composed of A (PB, 0.1 M, pH 7.4) and B (©/MeOH, 65/30, v/v). The sample injection volume was 5 μL, and the flow rate was 0.3 ml/min (A/B, 55/45, v/v). The temperatures of the sampler and column were set at 4 °C and 55 °C, respectively.

6.2.5 Characterization of nanoparticles

Particle size, PDI and ζ-potential were analyzed using a dynamic light scattering (DLS) instrument (Nano ZetaSizer, Malvern Instruments, UK). The samples were diluted to 0.1 mg/mL with Milli-Q water and measured at 25 °C.

The microstructure of nanoparticles was observed using transmission electron microscopy (TEM, JEM 1400Plus, JEOL Ltd., USA). Briefly, 5 μL of sample solution

(0.1 mg/mL) was added on a formvar/carbon grid and stood for 2 min. After removing the excess, the grid was washed with Milli-Q water. Then, the negative staining was conducted using 5 μL of phosphotungstic acid (1%, w/v). The grid was finally observed using TEM.

The chemical functionality of nanoparticles was assessed via a Fourier transform infrared spectroscopy (FTIR, Vertex 70, Bruker Inc., U.S.). Briefly, the samples were ground with dried potassium bromide and compressed into a 1 mm slice. They were scanned from 400 to 4000 cm^{-1} with a resolution of 4 cm^{-1}.

6.2.6 Re-dispersibility in Milli-Q water

The re-dispersibility of lyophilized nanoparticles was evaluated by redispersing in Milli-Q water. Briefly, freshly prepared samples were lyophilized into powders and then redispersed in Milli-Q water at a concentration of 1 mg/mL. Redissolved samples were observed for appearance by taking pictures. The analysis of particle size and PDI was conducted using ZetaSizer.

6.2.7 Thermal stability

The thermal stability was investigated by evaluating the changes in particle size and insulin stability at 80 °C, referring to the previous study [29]. Briefly, nanoparticles were dispersed in Milli-Q water at 1 mg/mL concentration. The dispersions were heated at 80 °C for predetermined times (0, 10, 20, 30 and 60 min) and then were placed into an ice bath for cooling. The particle size and insulin amount were measured using ZetaSizer and HPLC, respectively, following the methods described above.

6.2.8 Storage stability

The stability of nanoparticles within four weeks of storage at 4 °C was investigated. Nanoparticle dispersions (1 mg/mL) were prepared by dissolving in Milli-Q water. They were then placed in a fridge at 4 °C. The changes in particle size and the remaining insulin amount were monitored at various time points (0, 3, 7, 14, 21 and 28 days), using ZetaSizer and HPLC abovementioned.

6.2.9 Stability in the gastrointestinal tract

Here the stability of nanoparticles treated with or without enzymes in the GI tract was investigated, referring to the previous method with minor modifications [30, 31].

The GI tract consists of the gastric phase followed by the intestinal phase. For the gastric phase, samples were dispersed in an HCl solution (pH 1.2) with the final insulin concentration of 1 mg/mL, containing 1.6 mg/mL of pepsin. The mixture was incubated in a water bath at 37 °C under agitation of 250 rpm. Digesta samples were collected at predetermined time points (0, 30, 60 and 90 min), followed by pH adjustment to 7.0 using 1 M NaOH and subsequent cooling in an ice bath.

For the intestinal phase, the pH of the mixture after the 90-min gastric phase was adjusted to 6.8 using NaOH (1 M). Then it was mixed with the same volume of pancreatin solution (10 mg/mL) dissolved in PB (pH 6.8, 10 mM). The mixture was placed in a water bath for another 120-min incubation, stirring at 250 rpm, 37 °C. At predetermined time intervals (30, 60, 90 and 120 min), the digesta was collected and promptly cooled for subsequent analysis.

The particle size and insulin stability were investigated without adding enzymes, which were detected using ZetaSizer and HPLC, respectively. The SDS-PAGE method was used to examine the insulin stability under enzymes. The control groups (INS and KNP-INS) and blank (enzymes only) were also performed.

6.2.10 SDS PAGE

The intestinal digesta treated with enzymes, collected from **section 6.2.9**, was dissolved in NuPAGE LDS sample buffer (2×) containing a reducing agent. The mixture was heated at 70 °C for 10 min and then centrifuged at 10000 × g for 1 min. Then, 20 μL of each sample was loaded into a tricine gel containing 10-20% polyacrylamide. The separation was performed at 200 V, followed by gel staining with Coomassie brilliant blue G-250. After that, the gel was washed using a distaining solution (10% ethanol and 7.5% acetic acid) until the blue bands appeared in the transparent background. Finally, the gels were observed using Gelscanner (GS900, Bio-Rad, US).

6.2.11 Statistics

The data analysis was conducted using Microsoft Excel, while the figures were generated using Origin 2019 software and the Biorender website. The analysis was based on triplicate samples, and the results are presented as the mean values ± standard deviation (SD).

6.3 Results and discussion

6.3.1 Evaluation of techniques for coating nanoparticles

6.3.1.1 Optimization of $CaCl_2$ and alginate concentrations for inverse-gelation technique

ALG can form nanoparticles by ionotropic gelation with divalent cations [32]. However, excess Ca^{2+} may also result in KNP aggregation, affecting the generation of uniformly sized nanoparticles. Thus, the optimal concentration of $CaCl_2$ was initially investigated, along with the ALG concentration.

The results involving particle size, ζ-potential and morphology are shown in **Figure 6.2A-D**. As depicted in **Figure 6.2A**, 2 mM of $CaCl_2$ induced a slight decrease in the average particle size of KNP-INS, which reduced from about 130 nm to 100 nm. Increasing the $CaCl_2$ concentration ≥ 4 mM resulted in KNP-INS aggregation, with an average particle size over 348 nm. Higher $CaCl_2$ concentration (8-10 mM) even induced large aggregations and flocculation, with a size > 1600 nm. The reduced size at 2 mM was probably caused by the structural rearrangement of KNP-INS, forming more compact particles with the effect of Ca^{2+} [33]. Nevertheless, excessive Ca^{2+} could produce extensive particle aggregation and gravitational separation owing to the strong electrostatic interactions between particles [34]. Thus, 2 mM of $CaCl_2$ concentration would be applied for forming ALG-coated nanoparticles.

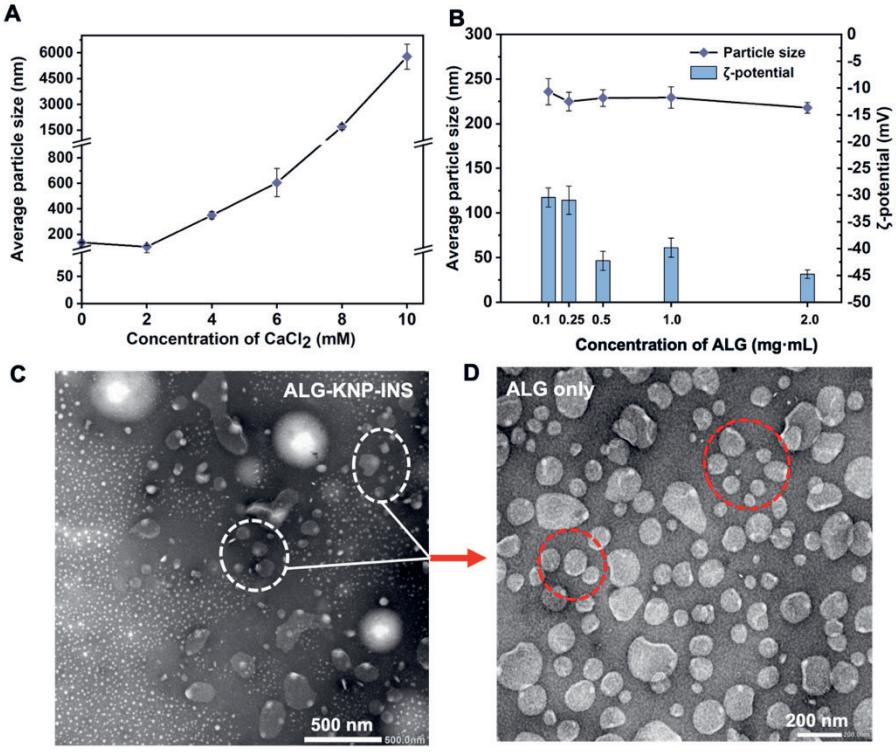

Figure 6.2. (A) Changes in average particle size of KNP-INS under various $CaCl_2$ concentrations (0-10 mM), (B) average particle size and ζ-potential of particles coated by ALG with varying concentrations (0.1-2 mg/mL), where $CaCl_2$ concentration was 2 mM, (C) TEM image of particles coated by 1 mg/mL ALG with 2 mM $CaCl_2$, and (D) TEM image of ALG-only at 1 mg/mL with 2 mM $CaCl_2$ following the same process. The data are presented as the mean values ± SD, n = 3.

The effect of varying ALG concentrations on average particle size and ζ-potential of ALG-coated nanoparticles is illustrated in **Figure 6.2B**. The findings suggest that increasing the ALG concentration (from 0.1 to 2 mg/mL) had minimal impact on the average particle sizes, which remained around 220 nm. The result indicates no significant decrease in ζ-potential with ALG ≥ 0.5 mg/mL, which reached about -42 mV, implying an adequate coating with ALG at 0.5 mg/mL. Similarly, the curcumin-encapsulated zein/caseinate-alginate nanoparticles showed a similar ζ-potential of -39.9 ± 1.2 mV [35]. A higher concentration (≥ 1.0 mg/mL) may produce excessive ALG-only nanoparticles. As confirmed by TEM images **(Figure 6.2C&D)**, 1.0 mg/mL of ALG yielded numerous ALG-only nanoparticles. The average particle size of ALG-only nanoparticles exceeded 200 nm, potentially contributing to an insignificant size variation in ALG-coated KNP-INS (**Figure 6.2B**). Hence, 0.5 mg/mL ALG would be

applied for forming ALG-coated KNP-INS via inverse gelation.

6.3.1.2 Optimization of $CaCl_2$ and alginate concentrations for gelation technique

Here the appropriate concentrations of ALG and $CaCl_2$ were investigated for the gelation method, and the results are shown in **Figure 6.3A-D**. The result from **Figure 6.3A** indicates an insignificant change in particle size with $CaCl_2 \leq 4$ mM, remaining at about 190 nm, while 8 mM $CaCl_2$ induced aggregation of ALG-coated KNP-INS with an average particle size surpassing 900 nm. The exposure of ALG to excess Ca^{2+} potentially led to the formation of large particles. Thus, 4 mM $CaCl_2$ would be applied to form ALG-coated nanoparticles.

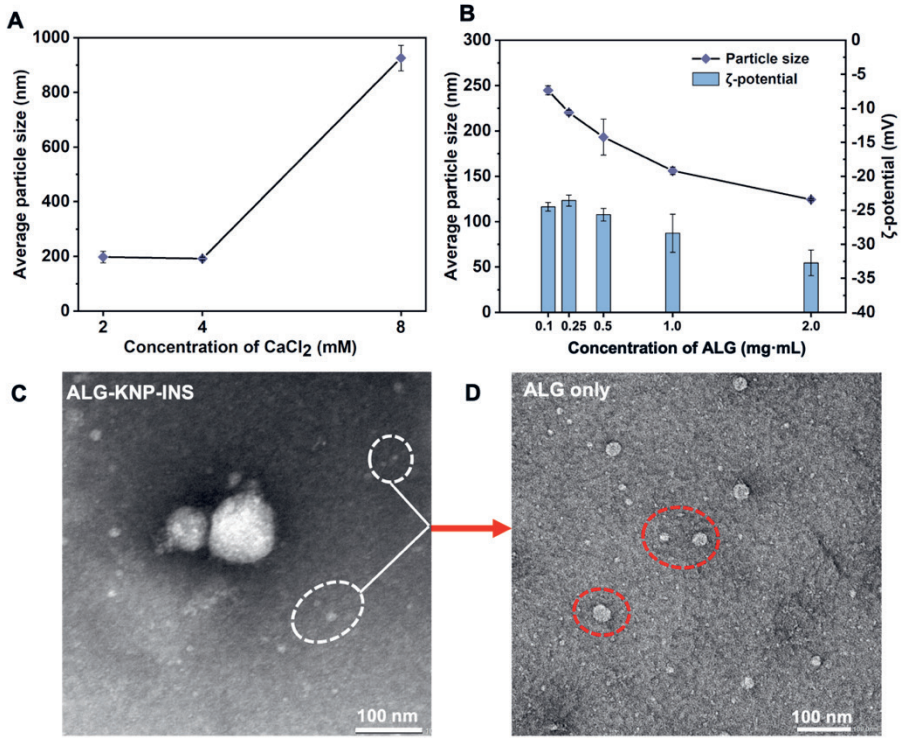

Figure 6.3. (A) Changes in average particle size of ALG-KNP-INS under various $CaCl_2$ concentrations (2-8 mM), where ALG concentration was 1 mg/mL, (B) average particle size and ζ-potential of particles coated by ALG with varying concentrations (0.1-2 mg/ml), where $CaCl_2$ concentration was 4 mM, (C) TEM image of particles formed by 1 mg/mL ALG and 4 mM $CaCl_2$, and (D) TEM image of ALG-only at 1 mg/mL with 4 mM $CaCl_2$. The data are presented as the mean values ± SD, n = 3.

The effect of various concentrations of ALG on particle size and ζ-potential is presented in **Figure 6.3B**. The results demonstrate that increasing ALG

concentrations (0.1-2 mg/mL) caused a decrease in the average particle size dropping from about 244 nm to 124 nm. The particle size of ALG-coated KNP-INS reached close to that of uncoated KNP-INS at 1 mg/mL ALG and decreased further at 2 mg/mL ALG. Excess ALG was inferred to produce a higher quantity of ALG-only particles characterized by smaller sizes, thereby contributing to the decrease in average particle size. Simultaneously, the ζ-potential result showed that an increasing ALG concentration ≥ 1 mg/mL caused an obvious decline below -28 mV, suggesting a potential excess level of ALG. This assumption was then visualized by TEM images, which is shown in **Figure 6.3C&D**. The results illustrate that a large number of ALG-only particles were formed at 1 mg/mL ALG with a size below 50 nm, thus contributing to the decrease of average particle size of ALG-coated KNP-INS. In this regard, 0.5 mg/mL ALG would be applied for formulating ALG-coated KNP-INS via gelation.

6.3.1.3 Comparison of gelation, inverse gelation and covalent crosslinking techniques

Here three techniques, gelation, inverse gelation and covalent crosslinking, were comprehensively evaluated by assessing particle size, PDI, ζ-potential, re-dispersibility and micromorphology of formulated nanoparticles, taking INS-only as control. Additionally, powdered nanoparticles provide advantages in transportation, storage, and incorporation into marketable products compared to their liquid-form counterparts. Thus, the size changes before and after freeze-drying were also determined. The results are presented in **Figure 6.4A-D**.

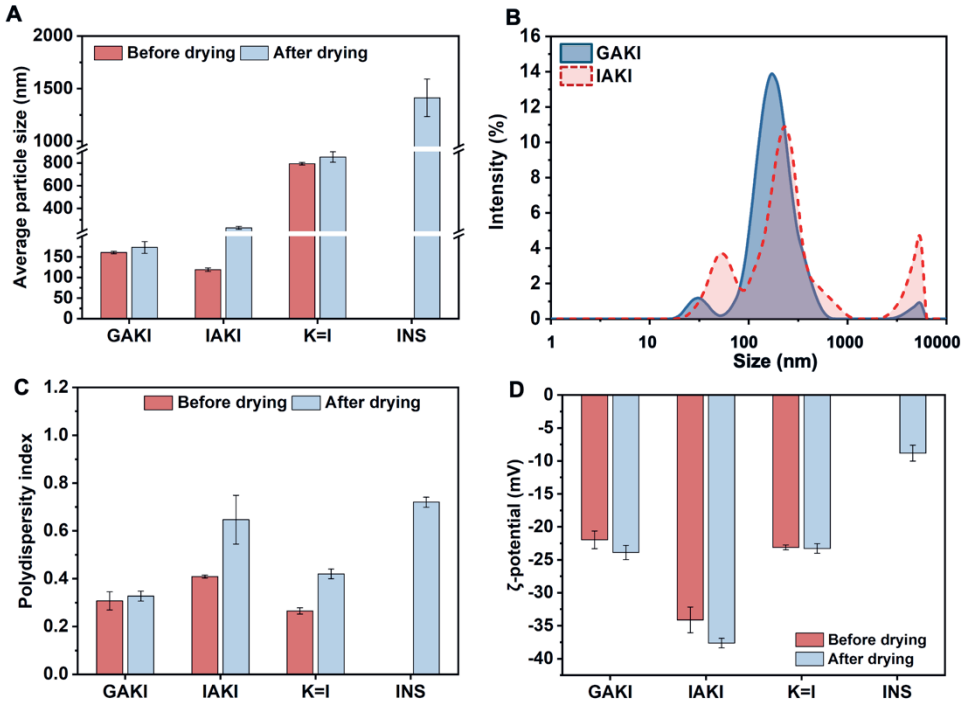

Figure 6.4. (A) Average particle size, (B) polydispersity index, (C) ζ-potential of various particles, and (D) size distribution of GAKI and IAKI. The particles included ALG-KNP-INS by gelation (GAKI), ALG-KNP-INS by inverse gelation (IAKI), covalently bonding (K=I) and insulin-only (INS). For gelation particles, the concentrations of $CaCl_2$ and ALG were 4 mM and 1 mg/mL, respectively, while they were 2 mM and 1 mg/mL, respectively, for inverse gelation. The data are presented as the mean values ± SD, n = 3.

As **Figure 6.4A** indicates, three techniques presented a positive effect on reducing insulin particle size, among which ALG-coated KNP-INS from both gelation and inverse gelation were significantly smaller (< 230 nm) than K=I (~851 nm). Additionally, the particle size of GAKI changed less before and after freeze-drying (ca. 160 and 173 nm respectively) while IAKI showed a tendency to increase after drying. Further analysis of the size distribution reveals that GAKI had a well-distributed profile with a small percentage of aggregations, whereas IAKI displayed a large peak above 2000 nm (**Figure 6.4B**). The PDI result confirms GAKI and K=I with a uniform size distribution due to the low PDI of about 0.31 and 0.27, respectively, whereas that of IAKI was about 0.41 (**Figure 6.4C**). In addition, the PDI of GAKI remained unchanged after drying, but that of IAKI and K=I was increased. The ζ-potential result depicts a negligible influence of freeze-drying on three types

of particles (**Figure 6.4D**). GAKI, IAKI and K=I had ζ-potential of about -23.89 mV, -37.6 mV and -23.3 mV, respectively.

The freeze-dried nanoparticles should be able to be re-dispersed for further application. Thus, the re-dispersibility and microstructure of various samples were observed and shown in **Figure 6.5A-D**. As displayed in **Figure 6.5A**, GAKI and IAKI were more uniformly dispersed in Milli-Q water, whereas INS showed a turbid appearance with large clusters. K=I dissolution was cloudy, indicating the large particles formed by strong covalent crosslinking. The microstructure of three types of nanoparticles is displayed in **Figure 6.5B-D**. The result demonstrates that K=I presented a disordered structure with flocculation. Conversely, GAKI and IAKI presented regularly spherical shapes. It should be noted that GAKI was revealed with a smaller particle size. These findings support the results about the size and PDI abovementioned (**Figure 6.4A&B**).

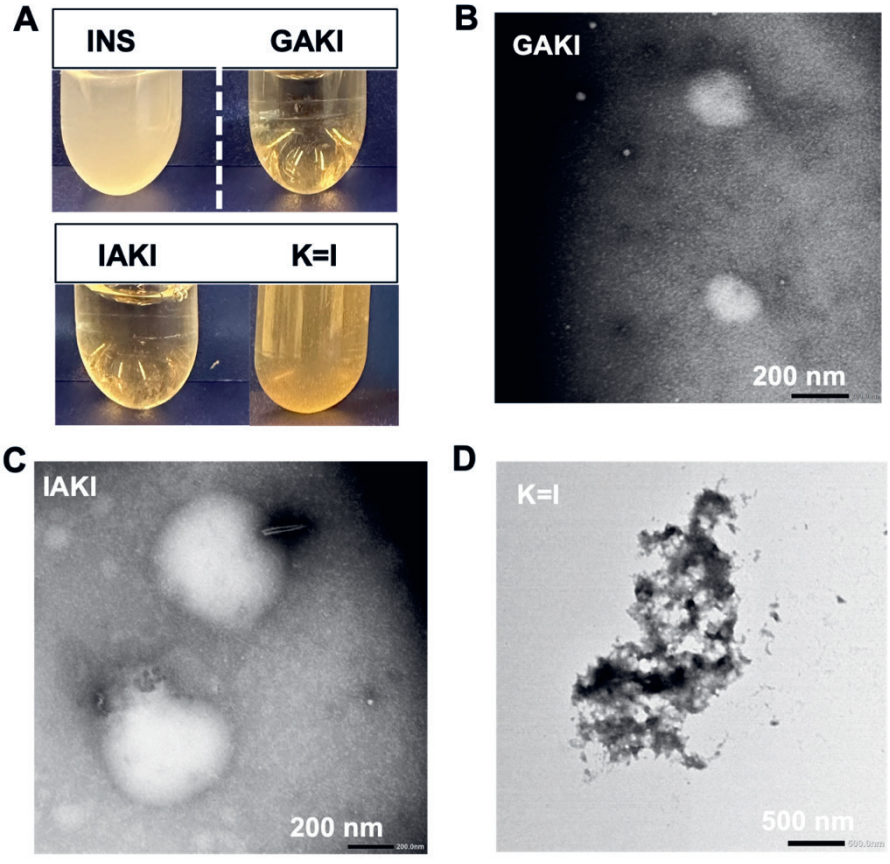

Figure 6.5. (A) Redissolution of various particles in Milli-Q water (1 mg/ml) and TEM images of (B) GAKI, (C) IAKI and (D) K=I.

To sum up, ALG-KNP coating played a role in reducing insulin aggregation and stabilizing particle size. The ALG-KNP coated nanoparticles exhibited small and uniform sizes in a spherical shape. In particular, the gelation technique showed an advantage in producing uniformly sized nanoparticles and preventing unwanted aggregation compared to inverse gelation and covalent crosslinking techniques. Therefore, the gelation technique will be employed in fabricating ALG-KNP-coated nanoparticles (ALG-KNP-INS), which will be subjected to further study.

6.3.2 Study on ALG-KNP-INS obtained via gelation technique

6.3.2.1 Formation of ALG-KNP-INS via gelation technique and particle size analysis

Insulin monomers demonstrate biological activity, however, they possess the least stable conformation and are prone to structural changes compared to hexamers [36-38]. In this study, we expect ALG-KNP-INS to mitigate insulin aggregation in the hexametric state with enhanced stability.

First, the formation of ALG-KNP-INS is visually illustrated in **Figure 6.6A**&**B**. As depicted in **Figure 6.6A**, ALG was successfully coated on KNP-INS located in the core. After transferring to $CaCl_2$ solution (**Figure 6.6B**), a hard shell was formed by crosslinking with Ca^{2+}. Additionally, the core-shell structure exhibited reduced particle size and improved spherical shape. The size distribution of ALG-KNP-INS would be further analyzed by taking ALG-INS, KNP-INS and INS as controls.

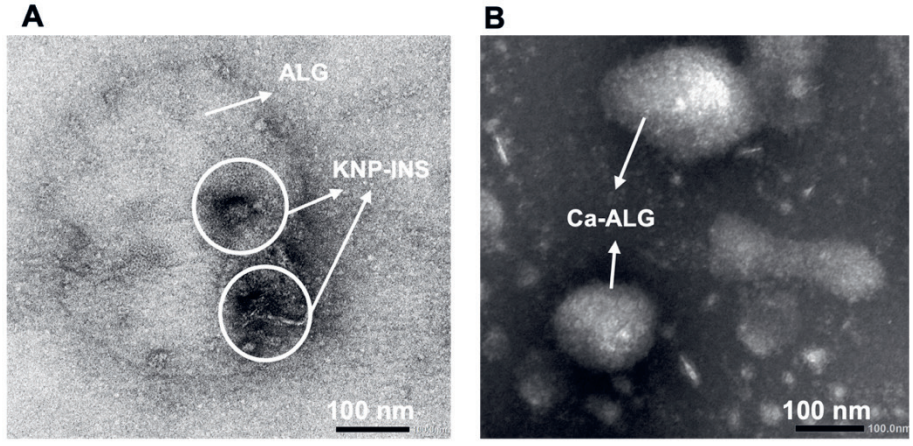

Figure 6.6. TEM images of freshly prepared ALG-coated KNPs-INS before transferring to $CaCl_2$ solution

(A), and after transferring to $CaCl_2$ solution (B). The concentrations of $CaCl_2$ and ALG were 4 mM and 1 mg/mL, respectively.

The result of particle size and resolution appearance is shown in **Figure 6.7A&B**. The result from **Figure 6.7A** suggests that KNP could effectively reduce INS aggregation (~1412 nm). The average particle size of ALG-KNP-INS and KNP-INS decreased to about 173 nm and 150 nm, respectively. Conversely, ALG-only coating exhibited less effect, with the average particle size of ALG-INS at about 1035 nm. Additionally, ALG-KNP-INS had the lowest PDI (~0.32) than others. It indicates the significant effect of ALG-KNP coating on improving the size distribution of INS. The PDI of KNP-INS, ALG-INS and INS was about 0.56, 0.89 and 0.72, respectively, demonstrating inferior size distribution. By further analyzing size distribution (**Figure 6.7B**), ALG-KNP-INS was confirmed with a more uniform size distribution than others. From the dissolution pictures depicted in **Figure 6.7B**, the transparent suspension of KNP was observed, indicating its stabilizing effect on particles with improved re-dispersibility and uniformity. Considering the above, ALG-KNP-INS presented good re-dispersibility and size distribution, attributes deemed crucial for nanoparticle application in food and pharmaceutical industries [39].

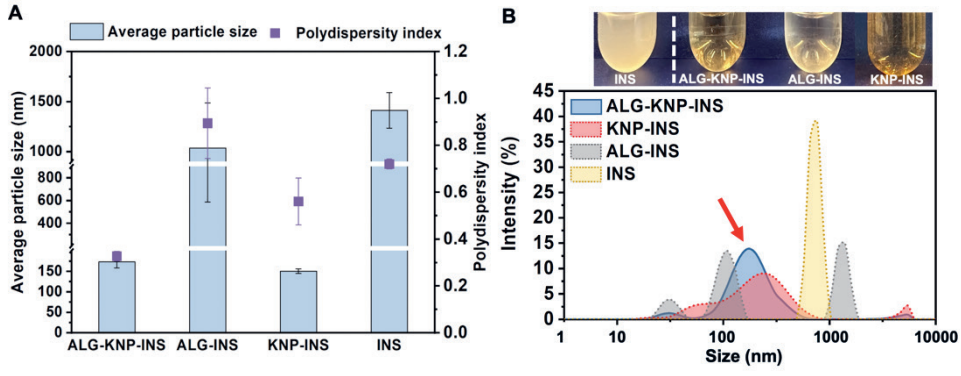

Figure 6.7. (A) Average particle size and polydispersity index and (B) size distribution of ALG-KNP-INS, ALG-INS, KNP-INS and INS. ALG-KNP-INS and ALG-INS were prepared via gelation, where the concentrations of ALG and $CaCl_2$ were 1 mg/mL and 4 mM, respectively. The data are presented as the mean values ± SD, n = 3.

6.3.2.2 Analysis of chemical functionality

The differences in chemical functionality of various nanoparticles were analyzed using FTIR. The result is shown in **Figure 6.8**. Here ALG-only presented characteristic peaks at around 830, 1040, 1100, 1430 and 1620 cm^{-1}. They were

consistent with the multiple vibration peaks of polysaccharides (900 to 1350 cm^{-1}) reported in literature [40]. The peaks at about 1040 and 1100 cm^{-1} were attributed to the C-O stretching vibrations and C-O-C stretching vibrations [41], and those at 1430 and 1620 cm^{-1} were ascribed to be carboxylate peaks (COO^-) [40, 42].

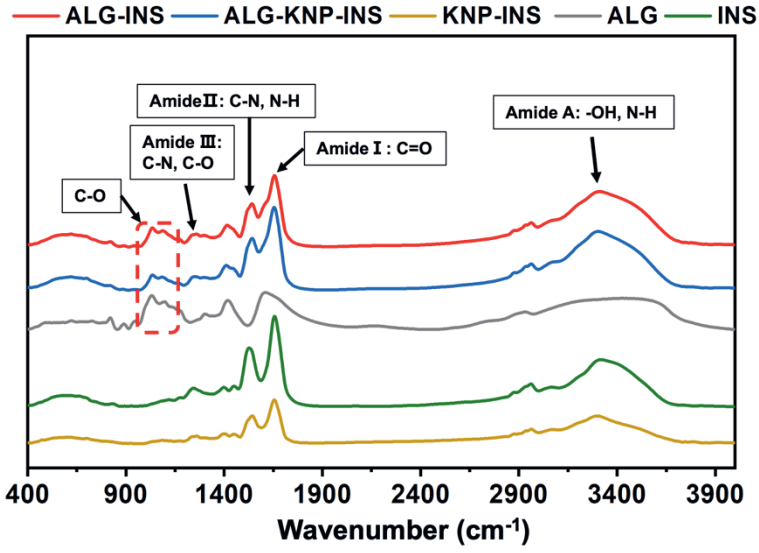

Figure 6.8. FTIR spectrum of ALG-KNP-INS, ALG-INS, KNP-INS and INS.

INS-only were observed with characteristic peaks located at about 1260, 1550, 1658 and 3300 cm^{-1}. The peak at around 1260 cm^{-1} was about the amide Ⅲ area involving C-N and C-O, while those at 1550 and 1658 cm^{-1} related to amide Ⅱ and amide Ⅰ, respectively, involving C-N, N-H bending and C=O [43-45]. The strong absorption at about 3300 cm^{-1} represented O-H stretching vibrations, indicating the formation of hydrogen bonds [46]. As **Figure 6.8** depicted, the spectrum of ALG-KNP-INS presented the characteristic peaks of both ALG-only and INS-only. The combination of FTIR analysis and formation visualization (**Figure 6.6**) suggest the successful coating of ALG on KNP-INS.

6.3.2.3 Analysis of microstructure

The microstructure of INS, ALG-INS, KNP-INS and ALG-KNP-INS is depicted in **Figure 6.9A-D**. The result suggests that INS aggregated and formed large clusters (**Figure 6.9A**), a phenomenon to be associated with self-association into hexamers [36]. The ALG-only coating was less effective in reducing insulin aggregation, since ALG-INS presented as large particles (**Figure 6.9B**). Nevertheless, KNP-INS

significantly enhanced the dispersity of insulin with reduced aggregation (**Figure 6.9C**). The particle size of KNP-INS decreased to about 150 nm in round shape. When focusing on ALG-KNP-INS (**Figure 6.9D**), the nanoparticles were uniformly dispersed without apparent clusters. The combination of ALG and KNP did not result in particle re-aggregation, suggesting the positive effect of KNP stabilization on particle dispersity. Moreover, ALG-KNP-INS displayed a regular spherical shape with a size below 200 nm. The findings of particle microstructure were consistent with the size analysis result (**Figure 6.7**).

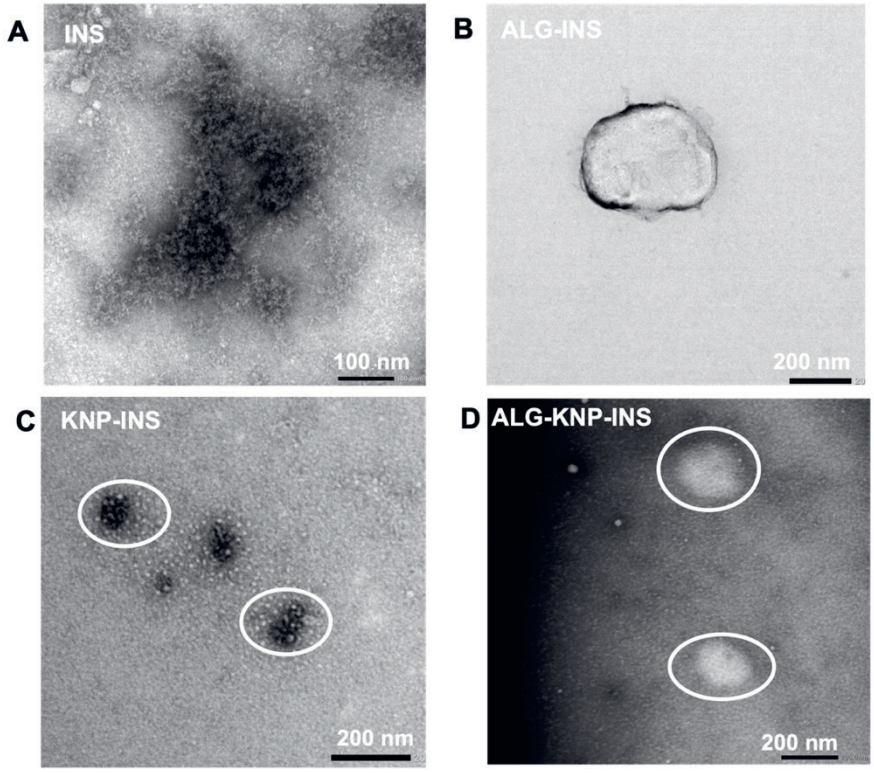

Figure 6.9. TEM images of (A) INS, (B) ALG-INS, (C) KNP-INS and (D)ALG-KNP-INS.

6.3.3 Study on the environmental and physiological stability

6.3.3.1 Analysis of thermal stability

Many food products are subjected to thermal treatments during processing, such as sterilization, pasteurization and utilization. Thus, inspecting the heating effect on the complex stability is essential [47]. Here the stability of nanoparticles was assessed by analyzing the changes in particle size, PDI and insulin stability with heating at

80 °C.

The result of particle size and PDI is depicted in **Figure 6.10A**. The results suggest that the average particle size of both ALG-KNP-INS and KNP-INS were less affected by heating, remaining below 200 nm. The particle size of ALG-INS fluctuated at around 1000 nm but with a tendency to reduce aggregation by prolonging heating time. INS exhibited thermal aggregation behavior, with particle size > 2000 nm under heating. The inter-molecule hydrophobic interactions possibly led to non-specific aggregation of the denatured polypeptide chains, which unfolded under heating [48]. Additionally, heating ≥ 10 min effectively decreased the PDI of KNP-INS from about 0.56 to 0.21, implying a more condensed size distribution. Heating ≤ 20 min maintained the PDI of ALG-KNP-INS at about 0.33, while time expansion over 30 min induced growing PDI to about 0.48, signifying a broadened size distribution.

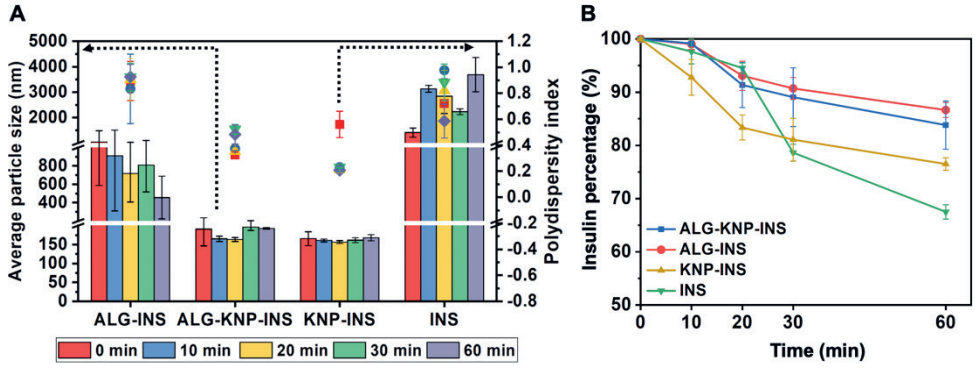

Figure 6.10. (A) Average particle size and polydispersity index and (B) insulin stability of ALG-KNP-INS, ALG-INS, KNP-INS and INS during 80 °C heating treatment. The data are presented as the mean values ± SD, n = 3.

The insulin stability result is illustrated in **Figure 6.10B**. The result shows that INS experienced minimal impact on insulin stability during 20 min heating, with insulin percentage exceeding 94%. However, degradation occurred abruptly when heating extended beyond 30 min, reaching about 67% at 60 min. The substantial stability within the initial 20 min was likely attributed to the hexameric state of insulin, which offered stability [49]. After heating for 30 min, insulin hexamers dissociated, leading to reduced thermal stability. Compared to INS, KNP-INS had lower insulin stability within the initial 20 min of heating, followed by a gradual decline to approximately 76% at 60 min. The insulin loaded by KNP primarily existed in monomers and presented as smaller particles, making them more susceptible to heating. ALG-INS

and ALG-KNP-INS exhibited insignificant differences in insulin stability (> 90%) within 20 min heating compared to INS. Nevertheless, the insulin stability of ALG-INS and ALG-KNP-INS obviously exceeded that of INS with further heating from 30 to 60 min, remaining over 83%. It implies the effect of ALG-coating on protecting insulin from heating.

Considering the above, it is evident that ALG coating has the potential to hinder the thermal aggregation of particles and safeguard insulin against thermal degradation. KNP contributes to stabilizing particle size, while its impact on preventing insulin degradation is comparatively less pronounced. Significantly, ALG-KNP-INS exhibits enhanced thermal stability at 80 °C, suggesting its suitability for thermal treatments during processing, such as pasteurization.

6.3.3.2 Analysis of storage stability

According to the Food and Drug Administration's recommendations, insulin should be stored in the fridge at 2-8 °C for long-term storage until expiration date [50]. Here, the effect of ALG-KNP coating on stabilizing insulin at 4 °C was investigated within 4 weeks of storage. The results are shown in **Figure 6.11A&B**.

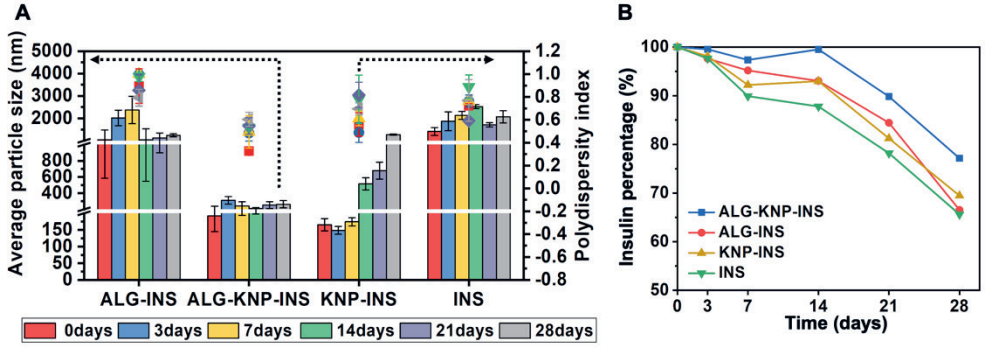

Figure 6.11. (A) Average particle size and polydispersity index, and (B) insulin stability of ALG-KNP-INS, ALG-INS, KNP-INS and INS during 4-weeks storage at 4 °C.

As **Figure 11A** illustrates, ALG-KNP-INS showed good size stability during 4-week storage, the average particle size of which remained at about 200 nm. KNP-INS exhibited size stability during the first week with an average particle size of around 150 nm. Subsequently, their average particle went up and reached about 1200 nm at the end of 4 weeks. INS tended to aggregate during 2-week storage and then dissociate. Insulin hexamers were likely dissociated into subunits, such as dimers

and monomers. ALG-INS showed an increase in particle size in the first week and then dropped to about 1000 nm when stored over 2 weeks, indicating an inferior size stability.

The insulin stability result (**Figure 6.11B**) indicates no noticeable decrease in insulin amount for ALG-KNP-INS during 2-week storage. In contrast, KNP-INS and ALG-INS slightly lost approximately 7% of insulin. The insulin amount of INS dropped below 90% after 1 week, and about 13% was lost after 2 weeks. Notably, the insulin amount in ALG-KNP-INS remained at about 90% when storing for 3 weeks. With further storage > 3 weeks, insulin exhibited a decrease in stability in all formulations. After storage for 4 weeks, the insulin amount in ALG-KNP-INS decreased to about 77%, whereas that of ALG-INS and KNP-INS were about 67% and 69% respectively. INS presented less than other groups, dropping to about 66%.

Thus the double coating of ALG-KNP had a superior effect on improving particle size stability and insulin stability during storage for 4 weeks at 4 °C. Both single coatings of ALG and KNP had limited impact on stabilizing particle size and preserving insulin during long-term storage.

6.3.3.3 Analysis of stability in the GI tract without enzymes

Insulin is highly susceptible to harsh environments during the GI tract, including extreme pH and enzymes [38]. Here the potential of ALG-KNP coating for oral delivery was explored. The simulated GI tract without enzymes was applied to investigate the influence of both physiological temperature (37 °C) and pH variation (1.2-6.8) on the stability of nanoparticles. Considering the inferior performance of ALG-INS discussed above (e.g. large particle size and poor re-dispersity), this part mainly investigated the stability of KNP-INS and ALG-KNP-INS.

The changes in particle size are shown in **Figure 6.12A**&**B**. The result depicted in **Figure 6.12B** illustrates that ALG-KNP-INS could not be well dissolved in simulated gastric fluid and exhibited as turbid clusters. Nevertheless, the clusters were efficiently redispersed upon transitioning to the simulated intestinal phase, forming a clear solution. Thus, the exact particle sizes were determined upon transitioning to the intestinal phase, taking INS and KNP-INS as controls (**Figure 6.12A**). As indicated, ALG-KNP-INS redispersed and decreased into small particles ranging from about 198 nm to 249 nm. It is noteworthy that ALG has been reported to exhibit pH sensitivity, remaining stable in acidic conditions and redissolving in alkaline

environments [51]. KNP-INS retained small (120-132 nm) during the first 90 min but then reached about 211 nm at 120 min, possibly caused by aggregation with prolonged incubation. The particle size of INS tended to increase from 318 nm to 501 nm when incubated in the intestinal phase. There should be a transition between monomers, dimers and hexamers. Additionally, the PDI of ALG-KNP-INS increased beyond the original value discussed in **section 6.3.2.1**, indicating a worsened size distribution. Li et al. have developed microbeads combining ALG and chitosan, which can protect insulin from the GI environment and realize controlled release [52]. Hence their protective effect on insulin needs to be explored.

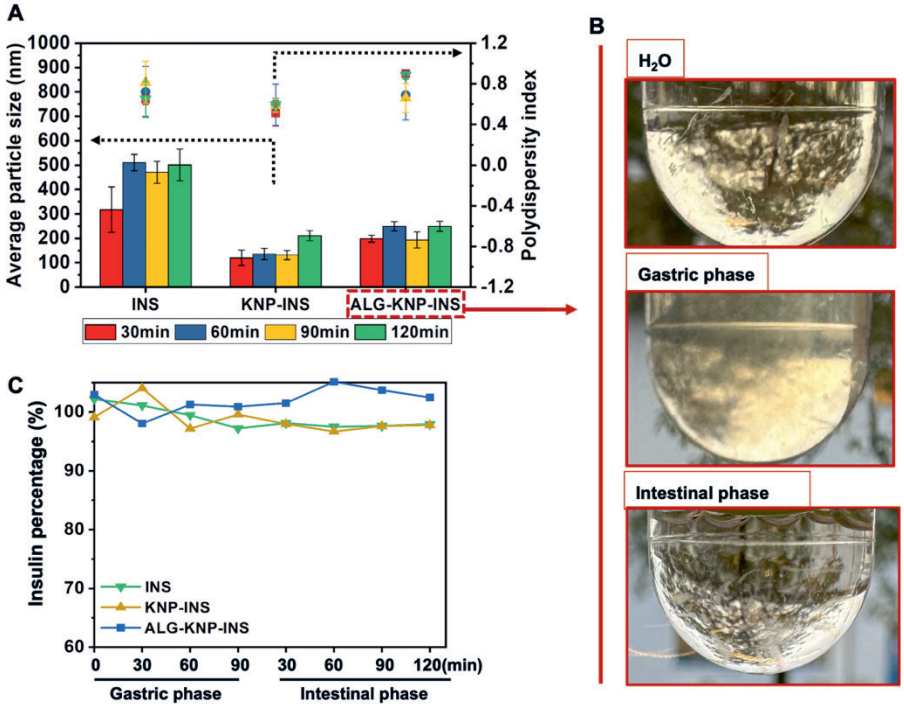

Figure 6.12. (A) Average particle size and polydispersity index of ALG-KNP-INS, KNP-INS and INS in the intestinal phase (120 min) switched from the gastric phase (90 min), (B) appearance of ALG-KNP-INS dispersed in various fluids, where the intestinal phase was switched from the gastric phase and (C) insulin stability of ALG-KNP-INS, KNP-INS and INS during the GI tract without enzymes.

The results of insulin stability are shown in **Figure 6.12C**. The result suggests that INS and KNP-INS exhibited a slight loss of insulin in the gastric phase, which was about 2.8% and 2.2%, respectively. Nevertheless, the intestinal environment did not significantly affect their insulin amount, remaining above 97% after the GI tract.

ALG-KNP-INS presented more robust insulin protection, where no insulin was found lost obviously after the GI tract. They were able to form clusters during the gastric phase and redisperse into nanoparticles below 250 nm when switching into the intestinal phase. Hence, ALG coating was validated with the potential to protect insulin in the non-enzyme GI tract.

6.3.3.4 Analysis of the insulin stability in the GI tract with enzymes

The ability of ALG-KNP-INS against enzymatic degradation in the GI tract was investigated, including treating with pepsin in the gastric phase (90 min) and pancreatin in the intestinal phase (120 min). The undegraded insulin in digesta was analyzed by SDS-PAGE (**Figure 6.13A-C**). The characteristic band of insulin was observed at around 5733.49 Da. Its variations in each sample indicate the stability of insulin over predetermined digestion times.

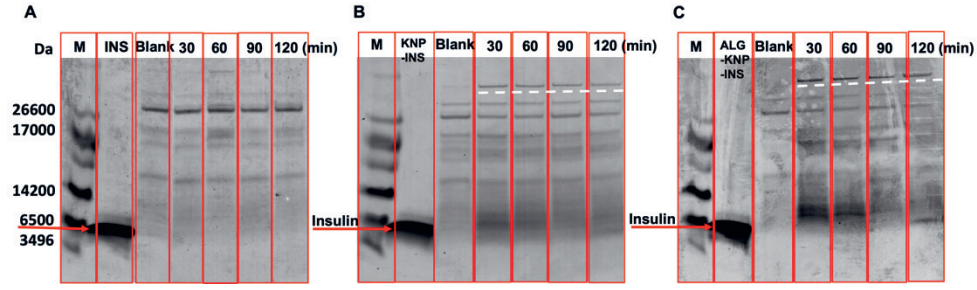

Figure 6.13. SDS-PAGE analysis of the digesta of INS (A), KNP-INS (B), and ALG-KNP-INS (C). The digesta was collected from the intestinal phase (30-120 min) that was switched from the gastric phase. "Blank" represents the trial with enzymes only.

As **Figure 6.13A** depicts, insulin was completely degraded by pepsin and pancreatin after 30 min during the intestinal phase, without showing the characteristic bands of insulin at around 5733.49 Da. The result depicted in **Figure 6.13B** demonstrates that the gel of KNP-INS presented characteristic bands of insulin. With time, those bands gradually get lighter. The remaining band at the end of the intestinal phase (120 min) is considered to be insulin although it can not be ignored that keratin peptides may also be present at this molecular weight range. Further studies regarding insulin qualification and quantification will be needed in the future. What is worth noting is that new bands, appeared on the top of the gel which might relate to the interactions between KNP-INS and enzymes. The results indicate the potential of KNP to protect insulin from enzymatic degradation to some extent. Similarly, clearer bands representing insulin were observed in the gel of ALG-KNP-INS

(**Figure 6.13C**), which remained undegraded after 120 min intestinal phase. At the top of the gel, again darker and clearer new bands were also observed. The observation at 90 min, which does not exhibit clear bands at ca. 6 kDa, is unexplained as the same material/sample at 120 min do exhibit bands in this region. Generally, the results indicate the potential effect of ALG-KNP coating on protecting insulin from enzymatic degradation in the GI tract.

6.4 Conclusion

This study developed a stability-enhanced nano-delivery system by incorporating ALG and KNP. The resultant nanoparticles (ALG-KNP-INS) from the gelation technique exhibited favorable particle size and spherical shapes. Here KNP was found to play a crucial role in reducing and stabilizing particle size, along with anti-digestion potential. Besides the improved size stability, ALG-KNP coating demonstrated potential enhancement in insulin stability under various environmental conditions (heating and storage). The size sensitivity of ALG-KNP coating made it resistant to harsh pH and enzymatic degradation in the GI tract. Incorporating KNP and ALG makes them a promising coating, protecting biomolecules from diverse attacks. A future study on insulin release and permeation across mucus and epithelium should be conducted. Our findings underscore the potential of ALG-KNP coating for enhancing nanoparticle performance, e.g. spherical shape, re-dispersibility and stability, and safeguarding biomolecules from various challenges. This study provides an insight into viable alternative to nano-delivery systems in diverse areas, e.g. food, nutraceutical and pharmaceutical areas.

6.5 References

1. S. Akula, A.K. Gurram, S.R. Devireddy, Self-microemulsifying drug delivery systems: an attractive strategy for enhanced therapeutic profile, International scholarly research notices, 2014 (2014).
2. Y. Li, J. Yao, C. Han, J. Yang, M.T. Chaudhry, S. Wang, H. Liu, Y. Yin, Quercetin, inflammation and immunity, Nutrients, 8 (2016) 167.
3. X. Huang, X. Huang, Y. Gong, H. Xiao, D.J. McClements, K. Hu, Enhancement of curcumin water dispersibility and antioxidant activity using core–shell protein–polysaccharide nanoparticles, Food Research International, 87 (2016) 1-9.
4. X. Wang, H. Sun, T. Mu, Materials and structure of polysaccharide-based delivery carriers for oral insulin: A review, Carbohydrate Polymers, (2023) 121364.
5. H. Nsairat, Z. Lafi, M. Al-Sulaibi, L. Gharaibeh, W. Alshaer, Impact of Nanotechnology on the Oral Delivery of Phyto-bioactive Compounds, Food Chemistry, (2023) 136438.
6. S.R. Pamshong, D. Bhatane, S. Sarnaik, A. Alexander, Mesoporous silica nanoparticles: An emerging approach in overcoming the challenges with oral delivery of PPs, Colloids and Surfaces B: Biointerfaces, (2023) 113613.
7. P. Anand, A.B. Kunnumakkara, R.A. Newman, B.B. Aggarwal, Bioavailability of curcumin: problems and promises, Molecular pharmaceutics, 4 (2007) 807-818.
8. A. Elsayed, M. Al-Remawi, N. Jaber, K.M. Abu-Salah, Advances in buccal and oral delivery of insulin, International Journal of Pharmaceutics, (2023) 122623.
9. D. Shen, H. Yu, L. Wang, A. Khan, F. Haq, X. Chen, Q. Huang, L. Teng, Recent progress in design and preparation of glucose-responsive insulin delivery systems, J Control Release, 321 (2020) 236-258.
10. L. Chen, Y. Lv, F. Zhong, Enhancing bioavailability of soy protein isolate (SPI) nanoparticles through limited enzymatic hydrolysis: Modulating structural properties for improved digestion and absorption, Food Hydrocolloids, 147 (2024) 109397.
11. A. Raza, U. Hayat, M. Bilal, H.M.N. Iqbal, J.-Y. Wang, Zein-based micro- and nano-constructs and biologically therapeutic cues with multi-functionalities for oral drug delivery systems, Journal of Drug Delivery Science and Technology, 58 (2020).
12. T. Zhang, L. Li, S. Chunta, W. Wu, Z. Chen, Y. Lu, Enhanced oral bioavailability from food protein nanoparticles: A mini review, Journal of Controlled Release, 354 (2023) 146-154.
13. H. Xu, Z. Shi, N. Reddy, Y. Yang, Intrinsically water-stable keratin nanoparticles and their in vivo biodistribution for targeted delivery, J Agric Food Chem, 62 (2014) 9145-9150.
14. M. Pakdel, Z. Moosavi-Nejad, R.K. Kermanshahi, H. Hosano, Self-assembled uniform keratin nanoparticles as building blocks for nanofibrils and nanolayers derived from industrial feather waste, Journal of Cleaner Production, 335 (2022).
15. X. Qin, X. Xu, Y. Guo, Q. Shen, J. Liu, C. Yang, E. Scott, H. Bitter, C. Zhang, A sustainable and efficient recycling strategy of feather waste into keratin peptides with antimicrobial activity, Waste Manag, 144 (2022) 421-430.
16. W. Zhao, R. Yang, Y. Zhang, L. Wu, Sustainable and practical utilization of feather keratin by an innovative physicochemical pretreatment: high density steam flash-explosion, Green Chemistry, 14 (2012).
17. Y. Esparza, N. Bandara, A. Ullah, J. Wu, Hydrogels from feather keratin show higher viscoelastic properties and cell proliferation than those from hair and wool keratins, Mater Sci Eng C Mater Biol

Appl, 90 (2018) 446-453.
18. S. Sharma, A. Gupta, S. Chik, C.G. Kee, B.M. Mistry, D.H. Kim, G. Sharma, Characterization of keratin microparticles from feather biomass with potent antioxidant and anticancer activities, Int J Biol Macromol, 104 (2017) 189-196.
19. P. Mura, F. Maestrelli, M. Cirri, N. Mennini, Multiple roles of chitosan in mucosal drug delivery: An updated review, Marine Drugs, 20 (2022) 335.
20. M.A.J. Shaikh, G. Gupta, A. Goyal, M.M. Gupta, O. Afzal, A.S.A. Altamimi, S.I. Alzarea, W.H. Almalki, I. Kazmi, P. Negi, Sodium alginate-based drug delivery for diabetes management: A review, International Journal of Biological Macromolecules, (2023) 123986.
21. N.M. Sanchez-Ballester, B. Bataille, I. Soulairol, Sodium alginate and alginic acid as pharmaceutical excipients for tablet formulation: Structure-function relationship, Carbohydrate Polymers, 270 (2021) 118399.
22. F. Maestrelli, P. Mura, M.L. González-Rodríguez, M.J. Cózar-Bernal, A.M. Rabasco, L.D.C. Mannelli, C. Ghelardini, Calcium alginate microspheres containing metformin hydrochloride niosomes and chitosomes aimed for oral therapy of type 2 diabetes mellitus, International journal of pharmaceutics, 530 (2017) 430-439.
23. T. Agarwal, S.G.H. Narayana, K. Pal, K. Pramanik, S. Giri, I. Banerjee, Calcium alginate-carboxymethyl cellulose beads for colon-targeted drug delivery, International journal of biological macromolecules, 75 (2015) 409-417.
24. D. Kothale, U. Verma, N. Dewangan, P. Jana, A. Jain, D. Jain, Alginate as promising natural polymer for pharmaceutical, food, and biomedical applications, Current drug delivery, 17 (2020) 755-775.
25. X. Qin, C. Yang, Y. Guo, J. Liu, J.H. Bitter, E.L. Scott, C. Zhang, Effect of ultrasound on keratin valorization from chicken feather waste: process optimization and keratin characterization, Ultrasonics Sonochemistry, (2023) 106297.
26. W. Li, F. Gao, J. Kan, J. Deng, B. Wang, S. Hao, Synthesis and fabrication of a keratin-conjugated insulin hydrogel for the enhancement of wound healing, Colloids and Surfaces B: Biointerfaces, (2019).
27. P. Liu, Q. Wu, Y. Li, P. Li, Y. Xiao, DOX-Conjugated keratin nanoparticles for pH-Sensitive drug delivery, Colloids and Surfaces B: Biointerfaces, 181 (2019) 1012-1018.
28. A. Najjar, M. Alawi, N. AbuHeshmeh, A. Sallam, A rapid, isocratic HPLC method for determination of insulin and its degradation product, Advances in Pharmaceutics, 2014 (2014).
29. C. Wang, B. Cui, Y. Sun, C. Wang, M. Guo, Preparation, stability, antioxidative property and in vitro release of cannabidiol (CBD) in zein-whey protein composite nanoparticles, Lwt, 162 (2022).
30. M. Li, Y. Sun, C. Ma, Y. Hua, L. Zhang, J. Shen, Design and Investigation of Penetrating Mechanism of Octaarginine-Modified Alginate Nanoparticles for Improving Intestinal Insulin Delivery, J Pharm Sci, 110 (2021) 268-279.
31. S. Li, N. Liang, P. Yan, Y. Kawashima, S. Sun, Inclusion complex based on N-acetyl-L-cysteine and arginine modified hydroxypropyl-beta-cyclodextrin for oral insulin delivery, Carbohydr Polym, 252 (2021) 117202.
32. S. De, D. Robinson, Polymer relationships during preparation of chitosan–alginate and poly-l-lysine–alginate nanospheres, Journal of Controlled Release, 89 (2003) 101-112.
33. M. Zhong, Y. Sun, Y. Sun, Y. Huang, B. Qi, Y. Li, The effect of salt ion on the freeze-thaw stability and digestibility of the lipophilic protein-hydroxypropyl methylcellulose emulsion, Lwt, 151 (2021).

34. K. Hu, D.J. McClements, Fabrication of biopolymer nanoparticles by antisolvent precipitation and electrostatic deposition: Zein-alginate core/shell nanoparticles, Food Hydrocolloids, 44 (2015) 101-108.
35. Y. Huang, Y. Zhan, G. Luo, Y. Zeng, D.J. McClements, K. Hu, Curcumin encapsulated zein/caseinate-alginate nanoparticles: Release and antioxidant activity under in vitro simulated gastrointestinal digestion, Current Research in Food Science, 6 (2023) 100463.
36. L. Jorgensen, P. Bennedsen, S.V. Hoffmann, R.L. Krogh, C. Pinholt, M. Groenning, S. Hostrup, J.T. Bukrinsky, Adsorption of insulin with varying self-association profiles to a solid Teflon surface—Influence on protein structure, fibrillation tendency and thermal stability, European journal of pharmaceutical sciences, 42 (2011) 509-516.
37. V. Sluzky, J.A. Tamada, A.M. Klibanov, R. Langer, Kinetics of insulin aggregation in aqueous solutions upon agitation in the presence of hydrophobic surfaces, Proceedings of the National Academy of Sciences, 88 (1991) 9377-9381.
38. E. Merisko-Liversidge, S.L. McGurk, G.G. Liversidge, Insulin nanoparticles: a novel formulation approach for poorly water soluble Zn-insulin, Pharmaceutical research, 21 (2004) 1545-1553.
39. M. Vandana, S.K. Sahoo, Optimization of physicochemical parameters influencing the fabrication of protein-loaded chitosan nanoparticles, Nanomedicine, 4 (2009) 773-785.
40. Q. Liu, Y. Jing, C. Han, H. Zhang, Y. Tian, Encapsulation of curcumin in zein/ caseinate/sodium alginate nanoparticles with improved physicochemical and controlled release properties, Food Hydrocolloids, 93 (2019) 432-442.
41. A. Sadiq, A. Choubey, A. Bajpai, Biosorption of chromium ions by calcium alginate nanoparticles, Journal of the Chilean Chemical Society, 63 (2018) 4077-4081.
42. A.J. Friedman, J. Phan, D.O. Schairer, J. Champer, M. Qin, A. Pirouz, K. Blecher-Paz, A. Oren, P.T. Liu, R.L. Modlin, Antimicrobial and anti-inflammatory activity of chitosan–alginate nanoparticles: a targeted therapy for cutaneous pathogens, Journal of Investigative Dermatology, 133 (2013) 1231-1239.
43. G. Han, Y. Li, Q. Liu, Q. Chen, H. Liu, B. Kong, Improved water solubility of myofibrillar proteins by ultrasound combined with glycation: A study of myosin molecular behavior, Ultrason Sonochem, 89 (2022) 106140.
44. F. Pourjavaheri, S. Ostovar Pour, O.A.H. Jones, P.M. Smooker, R. Brkljača, F. Sherkat, E.W. Blanch, A. Gupta, R.A. Shanks, Extraction of keratin from waste chicken feathers using sodium sulfide and l-cysteine, Process Biochemistry, 82 (2019) 205-214.
45. D. Wang, W. Li, Y. Wang, H. Yin, Y. Ding, J. Ji, B. Wang, S. Hao, Fabrication of an expandable keratin sponge for improved hemostasis in a penetrating trauma, Colloids Surf B Biointerfaces, 182 (2019) 110367.
46. J. Yuan, L. Guo, S. Wang, D. Liu, X. Qin, L. Zheng, C. Tian, X. Han, R. Chen, R. Yin, Preparation of self-assembled nanoparticles of epsilon-polylysine-sodium alginate: A sustained-release carrier for antigen delivery, Colloids Surf B Biointerfaces, 171 (2018) 406-412.
47. F. Liu, D. Wang, C. Sun, D.J. McClements, Y. Gao, Utilization of interfacial engineering to improve physicochemical stability of β-carotene emulsions: Multilayer coatings formed using protein and protein–polyphenol conjugates, Food Chemistry, 205 (2016) 129-139.
48. M. Al-Remawi, N. Jaber, A. Elsayed, D. Alsafadi, K.A. Salah, Stabilization of insulin using low molecular weight chitosan carbonate nanocarrier, Carbohydrate Polymers, 291 (2022) 119579.

49. J. Brange, Stability of insulin: studies on the physical and chemical stability of insulin in pharmaceutical formulation, (No Title), (1994).
50. K. Braune, L.A. Kraemer, J. Weinstein, A. Zayani, L. Heinemann, Storage conditions of insulin in domestic refrigerators and when carried by patients: often outside recommended temperature range, Diabetes Technology & Therapeutics, 21 (2019) 238-244.
51. T.M. Kumar, W. Paul, C.P. Sharma, M. Kuriachan, Bioadhesive, pH responsive micromatrix for oral delivery of insulin, Trends Biomater. Artif. Organs, 18 (2005) 198-202.
52. J. Li, H. Wu, K. Jiang, Y. Liu, L. Yang, H.J. Park, Alginate calcium microbeads containing chitosan nanoparticles for controlled insulin release, Applied Biochemistry and Biotechnology, 193 (2021) 463-478.

6.6 Supplementary materials

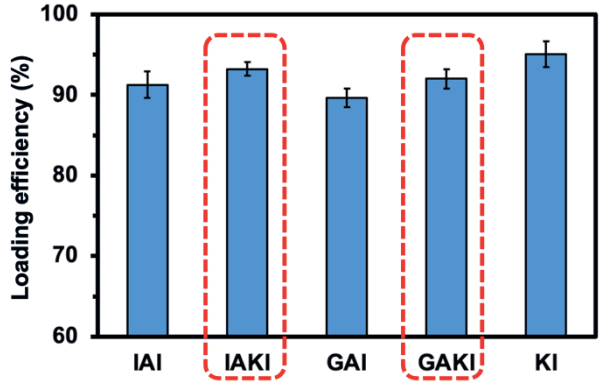

Figure S6.1. The insulin loading efficiency of various nanoparticles. The IAI and IAKI represent ALG-INS and ALG-KNP-INS fabricated via inverse gelation respectively; GAI and GAKI represent ALG-INS and ALG-KNP-INS fabricated via gelation respectively; KI represents KNP-INS fabricated via partial hydrolysis and pH shifting.

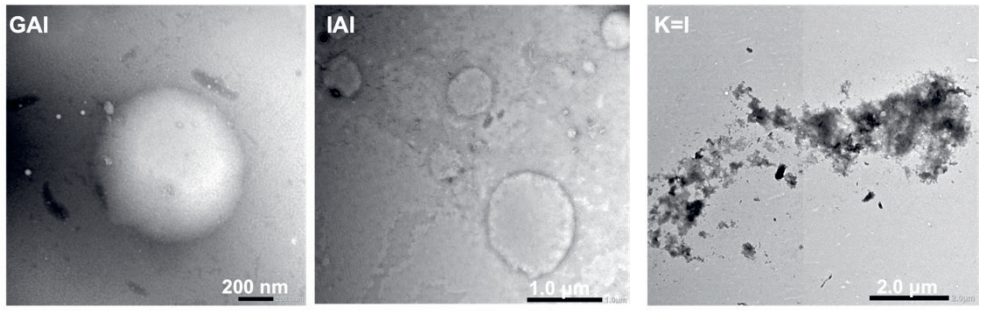

Figure S6.2. TEM of various samples. The GAI and IAI represent ALG-INS fabricated via gelation inverse gelation respectively; K=I represents KNP=INS fabricated via covalent crosslinking.


7

CHAPTER 7

General Discussion

7.1 Introduction

With the increasing demand for meat and eggs, chicken feathers are produced in a vast output annually. Chicken feathers contain over 90% of keratin, serving as a huge protein resource reservoir. Feather keratin presents biological potential owing to its appealing biological properties, e.g. biodegradability, biocompatibility, low-toxicity, wound healing, antibacterial ability, intrinsic stability and cell attachment and proliferation [1-4]. However, traditional techniques for feather utilization exhibit shortcomings such as time consumption, low productivity and chemical pollution, thus leading to underutilization and environmental pollution. Additionally, previous literature has reported the biological potential of feather keratin hydrolysate, e.g. antimicrobial and antioxidant ability [5]. However, there are a few investigations delving into the bioactivity of feather keratin hydrolysates. Most keratin-based products demonstrate low added economic and functional values, e.g. feeds and fertilizers. Moreover, researchers have emphasized the potential of keratin nanoparticles (KNPs) for enhancing biomolecule bioaccessibility in biomedical areas [2, 6]. However, the intrinsic stability owing to abundant disulfide bonds results in poor performance of KNPs, e.g. low water solubility and easy aggregation. This thesis will devise more efficient and sustainable strategies for keratin extraction and upcycled utilization from feather waste. Allied to it, the transformation of high-value products from feather waste will primarily focus on bioactive keratin peptides (KEPs) and nanoparticles.

There are three major objectives in this thesis: 1) devising more sustainable strategies for efficiently extracting/utilizing keratin; 2) delving into the potential bioactivities (antimicrobial and cell-penetrating ability) of keratin hydrolysates enriched with high value; 3) developing an optimal route for fabricating keratin-based nanoparticles with enhanced performance. In this regard, a strategy combining ultrasound and Cys-reduction for extracting keratin was optimized in **Chapter 2**. In **Chapter 3**, the strategy combining instant catapult steam explosion (ICSE) and enzymatic hydrolysis was proposed for preparing antimicrobial KEPs. **Chapter 4** delved into the cell-penetrating potential of KEPs for non-covalently delivering biomolecules. In **Chapters 5** and **6**, the novel routes for fabricating KNPs and stability-enhanced nanoparticles incorporating KNP and sodium alginate (ALG) were developed. In **Chapter 7**, the main findings (**Figure 7.1**) are summarized and suggestions for further research and development will be discussed.

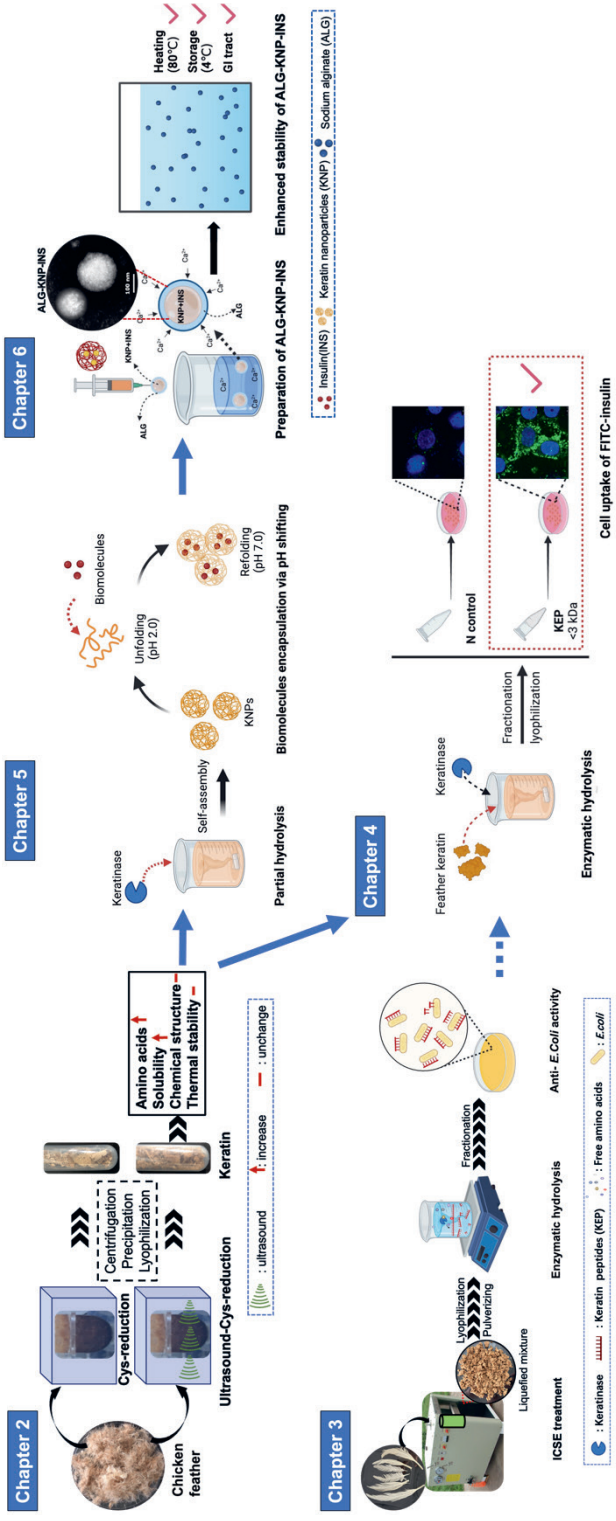

Figure 7.1. The main findings of the thesis

7.2 Effect of Cys-reduction assisted with ultrasound on extracting keratin

The current keratin extraction techniques face drawbacks such as time consumption, chemical pollution, keratin over-degradation, etc., thus limiting the wide utilization of feather waste [7]. Hence we proposed an alternative strategy enhancing efficiency and minimizing chemical pollution for extracting high-quality keratin in **Chapter 2**. Here, ultrasound was employed to assist in Cys-reduction, leveraging the effects of mechanical vibration, acoustic cavitation and the strong reducibility of Cys. As observed, ultrasound played a positive effect on feather deconstruction. The raw feather structure was physically deconstructed by moderate ultrasonic treatment, with the protein backbone remaining intact. Nevertheless, long-time (≥ 6h) ultrasonic treatment led to severe keratin degradation, resulting in a greater amount of small peptides and free amino acids as well as reduced thermal stability. Conversely, solely improving ultrasonic power presented a less negative impact. Aimed at a relatively high yield with minimal time consumption, the process of Cys-reduction assisted with ultrasound was optimized. The result indicates that 64% of keratin could be extracted under 130 W, 2.7 h and 15% of Cys concentration. The resulting keratin exhibited improved solubility in aqueous solutions without damage to amino acid composition and thermal stability.

7.2.1 Design of Cys-reduction assisted with ultrasound

Keratin is a promising candidate for biomaterials due to their merits of cost-effectivity, renewability and ready availability. Despite decades of progress in upcycling keratinous materials, keratin biomaterials still only represent a small fraction of the expansive biomaterials market [8]. One of the key reasons for this is the limitations in extraction use and application. Here we designed a strategy for keratin extraction by focusing on two aspects: process applicability and keratin quality. For process applicability enhancement, the optimization of chemical pollution and processing time were considered. Cys presents a potential eco-friendly alternative to reductive chemicals (e.g. mercaptoethanol and sodium dodecyl sulfate), which can be commercially produced via fermentation. The mechanical vibration and acoustic cavitation enable ultrasound to shorten processing time. Previously use of only ionic liquids and Cys-reduction techniques were reported to take about ≥ 10 h and 6-12 h, respectively [7, 9, 10]. In contrast, the Cys-reduction assisted with ultrasound was more timesaving (2.7 h) in this thesis.

Applying keratin-based biomaterials like biofilms, scaffolds, sponges and fibers often requires a more intact keratin structure. Thus, it is advisable to avoid the potential damage to the keratin backbone when devising a new strategy. Additionally, an improved solubility and dispersibility of keratin in aqueous solutions will benefit broadening its application. Thus, an aided technique that is beneficial for reducing inter- and intra-particle forces can be applied. In this thesis, ultrasound exhibited enhancement in improving keratin solubility without causing damage to its chemical structure.

However, our strategy did not significantly improve keratin yield (64%) than the yield reported in literature [9, 10], e.g. 64-71% of Cys-reduction-alone. One of the reasons could be the buoyancy of feathers floating on the buffer surface. It could be solved by adding an agitation in the ultrasonic device in the future. The other reason is likely the co-production of free amino acids and soluble peptides facilitated by ultrasound.

Nevertheless, the process demonstrated an advantage in enhancing the solubility of keratin in aqueous solutions, a property often constrained by robust inter/intramolecular forces. Beyond the above, no adverse effects on amino acid composition and thermal stability were observed. Given the benefits of timesaving, less chemical pollution and high-quality keratin, Cys-reduction assisted with ultrasound demonstrates its applicability for extracting solubility-enhanced keratin from chicken feathers, as well as other keratinous waste (e.g. wool and horns). It also provides insights into extracting protein from other resources with enhanced solubility using ultrasound.

7.3 Application of enzymatic hydrolysis assisted by ICSE yielding antimicrobial peptides

Earlier studies have highlighted the antimicrobial potential of feather keratin and its hydrolysates [5, 11]. However, there are few studies on preparing KEPs and their antimicrobial ability. Thus, **Chapter 3** aims to develop an efficient and sustainable strategy for producing antimicrobial KEPs. Here, the technique of enzymatic hydrolysis via various enzymes assisted with ICSE was employed. As indicated, the ICSE treatment at 1.5 MPa for 120 s was efficient in feather deconstruction, breaking disulfide bonds and polypeptide chains without severe degradation. Based on this condition, the enzymatic hydrolysis via keratinase was more effective in

deconstructing feathers than conventional enzymes, e.g. protamex, alcalase, papain and trypsin. About 90% of ICSE feathers were deconstructed into soluble peptides within 3 h, far more efficient than keratinase hydrolysis only as well [5]. Furthermore, the feather hydrolysate via keratinase was found with anti-*E.coli* ability, as opposed to other conventional enzymes. Consistent with most research [12, 13], the most effective peptides exist within 3 kDa with a high hydrophobic proportion containing rich key amino acids such as Cys, Gly and Leu. The research elucidated the positive effect of ICSE-assisted enzymatic hydrolysis in deconstructing feather waste. The anti-*E.coli* ability of feather KEPs by keratinase cleavage holds potential in converting feather waste into value-added antimicrobial products.

7.3.1 Design of enzymatic hydrolysis assisted with ICSE

Besides the demand for keratin as biomaterials, keratin hydrolysates exhibit potential for entirely different applications in biotechnological or food-related areas, such as valuable nutrients [7]. Typically, the bioactive KEPs hold promise for function-fortified applications with economic value added. In this regard, a more efficient and targeted strategy will be needed. Here the strategy design took similar process considerations into account as mentioned in **section 7.2.1**: processing time and chemical pollution. The ICSE technique and enzymatic hydrolysis were combined. ICSE can efficiently (in a few minutes) result in physical tearing and dissociation of feathers, rendering them more accessible to enzymatic hydrolysis [5]. Enzymatic hydrolysis can prevent severe damage to the backbone and functional properties of KEPs [14]. This combination significantly shorted processing time and required no chemicals, while the enzymatic hydrolysis alone could last over 20 h [5].

Furthermore, it is essential to take the KEP structure into consideration. It means that the potential damages of the process on KEP bioactivity should be avoided, such as amino acid composition, functional groups, molecular weight, etc. Antimicrobial peptides (AMPs) have been reported to be composed of 11-50 amino acids [15]. To circumvent possible damage, the ICSE conditions were optimized in our study. The conditions of 1.5 MPa and 120 s were determined to be optimal for minimizing the excessive production of free amino acids and small peptides < 2 kDa.

Nevertheless, there are still two remaining issues in the current study. First, ICSE treatment showed a low recovery yield of chicken feathers (~ 56%). The main reason was likely due to the cylinder of ICSE equipment being opened on a flat surface for

discharging pressure instantaneously, which made it hard to collect small particles and liquid. Similarly, a mass loss of wool was also found when treated with a steam explosion [16]. A high yield will require more precise equipment with a complete recycling process. Second, despite the improved efficiency of enzymatic hydrolysis, a high quantity of peptides without anti-*E.coli* ability was produced by ICSE treatment. This led to a higher minimal inhabitation concentration of feather hydrolysate (30 mg/mL) compared to other hydrolysates reported previously (e.g. 0.5 mg/mL) [12, 13]. This discrepancy stems from the constraints of the ICSE process. Despite optimizing ICSE conditions, the steam explosion is an uncontrollable and disordered process without targeted deconstruction. The most bioactive part could be fractionated and purified for more accurate and targeted applications, e.g. biomedicine.

It is noteworthy that gaining a deep understanding of the structure and degradation process of keratin will be imperative for an applicable strategy. An initial degradation of disulfide bonds is a crucial step for keratin deconstruction, making it vulnerable to enzymatic or chemical hydrolysis. An example of enzymatic degradation for producing amino acids from keratinous materials is illustrated in **Figure 7.2**. Here four enzymes were combined sequentially to break down disulfide bonds, interior and exterior of keratin, and oligopeptides. In this regard, it is advisable to employ a combination of various techniques, including physical, chemical and biological methods, for the sequential deconstruction of keratinous materials. Nevertheless, it should be noted that the potential drawbacks from the preceding technique may affect the subsequent technique efficacy and product quality, such as severe degradation and decreased enzymatic activity caused by the presence of reducing agents, etc.

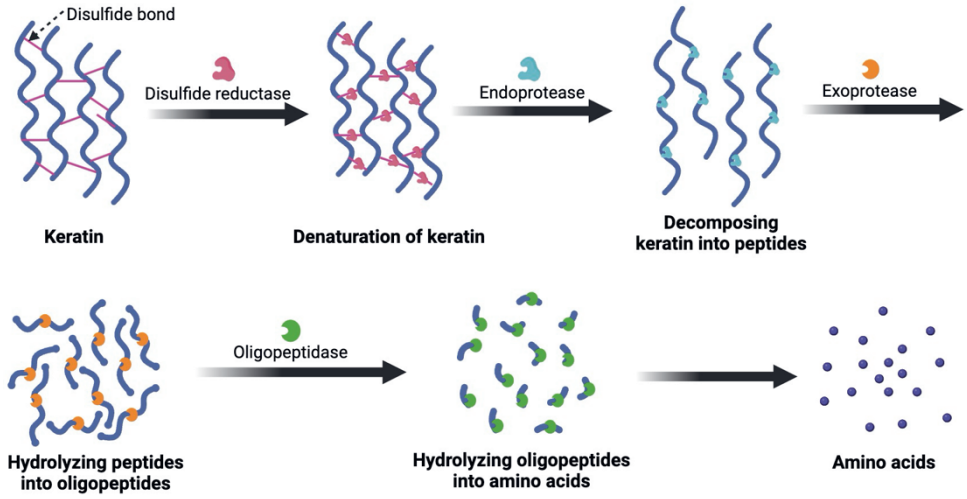

Figure 7.2. Sequential enzymatic keratin degradation process by disulfide reductases, endo-keratinases, exo-keratinases and oligo-keratinases [17].

7.3.2 Valorization of antimicrobial keratin peptides

AMPs derived from natural protein materials show prospect for substituting traditional antibiotics nowadays [18]. They avoid disrupting microecological balance and inducing bacterial resistance, which is a big concern to human health. In this thesis, the high hydrophobic ratio and special composition of amino acids (e.g. rich Cys) potentially contributed to anti-*E.coli* ability of KEPs. The mechanism probably involves two aspects. First, the hydrophobic residues inserted into the bacterial cell membrane and destabilized the water inlet. Second, the disulfide bridge with the cell membrane based on the β-sheet structures stabilized by Cys likely aided KEPs in traversing the membrane. It led to the formation of separation channels and disorganization of lipid bilayers [19-21].

The antimicrobial KEPs demonstrate promise for diverse applications. For instance, they could be formulated into nano hydrogel, wound dressings and biofilms fortified with antimicrobial ability. Hydrogel and wound dressings, with merits of bacteria inhibition, will offer potential in personal care products and pharmaceuticals, such as skincare and wound recovery. The KEPs biofilms will present an alternative to traditional plastic films, such as in food packaging applications. They will offer protection against microbial contamination, thereby extending the shelf life of food products. Additionally, their biodegradability helps mitigate plastic pollution concerns. Nevertheless, product performance, such as

mechanical properties and efficacy, should be considered. The performance enhancement can be achieved by incorporating other biopolymers (e.g. polysaccharides) and optimizing process conditions (e.g. KEP concentrations).

Furthermore, the antimicrobial KEPs perhaps possess cell-penetrating ability for delivering biomolecules. The AMPs and cell-penetrating peptides (CPPs) often share common physicochemical characteristics, such as hydrophobicity, amphipathicity, etc. [22, 23]. Considering this, the potential of KEPs as CPPs was investigated in the next chapter (**Chapter 4**).

7.4 The cell-penetrating ability of keratin peptides

Keratin has been found with cell adhesion and proliferation capacity, and KNPs could penetrate into kidney and liver cells [24, 25]. Nevertheless, there is a limited number of studies on the cell-penetrating capability of KEPs as carriers. **Chapter 4** demonstrates that KEPs promoted insulin labeled with fluorescein into Caco2 cells based on non-covalent bonding, exhibiting potential cell-penetrating ability. The cellular uptake mechanism was energy-dependent, mainly involving macropinocytosis. The results of fractionation and sequencing indicate that the most effective peptides consisted of 8-19 amino acids, characterized by hydrophobic, PP Ⅱ amphipathic and Cys-rich properties. The secondary and tertiary structure and intra/intermolecular forces probably also contributed to their cell-penetrating ability, e.g. high ratio of β-sheet to α-helix, disulfide bonds and hydrophobic residues. The β-sheet structure and disulfide scaffold with an "inside-out" feature tend to expose hydrophobic residues, potentially increasing interaction with the cell membrane [26, 27]. Conversely, small particle size and electrostatic interactions had less effect on the cell-penetrating ability of KEPs.

7.4.1 Valorization of cell-penetrating keratin peptides

The cell membrane remains one of the most formidable barriers hindering the entry of bioactive molecules entry into cells, particularly for mid- or large-size and hydrophilic molecules. The CPPs are an efficient approach to induce a cellular uptake process. They can address challenges of poor permeation and bioavailability of biomolecules through covalent or non-covalent interactions [28]. This thesis validated the cell-penetrating ability of KEPs, which can potentially transport biomolecules into cells through non-covalent bonding.

It exhibits merits in two aspects. First, naturally derived CPPs offer advantages over artificial CPPs, including cost-efficiency, biocompatibility, biodegradability and fewer residual chemicals. Second, non-covalent bonding is often advantageous over covalent bonding, due to its fabrication efficiency, simplicity, avoidance of chemical usage, etc. The cell-penetrating complexes can be conveniently formed by simply mixing KEPs and biomolecules through intermolecular interactions involving electrostatic, hydrophobic, coordination and other specific interactions. In contrast, covalent bonding may encounter problems like complexity, low connection efficiency, reduced expression efficiency and activity of biomolecules and generation of heterogeneous products.

However, using KEPs as CPPs presents its own set of challenges. The KEPs identified in this research consist of 24 peptides, suggesting that the complex exhibits potent penetrating activity only at higher concentrations, typically deemed unacceptable in clinical trials. Additionally, uncertainties persist regarding the bioavailability of biomolecules, e.g. physiological stability and targeting selectivity. The non-covalent approach may face challenges in maintaining sufficient stability under physiological conditions. The loaded biomolecules may be concentration-dependent and prone to be exchanged with other molecules (e.g. albumin and immunoglobulin) [29, 30]. Thus, further fractionation and purification of KEPs, along with the investigation into kinetic stability under physiological conditions, will be needed.

The KEPs hold the potential for enhancing a variety of drug and nutrient delivery systems. They can be made into diverse formulations, such as nanoparticles, nanofibers, emulsions, hydrogels and films. The incorporation of KEPs enables the enhancement of biomolecule bioaccessibility. Nevertheless, besides addressing the product performance aspects as mentioned in **section 7.3.2**, it is also crucial to propose various efforts and strategies to overcome the limitations in their targeted bioapplication, such as *in-vivo* stability, selectivity and efficiency. For example, strategies for stability enhancement, e.g. terminal modification and conjunctions to polymers, are executable. It is noteworthy that the potential cover and damage to bioactive sites should be avoided during modification. For example, polymer conjunction may cover the bioactive sites of KEPs, thus reducing their cell-penetrating ability.

7.5 Fabrication of keratin nanoparticles via partial hydrolysis and pH-shifting methods

Keratin is a potential protein substitute due to its intrinsic stability properties, cell adhesion and penetrating ability, etc. Nevertheless, the poor solubility and dispersibility in aqueous solution restrict its wide application as carriers, owing to the rich inter-and intra-molecule forces. Thus, **chapter 5** aims to develop an effective strategy for formulating self-assembly KNPs with improved solubility and dispersibility. Here enzymatic hydrolysis was found to be effective in breaking the robust molecule interactions of raw keratin. The degree of hydrolysis (DH) at 5% produced small nanoparticles (~ 123 nm) with improved water solubility (~ 94.5%). The resultant KNPs exhibited stability against enzymatic degradation during the gastrointestinal (GI) tract. Moreover, our results reveal the reversible "open-close" structure of KNPs upon pH shifting from 2.0 to 7.0. Based on this property, KNPs exhibited good capacity in encapsulating insulin and resveratrol. Nevertheless, higher DH (≥ 10%) resulted in more β-sheets and exposed hydrophobic residues of KNPs, producing more aggregation and denser clusters. Their structural transformation in response to pH shifting was inferior, accompanied by lower loading efficiency of biomolecules.

7.5.1 Design of partial enzymatic hydrolysis and pH shifting

Enzymatic hydrolysis is an eco-friendly method requiring limited chemicals and potentially lower energy than chemical and hydrothermal hydrolysis [7]. Partial hydrolysis by enzymes can disrupt various protein molecule interactions while preventing damage to its backbone and functional groups. This thesis demonstrates the positive effect of partial hydrolysis on fabricating self-assembled nanoparticles. Nevertheless, it is advisable to avoid a high degree of hydrolysis (≥ 10%) to prevent aggregation, reduced stability and loading efficiency.

Besides, the pH-shifting technique offers advantages such as low cost, simple operation, absence of organic solvents and functional properties. It has been favored for constructing nanocarriers utilizing egg white protein and soy protein [31]. However, there are fewer reports about the effect of pH shifting on keratin structures so far. This thesis innovatively found the applicability of pH shifting into biomolecule-loaded KNPs. The combination of partial enzymatic hydrolysis and pH shifting offers a novel and efficient strategy for fabricating KNPs. In fact, it also

provides new insights into the utilization of other protein resources.

However, several aspects still need attention. First, this strategy does not apply to acid-sensitive biomolecules. The unstable biomolecules will undergo degradation under acidic conditions when preparing biomolecule-loaded KNPs. Second, caution should be exercised in their application in acidic environments, as the unfolding of KNPs may diminish their protection of biomolecules. For example, the leaked biomolecules resulting from KNPs unfolding will be accessible to pepsin and degraded in the gastric fluid. In this regard, a protective coating can be constructed on KNPs in future studies to prevent KNPs from unfolding and biomolecule leakage. In the next chapter (**Chapter 6**), a coating formed by ALG was studied. Moreover, biomolecule-loaded KNPs could be a viable formulation when controlled release in an acidic environment is required. Future studies on biomolecule release and fortification under specific targeted environments can be conducted.

In addition to biomolecule encapsulation, KNPs also demonstrate potential for other applications. For example, the favorable solubility and stability resulting from partial hydrolysis enable KNPs to serve as emulsifiers, stabilizers and surfactants. KNPs are competitive candidates for applications in food, cosmetics and biomedical fields.

7.6 Keratin-based nanoparticles along with alginate coating

Protein-based nanoparticles are increasingly favored for orally delivering biomolecules. They offer enhanced water solubility, reduced aggregation and protection against harsh pH and enzymes. However, some face challenges in stability across different environments, leading to premature degradation and limited bioavailability. **Chapter 6** aims to address these issues by developing a stability-enhanced nano-delivery system based on KNPs from **Chapter 5**. Here, a protective coating of ALG was applied to safeguard KNPs from potential deconstruction under pH variations in the GI tract. The results indicate that the insulin (INS)-loaded double-coating nanoparticles (ALG-KNP-INS) via gelation technique displayed a small particle size of about 173 nm with improved dispersibility. They demonstrated enhanced stability in particle size and insulin under various environmental conditions (e.g. heating at 80 °C and long-term storage at 4 °C). Allied with this, KNP effectively reduced and stabilized particle size while exhibiting less pronounced insulin protection. While ALG improved insulin

protection, as opposed to the size aspect. Moreover, ALG-KNP-INS presented size sensitivity during the GI tract, showing aggregation in the gastric phase and re-dispersion in the intestinal phase with an average size below 250 nm. This potentially bolstered the safeguarding of insulin against enzymatic degradation. Therefore, the synergetic effect of KNP and ALG addressed the poor performance of insulin involving low solubility and instability under various environmental and physiological conditions.

7.6.1 Application of KNPs and ALG coating

The results regarding insulin-loaded KNPs (KNP-INS) indicated that KNPs played a crucial role in reducing and stabilizing particle size, alongside protecting partial insulin from enzymatic degradation. Despite the unfolding of KNPs in the gastric fluid, the potential release of insulin did not lead to complete degradation. KNPs might impede the access of pepsin to insulin. When switching to the intestinal phase, the refolding of KNPs further protected insulin from pancreatin degradation, whereas the escaped insulin from KNP entrapment underwent degradation. The ALG coating on KNP-INS potentially improved KNP-INS stability in the GI tract, coupled with the size changes under pH variations. In the gastric phase, the ALG-KNP-INS aggregated and shrunk into clusters, making KNP-INS inaccessible to pepsin. The potential variations of KNP-INS and ALG-KNP-INS are depicted in **Figure 7.3**.

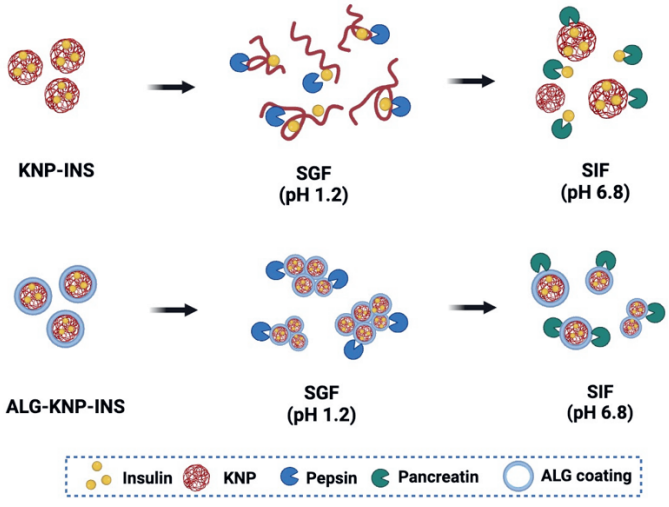

Figure 7.3. Potential variations of KNP-INS and ALG-KNP-INS in the GI tract. The GI tract includes the simulated gastric fluid (SGF) and simulated intestinal fluid (SIF).

Nevertheless, our method failed to quantify the insulin changes in the GI tract with enzymes. The enzymes might interact with nanoparticles, thus leading to difficulty in detecting insulin. In fact, we also observed a band beyond 30 kDa presenting in the gel with SDS-PAGE. In the future, separation and method optimization can be conducted for insulin quantification. Additionally, given that insulin is a property of peptides here, our study only explored the potential reactions of ALG-KNP-INS with major proteases using simplified GI fluids. The human GI tract is significantly more intricate, housing diverse enzymes and microorganisms, thus potentially may lead to slightly difference. Future research will require more realistic simulations of GI environments to delve deeper into such *in-vitro* studies. Moreover, our research did not involve the investigation into the reactivity of ALG-KNP-INS when encountering mucus, epithelial cells, blood environments, etc. Along with the mucoadhesion of ALG and cell adhesion/permeability of KNP, ALG-KNP-INS probably possesses high insulin bioavailability.

Despite the limitations abovementioned, the findings in this thesis provide insights into the potential of ALG-KNP coating for stability-enhanced delivery systems. It will be possible to encapsulate both hydrophilic and hydrophobic biomolecules (e.g. peptides and polyphenols) with enhanced solubility and dispersibility. Nevertheless, it is recommended to investigate the capacity of loaded biomolecules to penetrate mucus and epithelial cells when applying into oral route, as well as their release kinetics in physiological environments. Overall, the ALG-KNP coating is a potential formulation for biomolecule encapsulation and delivery in diverse fields, such as food, nutraceuticals and pharmaceuticals.

7.7 Outlook

According to the UN Food and Agriculture Organization (FAO), annual global poultry production is projected to exceed 24.8 billion animals by 2030 and 37.0 billion by 2050 [32, 33]. Consequently, keratinous waste production will increase substantially as a byproduct each year. Alongside keratinous waste from leather factories, wool, textiles and slaughterhouses, these byproducts pose significant threats to environmental and human health (water, air, and soil). It is estimated that over 65 million tons of keratinous waste are landfilled (−$400/t biomass) annually worldwide, resulting in a loss exceeding $26 billion. Valorizing biomass waste for various purposes, such as bulk chemicals and cattle feed, can add value ranging

from approximately $1000 to $70–200/t biomass, respectively [32, 34]. Using keratin-based materials in food, cosmetics and biomedical fields can generate significant economic value from keratinous waste. Given the above, innovations aimed at environmentally friendly biomass valorization offer substantial economic benefits, environmental sustainability and potential human health advantages.

This thesis proposed two strategies, Cys-reduction assisted with ultrasound and ICSE-keratinolysis, aimed at recycling keratin and preparing keratin hydrolysate, respectively. They demonstrate improved sustainability, efficiency and simplicity, resulting in solubility-enhanced keratin and antimicrobial KEPs. The strategies found their potential in extended applications with promising economic values. They also provide insights for utilizing other keratinous waste, as well as other protein resources. Additionally, developing techniques for preparing KNP-based nanocarriers further expanded their potential in nano-delivery systems, including but not limited to oral delivery systems. The merits such as enhanced solubility, dispersibility and stability bring more possibilities for keratin utilization in foods, cosmetics, biomedical materials, etc. The findings in this thesis will propel the advancement of keratin towards becoming a mainstream biomaterial.

As an exceptional biomaterial capable of converting waste into valuable resources, keratin warrants more attention and continued development. In the future, further research on the biological effects of keratin-based materials can be conducted at the cellular and molecular levels. A deeper understanding and clarification will facilitate the broad and precise application of keratin, potentially advancing it into the mainstream in the commercial market.

7.8 References

1. H. Xu, Z. Shi, N. Reddy, Y. Yang, Intrinsically water-stable keratin nanoparticles and their in vivo biodistribution for targeted delivery, Journal of Agricultural & Food Chemistry, 62 (2015) 9145-9150.
2. A. Aluigi, M. Ballestri, A. Guerrini, G. Sotgiu, C. Ferroni, F. Corticelli, M.B. Gariboldi, E. Monti, G. Varchi, Organic solvent-free preparation of keratin nanoparticles as doxorubicin carriers for antitumour activity, Mater Sci Eng C Mater Biol Appl, 90 (2018) 476-484.
3. J. Lin, X. Zhi, P. Li, X. Jiang, Y. Jiang, Triple stimuli-responsive keratin nanoparticles as carriers for drug and potential nitric oxide release, Materials Science and Engineering: C, (2018).
4. L. Wang, Y. Shang, J. Zhang, J. Yuan, J. Shen, Recent advances in keratin for biomedical applications, Advances in Colloid and Interface Science, (2023) 103012.
5. L. Guo, L. Lu, M. Yin, R. Yang, Z. Zhang, W. Zhao, Valorization of refractory keratinous waste using a new and sustainable bio-catalysis, Chemical Engineering Journal, 397 (2020).
6. M. Pakdel, Z. Moosavi-Nejad, R.K. Kermanshahi, H. Hosano, Self-assembled uniform keratin nanoparticles as building blocks for nanofibrils and nanolayers derived from industrial feather waste, Journal of Cleaner Production, 335 (2022).
7. A. Shavandi, T.H. Silva, A.A. Bekhit, A.E.A. Bekhit, Keratin: dissolution, extraction and biomedical application, Biomater Sci, 5 (2017) 1699-1735.
8. S. Feroz, N. Muhammad, J. Ratnayake, G. Dias, Keratin-Based materials for biomedical applications, Bioactive materials, 5 (2020) 496-509.
9. H. Xu, Y. Yang, Controlled De-Cross-Linking and Disentanglement of Feather Keratin for Fiber Preparation via a Novel Process, ACS Sustainable Chemistry & Engineering, 2 (2014) 1404-1410.
10. F. Pourjavaheri, S. Ostovar Pour, O.A.H. Jones, P.M. Smooker, R. Brkljača, F. Sherkat, E.W. Blanch, A. Gupta, R.A. Shanks, Extraction of keratin from waste chicken feathers using sodium sulfide and l-cysteine, Process Biochemistry, 82 (2019) 205-214.
11. C.D. Tran, F. Prosenc, M. Franko, G. Benzi, Synthesis, structure and antimicrobial property of green composites from cellulose, wool, hair and chicken feather, Carbohydrate Polymers, 151 (2016) 1269-1276.
12. S. Pezeshk, S.M. Ojagh, M. Rezaei, B. Shabanpour, Fractionation of Protein Hydrolysates of Fish Waste Using Membrane Ultrafiltration: Investigation of Antibacterial and Antioxidant Activities, Probiotics Antimicrob Proteins, 11 (2019) 1015-1022.
13. A. Mirzapour-Kouhdasht, M. Moosavi-Nasab, Y.M. Kim, J.B. Eun, Antioxidant mechanism, antibacterial activity, and functional characterization of peptide fractions obtained from barred mackerel gelatin with a focus on application in carbonated beverages, Food Chem, 342 (2021) 128339.
14. A. Brandelli, Bacterial keratinases: useful enzymes for bioprocessing agroindustrial wastes and beyond, Food and Bioprocess Technology, 1 (2008) 105-116.
15. T. Li, Q. Liu, H. Chen, J. Li, Antibacterial activity and mechanism of the cell-penetrating peptide CF-14 on the gram-negative bacteria, Escherichia coli, Fish Shellfish Immunol, 100 (2020) 489-495.
16. Tonin, C.; Zoccola, M., Aluigi, A., Varesano, A., Montarsolo, A., Vineis, C., Zimbardi, F., Study on the conversion of wool keratin by steam explosion. Biomacromolecules, 7 (2006) 3499-3504.
17. J. Qiu, C. Wilkens, K. Barrett, A.S. Meyer, Microbial enzymes catalyzing keratin degradation: Classification, structure, function, Biotechnol Adv, 44 (2020) 107607.
18. Z. Xie, Q. Zhao, H. Wang, L. Wen, W. Li, X. Zhang, W. Lin, H. Li, Q. Xie, Y. Wang, Effects of

antibacterial peptide combinations on growth performance, intestinal health, and immune function of broiler chickens, Poult Sci, 99 (2020) 6481-6492.

19. L. Wang, C.-e. Lai, Q. Wu, J. Liu, M. Zhou, Z. Ren, D. Sun, S. Chen, A. Xu, Production and characterization of a novel antimicrobial peptide HKABF by Pichia pastoris, Process Biochemistry, 43 (2008) 1124-1131.
20. F.A. Nobari Azar, A. Pezeshki, B. Ghanbarzadeh, H. Hamishehkar, M. Mohammadi, S. Hamdipour, H. Daliri, Pectin-sodium caseinat hydrogel containing olive leaf extract-nano lipid carrier: Preparation, characterization and rheological properties, Lwt, 148 (2021).
21. Q. Wu, J. Patočka, K. Kuča, Insect antimicrobial peptides, a mini review, Toxins, 10 (2018) 461.
22. Z. Guo, H. Peng, J. Kang, D. Sun, Cell-penetrating peptides: Possible transduction mechanisms and therapeutic applications, Biomedical reports, 4 (2016) 528-534.
23. K. Splith, I. Neundorf, Antimicrobial peptides with cell-penetrating peptide properties and vice versa, European Biophysics Journal, 40 (2011) 387-397.
24. H. Xu, Z. Shi, N. Reddy, Y. Yang, Intrinsically water-stable keratin nanoparticles and their in vivo biodistribution for targeted delivery, J Agric Food Chem, 62 (2014) 9145-9150.
25. H. Xu, S. Cai, L. Xu, Y. Yang, Water-stable three-dimensional ultrafine fibrous scaffolds from keratin for cartilage tissue engineering, Langmuir, 30 (2014) 8461-8470.
26. A. Kam, S. Loo, J.S. Fan, S.K. Sze, D. Yang, J.P. Tam, Roseltide rT7 is a disulfide-rich, anionic, and cell-penetrating peptide that inhibits proteasomal degradation, J Biol Chem, 294 (2019) 19604-19615.
27. X. Sun, W. Zhang, L. Zhang, S. Tian, F. Chen, Effect of ultrasound-assisted extraction on the structure and emulsifying properties of peanut protein isolate, Journal of the Science of Food and Agriculture, 101 (2021) 1150-1160.
28. G.C. Kim, D.H. Cheon, Y. Lee, Challenge to overcome current limitations of cell-penetrating peptides, Biochim Biophys Acta Proteins Proteom, 1869 (2021) 140604.
29. Y. Lu, E. Zhang, J. Yang, Z. Cao, Strategies to improve micelle stability for drug delivery, Nano research, 11 (2018) 4985-4998.
30. M. Bteich, An overview of albumin and alpha-1-acid glycoprotein main characteristics: highlighting the roles of amino acids in binding kinetics and molecular interactions, Heliyon, 5 (2019).
31. Y. Wang, L. Zhang, P. Wang, X. Xu, G. Zhou, pH-shifting encapsulation of curcumin in egg white protein isolate for improved dispersity, antioxidant capacity and thermal stability, Food Res Int, 137 (2020) 109366.
32. C.O. Tuck, E. Pérez, I.T. Horváth, R.A. Sheldon, M. Poliakoff, Valorization of biomass: deriving more value from waste, Science, 337 (2012) 695-699.
33. A.J. Poole, J.S. Church, M.G. Huson, Environmentally sustainable fibers from regenerated protein, Biomacromolecules, 10 (2009) 1-8.
34. K. Chojnacka, H. Górecka, I. Michalak, H. Górecki, A review: valorization of keratinous materials, Waste and Biomass Valorization, 2 (2011) 317-321.


S

SUMMARY

Chicken feathers, as a globally abundant animal byproduct, represent a vast protein reservoir with significant biological potential. As discussed in **Chapter 1**, keratin and its hydrolysates exhibit appealing merits, such as biocompatibility, biodegradability, cell adhesion and proliferation, antimicrobial and antioxidant ability, etc. However, keratin only holds a small fraction of the commercial market compared to other biomaterials. The limitations regarding its inherent stability and method of extraction result in resource waste and environmental problems. Developing enhanced techniques becomes the priority for promoting feather waste conversion. In this thesis, we propose two sustainable and efficient strategies for keratin extraction and keratin hydrolysates preparation respectively (**Figure 8.1, Chapters 2&3**). Additionally, to reach more economic benefits, we propose the conversion to bioactive keratin peptides (KEPs) and nanoparticles (KNPs), leveraging their biological properties. The antimicrobial and cell-penetrating KEPs are obtained from feather keratinolysis (**Figure 8.1, Chapters 3&4**). To overcome the common problems such as low water solubility and aggregation, a novel route for preparing KNPs with enhanced performance was developed (**Figure 8.1, Chapter 5**). Then, the stability of KNPs was further enhanced with a sodium alginate (ALG) coating (**Figure 8.1, Chapter 6**).

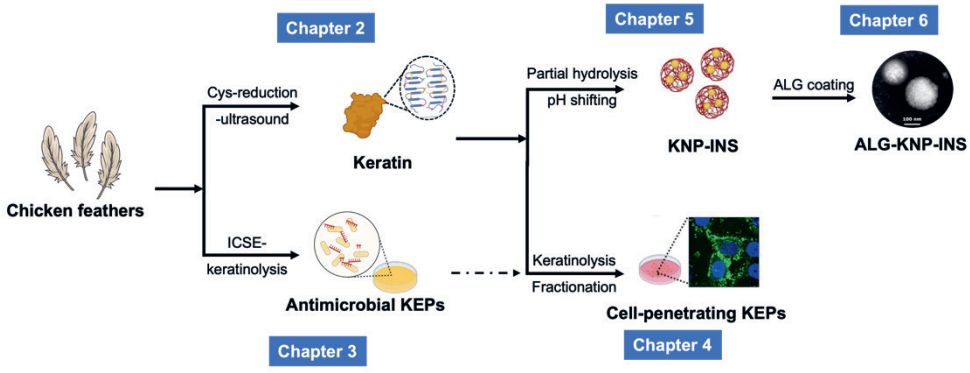

Figure 8.1. Overview of the thesis

In **Chapter 2**, a strategy of keratin recycling from chicken feathers combining ultrasound and Cys-reduction was investigated. The results indicate that ultrasound played a role in facilitating the feather deconstruction. However, a time of treatment ≥ 6h led to a large amount of small peptides and amino acids, as well as decreased yield and thermal stability of keratin. Conversely, solely by increasing ultrasonic power barely showed a significant impact. The recycled keratin under optimal

conditions (130 W, 2.7 h, and 15% Cys concentration) demonstrated improved solubility in aqueous solutions without damage to its chemical structure, thermal stability and amino acid composition. The study suggests the potential of ultrasound in recycling keratin from feather waste. The strategy combining ultrasound and Cys-reduction presents a time-saving alternative technique requiring no toxic reagent.

Besides recycling keratin, we also proposed a strategy for preparing feather hydrolysates (**Chapter 3**). Here the combination of instant catapult steam explosion (ICSE) and enzymatic hydrolysis was investigated. The results demonstrate that the ICSE treatment at 1.5 MPa for 120 s could deconstruct feathers without a large generation of small peptides and amino acids. Based on this, 90% of feathers were further deconstructed into soluble peptides by keratinases within 3 h, indicating a higher efficiency than other proteases, e.g. pepsin and trypsin. Additionally, the feather hydrolysate from keratinolysis exhibited anti-*E. coli* ability. The most active peptides were found to be below 3 kDa, exhibiting a high hydrophobic ratio and rich in specific amino acids such as Cys, Gly and Leu which potentially contributed to their antimicrobial ability. The findings indicates that ICSE-keratinolysis is an efficient strategy for valorizing feathers into antimicrobial KEPs.

Considering the findings in **Chapter 3** regarding the antimicrobial ability of KEPs, we proposed a hypothesis that KEPs might possess cell-penetrating ability. Therefore, **Chapter 4** delved into the cell-penetrating ability of KEPs with different molecular weights (Mw). The results demonstrate that the KEP < 3 kDa exhibited the highest cell-penetrating ability at 2 mg/mL, allowing efficient delivery of insulin into Caco2 cells without covalent bonding. The cellular uptake mechanism was energy-dependent, mainly involving macropinocytosis. The most effective components involved specific hydrophobic, PP Ⅱ amphipathic and Cys-rich peptides, e.g. RVVIEPSPVVV, PPPVVVTFP and CLPCRPCGPTPL. Additionally, the physicochemical characterization highlighted the potential contribution of rich hydrophobic residues and disulfide bonds, as opposed to small particle size and electrostatic interactions. These findings unveil the cell-penetrating ability of KEPs, suggesting the potential for non-covalently delivering biomolecules.

To overcome the challenges of KNPs regarding poor water solubility and aggregation, **Chapter 5** explored the preparation of performance-enhanced KNPs via partial hydrolysis and pH-shifting. The results show that the partial hydrolysis at a 5% degree of hydrolysis (DH) produced self-assembled spherical KNPs. The

KNPs exhibited small particle sizes of about 123 nm, along with great water solubility and stability against enzymatic degradation. Furthermore, we found that KNPs exhibited a reversible "open-close" structure between pH-shifting from 2.0 to 7.0. This was beneficial for fabricating insulin- and resveratrol-loaded nanoparticles. However, the KNPs at DH ≥ 10% presented more aggregation and denser clusters. They were also observed with inferior structural transformation reacting to pH-shifting and lower efficiency for loading biomolecules. The study indicates that partial hydrolysis (5% DH) combined with pH shifting is applicable for preparing biomolecule-loaded KNPs. Nevertheless, the application of KNPs in acidic environments should be avoided to prevent the deconstruction of KNPs.

Chapter 6 aims to address the remaining instability of KNPs under acidic conditions from **Chapter 5**, which may broaden their utilization in oral delivery systems. A coating of sodium alginate (ALG) was constructed on insulin (INS)-loaded KNPs for enhanced stability. The results indicate that double-coating nanoparticles (ALG-KNP-INS) via a gelation technique displayed small particle sizes of about 173 nm with spherical shapes alongside good re-dispersibility. Compared to the control groups, they presented enhanced stability under both heating treatment (80 °C) and storage at 4 °C for 4 weeks. Moreover, ALG-KNP-INS exhibited size changes responding to pH variations in the gastrointestinal tract, potentially protecting insulin against enzymatic degradation. The study highlights the positive effect of ALG-KNP coating on enhancing nanoparticle performance, such as size distribution, re-dispersibility and stability. The ALG-KNP coating is a potential formulation for enhancing the utilization of various biomolecules in diverse fields, including but not limited to oral delivery systems.

In **Chapter 7**, the thesis concludes with a summary of main results. The implications of our findings are discussed, and recommendations for future research are given.


A

ACKNOWLEDGEMENTS

I still remember how excited and grateful I was when given the opportunity to join the PhD program with a great supervisor team of Prof. Dr Johannes H. Bitter, Prof. Dr Chunhui Zhang and Dr Elinor L. Scott. The PhD journey encompassing four years and nine months, took me from the Chinese Academy & Agricultural Sciences (CAAS) in Beijing, China to Wageningen University & Research (WUR) in the Netherlands. It has been fulfilling period of personal and professional development for me. I would like to acknowledge the invaluable contributions of those who have supported me along the way.

I am immensely grateful to **Harry**, who has given me the opportunity to the Netherlands and perform a PhD at the BCT group. You let me know that I could start an email with "Hi Harry" instead of "Dear Prof. Harry". I really appreciate your patience on guiding me how to write a scientific proposal, an article and an abstract (I promise I got improved ☺). I learned "critical thinking" from you for the first time and started to think how important it is. I would like to thank you for always generously giving me affirmation and encouragement. The guidance and inspiration you have given me will shine like a lighthouse, illuminating the path to my future. Lastly, I would like to thank you for being so hospitable in hosting all the BCT barbecues and Christmas dinners. It is the most wonderful moments being with all BCT members.

I feel extremely grateful to **Chunhui Zhang** who agreed with Harry for allowing me to perform a PhD and supported me to the Netherlands. I have been lucky enough being your graduate student and finishing my MSc thesis under your supervision. I really appreciate that you have given me the scientific research enlightenment which strengthened my determination to pursue scientific research. You have been patiently supervising me on how to make a scientific research design and even how to prepare presentation slides. I will never forget that you reassured me not to be nervous for my first oral presentation. I greatly appreciate that you have always been there to offer excellent solutions whenever I had questions. I am grateful that you have been treating students as your own kids, which plays a vital role in my personal and academic development.

I could not be more grateful to **Elinor**, who has made great efforts supervising me. I have been thinking that you were a serious and incommunitive person, and even being a bit scared of you before I came to Wageningen. However, I realized how

wrong I was! You are such a kindly, optimistic and cheerful person. I would like to thank you for organizing the "first-week activity" to help me adapt to a new environment. I really enjoyed the relaxing and interesting talks with you at the coffee table. Your infectious laugh has been like a magic that cheers people up. I greatly appreciate for your ability of logical thinking and straightforward guidance when I was facing challenges regarding research. I am also grateful for your great patience and dedication to every nuance of my thesis. You delved into every sentence, leaving no detail unexplored. I feel lucky and happy to have you as my supervisor.

I would also like to thank my thesis committee-- **Aldrik Velders**, **Michel Eppink**, **Yuemei Lin** and **Carlos Cabrera** for taking the time to read and evaluate my thesis, also be my opponents.

I would like to thank all the staff of BCT for their contribution to my PhD thesis. **Susan**, you are such an amazing chromatography expert and painter! I am grateful for you helping me out with HPLC measurements whenever I got questions. Thank you for your painting of Rabbit which has been framed hanging up in my room. **Danielle**, thank you for helping me with the visa application and all other work behind the scenes. **Nadine**, thank you for never getting tired of helping me with chemicals and instruments. **Imogen**, thank you for exploring the micro-world of nanoparticles with me. **Guanna**, thank you for all the nice conversations and hope to play badminton with you someday! **Tomas**, it was nice to have been your running teammate and cheer for you. **Costas** and **Akbar**, I enjoyed the PhD trip to France with you and thank you for all the nice discussions.

I would also like to thank all the staff in Chinese Food Processing and Equipment Innovation Team, CAAS. **Xia Li**, I am grateful for your patiently listening to my concerns regarding research and life, offering me mental support and efficient solutions whatever the dilemma was. **Yujie Guo**, **Dong Han**, **Qingshan Shen**, **Yunhe Liu**, **Jiqian Liu**, **Xiong Xu** and **Yu Song**, thank you all for your invaluable support to my PhD project. You are such excellent seniors along my PhD journey!

Thank you also to all my fellows from WUR and CAAS. **Marlene**, **Laura**, **Jack, Umay** and **Zhaoxiang**, I am really grateful for all the talks and intro during my first week in BCT. **Umay**, you are such a warmful friend and thank you for accompanying me along my PhD journey in the BCT. **Matthijs**, thank you for sharing the nice cities for traveling and special candies with me. It has been nice time being your office mate.

Raghavendra and **Yangming**, thank you for the nice ping-pong and badminton times. **Ivo**, **Torin**, **Freek**, **Dmitry**, **Roel**, **Cynthia** and **Sanne**, it has been such an amazing and memorable PhD trip to France with you! **Ellis**, **Sybren**, **Gijs** and **Pedro**, thank you for being my lab mates and I have enjoyed the talks with you at the coffee table. **Feng**, **Mingming**, **Yufan**, **Zhaoxiang**, **Chenqiang** and **Mingzhao**, it was so nice to meet you in Wageningen and I feel lucky to be your friend. **Chuan Yang** and **Ruilin Li**, thank you for your invaluable contributions to my PhD thesis. Finally, I would like to express my special gratitude to **Ivo** and **Torin** for being my paranymphs!

I would also like to express my gratitude to all my friends. **Yusi Liu**, **Lei Deng**, **Xiyu Li**, **Ying Lv**, **Lina Hu**, **Feilong Yang**, **Zhuo Xu**, **Qiuhong Huang**, **Yaowu Wang**, **Mengxiao Sun, Xixu Jiang**, **Bingxin Wang** and **Meijun Chen**, thank you for your invaluable help, support and friendship. I have enjoyed all the sports, dinners and trips with you!

Finally, I would like to express my sincere gratitude to my parents and my sister for their supports. Without your tremendous understanding and encouragement over the past few years, it would be impossible for me to complete my studies.


A

ABOUT THE AUTHOR

Curriculum vitae

Xiaojie Qin was born in November 1993 in Shandong province, China. She obtained her bachelor's degree from the College of Food Science and Engineering of Northwest A&F University in 2016 in Xi'an city, Shanxi province. There she developed a strong interest in the area of food science and engineering. After graduation, she made a further study on the processing and storage of agricultural products at the Institute of Food Science and Technology of the Chinese Academy of Agricultural Sciences. Xiaojie completed her MSc thesis entitled "Preparation of yak bone powder and its anti-osteoporosis effect" under the supervision of Prof. Dr Chunhui Zhang. In September 2019, she received a scholarship fund from the China Scholarship Council for her Ph.D. study at the Biobased Chemistry & Technology group of Wageningen University & Research, the Netherlands. Her work focused on the valorization of chicken feathers supervised by Prof. Dr Johannes H. Bitter, Prof. Dr Chunhui Zhang and Dr Elinor L. Scott. The project, entitled "Valorization of chicken feathers: biobased nanocarriers for biomolecule delivery", was in close collaboration with the Institute of Food Science and Technology of the Chinese Academy of Agricultural Sciences. The most important results of her PhD research are presented in this dissertation.

Contact: xiaojie_qin0915@163.com

List of publications

Xiaojie Qin, Johannes H. Bitter, Chunhui Zhang, Elinor L. Scott. Preparation and evaluation of double-coated nanoparticles incorporating keratin and sodium alginate for enhanced stability. (To be submitted)

Xiaojie Qin, Johannes H. Bitter, Chunhui Zhang, Elinor L. Scott. Preparing keratin nanoparticles via partial hydrolysis and pH-shifting. (To be submitted)

Xiaojie Qin, Ruilin Li, Yujie Guo, Johannes H. Bitter, Elinor L. Scott, Chunhui Zhang. Enhanced delivery of biomolecules into Caco2 cells based on the cell-penetrating ability of keratin peptides. (Submitted for publication)

Xiaojie Qin, Chuan Yang, Yujie Guo, Jiqian Liu, Johannes H. Bitter, Elinor L. Scott, Chunhui Zhang. Effect of ultrasound on keratin valorization from chicken feather waste: Process optimization and keratin characterization, *Ultrasonics Sonochemistry*, 2023, 106297.

Xiaojie Qin, Xiong Xu, Yujie Guo, Qingshan Shen, Jiqian Liu, Chuan Yang, Elinor L. Scott, Johannes H. Bitter, Chunhui Zhang. A sustainable and efficient recycling strategy of feather waste into keratin peptides with antimicrobial activity, *Waste Management*, 2022, 144: 421-430.

Xiaojie Qin, Qingshan Shen, Yujie Guo, Jiqian Liu, Hongru Zhang, Wei Jia, Xiong Xu, Chunhui Zhang. An advanced strategy for efficient recycling of bovine bone: Preparing high-valued bone powder via instant catapult steam-explosion, *Food Chemistry*, 2021, 374.

Xiaojie Qin, Qingshan Shen, Yujie Guo, Xia Li, Jiqian Liu, Mengliang Ye, Hang Wang, Wei Jia, Chunhui Zhang. Physicochemical properties, digestibility and anti-osteoporosis effect of yak bone powder with different particle sizes, *Food Research International*, 2021, 145.

Hang Wang[1], **Xiaojie Qin**[1], Xia Li, Xiaoling Wang, Yinfeng Lei, Chunhui Zhang. Effect of chilling methods on the surface color and water retention of yellow-feathered chickens, *Poultry Science*, 2020, 99(4): 2246-2255.

Hang Wang, **Xiaojie Qin**, Xia Li, Xiaoling Wang, Hongwei Gao, Chunhui Zhang. Changes in the microbial communities of air- and water-chilled yellow feathered broilers during storage at 2 °C, *Food microbiology*, 2020, 87: 18-26.

Xiaojie Qin, Qingshan Shen, Chunhui Zhang, Hongru Zhang, Jia Wei. Preparation of instant yak bone powder by using instant catapult steam explosion and its physicochemical properties, *Transactions of the Chinese Society of Agricultural Engineering*, 2020, 36: 307-315. (In Chinese)

Hang Wang, **Xiaojie Qin**, Si Mi, Xia Li, Xiaoling Wang, Weijiang Yan, Chunhui Zhang. Contamination of yellow-feathered broiler carcasses: Microbial diversity and succession during processing, *Food Microbiology*, 2019, 83: 18-26.

Xiaojie Qin, Qingshan Shen, Wei Jia, Chunhui Zhang, Qiankun Zheng. Effect of ultrasonic-assisted degreasing on preparation and physicochemical properties of yak bone powder, *Transactions of the Chinese Society of Agricultural Engineering*, 2018, 36: 272-280. (In Chinese)

Overview of completed training activities

Discipline specific activities

Courses

Special Topics Agricultural Science and Technology Progress	Beijing, China, 2020
NanoBioPhysX Course	Wageningen, The Netherlands, 2022-2023
Advanced Course Microscopy and Spectroscopy in Food and Plant Sciences	Wageningen, The Netherlands, 2023
Healthy Food Design	Wageningen, The Netherlands, 2023
Rheology: The do's and don'ts	Wageningen, The Netherlands, 2023
Protein quality evaluation and application	Wageningen, The Netherlands, 2023

Conferences and symposia

Food Science and Technology Innovation Forum	Shanghai, China, 2021
International Forum on Food Safety and Health	Beijing, China, 2021
Summer Course Glycosciences——17th European Training Course on Carbohydrates[1]	Wageningen, The Netherlands, 2023
4th International Conference for Bioresource Technology[1]	Lake Garda, Italy, 2023
Immune Connection Event	Wageningen, The Netherlands, 2023

General courses

Scientific Research Integrity and Academic Ethics	Beijing, China,2020
Academic Writing and Presenting	Beijing, China, 2020
Effective Academic Development	Beijing, China, 2020
VLAG PhD week	Baarlo, The Netherlands, 2022
Project & Time Management	Wageningen, The Netherlands, 2022

Others

CAAS group meetings	Beijing/online, China, 2020-2024
Preparation of research proposal	Wageningen, The Netherlands, 2022
PhD study trip to France	Lyon & Paris, France, 2022
PhD scientific meetings	Wageningen, The Netherlands, 2022-2024
Weekly scientific meetings	Wageningen, The Netherlands, 2022-2024
BCT group meetings	Wageningen, The Netherlands, 2022-2024
Revision of Scientific articles	Wageningen, The Netherlands, 2022

[1] Poster presentation

The research presented in this thesis was performed within the close collaboration of Wageningen University & Research and Chinese Academy of Agricultural Sciences. The funding from China Scholarship Council (No. 202003250130) is greatly appreciated.

Financial support from Wageningen University for printing this thesis is gratefully acknowledged.

Cover artwork and design by Xiaojie Qin

Printed by Proefschriftmaken, the Netherlands